VOLUME 13 NUMBER 2 2020 ISSN 2218-7979
eISSN 2409-370X

International Journal of Biology and Chemistry

Al-Farabi Kazakh National University

International Journal of Biology and Chemistry is published twice a year by
al-Farabi Kazakh National University, al-Farabi ave., 71, 050040, Almaty, Republic of Kazakhstan
website: http://ijbch.kaznu.kz/

Any inquiry for subscriptions should be sent to:
Prof. Mukhambetkali Burkitbayev, al-Farabi Kazakh National University
al-Farabi ave., 71, 050040, Almaty, Republic of Kazakhstan
e-mail: Mukhambetkali Burkitbayev@kaznu.kz

EDITORIAL

The most significant achievements in the field of natural sciences are reached in joint collaboration, where important roles are taken by biology and chemistry. Therefore publication of a Journal, displaying results of current studies in the field of biology and chemistry, facilitates highlighting of theoretical and practical issues and distribution of scientific discoveries.

One of the basic goals of the Journal is to promote the extensive exchange of information between the scientists from all over the world. We welcome publishing original papers and materials of biological and chemical conferences, held in different countries (by prior agreement, after the process of their subsequent selection).

Creation of special International Journal of Biology and Chemistry is of great importance, since scientists worldwide, including other continents, might publish their articles, which will help to widen the geography of future collaboration.

The Journal aims to publish the results of the experimental and theoretical studies in the field of biology, biotechnology, chemistry and chemical technology. Among the emphasized subjects are: modern issues of technologies for organic synthesis; scientific basis of the production of physiologically active preparations; modern issues of technologies for processing of raw materials; production of new materials and technologies; study on chemical and physical properties and structure of oil and coal; theoretical and practical issues in processing of hydrocarbons; modern achievements in the field of nanotechnology; results of studies in various branches of biology, biotechnology, genetics, nanotechnology, etc.

We hope to receive papers from the leading scientific centers, which are involved in the application of the scientific principles of biological and chemical sciences on practice and carrying out research on the subject, related to production of new materials, technologies and ecological issues.

IRSTI 76.03.35 https://doi.org/10.26577/ijbch.2020.v13.i2.01

T.T. Nurkenov[1*], A.K. Tsoy[2], G.E. Zhusupova[1],
F.S. Olzhayev[2], M.Zh. Shertay[2], T.M. Shalakhmetova[1],
J.C.-M. Lee[3], Sh.N. Askarova[2]

[1]Al-Farabi Kazakh National University, Almaty, Kazakhstan
[2]Nazarbayev University, Nur-Sultan, Kazakhstan
[3]University of Illinois at Chicago, Department of Bioengineering, Chicago, USA
*e-mail: nurkenovtulendy@gmail.com

Therapeutic effectiveness of *Limonium gmelinii* extract in experimentally – induced ischemic brain damage *in vivo*

Abstract. One of the important directions in the treatment of ischemic stroke (IS) consequences is revascularization of the damaged brain areas including decreasing acute hypoxia and oxidative stress that occur in the ischemic tissue due to reperfusion syndrome after restoration of blood flow. Plant polyphenols are promising candidates capable of exerting a pronounced antioxidant and neuroprotective effects. There are a number of wild plants growing on the territory of Kazakhstan, and one of these plants containing significant number of polyphenols is *Limonium gmelinii* (*L. gmelinii*, genus *Limonium* Mill). In our study we have applied middle cerebral artery occlusion (MCAO) method to induce focal ischemic cerebral stroke in male Wistar rats. The results of assessment of sensorimotor functions in laboratory animals showed that MCAO resulted in sensorimotor deficiency. At the same time, partial recoveries of sensorimotor functions were observed in animals that were treated with extract of *L. gmelinii* after stroke compared to untreated animals. Similarly, histological analysis of the damaged brain regions has revealed focal coagulation necrosis with clearly visualized damaged regions in animals with MCAO, whereas brain tissue of animals exposed to *L. gmelinii* extract after stroke induction was partially restored. Our results demonstrate that extract of *L. gmelinii* possesses neuroprotective properties that require further investigations.

Key words: ischemic stroke, plant polyphenols, ROS, antioxidants.

Introduction

Acute cerebrovascular disease or stroke is one of the three most common cardiovascular diseases in the world [1]. According to WHO (2012), about 6.7 million fatal cases of stroke are recorded every year globally (http://who.int/mediacentre/factsheets/fs310/en/). Among all registered cases, 80% are ischemic strokes. Moreover, 95% of ischemic strokes (IS) are associated with complications of the embolic type arising from plaques located in the extracranial sections of the arterial system.

Given the prevalence of this pathology, as well as the association with high percentage of mortality and primary disability, IS is a global medical and social problem [2]. There is a clear dependence of the increase in the incidence of stroke with an age above 30 years [3; 4], with two thirds of all cases of stroke occurring at the age of 65 years or more [5]. The costs of treating this disease are also of great socio-economic importance. The costs of therapy and maintenance of patients who have undergone IS making up the major expenses of the healthcare industry in many countries around the world [6]. The continuing tendency to "rejuvenate" stroke, a high percentage of mortality and disability also highlights the importance and relevance of the study of stroke in young people. Thus, the development of stroke prevention methods and rehabilitation – based therapy is a very important task for many countries in the world.

Restoration and maintenance of systemic hemodynamics, conducting drug thrombolysis and hemangiocorrection are key circulation recovery methods. In recent decades, the most effective method of treating IS is considered to be medication thrombolysis targeted on restoration of the main blood flow in the affected area in order to prevent

irreversible changes in the brain tissue [7]. Data were obtained that thrombolysis in patients with IS in the acute phase of the disease helps to reduce mortality rate by 17% and reduces the development of disability rate by 25% [8]. However, due to the narrow temporary "therapeutic window" (not more than 3 hours after the development of stroke) and the high risk of developing hemorrhagic complications, the spectrum of therapy with recombinant tissue plasminogen is very limited [9-11]. In most cases, a significant proportion of patients are admitted to specialized hospitals at a later date and the main method for correcting IS is to conduct «standard» basic therapy using drugs aimed at normalizing the rheological properties of blood, antiplatelet, anti-coagulation therapy and maintaining brain tissue metabolism [12-14].

Studies have shown that despite the fact that the restoration of the main blood flow in the area of cerebral ischemia is critical, the subsequent development of reperfusion syndrome causes further damage to nerve tissues [15-17]. As a result of the action of ischemia of brain tissue and the development of reperfusion syndrome, a cascade reaction mechanism is launched, which is accompanied by the accumulation of products of free radical oxidation [18]. Considering the fact that escalation of ROS synthesis is noted both during and after brain ischemia, the products of oxidative reactions are of particular importance in ischemia and secondary cerebral hypoxia [19-23]. In this regard, the antioxidant therapy is justified even in a delayed manner, since one of the main mechanisms of cell death is oxidative stress [24; 25].

In recent decades, plant polyphenols have been of increasing interest due to their proven antioxidant properties and the ability to inactivate free radicals [26–31]; therefore, the search for new plant objects rich in bioavailable polyphenols is in high demand. One of the plants abundant in polyphenols is *Limonium gmelinii* (*L. gmelinii*), a representative of the genus *Limonium*, growing in large numbers in Kazakhstan [32; 33]. It was previously shown that the extract of polyphenols isolated from the roots of *Limonium gmelinii* has a wide range of therapeutic properties [31; 34; 35]. In addition, it neutralizes the toxic effect of the pro-inflammatory cytokine TNF-α, has antioxidant properties, inhibits endothelial cell activation, reduces the generation of ROS in endotheliocytes and astrocytes of the brain, inhibits the activation of the NADPH oxidase enzyme and blocks the development of oxidative stress in neurons, thus providing a complex protective effect and inhibiting the development of oxidative stress *in vitro* [36]. However, the question of what effect the extract of *Limonium gmelinii* has in case of ischemic stroke and *in vivo* reperfusion syndrome remained open. In this regard, the aim of the work was to evaluate the effectiveness of the use of the extract of polyphenols isolated from the roots of *Limonium gmelinii*, in conditions of ischemic brain damage *in vivo* in a model of laboratory animals.

Materials and methods

Preparation of polyphenol extract. Preparation of polyphenol extract was conducted at the Department of Chemistry and Chemical Technology, al-Farabi Kazakh National University according to a described previously method [31]. Briefly, the polyphenols from roots of *Limonium gmelinii* will be double extracted with 50% ethanol (1:6) for 5 hrs followed by vacuum drying in 40-60 °C.

Object of study. Outbred male Wistar rats weighing 280-300 g were used, which were kept in vivarium conditions, including a 12-hour day/night cycle, at a temperature of 22-23 °C. For the experiments, the animals were divided into 4 groups: 1 – control animals, 2 – animals with MCAO, 3 – animals with MCAO, which were treated with *Limonium gmelinii* extract intragastrically at a dosage of 200 mg / kg for 28 days, 4 – animals that received only *Limonium gmelinii* extract in the same dosage. A day before the induction of stroke, the next day, on the 14th and 28th day after induction, the sensorimotor functions of animals were evaluated. On day 29, control and experimental animals were euthanized under isoflurane anesthesia and brain samples were taken.

Ethical approval. The research related to animals use has been complied with all the relevant national regulations and institutional policies for the care and use of animals (Protocol №2 from 06.18.2015, the Local Ethical Commission of the Center for Life Sciences of Nazarbayev University, Astana).

Creating a model of ischemic stroke by middle cerebral artery occlusion (MCAO). For an experimental study of the effects of plant polyphenols on the brain, an IS model caused by occlusion of the middle cerebral artery (MCAO) was used. This model is characterized by the stability of damage to brain structures and is convenient for assessing the functional changes. The MCAO model differs from other experimental models in the ability to cause significant sizes of IS [37] and is similar to the development of IS in humans. When modeling a stroke, special material and equipment were used: an Olympus optical binocular microscope (Olympus,

Japan), a coagulator, a gas anesthesia system (Harvard Apparatus, USA), an Isoflurane inhalation anesthetic (5% solution), Lawton microsurgical instruments (Lawton, Germany), suture material: prolen 6/0, silk 6/0, vicryl 6/0 (Ethicon, USA) (Figure 1).

IS model has been reproduced by MCAO in rats according to a previously described protocol [38]. As a temporary obturator of the lumen of the middle cerebral artery, a 4/0 nylon monofilament with a thickened silicone tip (Doccol Corp. USA) was used, which was introduced under visual control into a.carotis interna to a level of 17-20 mm. In this position, the monofilament was left for 2 hours to create a focal zone of acute cerebral ischemia (Figure 2). To confirm the presence of focal ischemic stroke of the brain 24 hours after occlusion of the middle cerebral artery in laboratory animals, brain tissue was taken under isoflurane anesthesia.

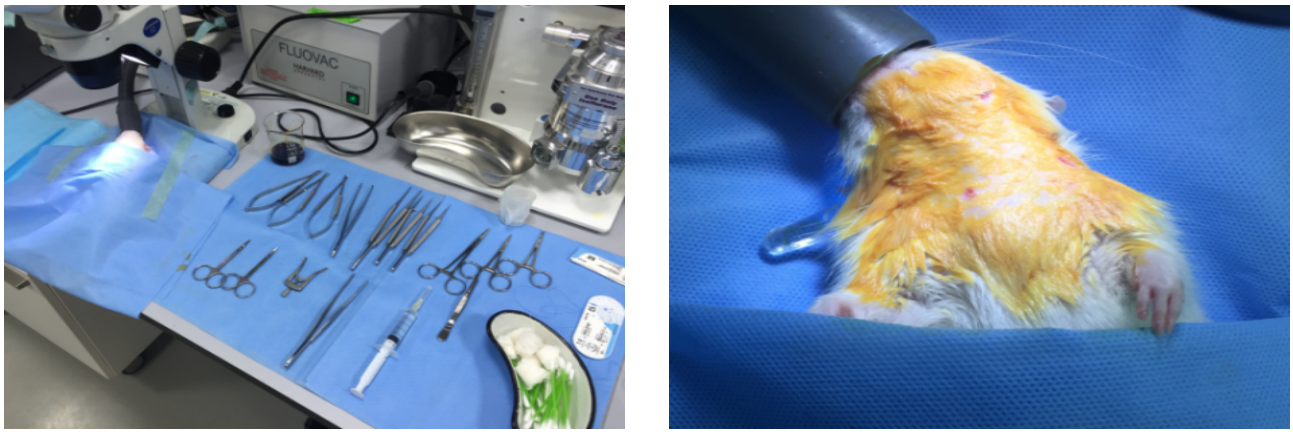

A B

Figure 1 – General view of the preoperative preparation.
Note: A – preoperative preparation; B – laying the animal on its back with the processing of the surgical field.

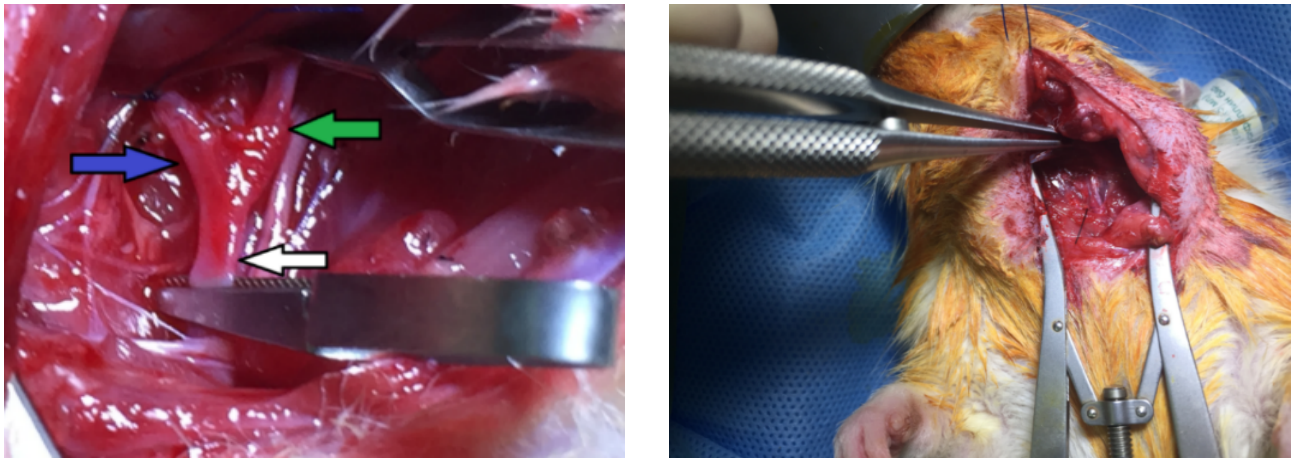

A B

Figure 2 – Model of middle cerebral artery occlusion (MCAO).
Note: A – mobilization of the common, external and internal carotid arteries: blue arrow – external, green arrow – internal, white arrow – common carotid artery; B – general view of the middle cerebral artery occlusion model (MCAO).

Evaluation of sensorimotor activity in laboratory animals. Analysis of locomotor functions of the front and hind legs of laboratory animals «Beam walk» balance test was performed. The rat was placed at the beginning of the board (wide part) and bright light was turned on, forcing the animal to move along a

narrowing path to the shelter (dark chamber). The entire testing process was recorded on a video camera installed at a sufficient distance from the test site, so the whole track got into the frame.

To assess the locomotor function of laboratory animals, the number of settings of the limb on the lower board (error), the amount of limb slipping from the upper board to the lower board (when the foot is placed on both boards) and the total number of steps taken from the start line to the animal's entrance into dark camera were calculated. Errors and slippage accounting was carried out for the front and hind legs separately. The videos were analyzed frame by frame using RealTimer software. The data obtained for three attempts were averaged. The severity of sensorimotor deficiency was calculated by the formula in percent:

$$\frac{\text{Error} + 0.5 * 100 * \text{Slipping}}{\text{Total number of steps}}$$

Preparation and analysis of histological slides of the brain. The rat brain was fixed in a 10% solution of neutral formalin. After fixation, the samples were washed from formalin, then brain samples were gradually dehydrated in 70%, 95%, 95%, 100%, 100% ethanol, followed by immersion in xylene. Thereafter samples embedded in paraffin blocks. Using a microtome (Leica, Germany), 5 μm thick sections were obtained, mounted on glass slides and spread on a warm table, then treated with xylene to exclude paraffin. Histological sections were rehydrated according to the reverse procedure in 100%, 100%, 95%, 95%, 70% ethanol, and in distilled water. After that, the sections were stained with hematoxylin-eosin. After staining, the slides were coated with Canadian balsam and analyzed under a microscope. Stained samples were analyzed using a Carl Zeiss Axio Vert light microscope (Carl Zeiss, Germany).

Statistical analysis. The data obtained are presented as mean ± standard error of the mean (Mean ± SEM). Standard deviations between experimental groups were evaluated using Student's t-test. Values were considered significantly different at $p \leq 0.05$.

Results and discussion

Induction of ischemic stroke by occlusion of the middle cerebral artery and administration of polyphenol extract. For the purpose of preoperative preparation, the animal was not given food and water on the day of surgery. To initiate inhalation anesthesia, the animal was placed in an anesthetizer chamber using a 5% Isoflurane solution under conditions of 1.0 L / min oxygen (O_2). The choice of anesthesia in favor of the inhaled anesthetic Isoflurane was determined due to the good controllability of anesthesia, the presence of interspecific universality of anesthesia, and the absence of toxic effects on the animal's body. The drug has a moderate irritant effect, pharyngeal and laryngeal reflexes become dull quickly, but there is some depression of the respiratory system. Heart rate and release practically do not change. Moreover, a decrease in stroke volume is compensated by an increase in heart rate. After immersing the animal in the surgical stage of anesthesia, a 1.5% level of Isoflurane was used to maintain anesthesia.

After recovery of the animal from anesthesia, signs of the development of ischemic lesion of a part of the brain in the basin of the middle cerebral artery were visually observed, which manifested as ptosis of the right eye and the development of paresis of the right upper limb. To confirm the development of focal ischemic stroke, a pathomorphological study of the brain was performed in some of the operated animals 24 hours after the operation. The remaining animals were slaughtered on the 29th day after the sensorimotor functions of the animals were evaluated.

It was found that in animals that were subjected to MCAO procedure, 24 hours after surgery, the presence of ischemic cerebral infarction was observed (Figure 3).

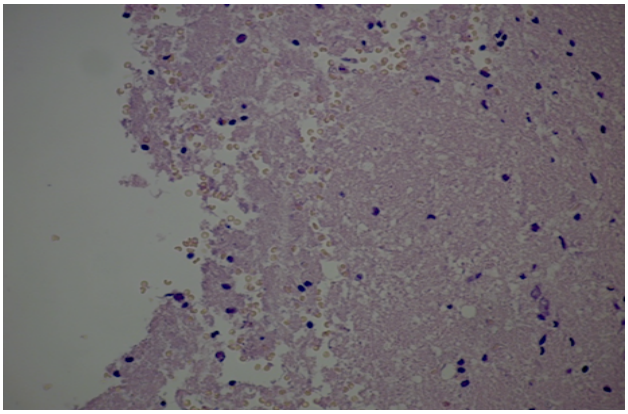

Figure 3 – Histostructure of the brain of rats with induced stroke. The center of ischemic infarction. Hematoxylin-eosin stain, x200.

Subcortical in the white matter and subcortical nodes, a focus of complete coagulation necrosis is found, in which the shadows of neurocytes, accumulations of red blood cells are visible. On the periphery of the focus of necrosis, widespread ischemic injuries of neurocytes were observed,

which lost most of their processes, extended and acquired an angular shape. Large focal hemorrhages were also observed in the cerebellum. In pear-shaped cells (Purkinje cells), homogenizing changes were observed in the form of a pale colored cell body, wrinkling of nuclei. The cells of the granular layer were in a state of dystrophy, the cytoplasm of part of the cells was vacuolated (Figure 4).

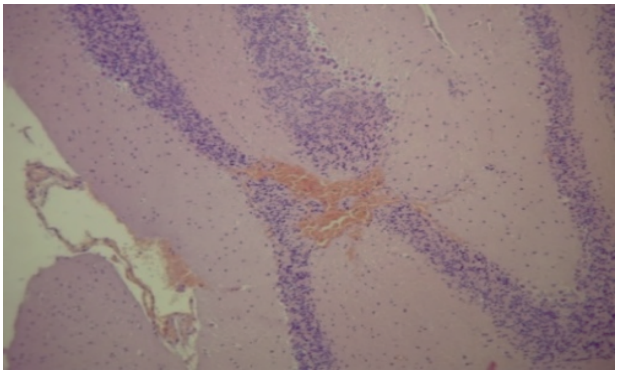

Figure 4 – Homogenizing changes and large-focal hemorrhages in the tissues of the cerebellum. Stained with hematoxylin and eosin, x100.

The presence of foci of ischemic infarction of the substance of the brain, as well as common ischemic damage to neurocytes of the cortex and white matter of the cerebral hemispheres, indicated the presence of ischemic stroke in the operated animals.

Assessment of sensorimotor functions in animals with induced stroke and exposed to Limonium gmelinii. The results of the analysis of motor function by the method of narrowing lane revealed a pronounced sensorimotor deficiency in all animals with induced stroke on the first day after MCAO (Figure 5).

After 2 and 4 weeks, a slight improvement in sensorimotor function was detected in animals with MCAO with no treatment. However, in animals that received extract of *Limonium gmelinii* after MCAO, a statistically significant improvement in the motor functions of the fore and hind limbs was observed after two weeks with a further decrease in sensorimotor deficiency compared to untreated animals.

Histological analysis of the brain of animals with induced stroke and exposed to extract of Limonium gmelinii. A histological examination of brain sections in animals without MCAO that received extract of *Limonium gmelinii*, as well as in animals of the control group, did not reveal pathological changes in the brain histostructure (Figure 6). Necrosis of neurons and glial cells was not observed, circulatory disorders were not detected. The nuclei of cells with clear boundaries were well detected in a light microscope.

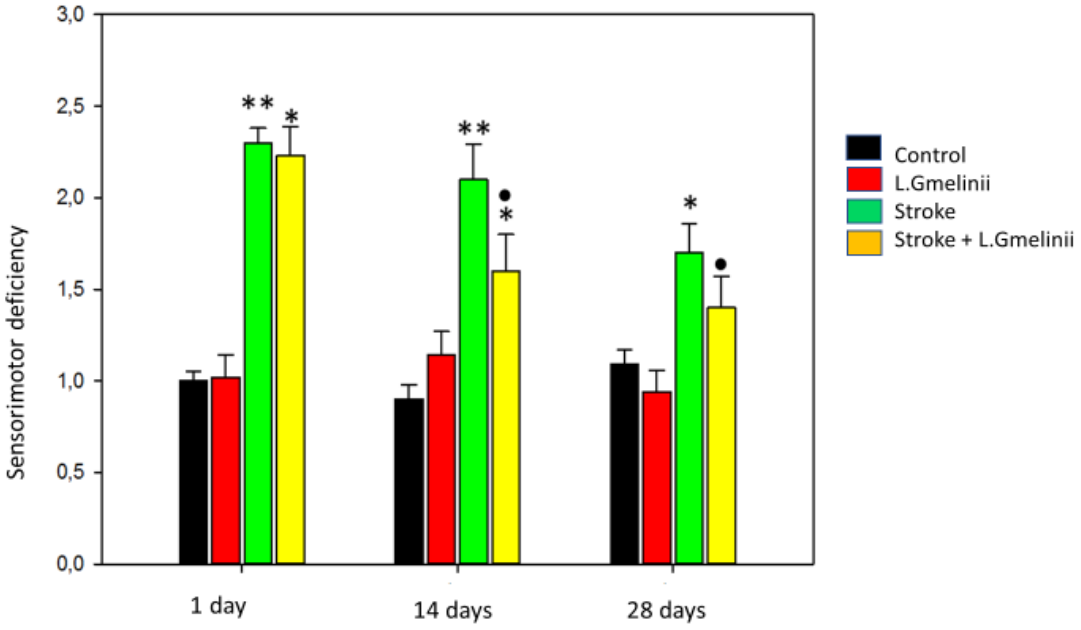

Figure 5 – Test results of sensorimotor functions in rats. ** – $p \leq 0.01$, * – $p \leq 0.05$ compared to the control, ● – $p \leq 0.05$, compared to animals with a stroke (Student's t-test).

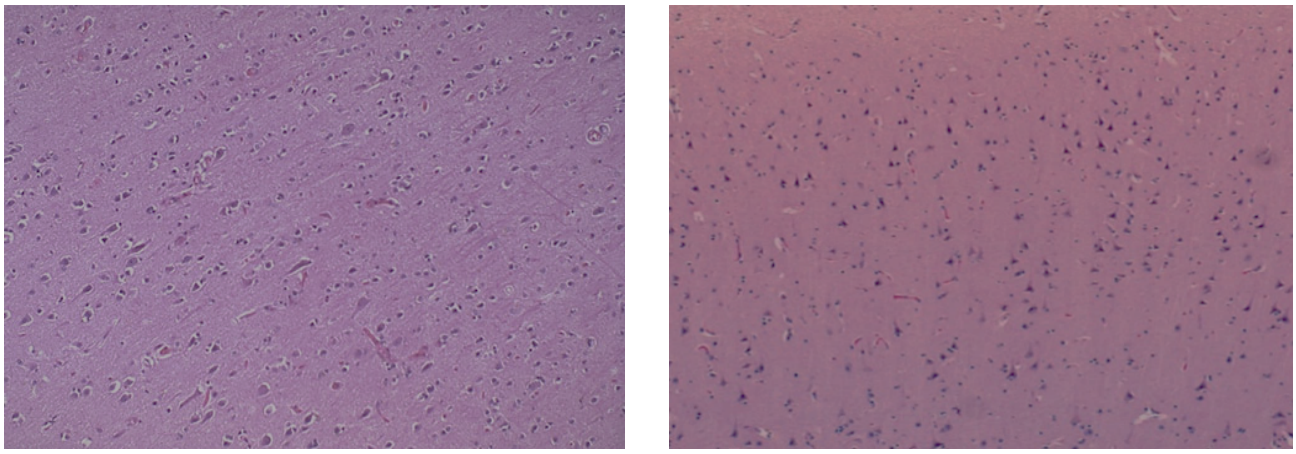

A B

Figure 6 – Normal histostructure of brain tissue of intact animals (A) and exposed to *Limonium gmelinii* without MCAO (B). Stained with hematoxylin and eosin, x100.

In animals with induced stroke, on the 29th day after MCAO, pathological changes in the histological structure of the brain were still observed (Figure 7). Shadows of neurons were observed in the foci of necrosis, hemolyzed erythrocytes were present in the areas of lysed cells. On the periphery of the focus of necrosis was determined ischemic damage to neurocytes. Outside the focus of necrosis in the cortex and extracortical areas of the cerebral hemispheres, medulla oblongata, and cerebellum, neurocytes were observed in the state of protein dystrophy. Foci of dystrophy, an increase in the number of microgliocytes were observed in glia. Foci of fibrosis were determined in the meninges.

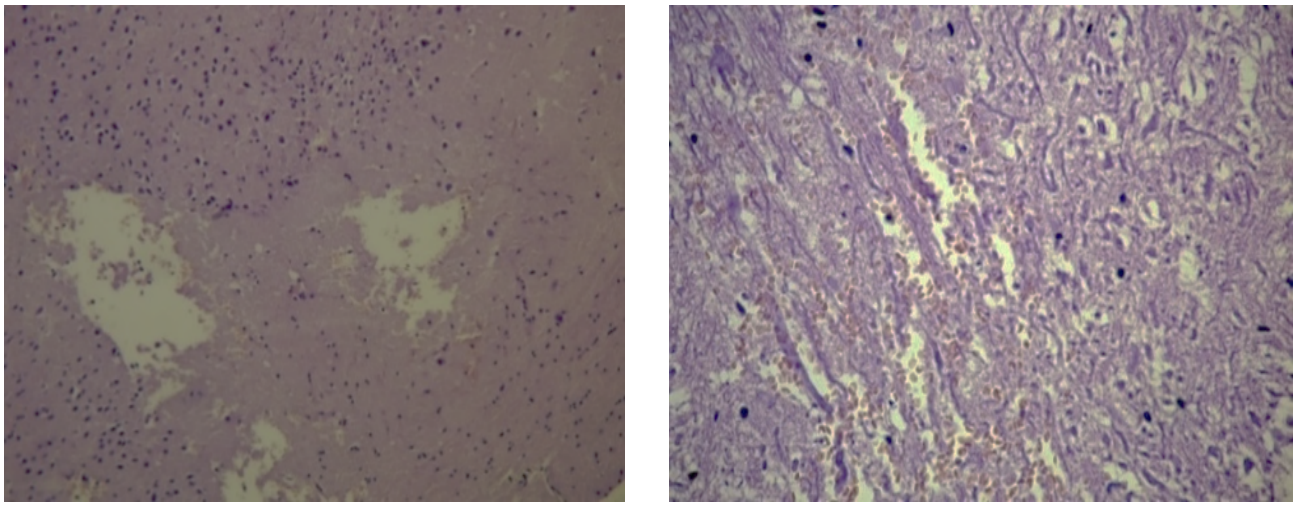

A B

Figure 7 – Foci of ischemic infarction. Note: A – In the histostructure of the brain; B – In the meninges. Stained with hematoxylin and eosin, x100.

Rats that received extract of *Limonium gmelinii* after stroke induction showed a slight improvement in the brain tissues (Figure 8). No extensive areas of necrosis were observed, although there were signs of frustration in the small foci. Along the periphery of small foci of necrosis, proliferation of astrocytic glia, isolated capillaries with red blood cell stasis were visible. Glia with foci of dystrophy,

an increase in the number of microgliocytes were also detected.

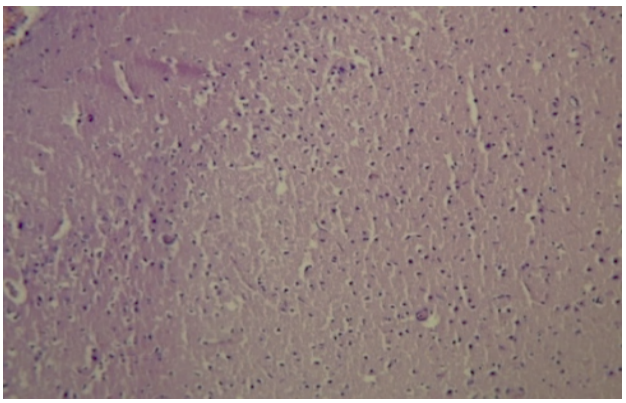

Figure 8 – Small focus of ischemic infarction. Stained with hematoxylin and eosin, x100.

Today plant polyphenols occupy a unique place in science as they potentially are capable of reducing the risk of the disease and might be used in treatment of such conditions as diabetes, cardiovascular disorders, atherosclerosis, neurodegenerative disorders and inflammation. Polyphenols are a structural class of mainly natural organic chemicals characterized by the presence of large multiples of phenol structural units. The number and characteristics of these phenol structures underlie the unique physical, chemical, and biological (metabolic, toxic, therapeutic, etc.) properties of particular members of the class. Polyphenols are rich in vegetables, fruits, grains, bark, roots, tea, and wine. Most polyphenols are generally known to possess potent antioxidant, anti-inflammatory, and anti-apoptotic properties, and their protective effects in ischemic injury have been demonstrated in a number of *in vitro* and *in vivo* studies [27; 28; 39; 40]. For example, magnolia polyphenols have been shown to attenuate oxidative and inflammatory responses in neurons and microglia cells [39]. Green tea polyphenols have also been proven to exhibit multiple neuro protective actions [41; 42]. However, the health effects of polyphenols depend on the chemical structure (eg, glycosylation, esterification, and polymerization) and bioavailability. Bioavailability appears to differ greatly between the various polyphenols, and the most abundant polyphenols in our diet are not those that have the best bioavailability profile [43]. Thus, new plant sources rich with bioavailable polyphenols are still in demand.

We have reported previously that root extract of *Limonium gmelinii* possesses significant hepatoprotective activity in CCl_4-induced liver damage, exceeding those of control flavonoids (silymarin and silibinin) [31]. The roots and rhizomes of the *Limonium gmelinii* (*Plumbaginaceae*) have been used in a traditional herbal medicine in Central Asia for hundreds of years. *Limonium gmelinii* contains a rich source of polyphenols, which is presented by flavonoids of oxidated type (7-14%), hydrolysable tannins and mono-, di and oligo forms of flavan-3-ols (40-60 %). The main monomeric flavane is (-)-epigallocatechin-gallate. Flavonoids of oxidated type are represented by 3,5,7,3',4',6' – hexahydroxy-flavane, isorhamnetin, quercetin, myricetin, their mono- and diglucosides (myricitrin, galactopyranosides of quercetin and myricetin, rhamnoglucoside of myricetin, rutin, etc.). Also, in extract composition was identified new flavone glycoside – Gmelinoside I [44]. 2-o-β-D-galloil and 2,3-o-β-D-digalloilglucose were isolated from hydrolized tannins. *Limonium gmelinii* extract also contains all known 20 natural α-aminoacids, 34 microelements, vitamins (C, E and ß-carotene) and xanthophylls.

Since both CCl_4-induced liver damage and ischemic brain damage are associated with oxidative cell injury and sterile immune response, in the present work we have evaluated therapeutic potential of *Limonium gmelinii* root extract on animal model of ischemic brain injury *in vivo*. Our results have demonstrated that the extract of *Limonium gmelinii* partially restored the motor functions and normalizes the morphology of the brain tissues damaged by MCAO, which allowed us to conclude that the *Limonium gmelinii* extract at a dose of 200 mg/kg per day for 28 days, has neuroprotective properties. However, further investigations are required in order to establish effective doses and active components of the extract.

Conclusion

Consequently, in the course of the work it was shown that in animals with MCAO and subsequent reperfusion in the basin of the middle cerebral artery of the brain, a focus of coagulation necrosis is determined, where dead cells of the nervous tissue are visualized, which indicates the development of focal cerebral infarction of ischemic origin. The histostructure of the brain tissue of animals that were exposed to *Limonium gmelinii* extract after stroke induction was partially restored. Moreover, in rats without MCAO, which were exposed to the studied extract, the histological picture of the brain did not differ from that in control animals. Hence, the

extract of *Limonium gmelinii* partially normalizes the histostructure of the damaged brain of animals with induced stroke, which indicates its neuroprotective effect in vivo; evaluation of the sensorimotor activity of laboratory animals with MCAO and administration of a polyphenol extract showed that the extract of *Limonium gmelinii* partially restores the musculoskeletal functions in rats with induced ischemic brain stroke.

Based on the above, the results obtained allow us to conclude that the *Limonium gmelinii* extract at a dose of 200 mg/kg per day for 28 days, has neuroprotective properties.

References

1 Donnan G.A., Fisher M., Macleod M., Davis S.M. (2008) Stroke. Lancet, vol. 371, no. 9624, pp. 1612-1623. https://doi.org/10.1016/S0140-6736(08)60694-77.

2 OECD. Health at a Glance (2011). OECD Publishing, OECD Indicators. http://dx.doi.org/10.1787/health_glance-2011-en.

3 Ellekjaer H., Holmen J., Indredavik B., Terent A. (1997) Epidemiology of stroke in Innherred, Norway, 1994 to 1996. Incidence and 30-day case-fatality rate. Stroke; a journal of cerebral circulation, vol. 28, no. 11, pp. 2180-2184. https://doi.org/10.1161/01.STR.28.11.2180.

4 Erkebaeva S.K., Nurguzhaev E.S., Gafurov B.G., Tuksanbaeva G.U. (2014) Prophylaxis of stroke in patients with cerebral ischemia with depressive syndrome. Neuroscience and Behavioral Physiology, vol. 44, no. 2, pp. 175-179. https://doi.org/10.1007/s11055-014-9893-6.

5 Feigin V.L., Forouzanfar MH, Krishnamurthi R, Mensah G.A., Connor M., Bennett D.A., Moran A.E., Sacco R.L., Anderson L., Truelsen T., O'Donnell M., Venketasubramanian N., Barker-Collo S., Lawes C.M., Wang W., Shinohara Y., Witt E., Ezzati M., Naghavi M., Murray C. Global and regional burden of stroke during 1990-2010: findings from the Global Burden of Disease Study 2010. (2014) Lancet, vol. 383, no. 9913, pp. 245-254. https://doi.org/10.1016/s0140-6736(13)61953-4.

6 Evers S.M., Ament A.J., Blaauw G. (2000) Economic evaluation in stroke research: a systematic review. Stroke; a journal of cerebral circulation, vol. 31, no. 5, pp. 1046-1053. https://doi.org/10.1161/01.STR.31.5.1046.

7 Lees K.R., Bluhmki E., von Kummer R., Brott T.G., Toni D., Grotta J.C., Albers G.W., Kaste M., Marler J.R., Hamilton S.A., Tilley B.C., Davis S.M., Donnan G.A., Hacke W., Allen K., Mau J., Meier D., del Zoppo G., De Silva D.A., Butcher K.S., Parsons M.W., Barber P.A., Levi C., Bladin C., Byrnes G. (2010) Time to treatment with intravenous alteplase and outcome in stroke: an updated pooled analysis of ECASS, ATLANTIS, NINDS, and EPITHET trials. Lancet, vol. 375, no. 9727, pp. 1695-1703. https://doi.org/10.1016/S0140-6736(10)60491-6.

8 Hacke W., Kaste M., Bluhmki E., Brozman M., Davalos A., Guidetti D., Larrue V., Lees K.R., Medeghri Z., Machnig T., Schneider D., von Kummer R., Wahlgren N., Toni D. (2008) Thrombolysis with alteplase 3 to 4.5 hours after acute ischemic stroke. The New England journal of medicine, vol. 359, no. 13, pp. 1317-1329. https://doi.org/10.1056/NEJMoa0804656.

9 Sandercock P., Wardlaw J.M., Lindley R.I., Dennis M., Cohen G., Murray G., Innes K., Venables G., Czlonkowska A., Kobayashi A., Ricci S., Murray V., Berge E., Slot K.B., Hankey G.J., Correia M., Peeters A., Matz K., Lyrer P., Gubitz G., Phillips S.J., Arauz A. (2012) The benefits and harms of intravenous thrombolysis with recombinant tissue plasminogen activator within 6 h of acute ischaemic stroke (the third international stroke trial [IST-3]): a randomised controlled trial. Lancet, vol. 379, no. 9834, pp. 2352-2363. https://doi.org/10.1016/S0140-6736(12)60768-5.

10 Kalogeris T., Baines C.P., Krenz M, Korthuis R.J. (2012) Cell Biology of Ischemia/Reperfusion Injury. Int Rev Cell Mol Biol., vol. 298, pp. 229-317. https://doi.org/10.1016/B978-0-12-394309-5.00006-7.

11 Laubach V.E., French B.A., Okusa M.D. (2011) Targeting of adenosine receptors in ischemia-reperfusion injury. Expert Opin Ther Targets., vol. 15, no. 1, pp. 103-118. 10.1517/14728222.2011.541441.

12 Amaro S., Llull L., Urra X., Obach V., Cervera Á., Chamorro Á. (2013) Risks and benefits of early antithrombotic therapy after thrombolytic treatment in patients with acute stroke. PLoS One, vol. 8, no. 8, e71132. https://doi.org/10.1371/journal.pone.0071132.

13 Bansal S., Sangha K.S., Khatri P. (2013) Drug Treatment of Acute Ischemic Stroke. Am J Cardiovasc Drugs, vol. 13, no. 1, pp. 57-69. https://doi.org/10.1007/s40256-013-0007-6.

14 Lansberg M.G., O'Donnell M.J., Khatri P., Lang E.S., Nguyen-Huynh M.N., Schwartz N.E., Sonnenberg F.A., Schulman S., Vandvik P.O., Spencer F.A., Alonso-Coello P., Guyatt G.H., Akl E.A. (2012) Antithrombotic and Thrombolytic Therapy for Ischemic Stroke: Antithrombotic Therapy and Prevention of Thrombosis, 9th ed: American College of Chest Physicians Evidence-Based Clinical

Practice Guidelines. Chest, vol. 141, no. 2 Suppl., pp. e601S-636S. https://doi.org/10.1378/chest.11-2302.

15 Matsuo Y., Onodera H., Shiga Y., Shozuhara H., Ninomiya M., Kihara T., Tamatani T., Miyasaka M., Kogure K. (1994) Role of cell adhesion molecules in brain injury after transient middle cerebral artery occlusion in the rat. Brain research, vol. 656, no. 2, pp. 344-352. https://doi.org/10.1016/0006-8993(94)91478-8.

16 McEver R.P. (2002) Selectins: lectins that initiate cell adhesion under flow. Curr Opin Cell Biol, vol. 14, no. 5, pp. 581-586. https://doi.org/10.1016/s0955-0674(02)00367-8.

17 Turkmen S., Cekic Gonenc O., Karaca Y., Mentese A., Demir S., Beyhun E., Sahin A., Gunduz A., Yulug E., Turedi S. (2016) The effect of ethyl pyruvate and N-acetylcysteine on ischemia-reperfusion injury in an experimental model of ischemic stroke. The American journal of emergency medicine, vol. 34, no. 9, pp. 1804-1807. https://doi.org/10.1016/j.ajem.2016.06.003.

18 Chen H., Yoshioka H., Kim G.S., Jung J.E., Okami N., Sakata H., Maier C.M., Narasimhan P., Goeders C.E., Chan P.H. (2011) Oxidative stress in ischemic brain damage: mechanisms of cell death and potential molecular targets for neuroprotection. Antioxid Redox Signal., vol. 14, no. 8, pp. 1505-1517. https://doi.org/10.1089/ars.2010.3576.

19 Busche M.N., Stahl G.L. (2010) Role of the complement components C5 and C3a in a mouse model of myocardial ischemia and reperfusion injury. Ger Med Sci., vol. 8. https://doi.org/10.3205/000109.

20 Elvington A., Atkinson C., Zhu H., Yu J., Takahashi K., Stahl G.L., Kindy M.S., Tomlinson S. (2012) The alternative complement pathway propagates inflammation and injury in murine ischemic stroke. J Immunol., vol. 189, no. 9, pp. 4640-4647. https://doi.org/10.4049/jimmunol.1201904.

21 Ferrari R.S., Andrade C.F. (2015) Oxidative Stress and Lung Ischemia-Reperfusion Injury. Oxid Med Cell Longev., vol. 2015. https://doi.org/10.1155/2015/590987.

22 Sharma V.K., Kawnayn G., Sarkar N. (2013) Acute ischemic stroke: comparison of low-dose and standard-dose regimes of tissue plasminogen activator. Expert Rev Neurother., vol. 13, no. 8, pp. 895-902. https://doi.org/10.1586/14737175.2013.827412.

23 Zhou T., Chuang C.C., Zuo L. (2015) Molecular Characterization of Reactive Oxygen Species in Myocardial Ischemia-Reperfusion Injury. Biomed Res Int., vol. 2015. https://doi.org/10.1155/2015/864946.

24 Tasoulis M., Douzinas E.E. (2016) Hypoxemic reperfusion of ischemic states: an alternative approach for the attenuation of oxidative stress mediated reperfusion injury. J Biomed Sci., vol. 23. https://doi.org/10.1186/s12929-016-0220-0.

25 Zozulya Yu.A., Baraboy V.A., Sutkova D.A. (2000) Free radical oxidation and antioxidant protection in brain pathology [Svobodnopadikal'noe okislenie i antioksidantnaja zashhita pri patologii golovnogo mozga]. M: Knowledge-M, 344 p. ISBN 5-93129-009-5.

26 Ross J.A., Kasum C.M. (2002) Dietary flavonoids: bioavailability, metabolic effects, and safety. Annual review of nutrition, vol. 22, pp. 19-34. https://doi.org/10.1146/annurev.nutr.22.111401.144957.

27 Simonyi A., Wang Q., Miller R.L., Yusof M., Shelat P.B., Sun A.Y., Sun G.Y. (2005) Polyphenols in cerebral ischemia: novel targets for neuroprotection. Mol Neurobiol., vol. 31, no. 1-3, pp. 135-147. https://doi.org/10.1385/MN:31:1-3:135.

28 Panickar K.S., Jang S. (2013) Dietary and plant polyphenols exert neuroprotective effects and improve cognitive function in cerebral ischemia. Recent Pat Food Nutr Agric., vol. 5, no. 2, pp. 128-143. https://doi.org/10.2174/1876142911305020003.

29 Zhao S., Kong W., Zhang S., Chen M., Zheng X., Kong X. (2013) Pretreatment with scutellaria baicalensis stem-leaf total flavonoid prevents cerebral ischemia-reperfusion injury. Neural Regen Res., vol. 8, no. 34, pp. 3183-3192.

30 Liu F.C., Tsai H.I., Yu H.P. (2015) Organ-protective effects of red wine extract, resveratrol, in oxidative stress-mediated reperfusion injury. Oxid Med Cell Longev., vol. 2015. https://doi.org/10.1155/2015/568634.

31 Shalakhmetova T.M., Zhusupova G.E., Askarova S.N. (2010) Antioxidative and hepatoprotective properties of phytomedicine extracted from Limonium Gmelinii. International Journal of Biology and Chemistry, vol. 1, no. 1, pp. 61-66.

32 Zhusupova G.E. (1997) Phytochemical study of the roots of saliniferous kermek (Gmelin) [Fitohimicheskoe issledovanie kornej kermeka solonchakovogo (Gmelina)]. Proceedings of the IV international conference on medical botany, P. 393.

33 Sivertsev I.I. (1997) Pharmacological study and therapeutic use of preparations of Kermek Gmelin [Farmakologicheskoe izuchenie i lechebnoe primenenie preparatov kermeka Gmelina]. Bulletin of the Academy of Sciences of the Kazakh SSR. Physiological series, pp. 75-87.

34 Smirnova G.V., Vysochina G.I., Muzyka N.G., Samoilova Z., Kukushkina T.A., Oktiabr'skii O.N. (2009) The antioxidant characteristics of

medicinal plant extracts from Western Siberia [Antioksidantnye svojstva jekstraktov lekarstvennyh rastenij Zapadnoj Sibiri]. Prikl Biokhim Mikrobiol., vol. 45, no. 6, pp. 705-709.

35 Markina O.V., Alekseeva L.P., Markin N.V. (2013) Effect of plant extracts on cytotoxic activity of Vibrio cholerae hemolysin [Vlijanie jekstraktov rastenij na citotoksicheskuju aktivnost' gemolizina vibrio cholerae]. Zh Mikrobiol Epidemiol Immunobiol, vol. 4, pp. 10-16.

36 Tsoi A.K., Zhusupova G.E., Olzhaev F.S., Shalakhmetova T.M., Nurkenov T.T., Shayakhmetov E.G., Abzhanova E.R., Turgambaeva A.M., Saparbaev S.S., Askarova Sh.N. (2017) Antioxidant and neuroprotective properties of phytopreparation from Gmelin Kermek [Antioksidantnye i nejroprotektornye svojstva fitopreparata iz kermeka Gmelina]. Bulletin of KazNU. Biological Series, vol. 71, no. 2, pp. 96-104.

37 Munoz-Elias G., Marcus A.J., Coyne T.M., Woodbury D., Black I.B. (2004) Adult bone marrow stromal cells in the embryonic brain: engraftment, migration, differentiation, and long-term survival. The Journal of neuroscience: the official journal of the Society for Neuroscience, vol. 24, no. 19, pp. 4585-4595. https://doi.org/10.1523/JNEUROSCI.5060-03.2004.

38 Uluc K., Miranpuri A., Kujoth G.C., Akture E., Baskaya M.K. (2011) Focal cerebral ischemia model by endovascular suture occlusion of the middle cerebral artery in the rat. Journal of visualized experiments, no. 48. https://doi.org/10.3791/1978.

39 Chuang D.Y., Chan M.H., Zong Y., Sheng W., He Y., Jiang J.H., Simonyi A., Gu Z., Fritsche K.L., Cui J., Lee J.C., Folk W.R., Lubahn D.B., Sun A.Y., Sun G.Y. (2013) Magnolia polyphenols attenuate oxidative and inflammatory responses in neurons and microglial cells. J Neuroinflammation, vol. 10, pp. 15. https://doi.org/10.1186/1742-2094-10-15.

40 Liu X., Wang Z., Wang P., Yu B., Liu Y., Xue Y. (2013) Green tea polyphenols alleviate early BBB damage during experimental focal cerebral ischemia through regulating tight junctions and PKCalpha signaling. BMC Complement Altern Med., vol. 13, no.1, pp. 187. https://doi.org/10.1186/1472-6882-13-187.

41 Abib R.T., Quincozes-Santos A., Nardin P., Wofchuk S.T., Perry M.L., Goncalves C.A., Gottfried C. (2008) Epicatechin gallate increases glutamate uptake and S100B secretion in C6 cell lineage. Mol Cell Biochem., vol. 310, no. 1-2, pp. 153-158. https://doi.org/10.1007/s11010-007-9675-3.

42 Mahler A., Mandel S., Lorenz M., Ruegg U., Wanker E.E., Boschmann M., Paul F. (2013) Epigallocatechin-3-gallate: a useful, effective and safe clinical approach for targeted prevention and individualised treatment of neurological diseases? EPMA J., vol. 4, no. 1, pp. 5. https://doi.org/10.1186/1878-5085-4-5.

43 Manach C., Scalbert A., Morand C., Remesy C., Jimenez L. (2004) Polyphenols: food sources and bioavailability. Am J Clin Nutr., vol. 79, no. 5, pp. 727-747. https://doi.org/10.1093/ajcn/79.5.727.

44 Kozhamkulova Z.A., Radwan M.M., Zhusupova G.E., Abilov Z., Rahadilova S.N., Ross S.A. (2010) Gmelinoside I, a new flavonol glycoside from Limonium gmelinii. Nat Prod Commun., vol. 5, no. 7, pp. 1061-1062. https://doi.org/10.1177/1934578X1000500715.

IRSTI 34.29.15 https://doi.org/10.26577/ijbch.2020.v13.i2.02

G. Sypabekkyzy[1, 2*], M. Sedlářová[3], Y.V. Rakhimova[1], B.D. Yermekova[1], L.A. Kyzmetova[1], A.M. Assylbek[1]

[1] Institute of Botany and Phytointroduction, Almaty, Kazakhstan
[2] Al-Farabi Kazakh National University, Almaty, Kazakhstan
[3] Palacký University in Olomouc, Olomouc, Czech Republic
*e-mail:gulnaz_92_21@mail.ru

Diversity of rust fungi on woody and shrubby vegetation of the Zailiysky Alatau

Abstract. Data on rust fungi on trees and shrubs of Zailiysky Alatau are significantly outdated (especially taxonomy of species). Therefore the aim of our work is to study the diversity of rust fungi on trees, shrubs and lianas of Zailiysky Alatau, to establish the distribution of species by host, gorge and absolute altitudes. Establishing the species composition of rust fungi associated with trees and shrubs, their distribution in the altitude zones and gorges of the Zailiysky Alatau is of scientific and practical importance. The material for the article was both the authors' own collections from the research area and the Institute's herbarium data. Preparation of specimens was carried out according to standard methods; they were studied and photographed using a Polyvar photomicroscope with Nomarsky interference optics. During the last decade we have determined 35 species of the rust fungi infecting trees and shrubs within the mycobiota of the Zailiysky Alatau. The material was combined both of the authors' own collections from numerous localities within the research area as well as herbarium samples from the Institute of Botany and Phytointroduction, Almaty. The most widely represented genera were *Phragmidium* and *Puccinia* (10 species each).The highest diversity, 23 rust species, has been recorded in the Turgen gorge of Zailiysky Alatau, although all identified species belonged only to 4 genera: *Gymnosporangium, Melampsora, Phragmidium,* and *Puccinia*. In the Big and Small Almaty gorges, similar number of rust species has been recorded (22 and 19, respectively). The lowest number of rust species, only 6, was noted in the Akterek gorge of the Zhetyzhol ridge, which is the western tip of the Zailiysky Alatau. The main species diversity was confined to heights of 1300–1900 m a.s.l., which corresponds to the small-leaved forests and dark coniferous forests and meadows belts. The value of the study and its practical importance lies in obtaining new data on the distribution of rust infections of various trees and shrubs in the territory of Zailiysky Alatau.

Key words: distribution, host plant, mycobiota, Pucciniales, species, woody-shrubby vegetation, Zailiysky Alatau.

Introduction

Rust fungi (Pucciniales, Pucciniomycotina, Basidiomycota), with ca 8000 described taxa, represent the most species-rich group of obligate plant pathogens. They are characterized by a complex life cycle, forming up to 5 dispersal stages in macrocyclic species, their life cycle can be realized either on one (autoecious) or two host plants (heteroecious) [1]. Host jump have been also very important for rust fungi phylogeny as revealed by recent molecular studies [2]. Zailiysky Alatau, one of the ranges of the Northern Tien Shan, is located in southeastern Kazakhstan and belongs to the Dzungar-Northern Tien Shan group of zonation types, including subnival vegetation (3300–3600 m a.s.l.), cryophytic (alpinotypic) meadows and meadows with *Kobresia* spp. (2800–3300 m a.s.l.), subalpinotype meadows and dwarf forests (2300–2800 m a.s.l.), dark coniferous forests and meadows (1700–2300 m a.s.l.), small-leaved forests (1400–1700 m a.s.l.), steppes (800–1400 m a.s.l.), and foothill deserts (700–800 m a.s.l.) [3].

The mycobiota of Zailiysky Alatau has been studied intensively since 1950's, resulting in three monographs [4-6]. G.S. Nevodovsky in 1956 provided a detailed description of rust fungi from the area of Kazakhstan, some of which were found in the Zailiysky Alatau [4]. However, this information is quite outdated (especially the taxonomy of species). The work of B.K. Kalymbetov from 1969 [5], dedicated to the mycobiota of Zailiysky Alatau, contained information about 249 species of rust

fungi, however, the species living in the adjacent territories of the Ketmen, Kungei and other ranges were also included in the monograph. The third monograph of S.A. Abiev from 2002 [6] provided a list and descriptions of rust fungi parasitizing on cereals of Kazakhstan. However, some of the recorded species are heteroecious, i.e. use trees and shrubs as intermediate hosts.

The aim of our work was to study the diversity of rust fungi on trees, shrubs and lianas of Zailiysky Alatau, and relate the distribution of species to host distribution, geographical location and altitude.

Materials and methods

The study was conducted in the Zailiysky Alatau ridge (southeastern region of Kazakhstan) for several years (2010, 2012-2019). Leaves of trees, bushes and lianas with typical rust symptoms were collected during field trips. The geographic location of each site was recorded using digital GPS (Germin). Digital camera Canon 600E was used for photographing of symptoms. Spores of rust fungi at different stages of development were stripped off the plant surface, placed in a drop of distilled water on a microscopic slide, examined and photographed using a photomicroscope Polyvar with Nomarski interference contrast optics (Reichert, Austria). Measurements of spores were made. Specimens were identified with use of determination literature focused on rust fungi [4, 7-10]. Dried specimens are stored in the herbarium of the Institute of Botany and Phytointroduction, Almaty, Kazakhstan (AA).

The systematic of the taxa is given in accordance with Kirk et al. [11]. Species of rust fungi located in the herbarium of the laboratory are also included in the checklist. The names of the host plants are given in accordance with the Plantarium database [12], while the names of fungal taxa and the names of taxon authors in accordance with the database Index Fungorum [13].

Results and discussion

At present, the mycobiota of the Zailiysky Alatau includes 35 species of the rust fungi on trees and shrubs (Table 1).The most widely represented genera are *Phragmidium* and *Puccinia* (10 species each).

Table 1– Number of species of rust fungi in the families and genera on woody-shrubby vegetation of Zailiysky Alatau

Families	Genera	Species
Coleosporiaceae	*Chrysomyxa*	2
Melampsoraceae	*Melampsora*	4
Phragmidiaceae	*Phragmidium*	10
Pucciniaceae	*Gymnosporangium*	5
	Puccinia	10
	Uromyces	1
Pucciniastraceae	*Melampsoridium*	1
	Pucciniastrum	1
Uropyxidaceae	*Tranzschelia*	1
Total	9	35

Checklist of rust fungi on woody-shrubby vegetation of the Zailiysky Alatau

The following abbreviations are accepted in the proposed list: ib. – ibidem, m a.s.l. – meters above sea level, SAG – Small Almaty gorge, BAG – Big Almaty gorge, IG – Issyk gorge, TG – Turgen gorge, PG – Prokhodnoye gorge. Most of the samples were collected by YV Rakhimova (abbreviated in the list as YVR), other collectors: MNK – MN Kuznetsova, LAK – LA Kyzmetova, GSN – GS Nevodovsky, UKJ – UK Jetigenova. The types of sporulation in the cycle of development of rust fungi are traditionally indicated by Roman numerals for brevity: 0 – spermogonia or pycnidia, I – aecia, II – uredinia, III – telia. Pucciniomycetes R. Bauer, Begerow, J.P. Samp., M. Weiss & Oberw. Pucciniales Clem. & Shear Coleosporiaceae Dietel

Chrysomyxa deformans (Dietel) Jacz. (III) – on *Picea schrenkiana* Fisch. & C.A. Mey., SAG, Medeo, 07.1924, AA Yachevsky, ib., 20.05.1938, MNK; Talgar gorge, 25.05.1952, SR Shvartsman; BAG,

below the peak Young geologist, the upper boundary of spruce forests, 2513 m a.s.l., 43º06′87.9″N, 76º59′19.0″E, 18.07.2012, YVR; PG, spruce forest, 1871 m a.s.l., 43°04′47.4″N, 76°54′28.5″E, 14.07.2019, AM Assylbek.

Chrysomyxa weirii H.S. Jacks. – on *Picea schrenkiana*, BAG, 14-27.05.1916, RN Abolin; Middle Talgar gorge, 06.06.1936; GSN; SAG, spruce forest, 26.05.1954, SR Shvartsman; PG, above the sanatorium Alma-Arasan, 2195 m a.s.l., 43º04′65.5″N, 76º54′27.5″E, 28.01.2012, YVR.

Melampsoraceae Dietel

Melampsora confluens (Pers.) H.S. Jacks. (II) – on *Ribes meyeri* Maxim., Talgar gorge, 06.06.1936, GSN.

Melampsora epitea Thüm. (II) – on *Salix* sp., Ayusai gorge, mixed forest, 1877 m a.s.l., 43°05′26.0″N, 76°56′51.9″E, 28.08.2018, LAK; BAG, 1950 m a.s.l., 43°06′18.6″N, 76°57′07.3″E, 04.06.2015, YVR; ib., spruce forest, 1571 m a.s.l., 43°05′59.2″N, 76°55′51.1″E, 23.05.2019, LAK; ib., border of spruce forest, 1579 m a.s.l., 43°06′00.5″N, 76°56′52.0″E, 23.05.2019, YVR; IG, the forest above the lake, 1761 m a.s.l., 43°14′43.1″N, 77°28′35.7″E, 14.07.2015, YVR; TG, at the confluence of the tributary with the Bear waterfall, 1427 m a.s.l., 43°16′28.9″N, 77°42′59.2″E, 27.07.2017, YVR; ib., above the village Batan, floodplain forest, 2143 m a.s.l., 43°13′46.0″N, 77°49′07.1″E, 16.08.2019, YVR; ib., path to the Bear waterfall, floodplain forest, 1942 m a.s.l., 43°16′37.5″N, 77°42′55.3″E, 12.07.2019, LAK, ib., path to Kairak waterfall, floodplain forest, 1737 m a.s.l., 43°13′55.8″N, 77°45′27.2″E, 12.07.2019, UKJ; PG, pine forest border, 1994 m a.s.l., 43°04′37.0″N, 76°54′28.6″E, 15.07.2019, LAK; Kastek range, Kastek gorge, 2036 m a.s.l., 42º59′08.0″N, 78º50′04.9″E, 08.09.2015, YVR; Zhetyzhol range, Akterek gorge, 1297 m a.s.l., 43º13′42.6″N, 75º22′11.0″E, 16.11.2014, YVR.

Melampsora populnea (Pers.) P. Karst. (II) – on *Populus alba* L., foothills, 900 m a.s.l., 18.06.1941, MNK; TG, above the village Batan, 2362 m a.s.l., 43°13′44.7″N, 77°49′06.6″E, 02.08.2016, YVR; on *P. laurifolia* Ledeb., TG, at the confluence of the tributary with the Bear waterfall, 1427 m a.s.l., 43°16′28.9″N, 77°42′59.2″E, 27.07.2017, YVR; on *P. tremula* L., Kamenskaya fissure, 08.08.1946, MNK; Ayusai gorge, spruce forest, 1831 m a.s.l., 43°05′43.4″N, 76°56′44.9″E, 27.08.2018, AM Assylbek, ib., birch forest, 1556 m a.s.l., 43°06′31.4″N, 76°54′43.8″E, 29.08.2018, LAK; on *Populus* sp., entrance to the canyon Aksai, 10.06.2011, YVR.

Melampsora salicina Desm. (II) – on *Salix arbuscula* L., Small Kemin gorge, 2300 m a.s.l., 04.09.1957, BK Kalymbetov; on *S. cinerea* L., SAG, the slope of Shaggy Hill, 03.07.1946, GSN; on *S. starkeana* Willd., SAG, spruce forests on the Kazachka river, 20.06.1945, MNK; on *Salix* sp., SAG, 2300 m a.s.l., 23.08.1945, MNK; Monk fissure, 03.06.1935, GSN; ib., 1641 m a.s.l., 43º13′39.8″N, 77º15′34.6″E, 07.09.2012, YVR; PG, above the sanatorium Alma-Arasan, spruce forest, 2103 m a.s.l., 43º04′10.6″N, 76º54′43.9″E, 27.07.2012, YVR; Aksai gorge, 15.08.2009, YVR; Ayusai gorge, 1754 m a.s.l., 43º05′61.5″N, 76º56′38.1″E, 14.07.2011, YVR; BAG, 1662 m a.s.l., 43º06′10.3″N, 76º56′61.8″E, 14.07.2011, YVR; SAG, Mynzhylki, 01.08.2015, RD Rakhimov; IG, near the lake, 1744 m a.s.l., 43º15′35.7″N, 77º29′10.1″E, 23.06.2011, YVR; TG, above the village Batan, right bank, 2362 m a.s.l., 43°13′44.7″N, 77°49′06.6″E, 02.08.2016, YVR; Kastek range, Kastek gorge, 1434 m a.s.l., 43º01′53.9″N, 75º57′98.2″E, 17.09.2011, YVR; Zhetyzhol range, Akterek gorge, 1129 m a.s.l., 43º15′14.2″N, 75º24′19.6″E, 27.06.2014, UKJ.

Phragmidiaceae Corda

Phragmidium andersonii Shear (III) – on *Dasiphora fruticosa* (L.) Rydb., SAG, Aman-Dzhailau valley, 2600 m a.s.l., 14.08.1936, GSN; ib., alpine meadow along the ridge of Kumbel, 3200 m a.s.l., 23.08.1945, GSN.

Phragmidium bulbosum (Fr.) Schltdl. (II, III)– on *Rubus caesius* L., foothills, Glubokaya fissure, 900 m a.s.l., 09.11.1945, MNK; TG, 12.06, 10.11.1938, GSN; BAG, 43º04′56.8″N, 76º58′50.5″E, 13.08.2009, YVR; Aksai gorge, 1359 m a.s.l., 43º07′232″N, 76º47′835″E, 10.06.2011, YVR; Kuznetsov fissure cordon, 1526 m a.s.l., 43°21′63.1″N, 77°40′68.1″E, 15.08.2013, YVR; TG, at the confluence of the tributary with the Bear waterfall, 1427 m a.s.l., 43°16′28.9″N, 77°42′59.2″E, 27.07.2017, YVR; ib., near the complex “Altyn Adam”, deciduous forest, 1173 m a.s.l., 43º19′47.3″N, 77º37′02.0″E, 18.08.2019, G Sypabekkyzy; Zhetyzhol range, Akterek gorge, 1113 m a.s.l., 43º15′17.1″N, 75º24′24.5″E, 27.06.2014, N Zhakhan; ib., 1120 m a.s.l., 43º15′17.1″N, 75º24′07.8″E, 27.06.2014, AK Dzhienbekov.

Phragmidium devastatrix Sorokin (III)– on *Rosa platyacantha* Schrenk, foothills, Glubokaya fissure, 900 m a.s.l., 11.06.1941, MNK; BAG, 1927 m a.s.l., 43º06′23.8″N, 76º56′46.4″E, 27.04.2018, UKJ; ib., trail to the Big Almaty peak, spruce forest, 1628 m a.s.l., 43°06′26.0″N, 76°54′46.6″E,

29.08.2018, YVR; neighborhood of Zhandosov, 43°10′14.0″N, 76°31′57.6″E, 02.12.2013, YVR; Karakastek gorge, 1353 m a.s.l., 43°02′08.6″N, 76°04′01.5″E, 03.08.2016, YVR; Zhetyzhol range, middle part of the Besmoyak gorge, 1944 m a.s.l., 43°06′21.7″N, 75°37′02.9″E, 06.07.2016, YVR; ib., 1801 m a.s.l., 43°06′11.6″N, 75°38′24.5″E, 06.07.2016, YVR; on *Rosa* sp., Talgar gorge, 12.09.1935; 10.04-06.06.1936, GSN; Kaskelen gorge, 5 km above the ecological post, 1313 m a.s.l., 43º06′23.8″N, 76º36′35.6″E, 07.07.2010, YVR; ib., 1307 m a.s.l., 43°06′16.3″N, 76°36′20.7″E, 03.08.2016, YVR; Ush-Konyr gorge, 1239 m a.s.l., 43º07′94.7″N, 76º30′85.4″E, 11.07.2010, YVR; pass of TG, 1344 m a.s.l., 43º31′64.6″N, 77º38′455″E, 15.08.2013, YVR; TG, floodplain forest, 1579 m a.s.l.,43°16′15.7″N, 77°44′22.9″E, 18.08.2019, AM Assylbek; Kastek range, Kastek gorge, 1854 m a.s.l., 42º59′70.7″N, 75º53′30.3″E, 29.06.2012, YVR; ib., 1977 m a.s.l., 43°00′41.8″N, 75°53′69.5″E, 28.06.2012, YVR; ib., 2036 m a.s.l., 42º59′08.0″N, 78º50′04.9″E, 08.09.2015, YVR; Zhetyzhol range, Akterek gorge, 1113 m a.s.l., 43º15′17.1′′N, 75º24′24.5″E, 27.06.2014, N Zhakhan; ib., 1069 m a.s.l., 43º15′30.6″N, 75º24′58.3″E, 26.06.2014, YVR; ib., 1297 m a.s.l., 43º13′42.6″N, 75º22′11.0″E, 16.11.2014, YVR; ib., 1094 m a.s.l., 43º15′25.7′′N, 75º24′40.6′′E, 26.06.2014, YVR.

Phragmidium fusiforme J. Schröt. (I) – on *Rosa alberti* Regel, Small Kemin gorge, Aktyuz, among juniper, 2400 m a.s.l., 06.09.1957, BK Kalymbetov; SAG, 20.06.1945, MNK; Kaskelen gorge, Kasymbek branch, 2122 m a.s.l., 43°02′08.1″N, 76°31′43.7″E, 03.06.2015, YVR; on *Rosa* sp., the upper reaches of the Pogansky fissure, 10.06.1937, GSN; Ayusai gorge, spruce forest, 1831 m a.s.l., 43°05′43.4″N, 76°56′44.9″E, 27.08.2018, AM Assylbek; PG, above the sanatorium Alma-Arasan, spruce forest, 2103 m a.s.l., 43°04′10.6″N, 76°54′43.9″E, 27.07.2012, YVR; TG, above the confluence of Karagaily, floodplain forest, 1446 m a.s.l., 43°16′29.4″N, 77°43′03.5″E, 21.05.2019, YVR; Kastek range, Kastek gorge, floodplain, 1812 m a.s.l., 42°59′99.3″N, 75°53′87.7″E, 29.06.2012, YVR.

Phragmidium kamtschatkae (H.W. Anderson) Arthur & Cummins (III) – on *Rosa platyacantha,* BAG, 1923 m a.s.l., 43º05′53.0″N, 76º57′12.8″E, 27.04.2018, SB Nurashov; on *Rosa* sp., Talgar gorge, 06.06.1936, GSN; BAG, spruce forest border, 1579 m a.s.l., 43°06′00.5″N, 76°56′52.0″E, 23.05.2019, YVR; TG, above the village Batan, spruce forest, 1757 m a.s.l., 43°14′10.0″N, 77°46′27.3″E, 22.05.2019, LAK; ib., floodplain forest, 1446 m a.s.l., 43°16′29.4″N, 77°43′03.5″E, 21.05.2019, YVR.

Phragmidium mucronatum (Pers.) Schltdl. (I) – on *Rosa* sp., SAG, Aman-Dzhailau valley, 2600 m a.s.l., 14.08.1936; TG, 12.06.1938, GSN; PG, spruce forest, 2069 m a.s.l., 43°04′18.9″N, 76°54′28.6″E, 15.07.2019, UKJ; Kastek range, Kastek gorge, 1854 m a.s.l., 42°59′70.7″N, 75°53′30.3″E, 29.06.2013, YVR.

Phragmidium rosae-lacerantis Dietel (II, III) – on *Rosa alberti*, Kaskelen gorge, neighborhood of the village of Izvestkovoe, 1845 m a.s.l., 43°01′56.9″N, 76°37′09.0″E, 19.09.2012, YVR; IG, forest above the lake, 1761 m a.s.l., 43°14′43.1′′N, 77°28′35.7′′E, 14.07.2015, YVR; SAG, Kok-Dzhailau pass trail, aspen forest, 1790 m a.s.l., 43°09′35.3″N, 77°01′43.0″E, 19.08.2019, YVR; TG, floodplain forest, 1516 m a.s.l., 43°16′11.1″N, 77°44′26.4″E, 16.08.2019, G Sypabekkyzy; on *R. platyacantha*, SAG, Kok-Dzhailau pass trail, aspen forest, 1790 m a.s.l., 43°09′35.3″N, 77°01′43.0″E, 19.08.2019, YVR; on *Rosa* sp., Zhetyzhol range, Akterek gorge, 1069 m a.s.l., 43º15′30.6″N, 75º24′58.3″E, 26.06.2014, YVR; ib., 1120 m a.s.l., 43º15′17.1″N, 75º24′07.8″E, 27.06.2014, AK Dzhienbekov; ib., 1033 m a.s.l., 43°15′43.7″N, 75°25′26.8″E, 26.06.2014, YVR; ib., 1113 m a.s.l., 43º15′17.1″N, 75º24′24.5′′E, 27.06.2014, N Zhakhan; ib., 1096 m a.s.l., 43º15′31.0′′N, 75º24′33.6′′E, 26.06.2014, GA Nam.

Phragmidium rubi-idaei (DC.) P. Karst. (III) – on *Rubus caesius* L., foothills, Glubokaya fissure, 900 m a.s.l., 09.11.1945, MNK; on *R. idaeus* L., Monk fissure, 24.08.1935; SAG, spruce forest, 2000 m a.s.l., 31.08.1946, MNK; BAG, spruce forest, 28.08.1922, Tupolev; ib., trail to the Big Almaty peak, spruce forest, 1628 m a.s.l., 43°06′26.0″N, 76°54′46.6″E, 29.08.2018, AM Assylbek; Ayusai gorge, spruce forest, 1776 m a.s.l., 43°05′45.5″N, 76°56′40.0″E, 27.08.2018, LAK; PG, above the sanatorium Alma-Arasan, spruce forest, 2103 m a.s.l., 43º04′10.6″N, 76º54′43.9″E, 27.07.2012, YVR; ib., near the waterfall, 1886 m a.s.l., 43°04′56.1″N, 76°54′27.4″E, 14.07.2019, UKJ, ib., above camp Young homebuilder, 1801 m a.s.l., 43°05′27.3″N, 76°54′22.3″E, 16.07.2019, LAK; TG, path to Kairak waterfall, 1814 m a.s.l., 43°13′23.6″N, 77°45′34.5″E, 12.07.2019, AM Assylbek.

Phragmidium saxatile Vleugel (I, II, III) – on *Rubus saxatilis* L., IG, floodplainforest above the lake, 29.08.1947, MNK.

Phragmidium tuberculatum Jul. Müll. (I, II, III) – on *Rosa albertii*, SAG, along the Kazachka river bed, 1800 m a.s.l., 09.09.1939, MNK; TG, above the village Batan, spruce forest, 1646 m a.s.l., 43°14′02.9″N, 77°46′24.4″E, 11.07.2019, LAK.

Pucciniaceae Chevall.

Gymnosporangium clavariiforme (Wulfen) DC. (I) – on *Crataegus* sp., SAG, MNK; on *Juniperus sibirica* Burgsd., IG, 12.06.1936, Zakharova; on *Malus domestica* Borkh., SAG, 1800 m a.s.l., 20.08.1945, MNK; on *M. sieversii* (Ledeb.) M. Roem., SAG, Kok-Dzhailau pass trail, 1960 m a.s.l., 43º09′37.9″N, 77º01′52.1″E, 15.08.2012, YVR; ib., Mynzhylki, 01.08.2015, RD Rakhimov; BAG, trail to the Big Almaty peak, mixed forest, 1477 m a.s.l., 43°06′37.0″N, 76°54′53.1″E, 29.08.2018, YVR; Aksai gorge, 1359 m a.s.l., 43º07′232″N, 76º47′835″E, 10.06.2011, YVR; Kuznetsov fissure, above the cordon, 1588 m a.s.l., 43º21′32.6″N, 77º40′94.8″E, 15.08.2013, YVR; PG, above camp Young homebuilder, 1801 m a.s.l., 43°05′27.3″N, 76°54′22.3″E, 16.07.2019, LAK; on *Malus* sp., Ayusai gorge, spruce forest, 1864 m a.s.l., 43°05′35.0″N, 76°56′52.9″E, 27.08.2018, YVR; ib., spruce forest, 1776 m a.s.l., 43°05′45.5″N, 76°56′40.0″E, 27.08.2018, UKJ; TG, at the confluence of the tributary with the Bear waterfall, 1427 m a.s.l., 43°16′28.9″N, 77°42′59.2″E, 27.07.2017, YVR; on *Pyrus* sp., BAG, trail to the Big Almaty peak, birch forest, 1556 m a.s.l., 43°06′31.4″N, 76°54′43.8″E, 29.08.2018, LAK; on *Sorbus tianschanica* Rupr., SAG, path to the Kok-Dzhailau pass, 1960 m a.s.l., 43º09′37.9″N, 77º01′52.1″E, 15.08.2012, YVR; Kuznetsov fissure, 1517 m a.s.l., 43º21′98.5″N, 77º40′46.5″E, 15.08.2013, YVR; BAG, trail to the Big Almaty peak, spruce forest, 1582 m a.s.l., 43°06′29.5″N, 76°54′43.8″E, 29.08.2018, AM Assylbek; TG, above the village Batan, 2362 m a.s.l., 43°13′44.7″N, 77°49′06.6″E, 02.08.2016, YVR; Kastek range, Kastek gorge, 2036 m a.s.l., 42º59′08.0″N, 78º50′04.9″E, 08.09.2015, YVR; PG, spruce forest, 1871 m a.s.l., 43°04′47.4″N, 76°54′28.5″E, 14.07.2019, AM Assylbek.

Gymnosporangium confusum Polwr. (I) – on *Cotoneaster melanocarpus* Fisch. ex Blytt, TG, above the village Batan, floodplain forest, 1910 m a.s.l., 43°13′46.8″N, 77°47′25.3″E, 11.07.2019, YVR; on *Crataegus almaatensis* Pojark., BAG, birch forest, 1507 m a.s.l., 43°06′15.7″N, 76°55′22.8″E, 23.05.2019, UKJ; TG, deciduous forest, 1281 m a.s.l., 43°17′21.4″N, 77°39′41.1″E, 20.05.2019, UKJ; ib., above trout farming, deciduous forest, 1040 m a.s.l., 43°19′00.7″N, 77°38′22.9″E, 20.05.2019, LAK; on *C. korolkowii* L. Henry, IG, 02.08.1935, GSN; TG, at the confluence of the tributary with the Bear waterfall, 1427 m a.s.l., 43°16′28.9″N, 77°42′59.2″E, 27.07.2017, YVR; on *C.songarica* K. Koch, SAG, 06.06.1946, MNK; on *Crataegus* sp., Ayusai gorge, spruce forest,1776 m a.s.l., 43°05′45.5″N, 76°56′40.0″E, 27.08.2018, UKJ; BAG, near Ayusai, 1662 m a.s.l., 43º06′10.3″N, 76º56′61.8″E, 14.07.2011, YVR; ib., 1754 m a.s.l., 43º05′615″N, 76º56′381″E, 14.07.2011, YVR; Right Talgar gorge, 1634 m a.s.l., 43º13′52.2″N, 77º17′47.7″E, 08.07.2010, S Userbayeva; IG, near the lake, 1744 m a.s.l., 43º15′35.7″N, 77º29′10.1″E, 23.06.2011, YVR; Kaskelen gorge, 1351 m a.s.l., 43º05′79.5″N, 76º36′63.0″E, 10.06.2011, YVR; Aksai gorge, 1487 m a.s.l., 43º06′44.7″N, 76º47′14.0″E, 10.06.2011, YVR; ib., 1115 m a.s.l., 43º09′18.1″N, 76º47′93.3″E, 10.06.2011, YVR; Kuznetsov fissure, 1517 m a.s.l., 43º21′98.5″N, 77º40′46.5″E, 15.08.2013, YVR; TG, path to Kairak waterfall, spruce forest, 1814 m a.s.l., 43°13′23.6″N, 77°45′34.5″E, 12.07.2019, AM Assylbek; ib., above the village Batan, spruce forest, 1901 m a.s.l., 43°13′55.2″N, 77°46′58.0″E, 11.07.2019, AM Assylbek; ib., above trout farming, deciduous forest, 1040 m a.s.l., 43°19′00.7″N, 77°38′22.9″E, 20.05.2019, LAK; ib., deciduous forest, 1281 m a.s.l., 43°17′21.4″N, 77°39′41.1″E, 20.05.2019, UKJ; Oi-Karagai gorge, 1866 m a.s.l., 43°11′68.0″N, 77°07′65.2″E, 20.09.2012, YVR.

Gymnosporangium fusisporum E. Fisch. (I) – on *Cotoneaster integerrimus* Medikus, SAG, 1400 m a.s.l., MNK; on *C. melanocarpus*, TG, path to Kairak waterfall, floodplain forest, 1737 m a.s.l., 43°13′55.8″N, 77°45′27.2″E, 12.07.2019, UKJ; on *C. Oliganthus* Pojark., SAG, Aman-Dzhailau valley, 14.08.1936, GSN; on *C. uniflorus* Bunge, BAG, near the lake, 2524 m a.s.l., 43º03′44.3″N, 76º59′22.5″E, 13.08.2009, YVR; on *Cotoneaster* sp., BAG, below peak Young geologist, 2513 m a.s.l., 43º06′87.9″N, 76º59′19.0″E, 18.07.2012, YVR; Kuznetsov fissure, 1588 m a.s.l., 43º21′32.6″N, 77º40′94.8″E, 15.08.2013, YVR; Kastek range, Kastek gorge, 1854 m a.s.l., 42º59′70.7″N, 75º53′30.3″E, 29.06.2012, YVR; ib., 2036 m a.s.l., 42º59′08.0″N, 78º50′04.9″E, 08.09.2015, YVR.

Gymnosporangium juniperi Link (I) – on *Sorbus tianschanica*, BAG, 07.09.1937; Middle Talgar gorge, 13.08.1936, GSN; TG, above the village Batan, 2143 m a.s.l.,43º13′46.0″N, 77º49′07.1″E, 16.08.2019, YVR.

Gymnosporangium turkestanicum Tranzschel (I) – on *Juniperus turkestanica* Kom., SAG, 3700 m a.s.l.,13.05.1915, R Abolin; ib., 2300 m a.s.l., 20.05.1946, MNK.

Puccinia atragenicola (Bubak) P. Syd. & Syd. (III) – on *Atragene sibirica* L., TG, above the village Batan, floodplain forest, 1910 m a.s.l., 43°13′46.8″N, 77°47′25.3″E, 11.07.2019, YVR; BAG, spruce forest, 2407 m a.s.l., 43°04′00.6″N, 76°59′14.7″E, 31.08.2018, UKJ.

Puccinia brachypodii G.H. Otth (0, I) – on *Berberis sphaerocarpa* Kar. & Kir., Monk fissure 03.06.1935; SAG, 1500 m a.s.l., 09.05.1946, 12.09.1946, MNK; BAG, 1923 m a.s.l., 43º05′50.1″N, 76º57′30.0″E, 27.04.2018, LAK; ib., spruce forest border, 1579 m a.s.l., 43°06′00.5″N, 76°56′52.0″E, 23.05.2019, YVR; ib., birch forest at the foot of the slope, 1507 m a.s.l., 43°06′15.7″N, 76°55′22.8″E, 23.05.2019, UKJ; TG, above the village Batan, spruce forest,1757 m a.s.l., 43°14′10.0″N, 77°46′27.3″E, 22.05.2019, LAK.

Puccinia coronata Corda (I)– on *Rhamnus cathartica* L., BAG, trail to the Big Almaty peak, birch forest, 1556 m a.s.l., 43°06′31.4″N, 76°54′43.8″E, 29.08.2018, LAK; Zhetyzhol range, Akterek gorge, 1129 m a.s.l., 43º15′14.2″N, 75º24′19.6″E, 27.06.2014, UKJ; ib., 1033 m a.s.l., 43º15′43.7″N, 75º25′26.8″E, 26.06.2014, YVR; on *Rhamnus* sp., Zhetyzhol range, Akterek gorge, 1113 m a.s.l., 43º15′17.1″N, 75º24′24.5″E, 27.06.2014, N Zhakhan.

Puccinia coronifera Kleb. (I) – on *Rhamnus cathartica*, foothills, 02.05.1932, ib., Glubokaya fissure, 27.05.1946, MNK; Kaskelen gorge, 1351 m a.s.l., 43º05′79.5″N, 76º36′63.0″E, 10.06.2011, YVR; Aksai gorge, 1487 m a.s.l., 43º06′44.7″N, 76º47′14.0″E, 10.06.2011, YVR; ib., 1115 m a.s.l., 43º09′18.1″N, 76º47′93.3″E, 10.06.2011, YVR; TG, above the confluence of the Karagayly river, floodplain forest, 1446 m a.s.l., 43°16′29.4″N, 77°43′03.5″E, 21.05.2019, YVR; ib., path to the Bear waterfall, 1436 m a.s.l., 43°16′33.1″N, 77°42′41.2″E, 22.05.2019, AM Assylbek; ib., above trout farming, deciduous forest, 1040 m a.s.l., 43°19′00.7″N, 77°38′22.9″E, 20.05.2019, LAK, ib., 1281 m a.s.l., 43°17′21.4″N, 77°39′41.1″E, 20.05.2019, UKJ.

Puccinia festucae Plowr. (I) – on *Lonicera caerulea* L., IG, at a lake, mixed forest, 02.08.1935, GSN; on *L. hispida* Pall. ex Roem. & Schult., TG, spruce forest border, 1687 m a.s.l., 43°15′12.2″N, 77°45′26.6″E, 20.05.2019, AM Assylbek; on *L. karelinii* Bunge ex P. Kir.,Big Kemin gorge, 2400 m a.s.l., 10.09.1957, BK Kalymbetov; BAG, spruce forest, 18.06.1941, MNK; SAG, 06.07.1936, MNK; foothills Kargaly gorge, 19.06.1941, MNK;on *L. tatarica* L.; BAG, spruce forest border, 1579 m a.s.l., 43°06′00.5″N, 76°56′52.0″E, 23.05.2019, YVR.

Puccinia graminis Pers. (0, I) – on *Berberis sphaerocarpa*, SAG, Kamenskaya fissure, 06.07.1931, Sukach and Bulatov; ib., 13.06.1946, MNK; Talgar gorge, 07.1931, GSN; Aksai gorge, 1115 m a.s.l., 43º09′18.1″N, 76º47′93.3″E, 10.06.2011, YVR; TG, deciduous forest, 1281 m a.s.l., 43°17′21.4″N, 77°39′41.1″E, 20.05.2019, UKJ; ib., above trout farming, deciduous forest, 1040 m a.s.l., 43°19′00.7″N, 77°38′22.9″E, 20.05.2019, LAK; ib., path to the Bear waterfall, floodplain forest, 1436 m a.s.l., 43°16′33.1″N, 77°42′41.2″E, 22.05.2019, AM Assylbek; BAG, spruce forest border, 1579 m a.s.l., 43°06′00.5″N, 76°56′52.0″E, 23.05.2019, YVR; Kastek range, Kastek gorge, 1854 m a.s.l., 42º59′70.7″N, 75º53′30.3″E, 29.06.2012, YVR; on *Berberis* sp., Uzyn-Kargaly gorge, above the dam, 1198 m a.s.l., 43º06′85.1″N, 76º26′01.7″E, 07.07.2010, YVR; Kaskelen gorge, at the base of the slope, 1313 m a.s.l., 43º06′23.8″N, 76º36′35.6″E, 07.07.2010, YVR; IG, near the lake, 1744 m a.s.l., 43º15′35. 7″N, 77º29′10.1″E, 23.06.2011, YVR.

Puccinia longirostris Kom. (III) – on *Lonicera hispida*, SAG, 03.07.1946, MNK; IG, 02.08.1935, GSN; Dzhaya gorge, 2700 m a.s.l., 09.06.1958, BK Kalymbetov; Ayusai gorge, spruce forest, 1888 m a.s.l., 43°05′18.4″N, 76°56′46.2″E, 28.08.2018, LAK; BAG, spruce forest, 1571 m a.s.l., 43°05′59.2″N, 76°55′51.1″E, 23.05.2019, LAK; ib., spruce forest border, 1579 m a.s.l., 43°06′00.5″N, 76°56′52.0″E, 23.05.2019, YVR; TG, above the village Batan, floodplain forest, 1910 m a.s.l., 43°13′46.8″N, 77°47′25.3″E, 11.07.2019, YVR; ib., above the confluence of the Karagayly river, floodplain forest, 1446 m a.s.l., 43°16′29.4″N, 77°43′03.5″E, 21.05.2019, YVR; PG, spruce forest, 2069 m a.s.l., 43°04′18.9″N, 76°54′28.6″E, 15.07.2019, UKJ**;** ib., 2085 m a.s.l., 43°03′59.7″N, 76°54′27.7″E, 15.07.2019, AM Assylbek**;** ib., floodplain forest, 1287 m a.s.l., 43°16′17.1″N, 77°44′18.9″E, 20.05.2019, YVR; ib., pine forest border, 1994 m a.s.l., 43°04′37.0″N, 76°54′28.6″E, 15.07.2019, LAK; on *L. olgae* Regel & Schmalh., SAG, Aman-Dzhailau valley, 2600 m a.s.l., 14.08.1936; ib., Talgar pass, 28.08.1946, MNK; on *L. semenovii* Regel, between the mountains of Maitobe and Araltobe, 2500 m a.s.l., 01.09.1957, BK Kalymbetov; on *L. karelinii* and on *L. altmannii* Regel & Schmalh., Small Kemin gorge, Aktyuz, among juniper, 2400 m a.s.l., 06.09.1957, BK Kalymbetov; on *Lonicera* sp., Kastek range, Kastek gorge, bushes, 1854 m a.s.l., 42º59′70.7″N, 75º53′30.3″E, 29.06.2012, YVR; BAG, path to the lake, 2111 m a.s.l., 13.08.2009, YVR.

Puccinia platypoda Syd. & P. Syd. (I, III) – on *Atraphaxis caucasica* (Hoffm.) Pavlov, IG, near the stream, 27.06.1937, M Prokopenko; on *A. frutescens* (L.) K. Koch, BAG, 12.09.1937; IG, 17.08.1937, MNK; on *A. pyrifolia* Bunge, Talgar gorge, 24.07.1935; TG, 12.10.1938, MNK.

Puccinia pygmaea Erikss.(I) – on *Berberis sphaerocarpa*, foothills, 02.06.1936, Dobrotvorskaya; ib., Kamenskaya fissure, 18.06.1930, Sukach and Bulatov; SAG, 13.06.1946, MNK; Monk fissure, 24.08.1935; Talgar gorge, 07.1936, GSN.

Puccinia recondita Roberge ex Desm. (I) – on *Atragene sibirica* L., SAG, spruce forest, 1600 m a.s.l., 16.06.1941, MNK; TG, floodplain forest, 1287 m a.s.l., 43°16′17.1″N, 77°44′18.9″E, 20.05.2019, YVR; ib., above the village Batan, spruce forest, 1646 m a.s.l., 43°14′02.9″N, 77°46′24.4″E, 11.07.2019, LAK; ib., path to Kairak waterfall, floodplain forest, 1862 m a.s.l., 43°12′48.6″N, 77°45′01.5″E, 13.07.2019, YVR; PG, near the waterfall, spruce forest, 1886 m a.s.l., 43°04′56.1″N, 76°54′27.4″E, 14.07.2019, UKJ; on *Atragene* sp., BAG, path to the lake, 2111 m a.s.l., 43º04′44.3″N, 76º59′01.8″E, 13.08.2009, YVR; on *Clematis orientalis* L., foothills, 25.06.1941, MNK; TG, path to the Bear waterfall, floodplain forest, 1436 m a.s.l., 43°16′33.1″N, 77°42′41.2″E, 22.05.2019, AM Assylbek; on *Clematis* sp., Uzyn-Kargaly gorge, above the dam, 1198 m a.s.l., 43º06′85.1″N, 76º26′01.7″E, 07.07.2010, YVR.

Uromyces cytisi J. Schröt. (III) – on *Caragana* sp., Kaskelen gorge, 5 km above the ecological post, 1313 m a.s.l., 43º06′23.8″N, 76º36′35.6″E, 07.07.2010, YVR; ib., 1307 m a.s.l., 43°06′16.3″N, 76°36′20.7″E, 03.08.2016, YVR.

Pucciniastraceae Gäum. ex Leppik

Melampsoridium betulinum (Pers.) Kleb. (II) – on *Betula pendula* Roth, SAG, spruce forest, 1400 m a.s.l., 18.09.1937, MNK; ib., trail to the Kok-Dzhailau pass, 1960m a.s.l., 43°09′37.9″N, 77°01′52.1″E, 15.08.2012, YVR; ib., 2113m a.s.l., 43°08′37.0″N, 77°00′56.2″E, 16.08.2012, YVR; Ayusai gorge, spruce forest, 1776 m a.s.l., 43°05′45.5″N, 76°56′40.0″E, 27.08.2018, LAK; IG, forest above the lake, 1761 m a.s.l., 43°14′43.1″N, 77°28′35.7″E, 14.07.2015, YVR; PG, near the waterfall, spruce forest, 1886 m a.s.l., 43°04′56.1″N, 76°54′27.4″E, 14.07.2019, UKJ; on *B. tianschanica* Rupr., SAG, spruce forest, 1700 m a.s.l., 14.08.1946, MNK; on *Betula* sp., Almaty Reserve, 07.09.1937; IG, near the lake, 02.08.1935; Talgar gorge, 24.07.1936, Sergazin; BAG, 1662 m a.s.l., 43º06′103″N, 76º56′618″E, 14.07.2011, YVR; IG, near the lake, 1744 m a.s.l., 43º15′35.7″N, 77º29′10.1″E, 23.06.2011, YVR.

Pucciniastrum areolatum (Fr.) G.H. Otth (II) – on *Padus avium* Mill., foothills, Kamenskaya fissure, 31.08.1933, K. Yatsynina; Talgar gorge, 24.08.1935; Middle Talgar gorge, 06.06.1936; IG, near the lake, 28.08.1938, MNK; on *Picea schrenkiana*, Talgar gorge, 23.06.1936; SAG, 05.05.1945, MNK.

Uropyxidaceae Cummins & Y. Hirats.

Tranzschelia pruni-spinosae (Pers.) Dietel (II, III) – on *Cerasus prostrate* (Labill.) Ser., IG, 17.08.1937, MNK.

The highest number of species (23) of rust fungi on trees and shrubs was recorded in the Turgen gorge of Zailiysky Alatau (Table 2). However, all identified species belonged only to 4 genera: *Melampsora, Gymnosporangium, Phragmidium,* and *Puccinia*. Similarly, to Turgen gorge, in the Big and Small Almaty gorges, high number of species of rust fungi on trees and shrubs was found (22 and 19, respectively). The lowest number of species (6) was detected in the Akterek gorge of the Zhetyzhol ridge, which is the western tip of the Zailiysky Alatau.

Table 2 – The number of species of rust fungi on trees and shrubs in the main gorges of Zailiysky Alatau

Genera	Gorges							
	BAG	SAG	Talgar	Prokhodnoye	Issyk	Turgen	Kastek	Akterek
Chrysomyxa	2	2	2	2	-	-	-	-
Gymnosporangium	3	3	2	1	2	4	2	-
Melampsora	3	1	1	2	2	3	2	2
Melampsoridium	1	1	1	1	1	-	-	-
Phragmidium	4	6	2	3	2	8	3	3
Puccinia	8	6	3	2	3	8	2	1
Pucciniastrum	-	-	1	-	1	-	-	-
Tranzschelia	-	-	-	-	1	-	-	-
Uromyces	1	-	-	-	-	-	-	-
Total	22	19	12	11	12	23	9	6

As obligate biotrophic parasites, rust fungi are tightly associated with their host plants which presence is the primary prerequisite for rust fungi distribution. In general, rust fungi can be found on trees and shrubs in many zones of the Zailiysky Alatau where the host plants can grow (Figure 1). As hosts for rust fungi, 22 species of trees, 30 shrubs, and 4 lianas were noted.

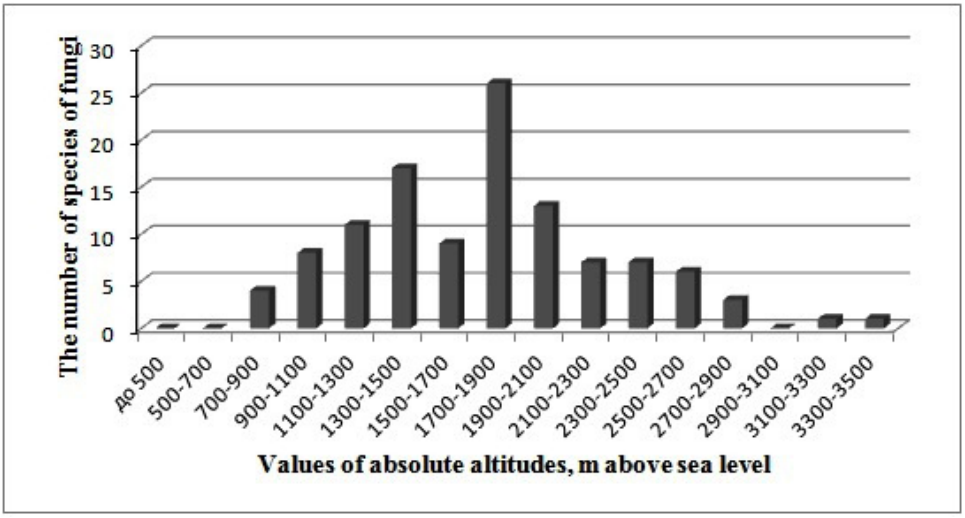

Figure 1 – Distribution of rust fungi species according to the vertical zoning

The main species diversity of rusts is confined to elevations of 1300–1900 m a.s.l., which corresponds to the small-leaved forests (1400–1700 m a.s.l.) and dark coniferous forests and meadows (1700–2300 m a.s.l.) belts, which are the hot spots of studied host plants distribution. In addition, rust fungi prefer habitats with humid conditions, which are typical in these zones. Due to low temperatures and high insolation subalpine and alpine belts are not ideal neither for the growth of host trees and shrubs or for the development of rust fungi.

Comparing distribution of recorded rust fungi with previous literary data [14–18], it should be noted that the greatest similarity was observed between the species composition of rust fungi on trees and shrubs of Zailiysky Alatau and Ketmen ridge [18] (Table 3). Some species are common to both ranges. Representatives of the genera *Pucciniastrum* and *Tranzschelia* are characteristic only of the Zailiysky Alatau.

Table 3 – Number of rust species in the Zailiysky Alatau and neighboring territories

Genera	Number of species				
	Zailiysky Alatau	Terskei ridge[14]	Chatkal and Kurama ridges[15]	Inner Tian Shan[16, 17]	Ketmen[18]
Chrysomyxa	2	2	-	1	1
Gymnosporangium	5	4	1	1	4
Melampsora	4	3	1	2	3
Melampsoridium	1	-	-	1	1
Phragmidium	10	4	-	1	8
Puccinia	10	6	-	4	7
Pucciniastrum	1	-	-	-	-
Tranzschelia	1	-	-	-	-
Uromyces	1	-	-	-	2
Total	35	19	2	10	26

On the woody-shrubby vegetation of the Terskey ridge, located in the south of the Zailiysky Alatau, only 19 species of rust fungi were noted [14]. An insignificant number of species in the Chatkal and Kuramin ranges [15] and the Inner Tian Shan ridges [16, 17] is explained by insufficient knowledge of these regions.

Conclusion

The presented work is devoted to the study of the diversity of rust fungi affecting trees, shrubs and lianas on the territory of the Zailiyskiy Alatau, and to the establishment of their distribution in terms of host plants, geography (location in separate gorges) and absolute heights. The material for the article was combined from both the authors' own collections from the research area and the Institute's herbarium data.

In the Zailiysky Alatau we have recorded 35 species of rust fungi on trees and shrubs, with the most spread genera *Phragmidium* and *Puccinia* (with 10 species of each). The Turgen gorge, as well as the Big and Small Almaty gorges, is characterized by high number of rust species (23, 22 and 19, respectively). The main factor influencing distribution of rust species is presence of host plants and optimal climatic conditions which corresponds to the small-leaved forests and dark coniferous forests and meadows belts in between 1300 and 1900 m a.s.l. The greatest similarity in the species composition of rust fungi on trees and shrubs of Zailiysky Alatau was detected with Ketmen ridge. Knowledge of the species composition and distribution of rust fungi will contribute to organize correctly practical measures to combat forest diseases in the territory of Zailiysky Alatau.

Acknowledgments

This work was financed by the Ministry of Education and Science of the Republic of Kazakhstan within the limits of the research program BR05236546 "Implementation by the State Botanical Gardens of the priority scientific and practical tasks of the Global Strategy for Plant Conservation as Sustainable Biodiversity Maintenance System" (Contract №340 from 03.04.2018).

References

1 Lorrain C., Gonçalves dos Santos K.C., Germain H., Hecker, A. and Duplessis, S. (2019) Advances in understanding obligate biotrophy in rust fungi. New Phytologist, vol. 222, no. 8, pp. 1190-1206. doi:10.1111/nph.15641

2 McTaggart A.R., Shivas R.G., van der Nest M.A., Roux J., Wingfield B.D., Wingfield M.J. (2016) Host jumps shaped the diversity of extant rust fungi (Pucciniales). New Phytologist, vol. 209, no. 8, pp. 1149-1158. doi: 10.1111/nph.13686

3 Rachkovskaya E.I., Volkova E.A., Khramtsov V.N., et al. (2003) Botanicheskaya geografiya Kazakhstana i Sredney Azii (v predelakh pustynnoy oblasti) [Botanical geography of Kazakhstan and Central Asia (within the desert region)]. St. Petersburg, 424 p. ISBN 5-201-11116-5.

4 Nevodovski G.S. (1956) Flora sporovykh rasteniy Kazakhstana. Rzhavchinny griby. [Flora of spore plants in Kazakhstan. Rust fungi.] Vol. 1. Alma-Ata: Nauka, 432 p.

5 Kalymbetov B.K. (1969) Mikologicheskaya flora Zailiyskogo Alatau (Severnyy Tyan'-Shan') [Mycological flora of Zailiysky Alatau (Northern Tien Shan)]. Alma-Ata, Nauka, 470 p.

6 Abiev S.A. (2002) Rzhavchinnyye griby zlakov Kazakhstana. [Rust fungi of cereals of Kazakhstan]. Almaty: Gylym, 296 p. ISBN 9965-07-054-7

7 Tranzshel V.G. (1939) Obzor rzhavchinnykh gribov SSSR. [Review of rust fungi of the USSR]. Moscow, Leningrad: Publishing House of the USSR Academy of Sciences, 426 p.

8 Rakhimova Y.V., Nam G.A., Yermekova B.D., Abiyev S.A., Jetigenova U.K., Yessengulova B.Z. (2015) The key to identify rust fungi in Kazakhstan. Turczaninowia, vol.18, no. 3, pp. 5-65. DOI: https://doi.org/10.14258/turczaninowia.18.3.18

9 Shivas R.G., Beasley D.R., McTaggart A.R. (2014) Online identification guides for Australian smut fungi (Ustilaginomycotina) and rust fungi (Pucciniales). IMA fungus, vol. 5, no. 2, pp. 195-202. doi:10.5598/imafungus.2014.05.02.03

10 Bahcecioglu Z., Gjaerum H.B. (2004) New and rare rust fungi (Uredinales) from Anatolia (Turkey) – 2. Mycotaxon, vol. 90, no. 1, pp. 55–68.

11 Kirk P.F., Cannon P.F., David J.C. and Stalpers J.A. (2008) Dictionary of the Fungi (10-th ed.). Wallingford: CAB International, 771 p. ISBN 978-0-85199-826-8

12 Plantarium, on-line determinant of plants (accessed on April 19th, 2020). http://www.plantarium.ru

13 Index Fungorum Database (accessed on April 19th, 2020). http://www.indexfungorum.org/names/names.asp

14 Domashova A.A. (1960) Mikoflora khrebta Terskey Alatoo Kirgizskoy SSR [Mycoflora of

Terskey Alatoo ridge of the Kyrgyz SSR]. Frunze, 242 p.

15 Gafforov Y., Abdurazzokov A., Yarasheva M. &OnoY. (2016) Rust Fungi from the Fergana Valley, Chatkal and Kurama Mountain Ranges in Uzbekistan.Stapfia, vol. 105, pp.161-175.

16 Beksultanova A.M. (2016) Analysis of micromycetes of the Jumgal district. Materials of the XIV All-Russian Scientific and Practical Conference with international participation Biodiagnostics of the state of natural and natural-technogenic systems. Book 2, Kirov, pp. 354-357.

17 Beksultanova A.M., Mosolova S.N. Pathogenic micromycetes of economically significant plant groups of the Jumgal river basin. News of the National Academy of Sciences of Belarus. Ser. Biological sciences, vol. 65, no. 1, pp. 82-87. https://doi.org/10.29235/1029-8940-2020-65-1-82-87

18 Rakhimova Y.V., Yermekova B.D., Kyzmetova L.A. (2017) Checklist of rust fungi from Ketmen ridge (southeast of Kazakhstan). Plant Pathology & Quarantine, vol. 7, no. 2, pp. 109–133. Doi 10.5943/ppq/7/2/4

IRSTI 31.27.17; 31.27.19 https://doi.org/10.26577/ijbch.2020.v13.i2.03

Hatice Aysun Mercimek Takcı[1]*, Pemra Bakirhan[2], Kıvılcım Caktu Guler[3]

[1]Faculty of Arts and Sciences, Department of Molecular Biology and Genetics,
Kilis 7 Aralık University, Kilis, Turkey
[2]Institute of Science and Technology, Kilis 7 Aralık University, Kilis, Turkey
[3]Faculty of Arts and Sciences, Department of Chemistry, Hacettepe University, Ankara, Turkey.
*e-mail: mersimek@hotmail.com

Urease purification from indigenous soil bacteria and accumulation of $CaCO_3$ crystals

Abstract. Recently, microbiologically induced calcite precipitation has been evaluated as an effective and eco friendly alternative to a repair technique in plugging of microcracks and pores in concrete for building trade. Enzymatic activity of urease synthesized by microorganisms has been induced for precipitation of $CaCO_3$ crystals. Urease activity and urease-induced calcium carbonate mineralization of indigenous soil bacteria (*Bacillus* spp.) isolated from Kilis, Turkey were studied. Total and specific urease activity of crude 19B intracellular enzyme sample were calculated as 0.67±0.003 EU/mL/min and 0.63±0.011 µmol/min/mg, respectively. Three protein bands (60.48, 23.27 and 20.17 kDa) indicating subunits of urease were detected by SDS-PAGE. Microbial calcium carbonate precipitation was analyzed by Scanning Electron Microscopy/Energy Dispersive X-Ray Analysis. Rhombohedral calcite crystals were clearly observed in SEM images. Element composition of precipitate was revealed to mostly comprise of calcium, carbon and oxygen. Results indicated that 19B strain may be evaluated for engineering applications such as remediation of concrete cracks and enhancing compressive strength of cement.

Key words: urease, *Bacillus* spp., microbial calcification, scanning electron microscopy, energy dispersive X-ray analysis.

Introduction

Urease (EC 3.5.1.5) obtained from jack bean (*Canavalia ensiformis*) is identified as the first nickel dependent metalloenzyme [1; 2]. It catalyzes the hydrolysis of urea to ammonia and carbamate and is the first enzyme to be crystallized. Carbamate formed as a result of ureolytic activity spontaneously decomposes carbonic acid. Urease was revealed to be a globulin protein with an isoelectric point of five by James Sumner in 1926 [3].

Urease is synthezised in several higher plants, yeast and microorganisms. Both plants and microorganisms use urease to supply ammonia as a nitrogen source [4; 5]. Prevailing number of eukaryotic ureases are represented by a single subunit including 840 amino acid residues. However, bacterial ureases are composed of three subunits, with e.g. 101, 106 and 567 amino acid residues identified for *Klebsiella aerogenes* urease. Exceptionally, *Helicobacter pylori* urease consists of two subunits, containing 238 and 569 acid residues [6].

Urease is an analytical tool widely used to determine urea content in blood, urine, alcoholic beverages, spring water and environmental wastewaters [7].

Ureases may be used as anticancer agents, antigen with strong stimulating ability in vaccines and in removal of urea from artificial kidney dialyzates [3; 7]. Ureases from *Staphylococcus*, *Lactobacillus*, and *Klebsiella aerogenes* are responsible of nitrogen metabolism in rumen sheep [3].

Recently, hydrolysis production of bacterial urease has been proposed as an effective alternative to cement [8]. Calcium carbonate deposits known as biocement, are calcite precipitation accumulated due to microbial urease activity [9]. Ammonia released after microbial ureolytic activity in surroundings leads to the accumulation of insoluble $CaCO_3$ by increasing pH. This is used for remediation of concrete cracks and thus increased compressive strength [10].

Consequently, the present study was focused on partial isolation of urease from indigenous soil bacterium, *Bacillus* spp., and accumulation of $CaCO_3$ crystals. Morphological properties of the latter were analyzed by scanning electron microscopy (SEM).

Materials and methods

All chemical materials in this study were supplied by Merck KGaA, Germany.

Isolation of urease producing Bacillus spp. Bacillus spp. were isolated from soil sample collected at Kilis, Turkey (36°43'48.6"N, 37°06'09.6"E). Following suspension by sterile water (1:9), soil sample was incubated at 65ºC for 30 min for stimulation of bacterial spores. 100 µL of this culture was inoculated using serial dilution technique on nutrient agar and incubated at 37°C for 24 h. Single colony was selected and maintained on nutrient agar slant for further identification and test of urease activity. Bacteria were identified by morphological (Gram staining, formation of spores and cell morphology) and standard microbiological procedures (catalase and urease test systems). To screen urease production by *Bacillus* strains, Christensen's agar medium was used, containing 20 g of urea, 1.0 g of peptone, 2.0 g of KH_2PO_4, 1.0 g of glucose, 5.0 g of NaCl, 15.0 g of agar, 0.012 g of phenol red indicator, pH 6.8±7.0. Strains were transferred to Christensen's urea agar, and incubated at 37°C for 48 h. According to the change of the medium color to pink from yellow with increase of pH, urease producing *Bacillus* strains were identified.

Urease purification from Bacillus strains. For preparation of bacterial inoculum, strains were grown overnight on Luria-Bertani broth at 37°C. Subsequently, 5 mL of inoculum was transferred into urea broth consisting of 1.0 g of peptone, 2.0 g of KH_2PO_4, 1.0 g of glucose, 5.0 g of NaCl and 100 mM/L urea. Cultures were incubated at 37ºC, 180 rpm for 24 h. Cells were harvested by centrifugation at 5500 rpm for 20 min after incubation. Following removal of supernatant, pellet was lyzed by suspending with 0.2 mg/mL lysozyme prepared in 0.05 M phosphate buffer (pH 7). Suspension was sonicated on ice for 30 s pulses within 5 min total period. Acquired crude enzyme was stored at -20ºC for further analyses (of enzymatic activity, total protein concentration and protein molecular weight).

Urease activity and total protein content. Amount of released ammonia was measured by phenol-hypochlorite reaction slightly modified in our lab [11]. Crude enzyme (50 µL) was added to 1.95 mL of substrate solution contaning 6.6 mg/mL of urea prepared in 0.05 M phosphate buffer (pH 7). This mixture was incubated at 37ºC for 5 min. Then, 500 µL of phenol-nitroprusside solution (0.1 g/mL phenol and 0.5 mg/mL sodium nitroprusside solutions prepared in distilled water) and alkaline sodium hypochlorite solution (5% NaOH and 26 mL/L NaOCl) at equal volume were added to this mixture. For monitoring of color development this mixture was incubated at 55ºC for 5 min in water bath. Subsequently to blue color formation, absorbance was measured at 630 nm. Calibration curve was plotted using ammonium sulfate standards (0-0.5 µmol/mL). One unit (U) of urease activity was calculated as amount of enzyme required for hydrolisation of 1 µmol of urea at 37ºC. Total protein concentration of crude enzyme was detected by Lowry assay [12].

SDS-PAGE analysis. Molecular weight of urease was determined according to Laemmli [13]. Optiprotein marker G252 (Applied Biological Materials ABM Inc., Canada) was used as a reference marker. Protein bands were monitored by staining with Coomassie Brilliant Blue R-250.

Morphological analysis of $CaCO_3$ minerals. 100 mL of overnight culture and 10% filtered urea were added to 500 mL of distilled water sample. Culture was incubated for one week at 180 rpm 37ºC and centrifuged at 5500 rpm for 20 min. $CaCO_3$ deposit (pellet) was dried on air at room temperature, in-house. After that, $CaCO_3$ crystals were observed by SEM [9]. Surface of the sample covering-stubs was coated by golden particles (Quorum Q150R Sputter Coater), viewed by SEM (FEI Quanta FEG 650) at 10 kV accelerating voltage.

Results and discusssion

Isolation and identification ureolytic Bacillus strains. Twenty aerobic, motile, Gram-positive, spore-forming, rod-shaped and catalase-positive bacterial strains were observed. Four of them were determined to be producing urease based on the medium color change to pink from yellow (Figure 1).

These isolates were entitled as 2B, 17B, 19B and XB. Similar findings related to urease activity in agar plate could be found in literature [14-17].

Intracellular urease activity. Intracellular urease activity in terms of unit (EU/mL/min) and total protein contents of crude enzyme samples are showed in Table 1.

The highest urease activity was calculated as 0.67±0.003 EU/mL/min in enzyme purified from 19B strain. The lowest activity was determined in 2B enzyme sample (0.38±0.000 EU/mL/min). As parallel to total urease activity, the lowest protein concentration was also recorded in 2B sample with 0.86±0.066 mg/mL. For specific activity measurement of enzyme purity in sample, the highest value was detected as 0.63±0.011 U/mg in 19B enzyme extract. 19B *Bacillus* isolate was revealed to show more urease activity (0.67±0.003 U/mL) and specific activity (0.63±0.011 µmol/min/mg) as compared to other isolates.

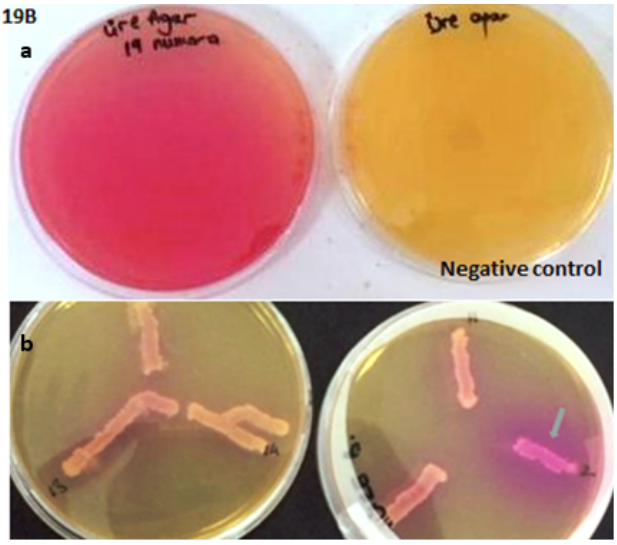

Figure 1 – Screening of urease-producing *Bacillus* spp. Note: (a) pink color indicating urease-producing, (b) yellow color indicating non-urease activity

Similarly, Tepe et al. (2019) intracellular urease purified using *Bacillus amyloliquefaciens* U17 isolated from calcareous soil of Denizli (Turkey) and specific enzyme activity found as 0.615±0.092 µmol/min/mg [18]. In other study, different bacterial strains were isolated from soil samples collected on the farm field to test urease activity of isolates. The value of urease activity varied within 0.072 and 0.88 U/mL [14]. Similar observations were reported by Kim et al. (2015). For *B. subtilis* having functional urease, detectable value of urease specific activity equaled to 0.113±0.006 U/mg protein [19]. Enzyme activity findings (0.55 U/mg) of urease extracted from bacterial sources reported by Mohammed et al. (2014) [20] were similar to our results.

Urease characterization. As can be seen from the Figure 2, the crude enzyme samples have many protein bands with different molecular weights. Protein bands belonging to urease in 19B sample were determined in comparison with bands having same molecular weight in other crude extracts.

Table 1 – Total and specific urease activities of cell-free enzyme samples

	Urease activity (EU/mL/min)	Protein amount (mg/mL)	Specific activity (µmol/min/mg)
2B	0.38±0.000	0.86±0.066	0.44±0.033
17B	0.65±0.003	1.30±0.022	0.50±0.006
19B	0.67±0.003	1.07±0.001	0.63±0.011
XB	0.58±0.014	1.08±0.004	0.53±0.011

Consequently, three protein bands (60.48, 23.27 and 20.17 kDa) indicating the subunits of urease were calculated. These findings of molecular weight exhibited similarity with previous study: 70, 60 and 55 kDa for *B. sphaericus* MTCC 5100 [21]; 66, 45, 29 and 15 kDa for *Proteus mirabilis* [20]; 11, 13 and 61 kDa for *B. pasteurii* [22].

Mineralogical results. Microbial cells adhere to different substrates for providing nutrition in natural environments. The cells metabolize nutrients to acquire energy resulting in minerals precipitated as by-product. The accumulation of calcium carbonate precipitates based on bacterial activities improves soil quality [15]. This accumulation is known as microbial induced calcite precipitation (MICP). As a result of biomineralization by ureolytic bacteria, $CaCO_3$ forms such as calcite, aragonite, vaterite and hydrated crystalline are obtained [18].

Morphological analysis of minerals for 19B strain having the highest urease activity was tested. Calcium carbonate precipitation potential of 19B strain was analyzed by SEM/EDX. Results are presented on Figure 3.

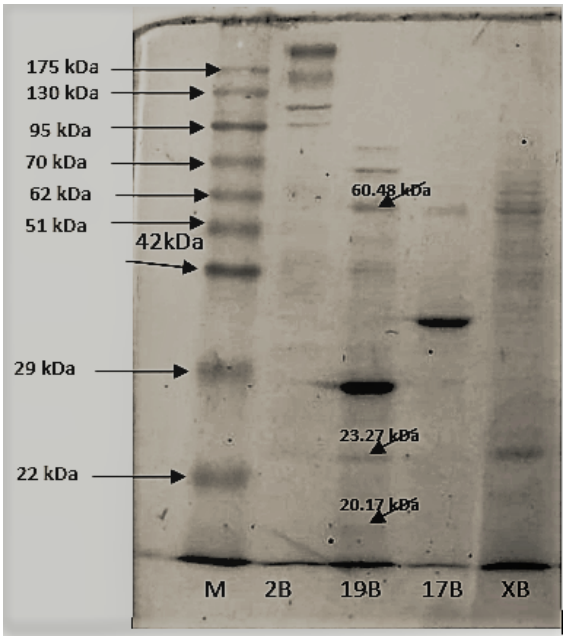

Figure 2 – Molecular weight analysis of ureases by SDS-PAGE using a 12% sperating gel. Note: M – marker DNA.

According to our results, calcites with a rhombohedral crystalline structure are clearly observed (Figure 3a). The EDX peaks (Figure 3b) and quantitative analysis (Table 2) belonging to rhombohedral crystalline show elemental composition of the precipitate.

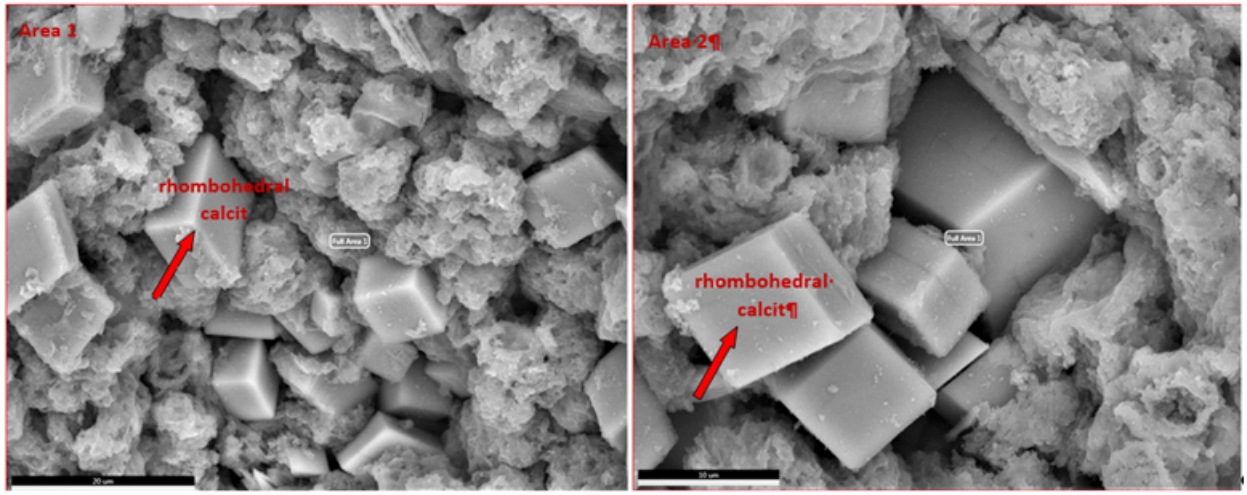

(a)

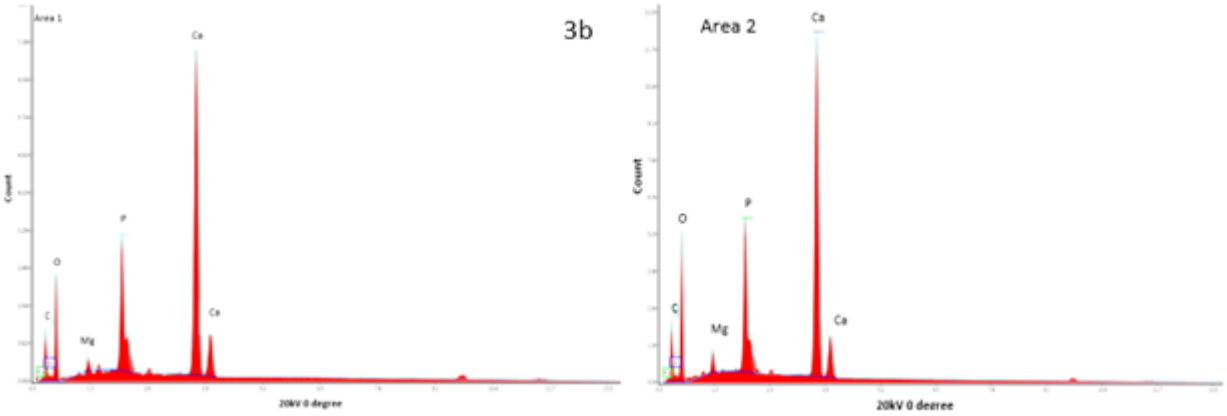

(b)

Figure 3 – SEM image of $CaCO_3$ minerals.
Note: (a) – SEM image of rhombohedral calcite produced by 19B urease activity; (b) – element analysis of precipitate.

Table 2 – EDX quantitative analysis of rhombohedral calcites

Element	Area 1		Area 2	
	Weight%	Atomic %	Weight%	Atomic %
C	10.14	17.73	10.13	17.19
O	42.52	55.81	46.12	58.77
Mg	0.94	0.81	1.42	1.19
P	8.69	5.89	8.8	5.79
Ca	37.71	19.76	33.54	17.06
Total	100.01	100.00	100.01	100.00

Composition of calcite observed to mostly consist of calcium, carbon and oxygen elements. This is indicated that rhombohedral crystalline formed as a result of microbial calcium carbonate precipitation. In EDX analysis, % weight of Ca produced by B19 was detected as 33.54-37.71 %.

Similar calcite morphologies to our results was showed by using *Sporosarcina pasteurii* strain ATCC 11859 [10]. Tao and Whenkun (2012) also indicated to the calcites or calcites/vaterite crystal forms of calcium carbonate precipitation induced by *Bacillus pasteurii* [23]. In other study, it was noted that B*acillus* strain with high urase activity showed high microbial calcification (calcite shape) [24]. Anitha et al. (2018) detected needle-like crystals of biocement produced by *Bacillus cereus* KLUVAA [5]. The calcium carbonate mineralization property of *Paenibacillus favisporus* U3 were revealed and rhombohedral vaterite and layered calcite crystals verified by mineralogical analyses by Tepe et. al. (2019) [18]. Present study and previous works indicated that different bacterial genus may produce different crystal structures, which may vary from strain to strain.

Conclusion

In this study, the $CaCO_3$ mineralization and urease activitiy properties of *Bacillus* strains, indigenous soil bacterium, were investigated. Four urease-producing *Bacillus* strains from Kilis soil were purified. Total and specific urease activity of crude 19B intracellular enzyme sample were calculated as 0.67±0.003 EU/mL/min and 0.63±0.011 μmol/min/mg, respectively. Urease was determined to be a trimeric enzyme of three 60.48, 23.27 and 20.17 kDa molecular weight subunits by SDS-PAGE. The rhombohedral crystalline calcite accumulation of B19 strain having high urease activity was revealed by SEM/EDX analysis. Our results emphasized that 19B strain may be evaluated for geological and engineering applications, such as remediation of concrete cracks and enhancing compressive strength of cement. The hardness and durability of biocement obtained by B19 bacterial suspension transferring to sand samples requires further research.

Acknowledgments

Authors would like to thank Kilis 7 Aralık University for laboratory provision and Cukurova University Central Research Laboratory for possibility to use SEM/EDS.

References

1 Balasubramanian A., Ponnuraj K. (2010) Crystal structure of the first plant urease from Jack Bean: 83 years of journey from its first crystal to molecular structure. J. Mol. Biol., vol. 400, pp. 274-283. https://doi.org/10.1016/j.jmb.2010.05.009.

2 Dixon N.E., Gazzola C., Blakeley R.L., Zerner B. (1975) Jack bean urease (EC 3.5.1.5). A metalloenzyme. A simple biological role for nickel? J. Am. Chem. Soc., vol. 97, pp. 4131-4133. https://doi.org/10.1021/ja00847a045.

3 Sujoy B., Aparna A. (2013) Enzymology, immobilization and applications of urease enzyme. Int. Res. J. Biologic. Sci., vol. 2, no. 6, pp. 51-56.

4 Mobley H.L.T., Hausinger R.P. (1989) Microbial ureases: significance, regulation, and molecular characterization. Microbiol Rev., vol. 53, pp. 85-108. https://doi.org/10.1128/MMBR.53.1.85-108.1989.

5 John A., Isaacson H. R., Bryant M.P. (1974) Isolation and characteristics of a ureolytic strain of Selenomonas ruminantium. J. Dairy Sci. vol. 57, pp. 1003-1014. https://doi.org/10.3168/jds.S0022-0302(74)85001-0.

6 Hausinger R.P., Karplus P.A. (2001) Handbook of metalloproteins. John Wiley Sons, Ltd., Chichester. P. 965.

7 Akkas T. (2016) Novel methods to prepare cross-linked enzyme aggregates (CLEA). challenging immobilization models – urease and pepsin. Dissertation, University of Sabanci, 95 p.

8 Krishnapriyaa S., Venkatesh Babub D.L., Prince Arulraj G. (2015) Isolation and identification of bacteria to improve the strength of concrete. Microbiologic. Res., vol. 174, pp. 48- 55. https://doi.org/10.1016/j.micres.2015.03.009.

9 Anitha V., Abinaya K., Prakash S., Seshagiri Rao, A., et al. (2018) Bacillus cereus KLUVAA mediated biocement production using hard water and urea. Chem. Biochem. Eng. Q., vol. 32, no. 2, pp. 257-266. https://doi.org/10.15255/CABEQ.2017.1096.

10 Okwadha G.D.O., Li J. (2010) Optimum conditions for microbial carbonate precipitation. Chemosphere, vol. 81, pp. 1143-1148. https://doi.org/10.1016/j.chemosphere.2010.09.066.

11 Azarno T. (2013) Optimization of urease production for the production of microbial biocement. Dissertation, University of Ege, 69 p.

12 Lowry O.H., Rosebrough N.J., Farra N.J., Randall R.J. (1951) Protein measurements with the

Folin phenol reagent. J. Biol. Chem., vol. 193, pp. 265-275.

13 Laemmli U.K. (1970). Cleavage of the structural proteins during assembly of the head of bacteriophage T4. Nature, vol. 227, pp. 680-685. https://doi.org/10.1038/227680a0.

14 Agarwal A., Banerje S., Dev K. (2015) Comparative characterization of urease secreting bacterial and fungal isolates from soil sample of farm fields. Int. J. Adv. Sci. Tech. Res., vol. 5, no. 4, pp. 138-150.

15 Bibi S., Oualha M., Ashfaq M.Y., Sulemimanb M.T. (2018) Isolation, differentiation and biodiversity of ureolytic bacteria of Qatari soil and their potential in microbially induced calcite precipitation (MICP) for soil stabilization. Royal Soc. Chem., vol. 8, pp. 5854-5863. https://doi.org/10.1039/C7RA12758H.

16 Cinar C. (2015) Isolation and characterization of Bacillus thuringiensis from olive tree related habitats. Dissertation, University of Izmir Institute Technology. 127 p.

17 Phanga I.R.K., Chanb Y.S., Wonga K.S., Lau S.Y. (2018) Isolation and characterization of urease-producing bacteria from tropical peat. Biocatal. Agric. Biotechnol., vol. 13, pp. 168-175. https://doi.org/10.1016/j.bcab.2017.12.006.

18 Tepe M., Arslan S., Koralay T., Mercan Dogan N. (2019) Precipitation and characterization of CaCO3 of Bacillus amyloliquefaciens U17 strain producing urease and carbonic anhydrase. Turkish J. Biol., vol. 43, pp. 198-208. https://doi.org/10.3906/biy-1901-56.

19 Kim J.K., Mulrooney S.B., Hausinge R.P. (2005) Biosynthesis of active Bacillus subtilis urease in the absence of known urease accessory proteins. J. Bacteriol., vol. 187, no. 20, pp. 7150-7154. https://doi.org/10.1128/JB.187.20.7150-7154.2005.

20 Mohammed S.O., Ahmed E.S., Hafez E.E., Khalid A., et al. (2014) Characterization and purification of urease enzyme from new Proteus mirabilis strain. J. Adv. Sci. Res., vol. 5, no. 4, pp. 8-11.

21 Kumar Singh A., Singh M., Verma N. (2017) Extraction, purification, kinetic characterization and immobilization of urease from Bacillus sphaericus MTCC 5100. Biocatal. Agric. Biotechnol., vol. 12, pp. 341-347. https://doi.org/10.1016/j.bcab.2017.10.020.

22 Follmer C., Real-Guerra R., Wasserman G.E., Olivera-Severo D., et al. (2004) Jackbean, soybean and Bacillus pasteurii ureases. Eur. J. Biochem., vol. 271, pp. 1357-1363. https://doi.org/10.1111/j.1432-1033.2004.04046.x.

23 Tao D., Wenkun Z. (2012) Optimization of calcium carbonate precipitation for Bacillus pasteurii. Appl. Mech. Mater., vol. 178-181, pp. 676-679. https://doi.org/10.4028/www.scientific.net/AMM.178-181.676.

24 Varenyum A., Mukherjeel A., Reddy M.S. (2010) Characterization of two urease-producing and calcifying Bacillus spp. isolated from cement. J. Microbiol. Biotechnol., vol. 20, no. 11, pp. 1571-1576. https://doi.org/10.4014/jmb.1006.06032.

IRSTI 34.15.23; 34.15.25; 34.23.33; 34.03.23 https://doi.org/10.26577/ijbch.2020.v13.i2.04

A.M. Belkozhayev[1, 2 *], R.Ye. Niyazova [1], C.M. Wilson[3, 4]

[1]Al-Farabi Kazakh National University, Almaty, Kazakhstan
[2] Structural and functional genomics laboratory of M.A. Aitkhozhin Institute of Molecular Biology and Biochemistry, Almaty, Kazakhstan
[3]Canterbury Christ Church University, School of Human and Life Sciences, Life Sciences Industry Liaison Lab, Sandwich, UK
[4] Novel Global Community Educational Foundation, Australia
* e-mail: ayaz_jarkent@mail.ru

The features of novel miRNAs interaction with mRNA candidate genes having trinucleotide repeats in coding sequences and untranslated regions

Abstract. Trinucleotide repeat disorders are a group of predominantly inherited neurological diseases caused by the expansion of repetitive sequences. miRNAs play major roles in transcriptional regulation and are expressed selectively and abundantly in the central nervous system. In the present research, MirTarget program predicted the miRNA-binding sites in mRNAs of genes with trinucleotide repeats. The MirTarget programme determines the following features of binding: the start of the initiation of miRNA binding to mRNAs; the localization of miRNA binding sites in 5'UTRs, CDSs and 3'UTRs; the free energy of binding; and the schemes of nucleotide interactions between miRNAs and mRNAs. In coding sequences the binding sites of ID00372.5p-miR with mRNA of *ATXN2, FMN2* and *MN1* genes having CAG (Q) repeats show the highest free binding energy**.** The mRNA of *ADRBK1, BRSK2, C11orf87* and *FMR1* genes have ID01508.5p-miR binding sites in 5'UTR with CGG repeated regions. Also, the binding sites of ID00296.3p-miR and ID01702.3p-miR in 5'UTR of *BLMH* gene interacted with CCG repeats. *DMPK* gene with CUG repeated regions have ID00522.5p-miR binding sites in 3'UTR. Based on these results, the interactions of ID00372.5p-miR, ID01508.5p-miR, ID00296.3p-miR, ID01702.3p-miR and ID00522.5p-miR and their target genes *ATXN2, FMN2, MN1, ADRBK1, BRSK2, C11orf87, FMR1, BLMH* and *DMPK* can be used for developing methods for diagnosing and therapeutic targets for neurological disorders.
Key words: miRNA, mRNA, binding site, coding sequence, untranslated regions, trinucleotide repeat.

Introduction

The extension of a tandem repeat array is responsible for disease pathology in a community of genetic disorders, repeat extension diseases including, Fragile-X syndrome (FXS) [1], amyotrophic lateral sclerosis (ALS) [2], Alzheimer's disease (AD) [3], Intellectual disability (ID) [4], Schizophrenia [5], Huntington disease [6] and neuromuscular and myotendinous junctions [7].The critical point in the development of new therapeutic strategies for neurological disorders (NDs) is identifying the role of miRNAs in normal cellular processes and understanding how dysregulated miRNA expression is responsible for their neurological effects, also dysregulation of miRNA has been implicated in different NDs [8]. miRNAs are group of 22-nucleotide short RNA sequences, which mediate the post-transcriptional gene silencing [9]. In neurological disorders, regulating the expression and processing of miRNAs, and the mechanisms by which miRNAs locate to their correct targets, is not yet fully understood [10]. The first researches of target prediction algorithms performance was carried out by TargetScanS, PicTar, DIANA-microT and EIMMO. TargetScanS, PicTar and miRanda used alone or as a union made the best trade off between sensitivity and specificity while TargetScan and DIANA-microT did not succeed [11]. Therefore in this study, using MirTarget program, we predicted the features of the interaction of miRNAs from a wide list of Londin *et al.* (Londin, 2015: 1106) with mRNA of candidate genes with trinucleotide repeats in coding sequences (CDS) and untranslated regions (UTRs).

Materials and methods

The nucleotide (nt) sequences of candidate genes of having trinucleotide repeats were downloaded from GenBank (http://www.ncbi.nlm.nih.

gov). The nucleotide sequences of human novel miRNAs were taken from Londin *et al.* (Londin, 2015: 1106) [12].The search for miRNA target genes were carried out using the MirTarget program, which was developed in our laboratory. The MirTarget program defines the following characteristics of miRNA binding to mRNAs: (a) the commencement of miRNA binding to mRNA; (b) the localization of miRNA binding sites in 5'UTRs, CDSs and 3'UTRs of the mRNAs; (c) the free energy of interaction between miRNA and the mRNA (ΔG, kJ/mole); and (d) the schemes of nucleotide interactions between miRNAs and mRNAs. This program found hydrogen bonds between adenine (A) and uracil (U), guanine (G) and cytosine (C), G and U, and A and C. The ratio ΔG/ΔGm (%) was counted for each site,where ΔGm equaled the free energy of a miRNA binding with its perfect complementary nucleotide sequence [13].

Results and discussion

A study of 3701 novel miRNAs binding to mRNAs of 371 genes of having nucleotide repeats showed that 41 genes were targets for seven miRNAs in CDS with CAG trinucleotide repeats. Also, in untranslated regions (5/3'UTRs) 52 miRNAs bind with 25 mRNA genes having CGG, CCG and CUG trinucleotide repeats with ΔG/ΔGm values equal to 85 % and more.

The binding sites of ID00372.5p-miR, ID03311.5p-miR, ID01508.5p-miR, ID00296.3p-miR, ID01702.3p-miR, ID00930.3p-miR, ID02986.5p-miR, ID00457.3p-miR and ID00522.5p-miR in mRNA of 59genes have the highest free binding energy from -101 kJ/mole to -123 kJ/mole in CDS with CAG trinucleotide repeat, and between -104 kJ/mole to -148 kJ/mole in 5'UTRand 3'UTR with CGG,CCG,CUG repeats withΔG/ΔGm value from 85% to 98%, respectively.

Table 1 shows that ID00372.5p-miR, ID03311.5p-miR, ID01508.5p-miR, ID00296.3p-miR and ID01702.3p-miR bind three or more mRNA genes. However in the CUG repeat region ID00930.3p-miR, ID02986.5p-miR, ID00457.3p-miR and ID00522.5p-miR bind only one gene mRNA. Moreover, 20 genes are targets of two or more miRNAs. For example, we can see that the mRNA of *ATXN1, ATXN2, ELMSAN1, FBXO11, FMN2, GIGYF2, IRS1, MED15, MEF2A* and *MN1* genes are targets for ID00372.5p-miR and ID03311.5p-miR in CDS. ID00296.3p-miR, ID01702.3p-miR, ID02986.5p-miR and ID00522.5p-miR can bind to the mRNAs of *AFF2, ANKH, ANKRD13D, BCL11A, BCL2L11, BLMH, BTF3L4, C4orf19*, *CA10* and *DMPK* genes in 5'UTR and 3'UTR.

Table 1 – The list of miRNAs binding sites in mRNA of two or more genes having trinucleotide repeats

miRNA	Gene	Region mRNA
ID00372.5p-miR	*ATXN1, ATXN2, ELMSAN1, FBXO11, FMN2, GIGYF2, IRS1 MED15, MEF2A, MN1*	CDS
ID03311.5p-miR	*AR, ATN1, ATXN1, ATXN2, ATXN7, CELF3, DACH1, DCP1B, DENND4B, DLX6, DNER, E2F4, EGR1, ELMSAN1, EP400, ERN1, FAM104A, FAM155A, FAM157A, FAM157B, FBXO11, FMN2, FOXJ2, FOXP2, FRMPD3, GIGYF2, HTT, IRS1, MAML3, MED15, MEF2A, MLL2, MN1, NCOR2, RUNX2, SMARCA2, TBP, TNRC6B, TOX3, ZNF384*	CDS
ID01508.5p-miR	*ADRBK1, B4GALT2, BRSK2, C11orf87, CARM1, CBL, CCDC93, FMR1*	5'UTR
ID00296.3p-miR	*AFF2, ANKH, ANKRD13D, BCL11A, BCL2L11, BLMH, BTF3L4, C4orf19, CA10*	5'UTR
ID01702.3p-miR	*ABCD3, AFF2, ANKH, ANKRD13D, BCL11A, BCL2L11, BLMH, BTF3L4, C4orf19, CA10*	5'UTR
ID00930.3p-miR	*ATP6V0B*	3'UTR
ID02986.5p-miR	*DMPK*	3'UTR
ID00457.3p-miR	C15orf39	3'UTR
ID00522.5p-miR	DMPK	3'UTR

From these binding sites, the mRNA genes of *ATXN2, ,FMN2, IRS1, MN1, ADRBK1, B4GALT2, BRSK2, C11orf87, CARM1, CBL, CCDC93* and *FMR1* have binding sites for ID00372.5p-miR and ID01508.5p-miR with the highest free binding energy equal to -121 and -123 kJ/mole in CDS with CAG, and 5'UTR with CGG repeated regions. Also, the binding sites of ID00296.3p-miR and ID01702.3p-miR with 5'UTR mRNA of *BLMH* and *C4orf19* genes having CCG repeats show the

highest free binding energy equal to -148 kJ/mole. The mRNA of *ATP6V0B, C15orf39* and *DMPK* genes with free binding energy from -118kJ/mole to -123kJ/mole have ID00930.3p-miR, ID00457.3p-miR and ID00522.5p-miR binding sites in 3'UTR with CUG repeated regions (Table 2).

Table 2 – The characteristics of miRNAs interaction with mRNA of having trinucleotide repeat genes with the highest free binding energy

miRNA	Gene	Start of site, nt	Region mRNA	ΔG, kJ/mole)	ΔG/ ΔGm,%	Length miRNA,nt	Nucleotide repeat
ID00372.5p-miR	*ATXN2*	654	CDS	-121	89	24	CAG
	FMN2	836	CDS	-123	90	24	CAG
	IRS1	2085	CDS	-121	89	24	CAG
	MN1	1861	CDS	-121	89	24	CAG
ID01508.5p-miR	*ADRBK1*	220	5'UTR	-123	85	23	CGG
	B4GALT2	137	5'UTR	-123	85	23	CGG
	BRSK2	103	5'UTR	-123	85	23	CGG
	C11orf87	17	5'UTR	-123	85	23	CGG
	CARM1	15	5'UTR	-123	85	23	CGG
	CBL	15	5'UTR	-123	85	23	CGG
	CCDC93	33	5'UTR	-123	85	23	CGG
	FMR1	101	5'UTR	-123	85	23	CGG
ID00296.3p-miR	*BLMH*	184	5'UTR	-148	94	25	CCG
	C4orf19	75	5'UTR	-148	94	25	CCG
ID01702.3p-miR	*BLMH*	184	5'UTR	-148	98	24	CCG
	C4orf19	75	5'UTR	-148	98	24	CCG
ID00930.3p-miR	*ATP6V0B*	901	3'UTR	-118	86	22	CUG
ID00457.3p-miR	*C15orf39*	4049	3'UTR	-118	87	22	CUG
ID00522.5p-miR	*DMPK*	2310	3'UTR	-123	87	23	CUG

From indicated in table 2 genes, especially *ATXN2, FMN2, MN1, ADRBK1, BRSK2, C11orf87, FMR1, BLMH* and *DMPK* genes are the major responsible causes forneurological disorders (Table 3). These genes are targets for ID00372.5p-miR, ID01508.5p-miR, ID00296.3p-miR, ID01702.3p-miR and ID00522.5p-miR. Moreover, below we discuss miRNAs binding sites with these genes and their functions in neurodevelopmental disorders (Table 3).

In CDS the mRNA of *ATXN2* gene has $(CAG)_{22}$ repeat between 658 to 726. Usually larger than 34 repeat CAG expansions in coding regions of the *ATXN2* gene are the cause of type 2 spinocerebellar ataxia (SCA2) [14]. Also, CAG repeats in the *ATXN2* gene were linked to an increased risk of amyotrophic lateral sclerosis (ALS) [15]. ID00372.5p-miR binding sites located from 654 nt to 677 nt, encodes polyQ with an interaction value ΔG/ΔGm of 89%.

The binding sites of ID00372.5p-miR in mRNA of *FMN2* and *MN1* genes have $(CAG)_6$ trinucleotide repeats of which binding sites started in 836 and 1861 nt in the CDS (Figure 1). *FMN2* was associated with synapse formation and deletion mutations are associated with intellectual disability, suggesting a role for *FMN2* in memory function in mice and humans [16; 17]. Also, recently research studies shows that *FMN2* was highly expressed in human hippocampal neurons and the mouse [18]. For patients with post-traumatic stress disorder (PTSD) and Alzheimer's disease (AD), *FMN2* is deregulated [18]. *MN1* gene, located on human chromosome 22, was first cloned in 1995 from a patient with t(4;22) (p16;q11) translocation meningioma, which in its first exon disrupts *MN1* [19]. *MN1* C-Terminal Truncation (MCTT) syndrome is a genetic disorder caused by an *MN1* gene alteration. A genetic modification of the *MN1* gene was related to intellectual disability (ID) [20].

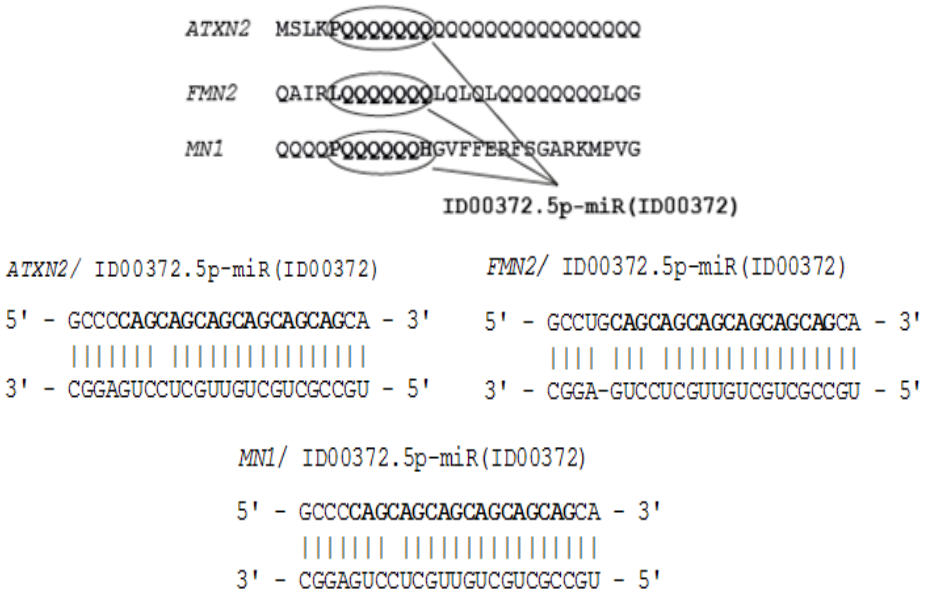

Figure 1 – The encoded oligopeptides and schemes of ID00372.5p-miR(ID00372) binding sites in CDS mRNA of *ATXN2, FMN2* and *MN1* genes

It can be seen from the figure 2 that the mRNA of four genes (*ADRBK1, BRSK2, C11orf87, FMR1*) are targets for ID01508.5p-miR in $(CGG)_8$ repeated regions in 5'UTR. It is known that these genes are responsible for the development of a number of neurodegenerative diseases.

Androgenic, beta, receptor kinase 1 *(ADRBK1)*, also known as *βARK, BARK*, or G-protein – coupled receptor kinase 2 (*GRK2*), produced serine / threonine intracellular kinase, a ubiquitous cytosolic enzyme that specifically phosphorylated the activated form of the beta-adrenergic and related G-protein – coupled receptors (GPCRs) [21-22]. *ADRBK1* related illnesses include heart disease and Alzheimer's disease [23].

BRSK2 interacts with many genes related to neurodevelopmental disorders including autism, tuberous sclerosis, developmental delay and intellectual disability [24].

The *C11orf87* is mainly found in brain tissue, also known as neuronal integral membrane protein 1 (NEURIM1). It is the only gene present within a locus known to harbour variations associated with schizophrenia in multiple genome-wide association studies in different populations, as well as association with self-reported educational achievement [25].

FMR1, located at Xq27.3, consists of 17 exons and measures approximately 38 kb [26]. CGG-repeat expansion in the 5′-untranslated region (5′UTR) of *FMR1*, inducing abnormal methylation of this region followed by transcriptional silencing, is the major recurrent mutagenic mechanism leading to the absence of FMRP. This regular expansion is thought to account for at least 99% of FXS cases [27]. Fragile-X syndrome (FXS) is the most widely recognised form of inherited intellectual disability (ID), and its neurodevelopmental phenotype often overlaps with autism spectrum disorder [28; 29].

Noticeably in Figure 3, ID00296.3p-miR and ID01702.3p-miR occupied the same binding site, starting from184 nt to 208 nt with $(CCG)_7$ repeats in 5'UTR mRNA of *BLMH* gene.

BLMH is involved in homocysteine metabolism and homocysteine constitutes a risk factor for Alzheimer's disease (AD). *BLMH* is important in cytoskeleton dynamics, preserves synaptic plasticity and can associate the inactivation of the *BLMH* gene with AD [30].

Other mRNA gene of *DMPK* was a target of ID00522.5p-miR, for example: ID00522.5p-miR was bound the gene mRNA of *DMPK* (between 2310 nt -2333 nt*)* with $(CUG)_5$ repeats in 3'UTR (Figure 4). A CUG repeat in *DMPK* is transcribed and is located in the 3- prime untranslated region (UTR) of an mRNA that is expressed in tissues affected by myotonic dystrophy [31]. Immunohistochemical staining revealed that *DMPK* is predominantly located at sites of human and rodent skeletal muscle neuromuscular and myotendinous junctions. The protein could also be seen in the neuromuscular junctions of adult and congenital DM muscle tissues, without any significant changes in structural organisation [32].

Figure 2 – The nucleotide sequences and schemes of ID01508.5p-miR binding sites in 5'UTR mRNA *of ADRBK1, BRSK2, C11orf87* and *FMR1* genes

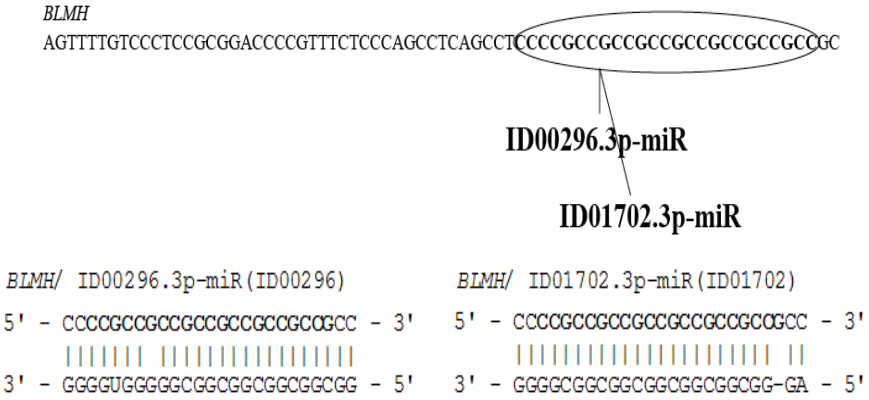

Figure 3 – The nucleotide sequences and schemes of ID01702.3p-miR binding sites in 5'UTR mRNA of *BLMH* gene

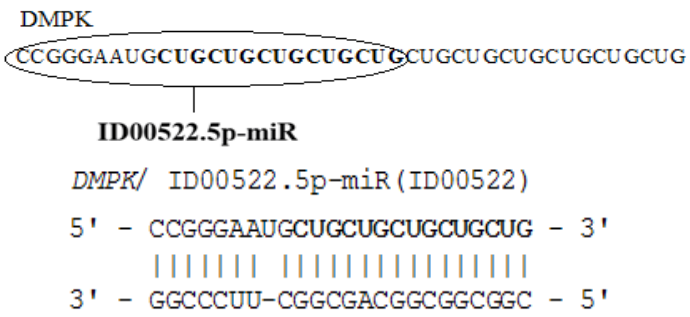

Figure 4 – The nucleotide sequence and scheme of ID00522.5p-miR binding site in 3'UTR mRNA of *DMPK* gene

Table 3 – Diseases and functions of miRNAs target genes which cause neurological disorders

Genes	Function	PMID	Disease	PMID
ATXN2	Ataxin-2 plays roles in a variety of cellular pathways including the maturation, translation and endocytosis of mRNA	27531668	2 spinocerebellar ataxia, amyotrophic lateral sclerosis(ALS)	25148523
FMN2	FMN2 plays an important role in the movement or differentiation of neurons	30227168	Intellectual disability, post-traumatic stress disorder, Alzheimer's disease (AD)	28768717
MN1	During embryogenesis, *MN1* plays a key role in the formation of membranous bones in the skull.	15870292	C-Terminal Truncation (MCTT) syndrome, intellectual disability (ID)	31834374
ADRBK1	*ADRBK1* plays a crucial role in fundamental cellular functions including cell proliferation , differentiation, and migration	25279970	Heart disease and Alzheimer's disease	30463058
BRSK2	*BRSK2* plays a major role in the distribution of synaptic vesicles, the development of synapse and neuronal polarisation	3448725	Autism, tuberous sclerosis, developmental delay and intellectual disability (ID)	30879638
C11orf87	The *C11orf87* is primarily expressed in brain tissue, also known as the neuronal integral membrane protein 1 (NEURIM1).	31959813	Schizophrenia	31959813
FMR1	The gene *FMR1* encodes FMRP with an amino terminal domain composed of structural modules, a tandem sequence of two domains Agenet / Tudor	29178241	Fragile-X syndrome (FXS)	28176767
BLMH	*BLMH* is an essential protective against death caused by Bleomycin and plays an important role in neonatal survival and the maintenance of epidermal integrity.	10200322	Alzheimer's disease	28781776
DMPK	The gene *DMPK* plays a major role in muscle, heart and brain cells.	20301344	Skeletal muscle neuromuscular and myotendinous junctions, myotonic dystrophy	8036515

Conclusion

Using the bioinformatic study of the characteristics of the interaction of novel miRNAs with mRNA of genes having trinucleotide repeats has not yet been performed. In the present research, for the first time MirTarget program was used to identify the interaction novel miRNAs with mRNA candidate genes having CAG, CGG, CCG and CUG trinucleotide repeats in coding sequences (CDS) and untranslated regions (UTRs).

We studied the characteristics of the interaction of miRNA with mRNA of genes having trinucleotide repeats. It has been identified five (ID00372.5p-miR, ID01508.5p-miR, ID00296.3p-miR, ID01702.3p-miR and ID00522.5p-miR) key associations of miRNAs and nine gene's mRNAs (*ATXN2, FMN2, MN1, ADRBK1, BRSK2, C11orf87, FMR1, BLMH* and *DMPK*) that have a free energy of interaction of -121 kJ/mole to – 148 kJ/mole.

The binding sites of ID00372.5p-miR, ID01508.5p-miR, ID00296.3p-miR, ID01702.3p-miR and ID00522.5p-miR and their target genes *ATXN2, FMN2, MN1, ADRBK1, BRSK2, C11orf87, FMR1, BLMH* and *DMPK* may be able to provide insights into pathogenesis mechanism and pave the way for the development of new diagnostic markers and therapeutic targets for neurological disorders. Addi-

tionally, the binding sites of the nucleotide sequences of novel miRNAs from Londin *et al.* (Londin, 2015: 1106) [12] with genes were derived from GenBank is not yet fully understood, therefore their function and target genes can be useful for understanding their physiological role in human diseaseas well as paving the way for new researches in the future studies. The research results can be used as a unified database as a basis for further experiments with animals and humans in biotechnology and medicine for early diagnosis, prevention and treatment of neurodegenerative diseases.

Acknowledgments

This study was supported by AP05132460 grant, MES RK, SRI of Biology and Biotechnology Problems, al-Farabi Kazakh National University. We thank Pyrkova A.Yu. for the help in the data analysis and interpretation.

References

1 Marwa Z., Hiu-Tung T., et al. (2020) FMR1 locus isoforms: potential biomarker candidates in fragile X-associated tremor/ataxia syndrome (FXTAS). Scientific Reports., vol. 10, no. 11099, pp.1-10. https://doi.org/10.1038/s41598-020-67946-y.

2 Sarah M., Ahmad A., Ammar A. (2017) What causes amyotrophic lateral sclerosis? F1000 Research., vol. 6, no.1, pp.1-10. https://doi.org/10.12688/f1000research.10476.1

3 Anil K., Jaskirat S., Amandeep G., et al. (2020) Alzheimer Disease. University of TN Health Science Center, 167 p. NBK499922.

4 Natasha M., Lacey H. (2017) Intellectual Disability and Language Disorder. Child AdolescPsychiatrClin., vol.26, no.3, pp. 539–554. https://doi.org/10.1016/j.chc.2017.03.001.

5 Arman D., Henry A. (2009) Neurological Disorders in Schizophrenia. PsychiatrClin North Am., vol. 32, no.4, pp. 719-57. https://doi.org/10.1016/j.psc.2009.08.004.

6 Frédérique Berger, et al. (2013) The impact of single-nucleotide polymorphisms (SNPs) in OGG1 andXPC on the age at onset of Huntington disease. Mutation Research., vol. 755, pp.115– 119. 10.2174/156652411794859250.

7 Richard J., Barohn M., Mazen M., et al. (2014) A pattern recognition approach to the patient with a suspected myopathy. NeurolClin., vol. 32, no. 3, pp.569. https://doi.org/10.1016/j.ncl.2014.04.008.

8 Mohammad A., Gohar M., Nigel H. (2015) Current Update on Synopsis of miRNA Dysregulation in Neurological Disorders. CNS NeurolDisord Drug Targets., vol.14, no. 4, pp. 492–501. https://doi.org/10.2174/1871527314666150225143637.

9 Chunmei W., Bingyuan J., Baohua Ch., Jing Ch. (2014) Neuroprotection of microRNA in neurological disorders. Biomed Rep., vol. 2 no. 5. pp. 611–619. https://doi.org/10.3892/br.2014.297.

10 Ramesh A., et al. (2006) MicroRNAs: regulators of gene expression and cell differentiation. Blood., vol.108, no.12, pp. 3646–3653. https://doi.org/10.1182/blood-2006-01-030015.

11 Londin E., Lohera P., Telonisa A.G., Quanna K., et al. (2015) Analysis of 13 cell types reveals evidence for the expression of numerous novel primate- and tissue-specific microRNAs. PNAS USA.,vol.112, no.10, pp.1106-1115. https://doi.org/doi: 10.1073/pnas.1420955112.

12 T.M. Witkos, E. Koscianska and W.J. Krzyzosiak. (2011) Practical Aspects of microRNA Target Prediction. Current Molecular Medicine., vol. 11, pp. 93-109. 10.1016/j.mrgentox.2013.04.020.

13 Ivashchenko A., Pyrkova A., Niyazova R. (2016) A method for clustering of miRNA sequences using fragmented programming. Bioinformation., vol. 12, no 1, pp. 15-18. https://doi.org/10.6026/97320630012015.

14 Stefan M. (2018) The complex structure of ATXN2 genetic variation. Neurol Genet., vol. 4, no.6, pp. 299. https://doi.org/10.1212/NXG.0000000000000299.

15 Daoud H., Belzil V., Martins S., Sabbagh M., Provencher P., Lacomblez L., et al. (2011) Association of long ATXN2 CAG repeat sizes with increased risk of amyotrophic lateral sclerosis. Arch Neurol. vol. 68, no.6, pp.739-42. https://doi.org/10.1001/archneurol.2011.111.

16 Peleg S., Sananbenesi F., Zovoilis A., Burkhardt S., Bahari-Java S., Agis-Balboa R., et al. (2010) Altered histone acetylation is associated with age-dependent memory impairment in mice. Science., vol.328, no.5979, pp.753-6. https://doi.org/10.1126/science.1186088.

17 Almuqbil M., Hamdan F., Mathonnet G., Rosenblatt B., Srour M. (2013) De novo deletion of FMN2 in a girl with mild non-syndromic intellectual disability. Eur J Med Genet., vol.56, pp.686–688. https://doi.org/10.1016/j.ejmg.2013.10.003.

18 Roberto C., Paulo S., Nelson R., Cemil K., Eva B., Michael G., Sanaz B. (2017) Formin 2 links neuropsychiatric phenotypes at young age to an increased risk for dementia. EMBO J., vol.36, no.19, pp.2815–2828. https://doi.org 10.15252/embj.201796821.

19 Fatemeh P., et al. (2020) Genetic Characterization and Risk Stratification of Acute Myeloid Leukemia. Cancer Manag Res., vol.12, pp. 2231–2253. https://doi.org 10.2147/CMAR.S242479.

20 Christopher C., Dan D., Angela E., et al. (2020) MN1 C-terminal truncation syndrome is a novel neurodevelopmental and craniofacial disorder with partial rhombencephalosynapsis. Brain., vol. 143, no. 1, pp. 55–68. https://doi.org/10.1093/brain/awz379.

21 Le S., Barrows N., Bradrick S., Pearson J. (2012) G protein-coupled receptor kinase 2 promotes flaviviridae entry and replication. PLoS Negl Trop Dis., vol. 6, no.9, pp.1820. https://doi.org/10.1371/journal.pntd.0001820.

22 Métayé T., Gibelin H., Perdrisot R., Kraimps J. (2005) Pathophysiological roles of G-protein-coupled receptor kinases. Cell Signal., vol.17, no.8, pp.917-28. https://doi.org/10.1016/j.cellsig.2005.01.002.

23 Degos V., Peineau S., Nijboer C., et al. (2013) G protein-coupled receptor kinase 2 and group I metabotropic glutamate receptors mediate inflammation-induced sensitization to excitotoxicneurodegeneration. Ann Neurol., vol.73, no 5, pp.667-678. https://doi.org/10.1002/ana.23868.

24 Saiyin H., Na N., Han X., Fang Y., Wu Y., Lou W., Yang X. (2017) BRSK2 induced by nutrient deprivation promotes Akt activity in pancreatic cancer via downregulation of mTOR activity. Oncotarget., vol.8, pp. 44669–44681. https://doi.org/10.18632/oncotarget.17965.

25 Mitra E., Adnan N., Lennart W. (2020) Transcriptome analysis of fibroblasts from schizophrenia patients reveals differential expression of schizophrenia-related genes. Scientific Reports., vol. 10., no. 630, pp. 1-10. https://doi.org/10.1016/j.nbd.2020.104740.

26 Maria J.S. (2020) Fragile X Syndrome and associated disorders: clinical aspects and pathology. Neurobiol Dis., vol.136, pp. 104-740. https://doi.org/10.1016/j.nbd.2020.104740.

27 Boyle L., Kaufmann W. (2010) The behavioral phenotype of FMR1 mutations. Am J Med Genet. vol.15, no.154, pp.469-76. https://doi.org/10.1002/ajmg.c.30277.

28 Tranfaglia M. (2011)The psychiatric presentation of fragile x: evolution of the diagnosis and treatment of the psychiatric comorbidities of fragile X syndrome. DevNeurosci., vol.33, no.5, pp. 337-48. https://doi.org/10.1159/000329421.

29 Mohan G., Abhilasha S., et al. (2017) Unraveling the genes implicated in Alzheimer's disease. Biomed Rep., vol. 7, no.2, pp.105–114. https://doi.org/10.3892/br.2017.927.

30 Ádám J., et al. (2016) Effect of Bleomycin Hydrolase Gene Polymorphism on Late Pulmonary Complications of Treatment for Hodgkin Lymphoma. Plos one. June., vol. 21, no. 6, pp. 1-10. https://doi.org/10.1371/journal.pone.0157651.

31 Beatriz L., Ruben A. (2008) Molecular Effects of the CTG Repeats in Mutant Dystrophia Myotonica Protein Kinase Gene. Curr Genomics., vol. 9, no.8, pp.509–516. https://doi.org/10.2174/138920208786847944.

32 Nalavade R., Griesche N., Ryan D., Hildebrand S., Krauss S. (2013) Mechanisms of RNA-induced toxicity in CAG repeat disorders. Cell Death Dis4., vol.4, no.8., pp. 752. https://doi.org/10.1038/cddis.2013.276.

IRSTI 34.31.27; 34.29.01 https://doi.org/10.26577/ijbch.2020.v13.i2.05

Ayse Gul Sarıkaya*, Seydi Ahmet Kavaklı

Bursa Technical University, Faculty of Forestry, Bursa, Turkey
*e-mail: aysegul.sarikaya@btu.edu.tr

Some morphological and phenological characteristics and volatile components of *Campanula rapunculus* L. var. *rapunculus*

Abstract. *Campanula* is one of the largest genus of the *Campanulaceae* family, represented by approximately 115 species in Turkey and is spread through Iran-Turan, Eastern Mediterranean and Mediterranean phytogeographical regions. The aim of the current study was to determine some morphological features, phenological characteristics and leaf-flower volatile components of *Campanula rapunculus* var. *rapunculus* collected in different sites of Uludag Mountain (Bursa). The average plant height was calculated as 37.21 cm, number of corolla was 2.4, the length of the corolla was 2.0 cm, calyx lobe length was 1.36 cm, leaf width was 1.7 cm and leaf length was 4.31 cm. Considering phenological features, it was measured that the first flowering ends in May, full flowering ends in June and late flowering ends in late July. A total of 32 different volatile components were detected in *Campanula rapunculus*. With the aid of gas chromatography-mass spectroscopy (GC-MS) of volatile components by solid phase microextraction technique (SPME), 3-Methylbutanal (10.87%), cis-3-Hexene-1-ol (9.85%) and 3-Octanol (9.62%) were identified as major components. In addition to its medicinal benefits, studies on *Campanula* genus, considered as food and ornamental plants, should be increased and its value should be revealed.

Key words: *Campanula*, solid phase microextraction technique, volatile components, morphological and phenological features.

Introduction

Plants demonstrate an extensive range of positive features, including antibacterial, anthelmintic, antihypertensive, antimutagenic, carminative, choleretic, sedative, antispasmodic, insecticide [1-8]. Medicinal and aromatic plants, which have never lost their importance throughout the history of mankind, are preferred extensively today with the rise of living standards [9,10].

Rich in medicinal and aromatic plants *Campanulaceae* is mostly presented by herbaceous or woody climber plants, rarely consisting of thick-bodied trees and bushes. *Campanula*, one of the largest genera of the *Campanulaceae* family, comprises around 300 species across the globe, especially in the northern hemisphere and Mediterranean region [11]. However, according to some records, the number of species of this genus is reported to be approximately 500 [12].

Leaves of *Campanula* are altered but can sometimes vary. Flowers are violet or blue, big and showy. Seeds are endospermic. Fruit is a capsule, it can rarely be a capsule with caps in some breeds, meaty grapes or dry and unopened [13-16].

The genus *Campanula* is represented by about 115 species in our country and has 43 taxa endemic at the species level [17]. *Campanula rapunculus* is a 2-year plant with a length of 50-100 cm. The lower stem and leaves are obovate, while the top ones are reduced. Flowers are unique but rarely, can be similar to 2-3 paniculae and long spica. Corolla is funnel-shaped, pale blue or whitish, slightly longer than calyx lobes. It has 3 stigmas. The taxon that blooms in May-July is 1500-2200 m in Uludag. It spreads between stunted junipers, shrubs and under the *Pinus-Fagus-Abies* forest at altitudes [18].

Bursa city and Uludag are one of the most important centers of plant diversity in Turkey. Different vegetation zones starting from the skirts of Uludag mountain to the summit and are located at different altitudes are very rare in the world and are of particular importance [18]. Under the focus of the current study were morphological characteristics, phenological features and leaf-flower volatile components of *Campanula rapunculus* var. *rapunculus* collected from different zones of Uludag.

Materials and methods

Object. Campanula rapunculus var. *rapunculus* collected from different points of Uludag mountain served the object of the study. During the field stud-

ies within 2018-2019 vegetation period, coordinates of distribution points of *Campanula rapunculus* var. *rapunculus* were taken with Garmin GPS Map 64 S. 20 different points, 20 x 20 m in size identified as sample areas representing different growing conditions (Figure 1; Table 1).

Figure 1 – Sampling areas within the study area – Uludag mountain, Bursa (Source: Google Earth®)

Table 1 – Information on the determined sample areas in the study area

Sample No.	Sampling Locations	Altitude	Aspect
	40°06,712' N-29°06,162' E	1707 m	NW
	40°06,751' N-29°06,243' E	1674 m	NE
	40°06,674' N-29°06,277' E	1649 m	NE
	40°06,821' N-29°06,805' E	1793 m	NW
	40°06,883' N-29°06,501' E	1677 m	SW
	40°07,009' N-29°06,454' E	1646 m	SW
	40°07,137' N-29°06,525' E	1685 m	W
	40°07,108' N-29°06,817' E	1744 m	NW
	40°08,006' N-29°06,971' E	1608 m	NW
	40°06,970' N-29°07,029' E	1701 m	N
	40°06,830' N-29°06,985' E	1830 m	NE
	40°06,675' N-29°07,008' E	1871 m	N
	40°06,174' N-29°07,541' E	1961 m	E

Table 1 continued

Sample No.	Sampling Locations	Altitude	Aspect
	40°06,035' N-29°07,854' E	1949 m	N
	40°06,389' N-29°07,656' E	1901 m	NE
	40°08,055' N-29°08,707' E	1671 m	W
	40°07,386' N-29°09,284' E	1741 m	NW
	40°06,889' N-29°09,475' E	1852 m	W
	40°06,764' N-29°04,957' E	1440 m	NW
	40°07,303' N-29°05,534' E	1521 m	W

Samples were taken from 20 areas with altitudes varying from 1440 to 1961 m above the sea level.

Analysis of morphological properties. Samples of *Campanula rapunculus* var. *rapunculus* were collected from sampling areas for determining of morphological features and storage in herbarium. In order to calculate the morphological measurements, digital diameter meter and meter, 30 plant length, number of corolla, length of corolla, calyx lobe length, leaf width and height were measured (Figure 2).

Figure 2 – Images of some morphological measurements on *Campanula rapunculus* var. *rapunculus*.
Note: a – plant height, b – corolla height, c – leaf width, d – leaf length. Photo by A.G. Sarıkaya

Estimation of phenological time. Field studies started on March, 2018. Along with some features of *Campanula rapunculus* characteristics of the spreading area were considered, such as topographic, soil, climate, other vegetation and altitude.

Analysis of volatile components. Leaves and flowers of *Campanula rapunculus* collected from the testing site, were dried at room temperature (25°C), leaves and flowers components were determined by the Peak Cavity-Solid Phase Micro Extraction (HS-SPME) technique combined with gas chromatography/mass spectrometry (GC/MS).

Samples of leaves and flowers taken as 2.5 g of each sample were placed in a 10 mL glass vial closed with a silicone cap and kept at 60°C for 30 minutes. The SPME apparatus was passed through 75 µm thin Carboxen/Polydimethylsiloxane (CAR/PDMS) coated fused silica fiber (Merck, Germany) to adsorb volatile compounds and then was directly injected into the capillary column (Rtx®-5MS 30 m x 0.25 mm I.D. df=0.25 µm, Restek, USA).

Device was connected to the same brand mass selector detector operated in hand mode (70 eV).

This process was repeated three times and the accuracy of the results was compared and the results were given as average. Helium with a flow rate of 1.61 mL per minute was used as the carrier gas. Injection and detection temperatures were set at 250°C. Retention Indices (RI) of the volatile components were calculated according to the C7-C30 alkane mixtures standard under the above-mentioned chromatographic conditions. The identification of the compounds was determined by comparison of mass spectra and compounds found in the spectral library (Wiley 7th edition, NIST 20, Tutor, FFNSC 3).

Results and discussion

Analysis of morphological properties and phenological time. Mean plant height of *Campanula rapunculus* collected from different points of Uludag was determined as 37.21 cm, number of corolla – 2.4, corolla length – 2.0 cm, calyx lop length – 1.36 cm, leaf width – 1.7 cm, leaf length – 4.31 cm (Table 2).

It was noted that first flowering started in early May, full flowering was in June and late flowering ended in late July. The color of the flowers varied from whitish and pale blue to bluish-purple and lilac-blue (Figure 3).

Table 2 – Morphological measurements of *Campanula rapunculus* var. *rapunculus*

Features	Smallest	Biggest	Mean
Plant height	25 cm	55.5 cm	37.21 cm
Number of corolla	2	3	2.4
Corolla length	1.4 cm	3 cm	2.0 cm
Calyx lop length	0.5 cm	2.4 cm	1.36 cm
Leaf width	0.5 cm	2.7 cm	1.37 cm
Leaf length	2.3 cm	7 cm	4.31 cm

Figure 3 – *Campanula rapunculus* var. *Rapunculus* at Uludag, Bursa
Note: a – general view, b – flower. Photo by S.A. Kavaklı

In the study by Davis [17], plant height of *Campanula rapunculus* was determined as 50-100 cm, number of corolla as 2-3, the length of the corolla as 1.2-2 cm, the calyx lobe length 0.9-1.6 cm, leaf width as 2 cm and the length as 4 cm. It was determined that morphological measurements other than the number of corolla differed from our study. Kaynak et al. [18] assessed the plant height of *Campanula rapunculus* as 50-100 cm, and the length of the corolla as slightly longer than the calyx lobes. The height of the plant differed from our study, though the fact that the length of the corolla and slightly longer than the calyx lobes supports our study.

In our study it was observed that first flowering began in early May, full flowering was observed in June, and flowering ended in late July. The color of the flower was determined to be whitish, pale blue, bluish-purple and lilac-blue. Kaynak et al. [18] determined the flowering time as May-July and color of the flower as whitish to pale blue. It was determined that the phenological time and flower color were the same in both studies, and in our study, the color of the flower was bluish-purple and lilac-blue.

Analysis of volatile components. Volatile components of *Campanula rapunculus* were determined by GC-MS using solid phase microextraction technique (SPME). A total of 32 different components were detected in *Campanula rapunculus*. 3-Methylbutanal (10.87%), cis-3-Hexene-1-ol (9.85%) and 3-Octanol (9.62%) were identified as the main components. Among volatile components, aromatic aldehydes were found to be high (Figure 4; Table 3).

Peak values seen on Figure 4 revealed the presence of 32 components.

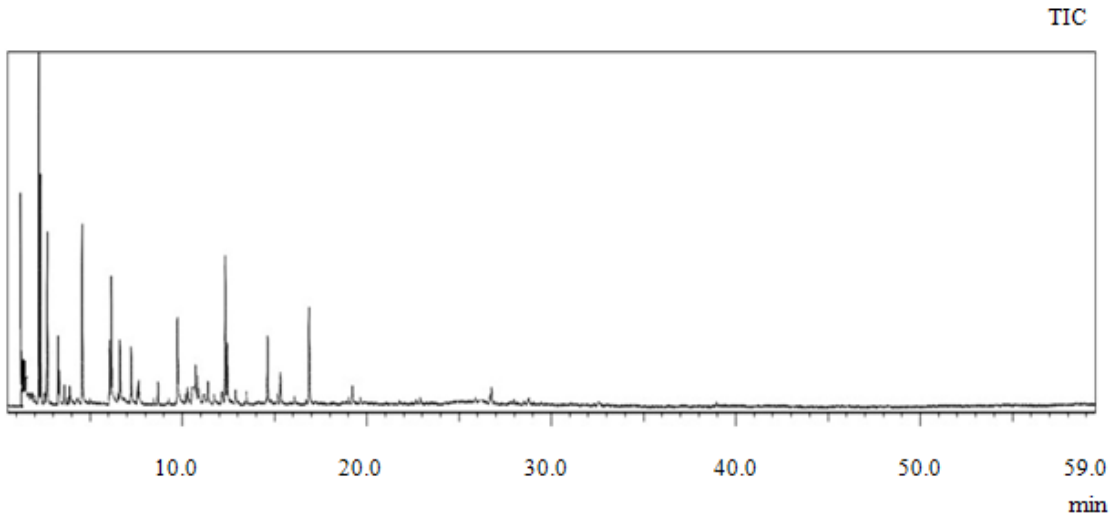

Figure 4 – Gas chromatogram of volatile components for *Campanula rapunculus* var. *rapunculus*

Table 3 – Leaf-flower volatile components of *Campanula rapunculus* var. *rapunculus*

	Retention time	Components	%	Formula	Class
	1.434	2-methyl-Pentanal	1.66	$C_6H_{12}O$	AA
	1.660	2-Methylpropanal	0.68	C_4H_8O	AA
	2.215	3-Methylbutanal	10.87	$C_5H_{10}O$	AAI
	2.304	2-Methylbutanal	7.36	$C_5H_{10}O$	AAI
	2.684	Sorbaldehyde	6.14	C_6H_8O	AA
	3.264	3-Methyl-1-butanol	1.82	$C_5H_{12}O$	AA
	3.331	2-methyl-1-Butanol	1.09	$C_5H_{12}O$	AA
	3.615	(E)-2-Pentenal	0.71	C_5H_8O	AAI
	3.888	1-Pentanol	0.42	$C_5H_{12}O$	AA

Table 3 continued

	Retention time	Components	%	Formula	Class
	4.573	Hexanal	5.74	$C_6H_{12}O$	AA
	6.057	(E)-2-Hexenal	3.13	$C_6H_{10}O$	AA
	6.149	cis-3-Hexene-1-ol	9.85	$C_6H_{12}O$	AA
	6.505	(Z)-2-Hexen-1-ol	0.84	C_6H_{12}	AA
	6.610	n-Hexanol	3.36	$C_6H_{14}O$	AA
	7.220	2-Heptanone	2.06	$C_7H_{14}O$	AA
	7.635	Heptanal	1.08	$C_7H_{14}O$	AA
	8.691	α-pinene	0.76	$C_{10}H_{16}$	MH
	9.740	Benzaldehyde	4.69	C_7H_6O	AAI
	9.840	3-Octanol	9.62	$C_8H_{16}O$	AAI
	10.397	3-Octanone	3.62	$C_8H_{14}O$	AAI
	10.650	(Z)-6-Octen-2-one	0.75	$C_8H_{14}O$	AAI
	11.145	2.4-Heptadienal	0.97	$C_7H_{10}O$	AA
	11.387	Octanal	0.81	$C_8H_{16}O$	AAI
	12.327	Limonene	5.67	$C_{10}H_{16}$	MH
	12.436	1.8-Cineole	2.49	$C_{10}H_{18}O$	OM
	12.885	Benzeneacetaldehyde	0.53	C_8H_8O	OC
	13.469	γ.-Terpinene	0.56	$C_{10}H_{16}$	MH
	14.622	Fenchone	2.66	$C_{10}H_{16}O$	OM
	15.320	Nonanal	1.87	$C_9H_{18}O$	AAI
	16.872	Camphor	6.96	$C_{10}H_{16}O$	OM
	19.212	Decanal	0.65	$C_{10}H_{20}O$	OM
	26.764	Caryophyllene	0.58	$C_{15}H_{24}$	SH
Total			100		
Component number			32		
AA: Aromatic alcohol			38.84		
AAI: Aromatic aldehyde			40.30		
MH: Monoterpene hydrocarbon			6.99		
OC: Other components			0.53		
OM: Oxygen monoterpene			12.76		
SH: Sesquiterpene hydrocarbon			0.58		

3-Methylbutanal (10.87%), cis-3-Hexene-1-ol (9.85%) and 3-Octanol (9.62%) were identified as the main components. 3-Methylbutanal component is used as a reagent for the production of pharmaceuticals and pesticides.

No study was found on the volatile components of *Campanula rapunculus* species. However, there are some researches on other *Campanula* species. In previous studies on volatile components of *Campanula* genus, Politeo et al. [19] identified the presence of 53 different components in *Campanula portenschlagiana*, and identified labda-13 (16), 14-dien-8-o as the main components. Chenxing et al. [20] identified 57 different components in *Campanula colorata* Wall. with 1,2-benzenedicarboxylic acid, butyloctyl ester, cedar camphor, hexadecanoic acid, dibutyl phthalate, tetradecanoic acid, caryophyllene oxide,

6,10,14-trimethyl-2-pentadecanone as main components. These results differ from the results presented in the current study.

Conclusion

Fresh leaves and roots of *C. rapunculus* are used raw (salad, etc.) or cooked (soup, tea, etc.) [21-24]. *Campanula rapunculus* is begining to appear more frequently in local street markets in the Umbria Region, Central Italy and used to treat inflammation of the oral cavity, also leaves used to treat warts, infusion of flowers used as a gargle [25]. It is known that leaves and roots were used as milk enhancer and stone reducer in Turkey, and today it is used in wound healing and constipation disorders [26-28]. *Campanula* species are especially rich in flavone and flavone glycosides. These species, which have decorative flowers, also find use as ornamental plants [29]. In addition to its medical benefits, it is recommended to increase the anatomical, physiological, molecular and biochemical studies of *Campanula* taxa, which are considered as food and ornamental plants. Thus, the value and importance of *Campanula* genus, which spread naturally in our country, can be revealed.

References

1 Alzoreky N.S., Nakahara K. (2003). Antibacterial activity of extracts from some edible plants commonly consumed in Asia. International Journal of Food Microbiology, vol. 80, no. 3, pp. 223-230.

2 Santoyo S., Lloria R., Jaime L., Ibanez E., Senorans F. J., Reglero G. (2006). Supercritical fluid extraction of antioxidant and antimicrobial compounds from Laurus nobilis 60 L. Chemical and functional characterization. European Food Research and Technology, vol. 222, no. 5-6, pp. 565-571.

3 Simić A., Soković M.D., Ristić M., Grujić-Jovanović S., Vukojević J., Marin P.D. (2004). The chemical composition of some Lauraceae essential oils and their antifungal activities. Phytotherapy Research, vol. 18, no. 9, pp. 713-717.

4 Berber I, Avşar C, Çine N, Bozkurt N, Elmas E. (2013). Sinop'da Yetişen Bazı Bitkilerin Metanolik Ekstraktlarının Antibakteriyal ve Antifungal Aktivitelerinin Belirlenmesi. Karaelmas Science and Engineering Journal, vol. 3, no.1, pp. 10-16.

5 Chandel Y.S., Metha P.K. (1990). Nematicidial properties of leaf extract of wild sage. Indian Journal of Agricultural Science, vol. 60, no. 11, pp. 781-790.

6 Trigg J. K. (1996). Evaluation of a eucalyptus-based repellent against Anopheles spp. in Tanzania. Journal of the American Mosquito Control Association, vol. 12, no.2, pp. 243-246.

7 Toroğlu S., Çenet M. (2006). Tedavi Amaçlı Kullanılan Bazı Bitkilerin Kullanım Alanları ve Antimikrobiyal Aktivitelerinin Belirlenmesi İçin Kullanılan Metodlar. Kahramanmaraş Sütçü İmam University Journal of Engineering Sciences, vol.9, no. 2, pp. 12-20.

8 Turan F., Gürağaç R., Sayın S. (2012). Su Ürünleri Yetiştiriciliğinde Esansiyel Yağlar, Türk Bilimsel Derlemeler Dergisi, vol. 5, no. 1, pp. 35-40

9 Kumar S.A. (2009). Plants-based Medicines in India. http://pib.nic.in/feature/feyr2000/fmay2000/f240520006.html. Accessed 21.09.2018.

10 Baytop T. (1999). Türkiye'de Bitkilerle Tedavi. Istanbul: Nobel Tıp Kitapevleri, 480 p. ISBN: 9789754200218.

11 Rosatti T.J. (1986). The genera of Spherocleaceae and Campanulaceae in the Southeastern U.S. Journal of the Arnold Arboretum, vol. 67, no.3, pp. 24-25.

12 Inceoğlu Ö. (1975). Akdeniz Bölgesine Ait Bazı Campanulaceae Polenleri Üzerinde Palinolojik Araştırmalar. Hacettepe Fen ve Mühendislik Bilimleri Dergisi, vol. 5, pp. 101-167.

13 Heywood J.T., Fonarow G.C., Costanzo M.R. (2007). High prevalence of renal dysfunction and its impact on outcome in 118,465 patients hospitalized with acute decompensated heart failure: a report from the ADHERE database. Journal of Cardiac Failure, vol.13, no.6, pp. 422-430.

14 Hickey M., King C. (1988). 100 Families of Flowering Plants. Cambridge: Cambridge University Press, pp. 130-133.

15 Warming E. (1895). Plantesamfund. Grundtraek af den økologiske Plantegeografi. Kjøbenhavn: Philipsens, 335 p.

16 McDonald M.B., Kwong F.Y. (2005). Flower seed: biology and technology. Wallingford: UK CABI Publishing, ISBN 0-85199-906-9.

17 Davis P.H. (1978). Flora of Turkey and the East Aegean Island. Edinburgh: Edinburgh University Press, vol. 1-9. ISBN: 9780748614097.

18 Kaynak G., Daşkın R., Yılmaz Ö. (2008). Bursa Bitkileri. Bursa: Uludağ Üniversitesi Yayınları, 865 p., ISBN: 9789756149355.

19 Politeo O., Skocibusic M., Burcul F., Maravic A., Carev I., Ruscic M., Milos M. (2013). Campanula portenschlagiana Roem. et Schult.: Chemical and Antimicrobial Activities. Chemistry and Biodiversity, vol. 10, no. 6, pp. 1072-1080.

20 Chenxing Z., Mi Z., Cheng X., Bao Cai L. (2014). Analysis on chemical constituents in essential oil from Campanula colorata. Journal of Plant Resources and Environment, vol. 23, no. 4, pp. 99-101.

21 Parada M., Carrio E., Valles J. (2011). Ethnobotany of food plants in the Alt Empordà region (Catalonia, Iberian Peninsula). Journal of Applied Botany and Food Quality, vol. 84, no.1, pp. 11-25.

22 Cornara L., Rocca A.L., Terrizzano L., Denta F., Mariotti M.G. (2014). Ethnobotanical and phytomedical knowledge in the North-Western Ligurian Alps. Journal of Ethnopharmacology, vol. 155, no. 1, pp. 463-484.

23 Arnold N., Baydoun L., Chalak-Th. R. (2015). A contribution to the flora and thnobotanical knowledge of Mount Hermon, Lebanon. Flora Mediterranea, vol. 25, no. 1, pp. 13-55.

24 Gras A., Serrasolses G., Valles J., Garnatje T. (2019). Traditional knowledge in semi-rural close to industrial areas: ethnobotanical studies in western Gironès (Catalonia, Iberian Peninsula). Journal of Ethnobiology and Ethnomedicine, vol. 15, no. 19, pp. 3-37.

25 Ranfa A., Bodesmo M. (2017). An Ethnobotanical investigation of traditional knowledge and uses of edible wild plants in the Umbria Region, Central Italy. Journal of Applied Botany and Food Quality, vol. 90, pp. 246-258.

26 Baytop T. (1984). Türkiyede Bitkilerle Tedavi: Geçmişte ve Bugün. Istanbul: İstanbul Üniversitesi Yayinlari, 520 p.

27 Baytop T. (1997). Türkçe Bitki Adları Sözlüğü [Dictionary of Turkish names of plants]. Ankara: Türk Dil Kurumu Yayınları, 578 p. ASIN: B002AX8YK.

28 Tümen G., Malyer H., Başer K.H.C., Aydın Öz S. (2006). Plants used in Anatolia for wound healing. Proceedings of the IVth International Congress of Ethnobotany (ICEB 2005), pp. 217-221.

29 Heywood V.H. (1978). Flowering Plants of the world. London: Batsford Ltd., ISBN: 9780192176745.

IRSTI 34.03.39 https://doi.org/10.26577/ijbch.2020.v13.i2.06

L.Zh. Gumarova[1*], D. Hillman[2], A.T. Mansharipova[3], G. Sadyrbayeva[1], M. Tauassarova[1]

[1]Laboratory of Chronobiology and Biophysics, Scientific Research Institute of Biology and Biotechnology Problems, Almaty, Kazakhstan
[2]University of Minnesota, Minneapolis, Minnesota, USA
[3]Kazakhstan-Russian Medical University, Almaty, Kazakhstan
[*]e-mail: gumarova.lyazzat@kaznu.kz

Geomagnetic, cardiovascular and geo-cardiovascular congruences of cycles: putative co-periodisms

Abstract. A sense for magnetism in humans and more broadly for nonphotic solar effects is not consciously perceived, even though the cosmos may have broad biospheric consequences. Associations are already documented for the human circulation and for mental and cellular functions with geo- and interplanetary magnetism. We compare interval estimates of periods in view of the ever-present uncertainties, congruence assess corresponding periods by the presence or absence of overlap between the CIs (95% confidence intervals) of the paired periods, found by the nonlinearly extended cosinors in time series of geomagnetic indices, Kp, quasi-logarithmic local index of the 3-hourly range, its derivatives Cp and C9, on the one hand and on the other hand in separate data sets of systolic (S) and diastolic (D) blood pressure (BP) and heart rate (HR) of 360 patients, each monitored ambulatorily (ABPM) for 24 hrs. Some circasemiseptan periods are shared by SBP, DBP and HR in female patients and further by C9 and Cp. Kp reveals a period of 4.31 days, with an even longer period found for SBP in men in the spectral region examined, the periods being picked because of their statistical significance in that spectral region. The gender differences in HR and SBP have their precedents in other regions of the circasemiseptan spectrum of these variables. The circaseptan coperiodisms between geomagnetic indices, Kp, Cp, C9 and cardiovascular system (SBP, DBP) in periodicity is clear for women patients only. The coperiodisms of HR with 10.7 C in 21 days period, and the circaseptan coperiodism again only of Kp with the BP were found.

Key words: geomagnetic, cardiovascular, patients, chronobiology, 24-hour blood pressure monitoring (ABPM), coperiodism, variability of vascular anomalies, variability of vascular disorders.

Introduction

Congruence or similarity in characteristics such as the period or phase of a spectral component in two or more concomitantly sampled time series of the same variables or of different variables within intracellular entities, cells, tissues, organs, organ systems, individuals, populations with spectral temporal characteristics of oscillations environmental factors such as space weather, ranging from infradians,multiples or submultiples of the week over transyears or trans- and cis-half-years to decadesis of undoubted scientific and practical interest, for example, for predicting an increase in the number of infectious diseases, or exacerbations of cardiovascular diseases and other non-communicable diseases [1-4].

Wobbly nature of some natural physical environmental and biospherical spectral components require an inferential statistical approach, e.g., according to Marquardt [5;6]. The congruence of anticipated components can be meaningfully assessed to approximate a yet-to-be-developed test of H_0: periodτ_1 (e.g., environmental τ) = τ_2 (e.g., biological τ) [= … = τ_k (e.g., sociological τ)], or the already available test at a fixed τ of H_0 : $\varphi_1 = \varphi_2$ [= … = φ_k] [7].

The overlap of CIs of the periodin two or more time series being compared by the cosinor [5; 6; 8] extended by Marquardt's algorithm [9] is the criterion for congruence. The same comparison also defines similarity and dissimilarity, the latter referred to as acongruence when the periods are separated by more than the length of a τwith its CI, admittedly an

arbitrary definition, to be refined as more data accumulate [10]. The search for congruence and similarity among periods based on CIs realizes that the changes in many physiological and geomagnetic variables are in part aeolian, i.e. nonstationary cycles that wax and wane in amplitude, A, to the point of disappearance and reappearance, that drift in period, sometimes bi- and trifurcating, and drift in phase, φ. These cycles are nonstationary in time and in space [11, 12].

Environmental about half-weekly periods are likely harmonics of the sun's rotation around its axis at the solar equator and influence geomagnetic indices like Kp. A likely double tidal contribution and its harmonics are difficult to separate, although this has been attempted in a newborn studied around the clock for 27 months [2]. Other harmonics are circadiseptans, described by Hermann Fritz in 1888, as an ~13.8-day cycle and by Franz Halberg [10]. With a different (selective) assortment, circaseptans have been found in an individual, in the form of congruent periods of blood pressure and heart rate with periods in the solar wind and/or the geomagnetic indices aa, Kp and/or Dst [13]. The biospheric circaseptans were damped but persisted in the absence of circaseptans in the area of sunspots [14]. Thus, a link between the sun and the earth's magnetism, and our heart and circulation was rendered extremely likely at multiseptan frequencies [10].

Non-photic solar effects in humans are not consciously perceived, that is, "felt", even though space may have wide biospheric implications [15; 10]. Associations are already documented for the human circulation and for mental and cellular functions with geo- and interplanetary magnetism [16-19]. Emphasis was placed on the study of shared frequencies or their reciprocals, the periods, period. Rather than looking for the same point estimates of period in paired nonstationary wobbly oscillations, we compare interval estimates of periods in view of the ever-present uncertainties. Consequently, congruence is a way to assess corresponding periods by the presence or absence of overlap between the CIs (95% confidence intervals) of the paired periods, found by the non-linearly extended cosinors in time series of geomagnetic indices, C9, Cp and Kp on the one hand and on the other hand in separate data sets of SBP (systolic blood pressure), DBP (diastolic blood pressure) and HR (heart rate) of treated cardiac patients, each monitored ambulatorily. Widely known researches studied the effect of the solar magnetic cycles of solar activity and magnetic storms on various aspects of human life, physiological parameters, and including cardiovascular system [13, 14, 17, 19]. Also are known geographical differences associated with superposition of geomagnetic and heliomagnetic fields, that local, specific for each of the geographical areas [3, 4]. Almaty in this aspect is a specific region, located in the foothills and earthquake-prone area, the population of this largest metropolis in Central Asia undergoes a more pronounced influence of the solar magnetic storms and the effect of the geomagnetic field more pronounced in connection with the periodic seismic activity, but we didn't found research related geomagnetic influence to cardiovascular diseases in this region.

Materials and methods

We performed this retrospective forward observational study in the "Smart health university city" Kazakh National university, Almaty, Kazakhstan from January 2018 to December 2019. We consecutively recruited patients older than 18 years patients with diagnosed hypertension after treatment. In total, 360 patients (167M +193F) were enrolled in this study. The TM-2430 monitor from A&D (Japan), BPLab monitor from OOO Petr Telegin (Russia) was used to measure BP and HR.

Averages per 24 hrs of HR and S or DBP were assigned to the calendar date of the monitoring and spectra of each time series as a whole (globally in time) were separately computed for men and women and for each variable. Mean values assigned to the date of monitoring were assembled irrespective of age into two separate series by gender. Basic congruences were subsequently sought and found among the series of the mean values of each of the individuals and each of the variables in each set, and further between the paired periods of geomagnetic and organismic time series, with focus on the about half-weekly (circasemiseptan) spectral region. A combination of linear and nonlinear cosinor methods [5, 6, 8, 9] served for temporally global analyses (of a time series as a whole). Plexograms, complemented by analyses of variance of the stacked data visualized signals detected by cosinor spectra [5, 6, 8]. For each series data were analyzed by sphygmochron [6], consisting of parametric and non-parametric assessments. Parametrically, by least squares (Figure 1), a two-component model, consisting of cosine curves with anticipated periods of 24 and 12 hours, is fitted to the data (Figure 2) yielding estimates of the MESOR (*M*, Midline Estimating Statistic Of Rhythm), 24-hour and 12-hour double amplitudes (2A) and acrophases (φ) [6].

The study was done after clearance from the local bioethical committee of the Al-Farabi Kazakh National University, IRB00010790, protocol No. IRB-A080) and consent was taken from all subjects.

Results and discussion

Non-parametrically, percentage time elevation, area of excess and timing of largest excess are determined by numerical integration. In addition to MESOR-hypertension, deviations from these chronobiological norms lead to diagnoses of CHAT (Circadian Hyper-Amplitude Tension) and/or ecphasia when the 24-hr BP-2A is excessive and/or the 24-hr BP- φ is outside acceptable limits but the 24-hr HR- φ is acceptable. These conditions along with an excessive pulse pressure (above 60 mmHg) and a deficient HR variability (standard deviation of HR <7.5 beats/min) constitute Vascular Variability Anomalies (VVAs) when present during one or a few days, or Vascular Variability Disorders (VVDs) when the abnormalities are confirmed over repeated week-long records in the absence of a persisting load [20]. Any two or more coexisting VVDs are referred to as Vascular Variability Syndromes (VVSs).

The figure 1 shows that after treatment, arterial hypertension, with which all patients were referred, remained in 27% of patients, in a small part, mainly women, the SBP mesor (2.5%) and the DBP MESOR (6.4%) fell even below the normocoridor, almost one third of patients (28.3%) had bradycardia, 22% of patients had no VVA, whereas 50% had multiple VVAs, Figure 1. CHAT of SBP and DBP, deficient heart rate variability, etc. were found, each of which increases the likelihood of complications of cardiovascular diseases, up to lethal [20].

The performed spectral analysis of the aggregate ABPM data and fluctuations in geomagnetic activity in the same time period revealed a number of periodicities up to month. Some circasemiseptan periods are shared by SBP, DBP and HR in female patients and further by C9 and Cp. Kp reveals a period of 4.31 days, with an even longer period found for SBP in men in the spectral region examined, the periods being picked because of their statistical significance in that spectral region. The gender differences in HR and SBP have their precedents in other regions of the circasemiseptan spectrum of these variables.

The circaseptan coperiodisms between geomagnetic indices, Kp, Cp, C9 and cardiovascular system (SBP, DBP) in periodicity is clear for women patients only, see Table 1. The coperiodisms of HR with 10.7 C in 21 days period, and the circaseptan coperiodism again only of Kp with the BP were found.

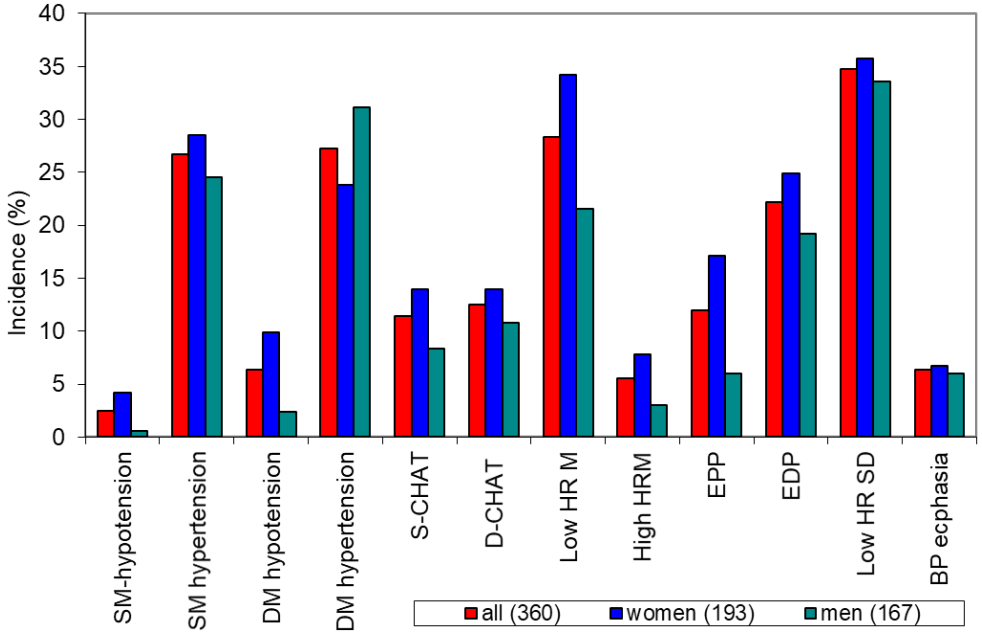

Figure 1– Incidence of VVAs in about 24-hr ABPM records obtained in routine hospital practice during consecutive two years
SM – SBP MESOR, DM – DBP MESOR, S-CHAT – Circadian Hyper-Amplitude-Tension (CHAT) of SBP, D-CHAT – CHAT of DBP, EPP – Excessive pulse pressure, EDP – Excessive double product, SD – standard deviation

Table 1 – Coperiodism geomagnetis and cardiovascular indices in circaseptan-monthly range

	SBP		DBP		HR		Kp	Ap	Cp	C9	10.7C
	men	women	men	women	men	women					
Period, days	7.9*; 9.1*	7*; 21*	9.1*	7*	14.4*; 21*	6.4*; 21*	7*; 14*	8.7**; 13.65*	14*	14*	15.6*; 21*

Note: *p<0.05; **p<0.001

However, acrophases in this circaseptan rhytms are not in same phase time, vascular answer time is differ with geomagnetic acrophases time for about 2-3 days. Earlier in the literature, the "anticipatory response" of heart rate, blood pressure and other physiological parameters has already been described, which can occur 2–3 days before the onset of magnetic storms [21]. This anticipatory effect was first discovered by Chizhevsky in the 1920s, and suggested that some unknown solar radiation was responsible for this [22, 23]. The increased radiation caused by coronal ejections reaches the Earth in 8 minutes, while the increased density and speed of the solar wind takes several days to reach the Earth's magnetosphere, resulting in a magnetic storm [21].

21-days period in HR, male and female patients both correlates to 10.7C geomagnetic indices. The dispersion of the acrophase time lies within the same range. Sex differences had been noted earlier in the circadian MESOR and circadian double amplitude of heart rate variability in the range of seconds and minutes. Moreover, an about 2-week cycle in the ECG was detected for heart rate only in women (not in men) [24].

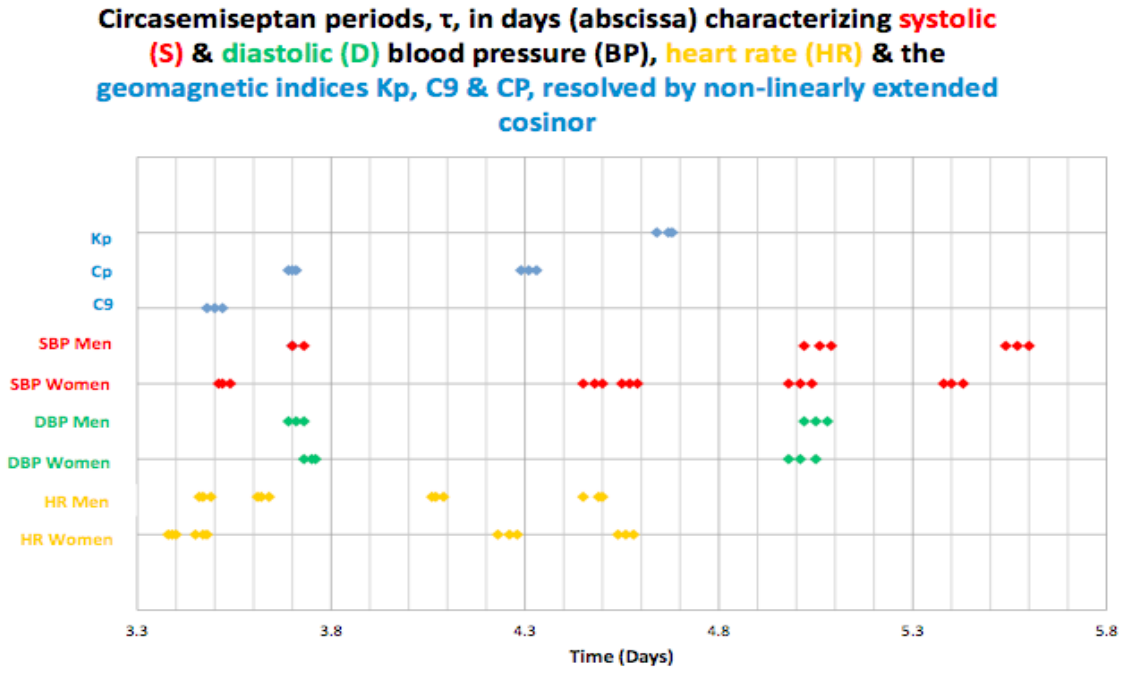

Figure 2 –Circasemiseptan coperiodism between geomagnetics indices (Kp, C9 & Cp) and the human circulation. Periods – in days, abscissa.

Figure 2 shows differences among variables and further differences between genders, as well as among the geomagnetic indices, which is consistent with previous studies [25]. Some circasemiseptan periods are shared by SBP, DBP and HR in female patients and further by C9 and Cp. Kp reveals a period of 4.31 days, with an even longer period found for SBP in men in the spectral region examined, the pe-

riods being picked because of their statistical significance in that spectral region. The gender differences in HR and SBP are also present in other regions of the circasemiseptan spectrum of these variables [21; 24].

Analysis of cardiovascular monitoring data for geomagnetic and other coperiodisms will be important to rule out chance contributing to congruence, once more than the 6 pooled time series examined herein on a few hundred patients become available on much larger data sets. Beyond establishing the degree of generality of congruences, one could try, notably on longer series, to implement a remove-and-replace approach [10; 25]. The relative merits of various helio- and geomagnetic indices, other than those here studied, could then also be examined in the light of biological coperiodisms, assuming that sooner or later a remove-and-replace or at least a subtract-and-add approach has found biospheric consequences, associated with changes with a geomagnetic coperiodism. In Figure 2, C9 and Cp seem to be closer to the human circulation than Kp.

Monitoring the environment by self-measurement of blood pressure on a population basis has already served to detect the after-effect of the Japanese earthquake and tsunami in Sendai in 2011 [26]. Staff measurements in Ladakh, Kashmir, India, have detected the paradecadal solar cycle's signature primarily in the systolic blood pressure of men and diastolic blood pressure of women, again on a population basis [26]. Ambulatory blood pressure measurements on a relatively small group of 11 subjects found an increase in systolic blood pressure for 2 days before the Sendai earthquake and tsunami [28]. The concomitant geomagnetic and cardiovascular monitoring may contribute to understanding cataclysms of societal health, including military and political affairs, that carry signatures of the sun in the decadal spectral range [10]. Coperiodisms in the circasemiseptan range involve a much shorter turn-around time for interpretation and are particularly pertinent to neonatology, when the infradians (near the circadians) dominate in the spectrum. Furthermore, in this range, by several methods, an association with the human heart has been validated by cross-spectral coherence with both geo- and interplanetary magnetism [10].

Conclusion

Some circasemiseptan periods are shared by SBP, DBP and HR in female patients and further by C9 and Cp. Kp reveals a period of 4.31 days, with an even longer period found for SBP in men in the spectral region examined, the periods being picked because of their statistical significance in that spectral region. The coperiodisms of HR with 10.7 C in 21 days period, and the circaseptan coperiodism again only of Kp with the BP were found. The circaseptan 7-days rhythms were significant in BP women' variable only, and in geomagnetic indices, for Kp, acrophases in this circaseptan rhytms are not in same phase time, vascular answer time differs with geomagnetic acrophases time for about 2-3 days. Such "anticipatory response" of blood pressure may contribute to work with bioindication of cataclysms.

Acknowledgment

This work was supported by a grant from the Ministry of Education and Science of the Republic of Kazakhstan, № AP05133311 "The study of the chronophysiological mechanisms of the human's cardiovascular system' adaptation to the environmental abiotic and socio-ecological factors"

References

1 Halberg, F., Düll-Pfaff, N., Gumarova, L., Zenchenko, T. A., Schwartzkopff, O., Freytag, E. M., Freytag, J., and Cornelissen, G. (2013) 27-day cycles in human mortality: Traute and Bernhard Düll, *History of Geo- and Space Sciences*, 4, 47–59, https://doi.org/10.5194/hgss-4-47-2013

2 Halberg F, Cornélissen G, Otsuka K, Watanabe Y, Beaty L, Gumarova L, Revilla M, Schwartzkopff O, Siegelova J, Singh R.B. Monitoring chronoosphere for knowing oneself and one's environs // *Geophysical processes and biosphere*, 2013, т.12, №4, с. 5-35 https://doi.org/10.21455/gpb

3 Gumarova L, Cornelissen G, Hillman D, Halberg F. Geographically selective assortment of cycles in pandemics: Meta-analysis of data collected by Chizhevsky. // *Epidemiology and Infection*, Volume 141, Issue 10, 2013 pp 2173-2184 https://doi.org/10.1017/s0950268812002804

4 Gumarova L, Cornelissen G. Terrestrial and solar magnetism' influence to diphtheria pandemics // *International Journal of Biology and Chemistry*. – 2016, volume 9, N.2, pp. 4-10https://doi.org/10.26577/2218-7979-2016-9-2-4-10

5 Halberg F. (1980) Chronobiology: methodological problems. Acta med rom, 18, pp. 399-440. http://dx.doi.org/10.4249/scholarpedia.3008

6 Refinetti R, Cornélissen G, Halberg F. (2007) Procedures for numerical analysis of circadian rhythms.

Biological Rhythm Research, vol. 38 no. 4, pp. 275-325. http://dx.doi.org/10.1080/09291010600903692.

7 Bingham C, Arbogast B, Cornélissen G, et al. (1982) Inferential statistical methods for estimating and comparing cosinor parameters. Chronobiologia, 9, pp. 397–439. PMID: 7168995. https://www.ncbi.nlm.nih.gov/pubmed/7168995

8 Cornélissen G, Halberg F. (2005) Chronomedicine. In: Armitage P, Colton T, editors. Encyclopedia of Biostatistics, 2nd ed. Chichester, UK: John Wiley & Sons Ltd. pp. 796-812.

9 Marquardt DW. (1963) An algorithm for least-squares estimation of nonlinear parameters. J Soc Indust Appl Math, 11, pp. 431-441. https://doi.org/10.1137/0111030

10 Otsuka, K., Cornelissen, G., Halberg, F. (2016). From Chronomics to Chronoastrobiology: Many Rhythms Are Control Information for Whatever We Do. Chronomics and Continuous Ambulatory Blood Pressure Monitoring, 53–98. doi:10.1007/978-4-431-54631-3_2

11 Halberg, F., Sothern, R. B., Watanabe, Y., Hillman, D., Best, W. R., Schwartzkopff, O., & Cornelissen-Guillaume, G. G. (2014). Signatures of space weather in the aging human blood circulation? In *Cardiovascular Health and Chronomics* (pp. 37-58). Nova Science Publishers, Inc.. ISBN 9781629489766

12 Cornélissen G, Hillman D, Katinas GS, et al. Geomagnetics and society interact in weekly and broader multiseptans underlying health and environmental integrity. *Biomed Pharmacother*. 2002;56 Suppl 2:319s-326s. https://doi:10.1016/s0753-3322(02)00310-4

13 Guillaume, G.C., Gubin, D., Beaty, L.A., Otsuka, K. (2020) Some near-and far-environmental effects on human health and disease with a focus on the cardiovascular system // International Journal of Environmental Research and Public Health, 17, 3083; https://doi.org/10.3390/ijerph17093083

14 Cornélissen G, Halberg F, Wendt HW, Bingham C, Sothern RB, Haus E, Kleitman E, Kleitman N, Revilla MA, Revilla M Jr, Breus TK, Pimenov K, Grigoriev AE, Mitish MD, Yatsyk GV, Syutkina EV. (1996) Resonance of about-weekly human heart rate rhythm with solar activity change. *Biologia (Bratislava),* 51, pp. 749-756.

15 Kamide Y. (2005) We reside in the sun's atmosphere. *Biomedicine & Pharmacotherapy* 59p. (Suppl 1): S1-S4. PMID: 16275476. https://doi.org/10.1016/S0753-3322(05)80001-0

16 Cornélissen G, Grambsch P, Sothern RB, Katinas G, Otsuka K, Halberg F. Congruent biospheric and solar-terrestrial cycles. Journal of Applied Biomedicine 2011; 9: 63-102. https://doi.org/10.2478/v10136-009-0023-7

17 Halberg F, Cornélissen G, Grambsch P, McCraty R, Beaty L, Siegelova J, Homolka P, Hillman DC, Finley J, Thomas F, Kino T, Revilla M, Schwartzkopff O. (2009) Personalized chronobiologic cybercare; other chronomics' progress by transdisciplinary cycles' congruences: Season's Appreciations. J Appl Biomed 2011; 9: 1-34. https://doi.org/10.2478/v10136-009-0022-8

18 Jozsa R, Halberg F, Cornélissen G, Zeman M, Kazsaki J, Csernus V, Katinas GS, Wendt HW, Schwartzkopff O, Stebelova K, Dulkova K, Chibisov SM, Engebretson M, Pan W, Bubenik GA, Nagy G, Herold M, Hardeland R, Hüther G, Pöggeler B, Tarquini R, Perfetto F, Salti R, Olah A, Csokas N, Delmore P, Otsuka K, Bakken EE, Allen J, Amory-Mazaudier C. (2005) Chronomics, neuroendocrine feedsidewards and the recording and consulting of nowcasts – forecasts of geomagnetics. Biomed &Pharmacother; 59 (Suppl 1): S24-S30. https://doi.org/10.1016/s0753-3322(05)80006-x

19 Kuzmenko, N.V.; Shchegolev, B.F.; Pliss, M.G., Tsyrlin, V.A. (2019) Influence of weak geomagnetic disturbances on rat's cardiovascular system in natural and shielded geomagnetic field conditions. // Biophysics, Vol: 64, Issue 1, pp.:131-139 https://doi.org/10.1134/S0006302919010162

20 Halberg, F., Cornélissen, G., Otsuka, K., Siegelova, J., Fišer, B., Dušek, J., Homolka, P., de la Peña, S.S., Singh, R.B. (2011) Extended consensus on need and means to detect vascular variability disorders (VVDs) and vascular variability syndromes (VVSs) World Heart Journal, Volume 4, Issue 4, pp 279-305, ISSN: 1556-4002

21 McCraty R, Atkinson M, Stolc V, Alabdulgader AA, Vainoras A, Ragulskis M. (Jul 13, 2017) Synchronization of Human Autonomic Nervous System Rhythms with Geomagnetic Activity in Human Subjects. Int J Environ Res Public Health.; 14(7):770. https://doi:10.3390/ijerph14070770

22 Khabarova O. Investigation of the tchizhevsky-velhover effect. Biophysics. 2004;49:S60-67

23 Chizhevsky A.L. About one type of specifically bioactive or Z-radiation from the Sun. In book: Cosmic pulse of life: earth in the arms of the sun; Heliotaraxia. M., Mysl, 1995, pp. 725-738. ISBN 5-244-00776-IX

24 Cornélissen G, McCraty R, Atkinson M, Halberg F. (June 3, 2010) Gender differences in

circadian and extra-circadian aspects of heart rate variability (HRV). Time Series (not spotcheck) Evidence-Based Holistic Approach to Health, 1st International Workshop of the TsimTsoum Institute, Krakow, Poland, pp. 27-28. https://doi.org/10.1037/e537902011-001

25 Halberg F, Cornélissen G, Sothern RB, Katinas GS, Schwartzkopff O, Otsuka K. (Invited presentation, Nishinomiya-Yukawa International & Interdisciplinary Symposium 2007, What is Life? The Next 100 Years of Yukawa's Dream, Yukawa Institute for Theoretical Physics, Kyoto University, October 15-20, 2007. Progress of Theoretical Physics 2008) Cycles tipping the scale between death and survival. Pp. 153-181. https://doi.org/10.1143/PTPS.173.153

26 Satoh M, Kikuya M, Ohkubo T., Imai Y. (2011) Acute and subacute effects of the great East Japan earthquake on home blood pressure values., vol. 58, no. 6. https://doi.org/10.1161/hypertensionaha.111.184077

27 Otsuka Ku, Yatagai A, Nakaoka T, Otsuka Ke, Otsuka Y, Ishikawa M, Watanabe Y, Okumiya K, Matsubayashi K, Norboo T, Cornélissen G, Halberg F. (4-8 June 2012) Astro-glocal spatially and temporally (global & local) comprehensive health watch especially at high altitude. Proceedings, Space Weather Effects on Humans in Space and on Earth, Moscow, pp. 31-32. https://doi.org/10.1007/978-4-431-54631-3_22

28 Watanabe Y, Halberg F, Otsuka K, Cornélissen G. (19-21 September 2011. London: SWB International Publishing House; 2012) Physiology and earthquakes, focusing on that in 2011 in East Japan. Proceedings, Natural Cataclysms and Global Problems of the Modern Civilization, Istanbul, pp. 260-264.

IRSTI 34.23.53 https://doi.org/10.26577/ijbch.2020.v13.i2.07

O.K. Khamdiyeva*, Z.B. Tileulesa, G.S. Baratzhanova,
S.S. Murzataeva, E.M. Khussainova, S. Abdikerim,
A. Childebayeva, L.D. Djansugurova

Institute of General Genetics and Cytology CS MES RK, Almaty, Kazakhstan
*e-mail: azadahamdieva@gmail.com

Next Generation Sequencing in diagnosis of mitochondrial epilepsy

Abstract. Epilepsy is a common manifestation of mitochondrial disorders, in addition mitochondrial oxidative stress may play an important role in epileptogenesis since it affects the excitability of neurons. Mitochondrial diseases are often difficult to diagnose unless the symptoms are clearly identified as a part of a specific mitochondrial mutation. The use of next-generation sequencing would lead to the rapid identification of genes associated with epilepsy syndromes. In this study, we evaluate the applicability of the NGS method for diagnosis of mitochondrial epilepsy by clinicians and laboratories in Kazakhstan. We performed complete mitochondrial genome sequencing on the Illumina MiSeq platform for 6 patients with epilepsy. Using the MITOMAP and HmtDB databases, we identified three pathogenic variants (MT-ND1 m.3697G> A, m.5628T> C and m.7547T> C) leading to the development of epilepsy, additionally we found 6 variable sites (m.5586C> T, m.10095C> T, 514_515delCA, 16180_16181delAA, C514.CACACA, A955. ACCCC), the clinic of which was not previously mentioned in the literature. Our preliminary study suggests that mitochondrial genes potentially play a role in the pathogenesis of epilepsy and mutations in these genes cause various forms of epilepsy. It is necessary to elucidate the main mechanisms and participation of variants of mtDNA haplogroups in the development of epilepsy to apply the NGS method in diagnosis of mitochondrial epilepsy.

Key words: Epilepsy, Next Generation Sequencing, mitochondrial DNA, mutation.

Introduction

Epilepsy is a chronic neurological disease with a high degree of genetic heterogeneity, which is accompanied by recurrent unprovoked seizures and has different clinical manifestations. The overall incidence of epilepsy is 61.4 per 100,000 people [1]. Long course, low cure rates, and high rates of disability from illness have a profound impact on patients and society. In recent years, numerous studies have been conducted on the pathogenesis of epilepsy, but despite this, the exact mechanism of the disease has not been fully understood. Presumably 20-30% of epilepsy cases are caused by acquired conditions, such as skull trauma, previous stroke, brain tumors, previous infectious diseases of the brain [2, 3], but the remaining 70-80% of cases are caused by one or more genetic factors [4].

Mitochondrial dysfunction and oxidative stress are considered as factors that play a role in the pathogenesis of a number of neurological diseases, including epilepsy [5]. Many studies show the relationship between mitochondrial dysfunction and epilepsy, but most of them does not study mitochondrial genome (mtDNA) of patients suffering mitochondrial diseases which would be extremely important for determining the role of mitochondrial genome in the development of disease and for the treatment of patients as mitochondrial epilepsy is often difficult to treat and resistant to antiepileptic drugs. Diagnosis of mitochondrial disease is often challenging unless the symptoms are clearly identified as part of a specific mitochondrial mutation [6].

Screening for mutations of the underlying genetic defects in epilepsy is often complicated by the many presumably responsible genes. Next Generation Sequencing (NGS) is a valuable and reliable diagnostic tool for massively parallel sequencing of as many genes as possible, and it is a fast and cost-effective diagnostic method to analyze genetic cause of epilepsy [7].

The use of NGS technologies in research and diagnostic laboratories has led to the rapid identifica-

tion of genes associated with epilepsy syndromes. In this study, we will evaluate the suitability of the NGS method for diagnosis of mitochondrial epilepsy by clinicians and laboratories in Kazakhstan.

Materials and methods

Patients. The study protocol was approved by the local ethics committee of the Kazakh-Russian Medical University (protocol No. 51 from 05.09.2017). The studies included three patients with epileptic encephalopathy and three patients with myoclonic epilepsy. All patients were treated at SVS clinic (Almaty, Kazakhstan). When collecting biological material, patients filled out a questionnaire and signed an informed consent form.

DNA isolation and sequencing. Total DNA was extracted by GeneJet Genomic DNA Purification Kit (Thermo Fisher Scientific, USA) according to the protocol recommended by the manufacturer. We used MiSeq Sequencing Platform (Illumina, USA) and Nextera XT Library Prep Kit to sequence the entire human mitochondrial DNA (mtDNA) genome. During sample preparation, the mtDNA genome was amplified in two PCRs to generate two long fragments spanning the entire human mitochondrial genome (16,569 bp). The amplicons were quantified and pooled before library preparation.

Primers
MTL-F1 5'- AAA GCA CAT ACC AAG GCC AC -3'
MTL-R1 5'- TTG GCT CTC CTT GCA AAG TT -3'
MTL-F2 5'- TAT CCG CCA TCC CAT ACA TT -3'
MTL-R2 5'- AAT GTT GAG CCG TAG ATG CC -3'

Data analysis. Raw FASTQ files were processed and mapped to the mitochondrial reference rCRS using Eager [8]. Genotyping was performed using GATK HaplotypeCaller and Genotype GVCF [9]. Geneious software version 2019.2.1 was used to visually assess the sequencing depth and the quality of genotype calling [10]. The genome for alignment is the Revised Cambridge Reference Sequence (rCRS), a mtDNA genome used by the Forensic Genomics community. Confirmed differences from the CRS were compared to previously reported mutations or polymorphisms listed in the MITOMAP database (http: //www.mitomap.org) and HmtDB (http://www.hmtdb.uniba.it).

Results and discussion

Mitochondrial diseases encompass a genetically and clinically heterogeneous group of diseases caused by defects in mitochondrial oxidative phosphorylation. Epilepsy is a common manifestation of mitochondrial disorders; in addition, mitochondrial oxidative stress may play an important role in epileptogenesis, as it affects the excitability of neurons [11].

mtDNA mutation analysis. We sequenced using NGS the mitochondrial genome of 6 patients with epileptic encephalopathy and myoclonic epilepsy. Bioinformatic analysis of NGS data showed the presence of 115 mutations, of which 80 mutations are localized in genes encoding proteins; the D-loop was also a sensitive region in which we found 35 variable sites. Using the MITOMAP and HmtDB databases, we found 21 missenses, 41 synonymous variants, 11 mutations in the 12S rRNA and 16S rRNA genes, 5 mutations in the tRNA genes (MT-TA, MT-TC, MT-TD, MT-TH, MT- TR) and two mutations in the regulatory region of the MT-NC3 gene. The distribution of variable sites in each gene is shown in Figure 1.

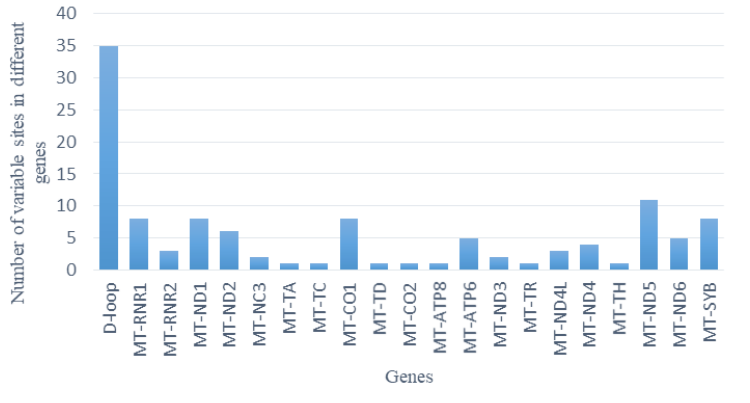

Figure 1 – The distribution of variable sites in each gene

Variable sites in the MT-ND5 gene were more frequent (11 mutations), 8 mutations were found in the MT-RNR1, MT-CO1, MT-ND1 and MT-CYB genes, 6 mutations were in the MT-ND2 gene, 5 variable sites were identified in the MT-ND6 and MT-ATP6 genes, 4 variable sites were in the MT-ND4 gene, the MT-RNR2 and MT-ND4L genes each had 3 variable sites, the MT-ND3 and MT-NC3 genes had 2 mutations. The least variable sites were in the genes of the transport RNA, 1 each in the genes MT-TA, MT-TC, MT-TD, MT-TH, and MT-TR. According to the MITOMAP and HmtDB databases, 26 mutations were associated with the development of epilepsy, 17 of them (Table 1) of them occurred in positions associated with haplogroups, and 9 mutations (Table 2) were directly involved in the development of epilepsy.

Table 1 – Variable sites of mtDNA associated with epilepsy and haplogroups

POS	Locus	Mutation type	AA Change		Population frequency	
				dbSNP ID	MITOMAP	1000G
152	MT-HV2	T→C		rs117135796	26.319%	NA
183	MT-HV2	A→G		rs113913230	0.6%	0.0078
961	12S rRNA	T→C		rs3888511	0.9%	0.0066
1736	16S rRNA	A→G		rs193303006	2.7%	0.0477
5628	MT-TA	T→C		rs1556423015	0.19%	0.0062
6671	MT- CO1	T→C	Syn: His256 His	rs1978028	0.7%	0.0033
6962	MT-CO1	G→A	Syn: Leu353Leu	rs1970771	2.4%	0.0271
7547	MT-TD	T→C		rs879076142	0.107%	NA
7738	MT-CO2	T→C	Syn: Thr51Thr	rs878875354	0.2%	NA
8794	MT-ATP6	C→T	Non-syn: His90Tyr	rs2298007	2.8%	0.045
8887	MT-ATP6	A→G	Non-syn: Ile121Val	rs1556423565	0.2%	0.0029
10310	MT-ND3	G→A	Syn: Leu84Leu	rs41467651	3.6%	0.0382
10410	MT-TR	T→C		rs200478835	0.5%	0.0054
10609	MT-ND4L	T→C	Non-syn: Met47Thr	rs200487531	2.4%	0.0255
13368	MT-ND5	G→A	Syn: Gly344Gly	rs3899498	5.0%	0.023
14569	MT-ND6	G→A	Syn: Ser35Ser	rs386420019	2.5%	0.0233
14668	MT-ND6	C→T	Syn: Met2Met	rs28357678	4.1%	0.0468

Mainly single nucleotide substitutions were found in genes encoding proteins, most of them are synonymous (7 variants: His256 His, Leu353Leu, Thr51Thr, Leu84Leu, Gly344Gly, Ser35Ser, Met-2Met). The frequency of these mutations according to the MITOMAP database was less than 5% in the population. The frequency of the three missense mutations found in the protein encoding genes (His90Tyr, Ile121Val, Met47Thr) was less than 2.8%. Non-synonymous single nucleotide substitutions may result in dysfunction of the protein, which may cause epileptic seizures. Thus, single nucleotide substitutions found in the MT-ATP6 gene can cause the development of epileptic syndromes NARP and Leigh [12].

Thus, we identified 4 synonymous variants (Met-100Met, Ala375Ala, Ile123Ile, Leu36Leu); three non-synonymous (Gly131Ser, Thr112Ala, Hr194 Ala), and two variable regions were found in rRNA genes (m.955A> C, m.2706A> G).

The pathogenic mutation of MT-ND1 gene (Non-syn: Gly131Ser) was previously described by Kirby et al. in patients with MELAS syndrome [13]. Our study confirms the clinical significance of this mutation, as it was found in a patient with epileptic encephalopathy and was possibly the cause of epileptic seizures.

The protein encoded by the MT-ND1 gene is one of the main components that form the hydrophobic core of complex I of the mitochondrial OXPHOS complexes [14]. Defects in the respiratory chain disrupt its functioning, reduce the gradient of the mitochondrial proton potential and interfere with the synthesis of ATP in mitochondria, even if ATP synthetase is not affected [15].

Table 2 – Variable sites of mtDNA associated with epilepsy

POS	Locus	Mutation type	AA Change		Population frequency	
				dbSNP ID	MITOMAP	1000G
955	12S rRNA	A→C		rs1556422497	0.006%	0.0004
2706	16S rRNA	A→G		rs2854128	78.9%	NA
3697	MT-ND1	G→A	Non-syn: Gly131Ser	rs199476122	NA	0.0004
4769	MT-ND2	A→G	Syn: Met100Met	rs3021086	97.6%	NA
7028	MT-CO1	C→T	Syn: Ala375Ala	rs2015062	80.8%	NA
8860	MT-ATP6	A→G	Non-syn: Thr112Ala	rs2001031	98.5%	NA
12705	MT-ND5	C→T	Syn: Ile123Ile	rs193302956	41.8%	NA
14854	MT-CYB	C→T	Syn: Leu36Leu	rs1057516071	0,012%	NA
15326	MT-CYB	A→G	Non-syn: Hr194Ala	rs2853508	98.65%	NA

Two mutations found in the transport RNA genes (m.5628T> C and m.7547T> C) are predicted to be pathogenic (disease Score: 0.75 and 0.5) according to the HmtVar Pathogenicity Prediction database. Over the past 20 years, many studies have found links between inherited population variants of mtDNA and neurological diseases. Since the first association of Leber hereditary optic neuropathy (LHON) with mitochondrial haplogroup J in the late 90s was revealed [16-19], many other mitochondrial disorders along with classic neurodegenerative diseases such as Parkinson's disease (PD), Alzheimer's disease (AD), disseminated sclerosis (MS) and amyotrophic lateral sclerosis (ALS) were also associated with mitochondrial disfunction [20].

In the case of MELAS, a study of 142 unrelated french families with the m.3243A> G mutation found statistically significant under-representation of the mutation in patients with haplogroup J [21]. Analysis of the same mutation in a smaller sample of the Spanish population found no association [22].

The increased risk of diseases with a mitochondrial contribution to pathogenesis is most likely determined by the balance between beneficial and damaging mtDNA mutations in haplogroups. In the case of some haplogroups, the balance tends more towards the harmful side. Deleterious mtDNA mutations are supposed to be population-specific, that is one variant may be associated with disease in one population but not in another [23].

Using the next-generation sequencing we revealed 6 variable sites in patients with epilepsy, the clinic of which was not previously mentioned in the literature (Table 3).

Table 3 – Variants of unknown significance

POS	Locus	Mutation typy	AA Change	dbSNP ID	Population frequency	
					MITOMAP	1000G
514	D-loop	GCA→ GCACACA			0.061%	
514-515	D-loop	GCA→ G			23.838%	
955	12S rRNA	A→ACCCC			NA	
5586	MT-NC3	C→T		rs879067503	0,104%	
10095	MT-ND3	C → A	Non-syn: Leu13Met		0.002%	
16179	D-loop	CAA → C		rs371240719	0,00%	0.0084

Genetic variants with unknown significance were mainly found in regulatory regions and were represented by deletions (514_515delCA and 16180_16181delAA), insertions (C514.CACACA and A955.ACCCC) and single nucleotide substitutions (m.5586C> T and m.10095C> A).

Deletion of 514_515delCA was detected in 3 patients with epileptic encephalopathy and in 1 with myoclonic epilepsy. The pathogenicity of these variable sites has been tested in the MITOMAP and HmtDB databases and has not been confirmed. A non-synonymous mutation in the MT-ND3 gene resulted in the substitution of the amino acid leucine for methionine at position 13. The pathogenicity of this mutation was confirmed in the HmtDB database (disease Score: 0.71) and its population frequency is 0.002%, but despite this, the clinic of this mutation is not described. Previously, mutations in the MT-ND3 gene have been described for patients with Lee syndrome and MELAS [24]. Xiao-Li Fu et al. described the T10158C mutation in the MT-ND3 gene for patients with mitochondrial encephalopathy [25]. In our case, the MT-ND3 gene mutation m.10095C> A was found in a patient with epileptic encephalopathy.

Conclusion

Advances in DNA sequencing and interpretation of genetic variation are rapidly changing our understanding of the etiology of epilepsy, which affects clinical diagnostic and treatment protocols. In developed countries, genetic testing for epilepsy is rapidly entering clinical practice, helping to accurately diagnose the type of epilepsy, establish hereditary epileptic syndromes, predict the course of the disease, choose specific treatment, and identify the risk of developing epilepsy for other family members. Unfortunately, in Kazakhstan, genetic methods for diagnosing epilepsy have not yet been introduced into medical practice. Many patients from Kazakhstan and Central Asia apply to laboratories in other countries for molecular genetic diagnosis of epilepsy.

Our preliminary study suggests that mitochondrial genes potentially play a role in the pathogenesis of epilepsy and identify subgroups of patients with different clinical phenotypes. To apply the NGS method in the diagnosis of mitochondrial epilepsy by clinicians and laboratories, it is necessary to determine the main mutations associated with the development of the disease and elucidate the role of haplogroup variants associated with the development of epilepsy. For this purpose, we plan to increase the sample and sequence of mtDNA in patients with epilepsy in the Kazakhstani population.

Acknowledgments

We would like to express our gratitude to Professor Sergey V. Savinov, the director of the SVS clinic by V.M. Savinov (Almaty, Kazakhstan) and doctors for the help in collecting biosamples and clinical testing of patients. We also thank all volunteers involved in research. This work was supported by the grant AP05131747 “The study of molecular genetic aspects of hereditary forms of epilepsy in populations from Kazakhstan” CS MES RK, 2017-2019.

References

1 Fiest K.M., Sauro K.M., Wiebe S., Patten S.B., et al. (2017) Prevalence and incidence of epilepsy: A systematic review and meta-analysis of international studies. Neurology. vol. 88, no. 3, pp. 296–303. https://doi.org/10.1212/WNL.0000000000003509.

2 Patel M. (2004) Mitochondrial dysfunction and oxidative stress: cause and consequence of epileptic seizures. Free Radic Biol Med. vol. 37, no. 12, pp. 1951–1962. https://doi.org/10.1016/j.freeradbiomed.2004.08.021.

3 Turnbull J., Lohi H., Kearney J.A., Rouleau G.A., et al. (2005) Sacred disease secrets revealed: the genetics of human epilepsy. Hum Mol Genet. vol. 14, no. 2, pp. 2491–2500. https://doi.org/10.1093/hmg/ddi250.

4 Olson H., Shen Y., Avallone J., Sheidley B.R., Pinsky R., Bergin A.M., et al. (2014) Copy number variation plays an important role in clinical epilepsy. Ann Neurol. vol. 75, pp. 943–958. https://doi.org/10.1002/ana.24178.

5 Vasenina E.E., Levin O.S. (2013), Oxidizing stress in patogeneza of neurodegenerate diseases: possibilities of therapy. Modern therapy in psychiatry and neurology. no. 13-14. pp. 39-46.

6 Chevallier J.A., Von Allmen G.K., Koenig M.K., (2014) Seizure semiology and EEG findings in mitochondrial diseases. Epilepsia. vol. 55, pp. 707–712. https://doi.org/10.1111/epi.12570.

7 Dunn P., Albury L.C., Maksemous N., Benton M.C., et al., (2018) Next Generation Sequencing Methods for Diagnosis of Epilepsy Syndromes. Front Genet. vol. 7, no. 9, pp. 20. https://doi.org/10.3389/fgene.2018.00020.

8 Peltzer A., Jäger G., Herbig A., Seitz A., et al., (2016) EAGER: efficient ancient genome reconstruction. Genome Biology. vol. 17, no. 60. https://doi.org/10.1186/s13059-016-0918-z.

9 Poplin R., Ruano-Rubio V., DePristo A.M., Fennell J.T., et al. (2017) Scaling accurate genetic variant discovery to tens of thousands of samples. https://doi.org/10.1101/201178

10 Kearse M., Moir R., Wilson A., Stones-Havas S., et al., (2012) Geneious Basic: An integrated

and extendable desktop software platform for the organization and analysis of sequence data. Bioinformatics. vol. 28, no. 12, pp. 1647–1649. https://doi.org/10.1093/bioinformatics/bts199.

11 Duncan J.S., Sander J.W., Sisodiya S.M., et al., (2006) Adult epilepsy. Lancet. vol. 367, no. 9516, pp. 1087-1100. https://doi.org/10.1016/S0140-6736(06)68477-8.

12 Dautant A., Meier T., Hahn A., et al., (2018) ATP synthase diseases of mitochondrial genetic origin. Front Physiol. vol. 9,329. https://doi.org/10.3389/fphys.2018.00329.

13 Kirby D.M., McFarland R., Ohtake A., Dunning C., et al., (2004) Mutations of the mitochondrial ND1 gene as a cause of MELAS. Journal of Medical Genetics. vol. 41, no. 10, pp. 784-789. https://doi.org/10.1136/jmg.2004.020537.

14 Sharma L., Lu J., Bai Y. (2009). Mitochondrial Respiratory Complex I: Structure, Function and Implication in Human Diseases. Current Medicinal Chemistry. vol. 16, no. 10, pp. 1266–1277. https://doi.org/10.2174/092986709787846578.

15 James A.M., Murphy M.P. (2002) How Mitochondrial Damage Affects Cell Function J Biomed Sci. vol. 9, no. 6, pp. 475-87. https://doi.org/10.1159/000064721.

16 Torroni A., Huoponen K., Francalacci P., Petrozzi M., et al., (1996) Classification of European mtDNAs from an analysis of three European populations. Genetics. vol. 144, pp.1835–1850.

17 Carelli V., Ghelli A., Ratta M., Bacchilega E., et al., (1997) Leber's hereditary optic neuropathy: biochemical effect of 11778/ND4 and 3460/ND1 mutations and correlation with the mitochondrial genotype. Neurology. vol. 48, pp. 1623–1632.

18 Hofmann C., Courtillot V., Féraud G., Rochette P., et al., (1997) Timing of the Ethiopian flood basalt event and implications for plume birth and global change. Nature. vol. 389, pp. 838-841.

19 Chinnery P.F., Gomez-Duran A., (2018) Oldies but Goldies mtDNA Population Variants and Neurodegenerative Diseases. Front. Neurosci. Vol. 12. https://doi.org/10.3389/fnins.2018.00682

20 Rocher C., Taanman J.W., Pierron D., Faustin B., et al., (2008) Influence of mitochondrial DNA level on cellular energy metabolism: implications for mitochondrial diseases. Journal of Bioenergetics and Biomembranes. vol. 40, no. 59, pp. https://doi.org/10.1007/s10863-008-9130-5.

21 Torroni A., Campos Y., Rengo C., Sellitto D., et al. (2003) Mitochondrial DNA haplogroups do not play a role in the variable phenotypic presentation of the A3243G mutation. Am J Hum Genet. vol. 72, no. 4, pp. 1005-1012. https://doi.org/10.1086/373936.

22 Breen M.S., Kondrashov F.A., (2010) Mitochondrial pathogenic mutations are population-specific. Biol Direct. vol. 5, no. 68. https://doi.org/10.1186/1745-6150-5-68.

23 Taylor R.W., Singh-Kler R., Hayes C.M., Smith P.E., Turnbull D.M. (2001) Progressive mitochondrial disease resulting from a novel missense mutation in the mitochondrial DNA ND3 gene. Ann Neurol. vol. 50, no. 1, pp. 104-107. https://doi.org/10.1002/ana.1084.

24 Crimi M., Papadimitriou A., Galbiati S., et al. (2004) A new mitochondrial DNA mutation in ND3 gene causing severe Leigh Syndrome with early lethality. Pediatr Res. vol. 55, no. 5, pp. 842-846. https://doi.org/10.1203/01.PDR.0000117844.73436.68.

25 Fu X., Zhou X., Shi Z., Zheng W., (2019) Adult-onset mitochondrial encephalopathy in association with the MT-ND3 T10158C mutation exhibits unique characteristics: A case report. World J Clin Cases. vol. 7, no. 9, pp. 1066-1072. https://doi.org/10.12998/wjcc.v7.i9.1066.

IRSTI 34.31.21 https://doi.org/10.26577/ijbch.2020.v13.i2.08

Z. Zakaria[1*], L. Bekbayeva[1,2], A.V. Goncharova[3], E.-S. Negim[4]

[1]School of Distance Education, Universiti Sains Malaysia, Penang, Malaysia
[2]S.D. Asfendiyarov Kazakh National Medical University, Almaty, Kazakhstan
[3]Al-Farabi Kazakh National University, Almaty, Kazakhstan
[4]Kazakh-British Technical University, School of Chemical Engineering, Almaty, Kazakhstan
*e-mail: zuraini@usm.my

Effects of blended polyvinyl alcohol/urea on the growth, yield and chemical content of tomato (*Lycopersicon esculentum* L. Mill)

Abstract. Tomato (*Lycopersicon esculentum* L. Mill) is one of the most important solanaceous vegetables widely cultivated in the world. The growth yield and chemical content of tomato (*Lycopersicon esculentum* L. Mill) treated with nitrogen fertilizers (PU) were investigated. Nitrogen fertilizers were based on polyvinyl alcohol blended with three different composites of urea (PU35, N: 8.45%; PU50, N: 34.1%, and PU65, 44.04%). In each of the five replicates of the treatments, 500 mL (1% w/v) of PU was applied directly to the soil. The first treatment was given at 15-day-old seedlings. Thereafter, treatments were given at intervals of 15 days (6 times) each until 90 days. Final harvest was at 112 days. Data was analyzed using variance analysis (ANOVA) and compared using control without fertilizer. The vegetative growth, leaf and fruit chemical composition, and flowering and fruiting of tomato responded positively to PU fertilizers compared to control plants. However, application of PU50 (nitrogen content 34.1%) gave significant increase in vegetative growth, chlorophylls a and b, flower and fruit characteristics more than PU35, PU65 and control.

Key words: Nitrogen fertilizers, tomato, growth, yield, parameters.

Introduction

Tomato (*Lycopersicon esculentum* Miller) belongs to the family *Solanaceae* and is an important vegetable crop grown throughout the world under field and greenhouse conditions [1-5]. Growing tomato is difficult due to many constraints (diseases, climate, nutrition, etc.), while the fruit itself has to meet certain market requirements. Numerous authors have studied the effects of different plant nutrients on the yield and quality of tomato and it becomes clear that some of these nutrients play key role in tomato production [2-8]. Nitrogen is one of the most important elements for plant growth, development and nutrition. Among commonly used are ammonium-, nitrate-, amide- and cyanamide-nitrogen fertilizers [6]. A number of researchers have studied the effects of nitrogen fertilizers on growth and yield components of tomato plants [7-11]. They reported that nitrogen application showed an increase in stem length, number of flowering branches and total plant dry weight. The amount of nitrogen required for optimal growth is between 2-5 % of plant dry weight. A higher supply of nitrogen has side effects such as delayed senescence, change in plant morphology, i.e., smaller roots and higher shoot/root dry weight ratio. Therefore, management of nitrogen fertilizers such as rate, type and application time are very important [12,13]. Asit et al. [5] reported that urea fertilization at the rate of 1,000 ppm increased tomato plant height (136.2 cm), number of leaves (30.73), number of green fruits per plant at harvest (21.08), number of flower clusters (11.89), number of flowers (75.18), fruit clusters (5.81), fruits per cluster (4.14), fruits per plant (21.49), and fruit length (4.72 cm), fruit diameter (6.58 cm) and weight of individual fruit (151.0 g). Mercado et al. [14] evaluated the impact of different concentrations of nitrogen on tomato seedling production. The nitrogen fertilizer was based on N-NO^{3-} with different concentrations of 4, 8, 12 and 16 mEq/L with highest morphological values at 16 mEq/L and shortened production time of seedlings for transplant. Nitrogen had the largest effect on yield and quality of tomato [15]. Number of authors reported that increased concentration of nitrogen fertilizer led to increase in nitrogen content in plant leaves [16,17]. Increase of nitrogen content results in increased protein concentration and consecutive increase in plants vegetative growth [18]. When urea fertilizer inputs to the soil system exceed

the crop needs, there is a possibility that half of the applied fertilizer escapes to the environment due to leaching, surface runoff, decomposition and ammonium volatilization in the soil as only a fraction is actually absorbed by plants. The objective of this study was to investigate nitrogen fertilizers based on polyvinyl alcohol blended with different concentrations of urea on vegetative growth, yield and quality of tomato plants. With the use of PVA/U systems, nutrients are released at a slower rate throughout the seasons, and plants are able to take up most of the nutrients without waste by leaching.

Materials and methods

Synthesis of nitrogen fertilizers. The nitrogen fertilizers based on polyvinyl alcohol (PVA) with urea (U) were synthesized with composition ratios of 65: 35 (PU35), 50: 50 (PU50) and 35: 65 (PU65) respectively by blending polymerization in presence of acetic acid as catalyst. The preparation of nitrogen fertilizers and methods of analysis (^{1}H NMR, FTIR, SEM, DSC and TGA) have been described in a previous investigation [19]. The elemental analysis was carried out for the determination of carbon, nitrogen and oxygen content in the fertilizers as shown in Table 1.

Table 1 – Elemental composition of nitrogen fertilizer

Elements	C (%)	N (%)	O (%)
PU35	49.41	8.45	42.15
PU50	28.79	34.09	37.58
PU65	21.54	44.04	34.42

The analysis was performed on a Vario Micro Elemental Analyzer (Elementar, Germany). The chemical structure of PU is presented on Figure 1.

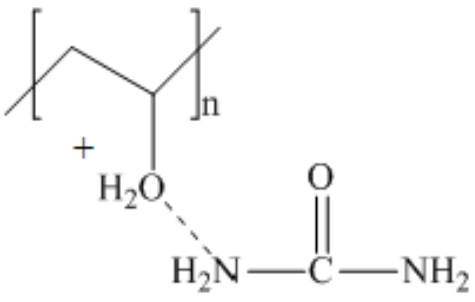

Figure 1 – Nitrogen fertilizer [polyvinyl alcohol + urea (PU)]

Nitrogen fertilizers (PU) were used in a constant concentration of 1% w/v using dH_2O.

Experimental design and treatments. The crop plant selected for the present study was *Lycopersicon esculentum* (tomato). The hybrid tomato seeds (Pearl – F1) were purchased from the local market and kept for one hour in a glass beaker with fresh water. Only the seeds that settled at the bottom of the beaker were used for the experiment. Seeds were carefully sowed in plastic trays and regular sprinkling with water was performed to keep the compost soil moist. After two weeks, germinated seedlings were transferred and planted in plastic pots. The seedlings were pushed 5 cm deep into the soil and the depression was then loosely covered back by the soil. The soil was air-dried, sieved and packed (13.5 kg/pot), and was properly filled in 15 pots.

Each pot was labelled with the pot number and the date of sowing of the seeds were recorded to determine the offset date for analysis. The day on which the seedlings were planted in the pot was treated as day zero. The plants were watered every day or on alternate days depending on the requirement.

All 3 sets were prepared in five replicates, with nitrogen fertilizer treatment given to the plants namely PU and a set of control pants. In each of the treatment, 500 mL (1% w/v) of PU was applied directly to the soil. The first treatment was given at 15-day-old seedlings. Thereafter, treatments were given at intervals of 15 days each until 90 days. The control set was watered only with tap water without any fertilizers.

Physical and chemical properties of the soil. In order to know the type and properties of soil used for the experiment, its physical and chemical properties were analyzed prior to addition of the nitrogen fertilizer (PU). Results are presented in Table 2. The ingredients of the experimental soil were a mixture of clay (56.63%), fine sand (14.22%), and silt (24.15%). The chemical properties of the soil were 1.4 mhos/cm^3, 81.0 ppm N, 3.04 ppm P, 40.8 ppm K, 0.6 ppm of organic matter and pH was 7.8.

Data recorded on vegetative growth. Plant height, number of main lateral branches, number of leaves, leaf area as well as fresh and dry weights of shoots were recorded at 4- and 8-weeks after transplanting.

Study of chemical composition. Leaf disks were taken at 4- and 8-weeks after transplanting to determine chlorophyll a, b according to the method described by Sartory and Grobbelaar [20]. Total carbohydrate content in dry matter of leaves was determined ин spectrophotometrically method described by Dubois et al. [21]. Nitrogen, phosphorus and potassium

elements were determined in the leaves of tomato plants via digestion procedure according to Piper [22]. Nitrogen content was determined by modified micro-Kjeldahl method as described by Pregl [23]. Phosphorus content in the sample was estimated using ammonium molybdate method according to Chapman and Pratt [24]. Potassium was determined using flame photometer according to reference [24].

Table 2 – Physical and chemical properties of the soil.

Physical properties (percentage of mixed type of soil)	
Sand (%)	14.22
Silt (%)	24.15
Clay (%)	56.63
Soil texture	Clay **loam**
Chemical properties	
pH	7.8
Ec (mhos/cm^3)	1.4
Available N (ppm)	81.0
Available P (ppm)	3.04
Available K (ppm)	40.8
Organic matter (%)	0.6

Study of flowering and fruit yield. Node number bearing the first flower, number of flower clusters per plant, number of flowers per cluster, number of flowers per plant, weight and number of fruits per plant were recorded.

Study of physical characteristics of fruits. Fruit shape index was calculated using the ratio of vertical to horizontal diameters. Fruit volume was determined by immersion method.

Study of chemical characteristics of fruits. Soluble solids content (SSC) was determined by hand refractometer according to the method described by AOAC, 1965 [25]. Titratable acidity was determined using the method described by AOAC, 2005 [26] and AOAC, 1970 [27]. Ascorbic acid content (vitamin C) was determined as described by AOAC, 1970 [27]. Lycopene in the tomato samples was extracted with hexane: ethanol: acetone (2:1:1) (v/v) mixture following the method of Sharma and Le Maquer [28].

Statistical analysis. The data calculated on different variables were subjected to analysis of variance (ANOVA) to observe the differences among the treatments and their interactions. Means were separated using Least Significant Difference (LSD at 5%) test. Statistical computer software Statistix 8.1 was used for computing the ANOVA and LSD [29,30].

Results and discussion

Plant height (cm). The plant height (cm) of the tomatoes treated with different nitrogen levels at 4 and 8 weeks is presented in Figure 2. As a result of the increased nitrogen rate up to PU50 (N: 34.1 %), the plant height of tomatoes is increased compared to other treatments. The plants fertilized with PU35 (N: 8.45 %) gave the tallest plant at 4 weeks (93.125 cm), while PU50 (N: 34.1 %) gave the tallest plant at 8 weeks (129 cm) compared with control (84.5 and 118.33 cm respectively). The highest N-rate of PU65 (N: 44.04 %) caused a decrease in plant height in comparison with PU35 (N: 8.45 %) lowest N-rate. The increase in plant height with N-fertilizer is attributed to the fact that nitrogen promoted plant growth which resulted in the progressive increase in plant height [31; 32]. Some investigators reported that nitrogen fertilizers including urea (46% N), ammonium sulphate nitrate (26% N), ammonium sulphate (21% N) increased plant height [31-34].

Number of lateral branches. Figure 3 shows maximum number of lateral branches per tomato plant fertilized with PU35 (N: 8.5%) at 4 and 8 weeks. PU50 (N: 34.1 %) and PU65 (N: 44.04 %) showed lower number of lateral branches per plant than PU35 and control at 4 and 8 weeks. Increases in nitrogen level within limit are associated with increase in number of lateral branches per plant [35-37]. The same behavior was reported by authors [33] when they studied synthetic polymer and nitrogen fertilizer on tomato plants. These results were also in harmony with those reported by authors [38] on mandarin. The researchers indicated that using mineral nitrogen fertilizer increased number of lateral branches per plant.

Number of leaves per plant. Increases in plant height resulted in an increase in the leaf number per plant as shown in Figure 4. Plants fertilized with PU35 (N: 8.5 %) resulted in the highest number of leaves per plant (51.5, 108.5), while the lowest number of leaves per plant was related to plant treated with PU65 (N: 40.3 %) 41 & 90.35 in the 4- and 8-weeks respectively. This is attributed to the response of tomato plants growth to nitrogen fertilizer (PU) and contributed to producing new shoot and increasing the number of leaves per plant [39]. Authors reported that number of leaves per tomato plant increased with increasing nitrogen rate in fertilizer [31, 40].

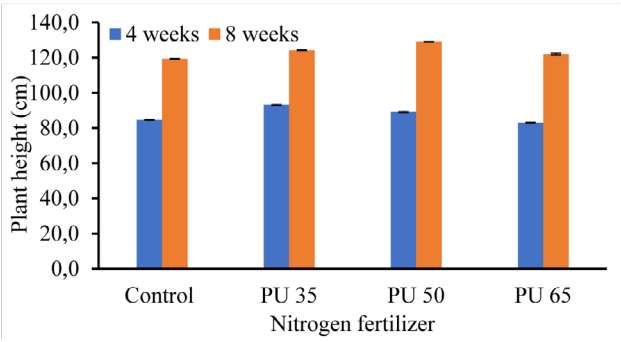

Figure 2 – Effect of nitrogen fertilizer on plant height of tomato

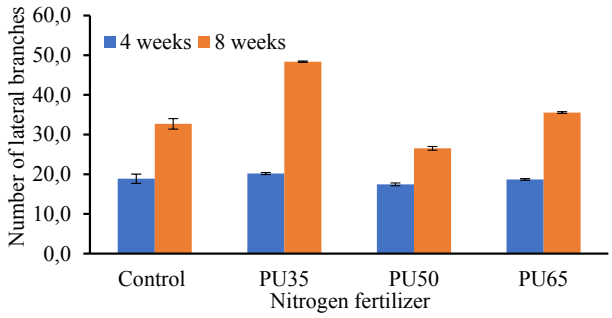

Figure 3 – Effect of nitrogen fertilizer
on the number of lateral branches per tomato plant.

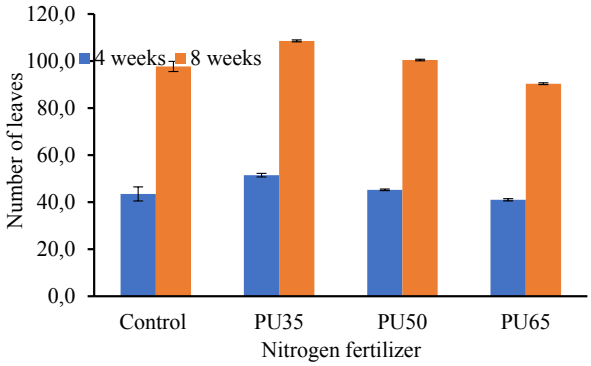

Figure 4 – Effect of nitrogen fertilizer
on the number of leaves per plant tomato

Leaf area (cm²). Figure 5 shows leaf area of tomato plants fertilized with different nitrogen levels (PU) compared with control (without fertilizers) at 4 and 8 weeks. When the levels of nitrogen are increased from 8.5 % (PU35) to 34.1 % (PU50), the leaf area of the tomato plants increased from 215.3 cm² to 248.2 cm² respectively at 4 weeks, and from 227.2 cm² to 265.5 cm² respectively at 8 weeks, due to the increase of photosynthetic activities of the leaf, which is directly responsible to increment leaf area of the plant [41]. At PU65 (N: 44.04 %) the leaf area reduced but was higher than the control. This effect of nitrogen on increasing leaf area of tomato plants was also observed by authors [42-44].

Fresh and dry weight of shoots (g/ plant). Figure 6 shows that the highest fresh and dry weights of tomato shoots were recorded by plants fertilized with PU50 (N: 34.1 %) at 4 and 8 weeks. On the other hand, tomato plants fertilized with PU65 (N: 44.04 %) exhibited the lowest fresh and dry weights of shoots but still higher than the control plants (without treatment). It was evident that PU fertilizer treatment caused an increase in the fresh and dry weights of shoots, especially PU50. The increase in fresh and dry weight of shoots attributed to the fact that nitrogen promotes plant growth [45]. The same behavior was reported by authors [46,47] when he studied the effect of different levels of urea on the growth and yield of tomato. The results showed that tomato plants fertilized with urea 150 mg per kg of soil gave the highest fresh and dry weights in comparison with plants fertilized with urea 200 mg per kg of soil.

Chlorophyll (a, b) content (mg/ dm²). The role of nitrogen as a macronutrient essential for plant growth and development is well known. Nitrogen is the component of protoplasmic proteins, enzymes, amino acids, nucleic proteins and chlorophyll. Therefore, plant growth vigor is greatly affected by increasing or decreasing level of nitrogen application. The effect of nitrogen fertilizer (PU) with different levels of nitrogen on chlorophyll (a and b) contents in the tomato leaves at 4 and 8 weeks is shown in Figure 7. Generally, all N-fertilizer treatments caused an increase in the chlorophylls a and b content of the leaves as compared to the control. The highest content of the photosynthetic pigments was obtained from tomato plants fertilized with PU50 (N: 34.1 %) at 4 and 8 weeks. This favourable effect of N-application on plant growth might be due to the vital role of nitrogen on the synthesis of plant proteins, chlorophyll and enzymes. This result was in agreement with authors [46, 47] on tomato. If nitrogen was added at high levels more than 34.1% the depression effect of fertilizer on plant growth should be expected as shown by the treatment PU65, N: 44.04%. However, there were investigators who mentioned positive effects of heavy N-application on plant growth [48].

Carbohydrate content (%). The carbohydrate content in leaves of tomato plants fertilized with PU fertilizer at 4 and 7 weeks is shown in Figure 8. The treatment plants with all PU fertilizers resulted in high carbohydrate content in leaves compared with the control plants. The carbohydrate content increased with increasing nitrogen from 8.5 % (PU35) to 34.1 % (PU50) but decreased with nitrogen of

44.04 % (PU65). The increase of carbohydrate content is attributed to the increasing in the process of photosynthesis and pigments [49]. Furthermore, PU as N-fertilizer enhanced carbohydrate content in the leaves of tomato plants. The same behavior was reported by authors [50] when they studied the effect of different nitrogen fertilizers on the carbohydrate content in leaves of wheat.

Nitrogen, phosphorus and potassium content (%). Figure 9 shows the effect of a variety of nitrogen fertilizer (PU) on the nutrient percentage of tomato leaves at 4 and 8 weeks. PU fertilizer had a high significant effect on nitrogen percentage, no significance on phosphorus percentage, and low significance of potassium percentage in the tomato leaves. An increase in nitrogen content in fertilizer (PU), increased the nitrogen and potassium percentages in the leaves of tomatoes at 4 and 8 weeks. Nitrogen is the most important nutrient for the synthesis of proteins and the enhancement nutrient content in the leaves of plant including nitrogen and potassium content [18]. The obtained data was in accordance with those previously reported by authors [51,52] who reported that N-fertilizer increased the leaf nitrogen concentration.

Characteristics of flowers. Figure 10 indicates that the node number bearing the first flower as compared to the control increased due to nitrogen fertilizer (PU) application and this effect was more evident with PU50 (N: 34.1 %). Number of flower cluster per plant, number of flowers per cluster and number of flowers per plant significantly increased with increasing the content of nitrogen in PU fertilizers from 8.5% (PU35) to 34.1 % (PU50) and decreased with increasing content of nitrogen 44.04 % (PU65).

The greatest number of flowers per plant was observed when the tomato plants were fertilized with PU50 (N: 34.1 %) while the lowest number of flowers was observed when the plants were fertilized with PU65 (N: 44.04 %) (Figure 11). Authors [40-47] reported that tomato plants treated with nitrogen fertilizer produced higher number of flowers than the control plants. The increase flower numbers might be due to increased content of available nitrogen which promotes better vegetative growth and enhances flower of tomatoes. From the Figure 11, it is clear that the nitrogen fertilizer (PU) promotes the production of flowers up to PU50 (N: 34.1 %) at which further increase in the fertilizer do not bring a significant increase in the flowers

Characteristics of fruits

Number of fruits per plant. Fruit number is the most impressive feature of all physiological process and plant growth phenomenon that express the response of plants to applied substances.

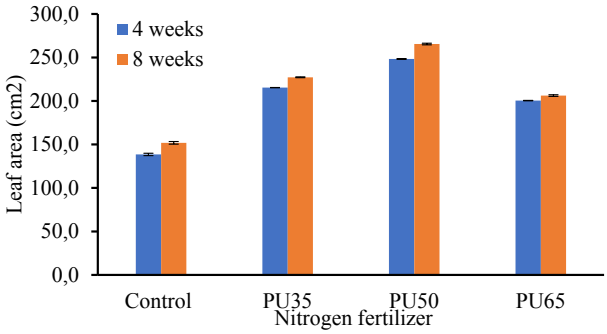

Figure 5 – Effect of nitrogen fertilizer on the leaf tomato area.

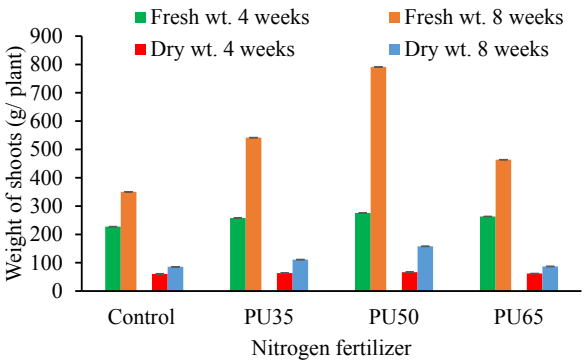

Figure 6 – Effect of nitrogen fertilizer on shoot fresh and dry weights per tomato plant.

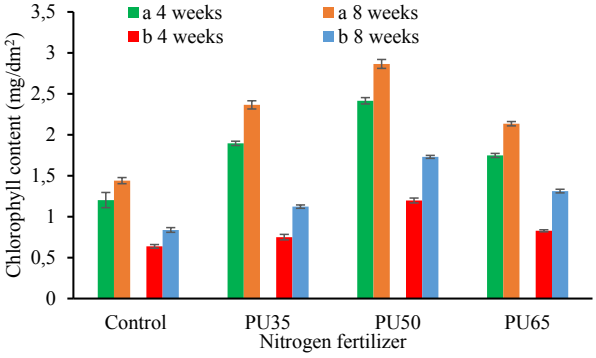

Figure 7 – Effect of nitrogen fertilizer on chlorophylls a and b in leaves of tomato plants.

Tomato plants fertilized with PU enhanced the number of fruits per plant than control plants as shown in Figure 12. Increasing the nitrogen content in PU fertilizer from 8.5 % (PU35) to 34.1 % (PU50) increased the number of fruits per plant from 27.73 to 29.85. At nitrogen level 44.04 % (PU65), the number of fruits was lower. This is attributed to the increase in the number of flowers per plan with increasing the

content on nitrogen in the fertilizer. The result was in agreement with authors [53, 46, 31] who reported increased in the fruit number with increasing rate of nitrogen fertilizer. This could be attributed to the increased uptake of nitrogen and its associated role in chlorophyll synthesis (and hence the process of photosynthesis and carbon dioxide assimilation) leading to enhanced number of flowers and fruits.

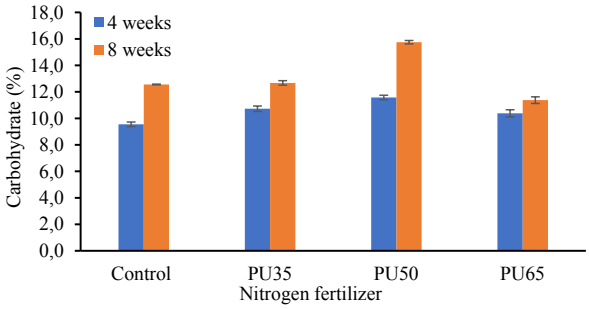

Figure 8 – Effect of nitrogen fertilizer on carbohydrate in leaves of tomato plant.

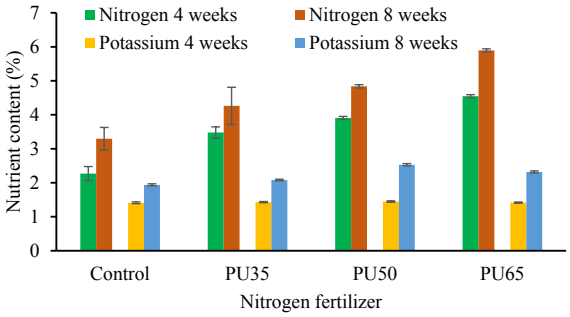

Figure 9 – Effect of nitrogen fertilizer on nitrogen and potassium percentages in leaves of tomato plants.

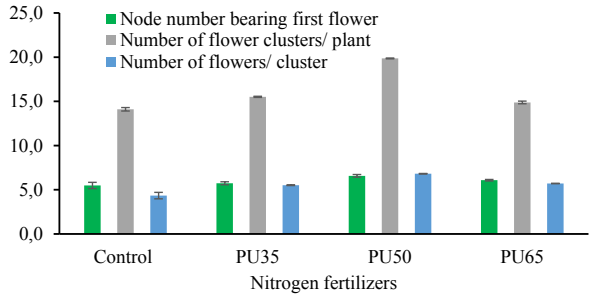

Figure 10 – Effect of N-fertilizer on node number bearing first flower, number of flower clusters per plant and number of flowers per cluster

Weight and volume of fruits. Data of the average fruit weight (Figure 13), volume (Figure 14) and shape index (Figure 15) produced by tomato plants fertilized with nitrogen fertilizer showed that PU fertilizer resulted in an increase in these parameters over control. Maximum values were recorded in tomato plants treated with PU50 (N: 34.1 %) and lowest values recorded in plants treated with PU65 (N: 44.04 %). Figure 13 shows the highest weight (69.8 gm) of fruits were obtained with PU50 (N: 34.1%) treatment, while lowest weight (50.83 gm) of fruits were observed for PU65 (N: 44.04 %) treatment.

Figure 14 shows that nitrogen fertilizers had a significant favorable effect on the fruit volume as compared to the control plants. The maximum significant values were obtained as a result of PU50 treatment. The increment was 20 % for for volume of fruit as compared to control plants.

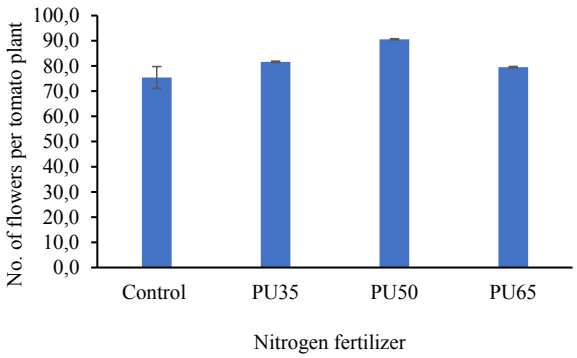

Figure 11– Effect of nitrogen fertilizer on number of flowers per tomato plant.

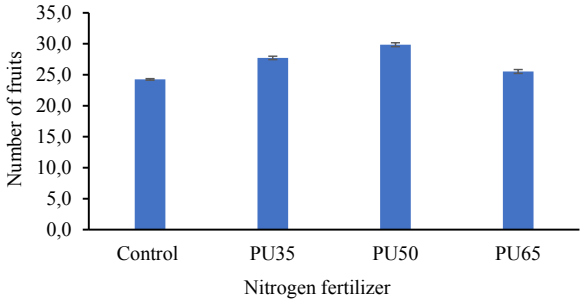

Figure 12 – Effect of nitrogen fertilizer on number of fruits per tomato plant.

The effects of the nitrogen fertilizers (PU) on the shape index of fruits showed an increase over the control except for treatment with PU50 (Figure 15). Tomato plants treatment with PU50 gave the highest shape of index fruits shape index (1.19) but PU65 gave the lowest shape index of fruits (1.12). The increased fruit weight, volume and shape index of tomato fruits under PU application could be attributed to the positive effect of nitrogen with balanced fertilization which increased weight, volume and shape index of fruit. The increments of the physical characters of tomato fruits response to nitrogen fertilizer were also reported by authors [54, 46, 47].

Chemical composition of fruits. Figure 16 shows that the SSC increased from 4.45 % to 5.48% with increasing nitrogen from 8.5 % (PU35) to 34.1 % (PU50) and decreased from 5.48% to 4.3% with increasing nitrogen of 34.1 % (PU50) to 44.04 % (PU65), but still more than the control. This might be due to the characteristics of N, which usually plays a role in increasing the amount of foliage, the quantity of chlorophyll, and ultimately the photosynthetic activity of the plant [46, 47]. However, Warner et al. (2004) [55] indicated that nitrogen did not affect the SSC of tomato fruits. Factors that might also influenced the solid content of tomato fruits include the number of fruits, rate of assimilates exported from leaves, rate of assimilates imported by fruits and fruit carbon metabolism.

The titratable acid of tomato fruits significantly increased with increasing nitrogen rate in PU fertilizer. Tomato plants fertilized with PU50 (N: 34.1 %) gave the highest percentage of acid (0.79 %) while plants fertilized with PU65 (N: 44.04 %) gave the lowest percentage of titratable acid (0.68 %) though higher than the control as shown on Figure 16. Wang et al. (2007) [56] reported that nitrogen was related to improved fruit shape, the reduction of ripening disorders, and an increase in fruit acid concentration, which subsequently improved the taste.

PU65 fertilizer reduced the ascorbic acid (vitamin C) and lycopene content (Figure 17). Rodriguez et al. (1994) [57] also reported that higher nitrogen fertilization decreased the vitamin C content and also worsened the fruit color. In this study, the highest values of ascorbic acid and lycopene contents were recorded with PU50 (N: 34.1 %).

This result was in agreement with previously reported results by Kobryń and Hallmann (2005) [57], whereas lycopene content increased with different nitrogen rates to 50 %. In fact, De Pascale et al. (2006) [12] suggested that since lycopene was synthesized by the isoprenoid pathway, nitrogen fertilizer enhanced the enzymes in this pathway therefore increasing the lycopene concentration in the fruits.

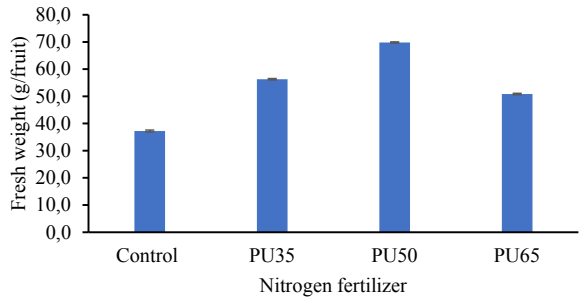

Figure 13 – Effect of nitrogen fertilizer on the fresh weight of tomato fruits.

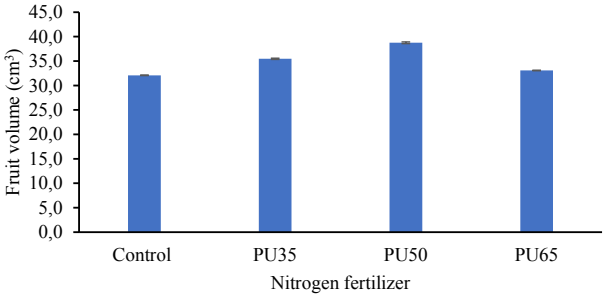

Figure 14 – Effect of nitrogen fertilizer on the volume of tomato fruits.

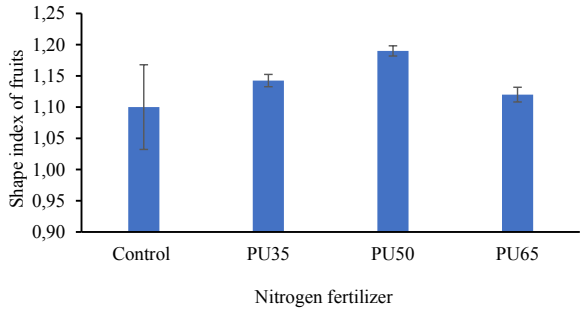

Figure 15 – Effect of nitrogen fertilizer on the shape index of tomato fruits

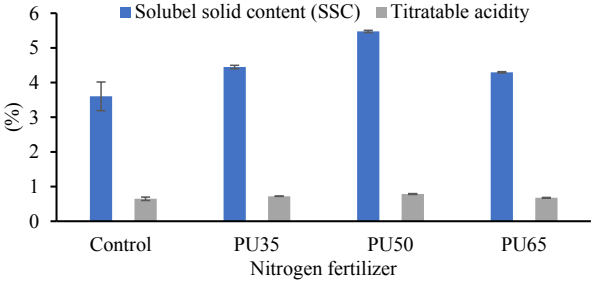

Figure 16 – Effect of nitrogen fertilizer on SSC and titratable acidity in tomato fruits.

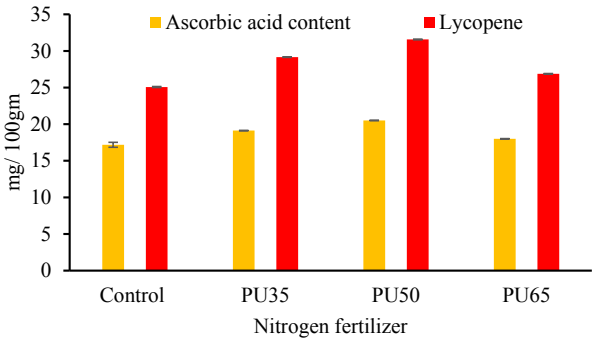

Figure 17 – Effect of nitrogen fertilizer on ascorbic acid and lycopene in tomato fruits.

Conclusion

The results revealed that nitrogen fertilizers based on polyvinyl alcohol blended with various ratios of urea [PU35 (N: 8.5 %), PU50 (N: 34.1%), PU65 (N: 44.0%)] affected vegetative growth of tomato plants. It was observed that PU35 treatment with nitrogen content (8.45%) was found to be the best treatment for the number of lateral branches and leaves per plant. Whereas the application of PU50 (nitrogen content 34.1%) resulted in a significant increase in other vegetative growth, chlorophylls a and b, flower and fruit characteristics higher than PU35, PU65 and control plants. Tomato fruit yields (23%) were best applied to PU fertilizers with a nitrogen content of 34.1% (PU50).

References

1 Akanbi W.B., Dris R., Togun A.O. (2003) Influence of compost and nitrogen fertilizer on growth, nutrient uptake and fruit yield of tomato (Lycopersicon esculentum). Crop. Res., vol 26, pp. 98-105.

2 Ahmet D, Hasan D, Tolga K, Hesna P, Mustafa G, Ali C. (2018) Yield and nutrient uptake improvement of chickpea (Cicer arietinum L.) by dressing fertilization and nitrogen doses. Conference Proceedings, Vol. 1, pp. 51-57. https:// doi: 10.2478/alife-2018-0008

3 Andersen P.C., Rhoads F.M., Olson S.M., Brodbeck B.V. (1999) Relationships of nitrogenous compounds in petiole sap of tomato to nitrogen fertilization and the value of these compounds as a predictor of yield. Hort. Science, vol. 34, pp. 254-258. https://doi:10.21273/HORTSCI.34.2.254

4 Aroiee H., Omidbaigi R. (2004) Effects of nitrogen fertilizer on productivity of medicinal pumpkin. Journal of Acta Horticulture, vol. 629, pp. 415–419. https:// doi:10.17660/ActaHortic.2004.629.54

5 Asit B.M., Abdullah A.M. (2011) Effect of foliar application of urea on the growth and yield of tomato. Frontiers of Agriculture in China, vol. 5, no. 3, pp. 372-374. https://doi.org/10.1007/s11703-011-1089-z

6 Cui X, Yan Q.-W., Sun J.-I., Xiao S, Xie F.-C., Chen Y.-J. (2014) Research Progree on Nitrogen use and Plant Growth. Journal of Northeast Agricultural University, Vol. 21, pp. 68-74. https://doi.org/10.1016/S1006-8104(14)60036-2

7 Souri M.K., Dehnavard S. (2018) Tomato plant growth, leaf nutrient concentrations and fruit quality under nitrogen foliar applications. Advanced in Horticultural Science, vol. 32, no. 1, pp. 41-47. https:// doi:10.13128/ahs-21894

8 Soval-Villa M., Guertal EA, Wood CW. (2000) Tomato leaf chlorophyll meter readings as affected by variety, nitrogen form, and nighttime nutrient solution strength. J. Plant Nutr, vol. 23, pp. 649–661. https://doi.org/10.1080/01904160009382047

9 Heeb A, Lundegårdh B, Ericsson T, Savage GP. (2005) Effects of nitrate-, ammonium-, and organic-nitrogen-based fertilizers on growth and yield of tomatoes. Journal of Plant Nutrition and Soil Science, vol. 168, no.1, pp. 123-129. https://doi.org/10.1002/jpln.200420420

10 Horchani F, Hajri R, Aschi-Smiti S. (2010) Effect of ammonium or nitrate nutrition on photosynthesis, growth, and nitrogen assimilation in tomato plants. J. Plant Nutr. Soil Sci., vol. 173, pp. 610–617. https://doi.org/10.1002/jpln.201000055

11 Akanbi WB, Akande MO, Adediran JA. (2005) Suitability of composted maize straw and mineral nitrogen fertilizer for tomato production. J. Veg. Sci., vol. 11, no. 1, pp. 57-65. https://doi.org/10.1300/J484v11n01_06

12 De Pascale S, Tamburrion R, Maggio A, Barbieri G, Foglioano V, Pernice R. (2006) Effect of nitrogen fertilization on the nutritional value of organically and conventionally grown tomatoes. Acta Horticulturae, vol. 700, pp. 107-110. https://doi.org/10.17660/ActaHortic.2006.700.14

13 Mukta S, Rahman MM, Mortuza MG. (2015) Yield and Nutrient Content of Tomato as Influenced by the Application of Vermicompost and Chemical Fertilizers. J. Environ. Sci. & Natural Resources, vol. 8, pp. 115-122. https://doi: 10.3329/jesnr.v8i2.26877

14 Mercado AL, Enrique RG, Jorge LCS, Alfredo LH, Juan SA. (2014) Evaluation of different concentration of nitrogen for tomato seeding production (Lycopersicon esculentum Mill.). Universal Journal of Agricultural Research, vol. 2, no. 8, pp. 305-312. https:// doi:10.13189/ujar.2014.020804

15 Ning XJ, Yu HJ, Jiang WJ, Liu XR. (2012). Effects of nitrogen rate on the growth, yield and quality of tomato in greenhouse fertilization with biogas slurry. Acta Hortic, vol. 927, pp. 989-994. https://doi.org/10.17660/ActaHortic.2012.927.122

16 Robin LW, Ian GB, Jeff M. (2001) Responses of plant growth rate to nitrogen supply: a comparison of relative addition and N interruption treatments. Journal of Experimental Botany, Vol. 52, no. 355, pp. 309–317. https://doi.org/10.1093/jexbot/52.355.309

17 Sheppard SC, Bates TE. (1980) Yield and chemical composition of rape in response to nitrogen, phosphorus and potassium. Can. J. Soil Sci., vol. 60, pp. 153-162. https://doi.org/10.4141/cjss80-019

18 Khorshidi MG, Moradpoor S, Ranji A, Karimi B, Amiri Khorie MM. (2014) Effect of different levels of nitrogen fertilizer and plant density on yield and yield components of canola. Scientific Journal of Crop Science, vol. 3, no 10, pp. 109-114. doi: 10.14196/sjcs.v3i10.1719.

19 Negim ES, Lyazzat B, Hanan A. Yeligbayeva G. (2018) The effect of blend ratios on physicomechanical properties and miscibility of cross-linked poly (vinyl alcohol)/urea blends. Journal of Physiscs Conference Series vol 1123, no. 1, pp. 1-9. doi:10.1088/1742-6596/1123/1/012066

20 Sartory DP, Grobbelaar JU. (1984) Extraction of chlorophyll a, from freshwater phytoplankton for spectrophotometric analysis. Hydrobiologia, vol. 114, pp. 177-187. https://doi.org/10.1007/BF00031869

21 Dubois M, Gilles KA, Hamilton J, Roberts R, Smith F. (1956) Colorimetric method for determination of sugar and related substances. Ann. Chem., vol. 28, pp. 350-356. https://doi.org/10.1021/ac60111a017

22 Piper CS. (1947) Soil and Plant Analysis. The Univ. of Adelaide, pp. 258- 275. ISBN 13: 9789387869356

23 Pregl F. Quantitative Organic Microanalysis. 4th Ed. J.&A. Churchill, Ltd., London (1945).

24 Chapman HD, Pratt PF. (1961) Methods of analysis for soil, plant and water. Univ. Calif. Davic. Agric. Sci.: U.S.A.

25 AOAC. (1965) Official Method of Analysis of Association of Agricultural Chemists (10th Ed.).

26 AOAC. (2005) Official Method of Analysis of Association of Agricultural Chemists (15th Ed.).

27 AOAC. (1970) Official Method of Analysis of Association of Agricultural Chemists (10th Ed.).

28 Sharma Le Maguer. (1996) Lycopene in tomatoes and tomato pulp fractions. Italian Journal of Food Science, vol. 2, 107-113.AGR: IND20527801

29 Jan MT, Shah P, Hollington PA, Khan MJ, Sohail Q. (2009) Agriculture Research: Design and Analysis. 1st ed. Dept. of Agronomy, KP Agric. Univ. Peshawar.

30 Mead R, Currnow RN, Harted AM. (1993) Statistical Methods in Agricultural and Experimental Biology. (2nd Ed.), pp. 54-60.

31 Chen JS, Zhu RF, Zhang YX. (2013) The effect of nitrogen addition on seed yield and yield components of Leymus chinensis in Songnen Plain, China. Journal of Soil Science and Plant Nutrition, vol. 13, no. 2, pp. 329-339. http://dx.doi.org/10.4067/S0718-95162013005000027.

32 Mohamed EHA. (2011) Effect of different nitrogen sources on growth, yield and quality of fodder maize (Zea mays L.). J. Saudi Soc. Agric. Sci., vol. 10, pp. 17-23. https://doi.org/10.1016/j.jssas.2010.06.003

33 Najaf DS, Alemzadeh AN, Sedighie DF. (2008) Effect of different levels of nitrogen fertilizer with two types of bio-fertilizers on growth and yield of two cultivars of tomato (Lycopersicon esculentum Mill). Asian Journal of Plant Science, vol. 7, no. 8, pp. 757-761. https://doi:10.3923/ajps.2008.757.761

34 Qiang Z, Min Z, Qiang MA. (2012) Copper-based foliar fertilizer and controlled release urea improved soil chemical properties, plant growth and yield of tomato. Scientia Horticulturae, vol. 143, pp. 109-114. https://doi:10.1016/j.scienta.2012.06.00

35 Maqsood MA, Awan UK, Aziz T, Arshad H, Ashraf N, Ali M. (2016) Nitrogen management in calcareous soils: problems and solutions. Pakistan Journal of Agricultural Sciences, vol. 53, no. 1, pp. 79–95. http://doi:10.21162/PAKJAS/16.4867

36 Courty PE, Smith P, Koegel S, Redecker D, Wipf D. (2015) Inorganic nitrogen uptake and transport in beneficial plant root-microbe interactions. Critical Reviews in Plant Sciences, vol. 34, no. 1–3, pp. 4–16. http://doi:10.1080/07352689.2014.897897

37 Babajide PA, Oyeleke OA. (2014) Evaluation of sesame (Sesamum indicum) for optimum nitrogen requirement under usual farmers' practice of basal organic manuring in the Savanna ecoregion of Nigeria. Journal of Natural Sciences Research, vol. 4, no. 17, pp. 2224–3186.

38 Huang FS, Zhang HS, Qian HNQ. (1995) Study on the effect of organic manures and leaf spraying P and K on the fruit quality of extra early Satsuma mandarin. China Citrus, vol. 24, no. 2, pp. 31- 32.

39 Yohannes KW, Belew D, Debela A. (2013) Effect of farmyard manure and nitrogen fertilizer rates on growth, yield and yield components of onion (Allium cepa L.) at Jimma, Southwest Ethio-

pia. Asian J. Plant Sci., vol. 12, pp. 228-234. http://doi:10.3923/ajps.2013.228.234

40 Fan XH, Li YC. (2009) Effects of slow-release fertilizers on tomato growth and nitrogen leaching. Communications in Soil Science and Plant Analysis, vol. 40, no. 21-22, pp. 3452-3468. https://doi.org/10.1080/00103620903326016

41 Liu F, Yang W, Wang Z, Xu Z, Liu H, Zhang M, Liu Y, An S, Sun S. (2010) Plant size effects on the relationships among specific leaf area, leaf nutrient content, and photosynthetic capacity in tropical woody species, Acta Oecologica, vol. 36, pp. 149-159. https://doi.org/10.1016/j.actao.2009.11.004

42 Ayeni LS, Omole TO, Adeleye EO, Ojeniyi SO. (2010) Integrated application of poultry manure and NPK fertilizer on performance of tomato in derived savannah transition zone of Southwest Nigeria. Nature and Science, vol. 8, no. 2, pp. 50-54.

43 Mahila M, Jodhpur PG. (2010) Growth and productivity of tomato (Lycopersicon esculentum Mill.) grown in greenhouse as affected by organic, mineral and bio-N-fertilisers. Sci. & Cult., vol. 76, no.3–4, pp. 128-131.

44 Dawa KKA, Al-Gazar TM, Abdel-Fatah AM. (2013) Effect of chicken manure combined with bio-fertilizers, mineral fertilizer and some foliar applications on: 1-vegetative growth and some chemical constituents of tomato leaves. J. Plant Production, Mansoura Univ., vol. 4, no.10, pp. 1555-1570.

45 Vaezzadeh M, Naderidarbaghshahi M. (2012) The effect of various nitrogen fertilizer amounts on yield and nitrate accumulation in tubers of two potato cultivars in cold regions of Isfahan (Iran). Intl J Agri Crop Sci., vol. 4, no. 22, pp. 1688-1691.

46 Masome H. (2013) Effects of different levels of urea on the growth and yield of tomato. J. Nov. Appl Sci., vol. 2, no. 3, pp. 1031-1035.

47 Masome H, Sepideh K. (2014) Effects of ammonium nitrate on the growth and yield of different plant tomato (Lycopersicon esculentum). J. Nov. Appl Sci., vol. 3, no. 2, pp. 142-144.

48 Tangolar S, Tarim G, Ada M, Alkan Torun A, Ertargn E. (2019) Effect of different nitrogen and potassium levels on yield and quality of two early grape cultivars in different soilless media. Act Hortic, vol. 1241, pp. 349-356. https://doi.org/10.17660/ActaHortic.2019.1242.49

49 Abd El-al F.S. (2009) Effect of urea and some organic acids on plant growth, fruit yield and its quality of sweet pepper (Capsicum annum). Research Journal of Agriculture and Biological Sciences, vol. 5, no. 4, pp. 372-379.

50 Abd-El-Hamied AS, Abd El-Hady MA. (2018) Response of Tomato Plant to Foliar Application of Calcium and Potassium Nitrate Integrated with Different Phosphorus Rates under Sandy Soil Conditions. Egypt. J. Soil Sci., Vol. 58, No.1 pp. 45-55. https://doi:10.21608/ejss.2017.1645.1126

51 Elahe S, Shirin S. (2017) Investigating of N and K Fertilizers on Yield and Components of Soybean (Glycine max (L.) Merr.). Journal of Agricultural Science, Vol. 9, pp. 85-94. https://doi.org/10.5539/jas.v9n10p85

52 Aminifard MH, Aroiee H, Nemati H, Azizi M, Khayyat M. (2012) Effect of nitrogen fertilizer on vegetative and reproductive growth of pepper plants under field conditions. Journal of Plant Nutrition, Vol. 35, pp. 235-242.

a. DOI: 10.1080/01904167.2012.636126.

53 Shamima Na, Kamal AM , Siddiky MA, Rannu RP, Islam MS. (2014) Effect of nitrogen, phosphorus, potassium and sulphur on the yield of mango. Bangladesh J. Agril. Res. Vol 39, pp. 631-640. https:// doi: 10.3329/bjar.v39i4.22542.

54 Abrha K, Gebremedhin W. (2014) Fruit quality and Net income response of tomato (Lycopersicon esculentum Mill.) Two Different Levels of Nitrogen and Plant Population in Alamata, Ethiopia. International Journal of Scientific & Technology Research, vol. 3, no. 9, pp. 125-128. https://hdl.handle.net/10568/49596

55 Warner J, Zhang TQ, Hao X. (2004) Effects of nitrogen fertilization on fruit yield and quality of processing tomatoes. Can. J. Plant Sci. 84, 865–871. https://doi.org/10.4141/P03-099

56 Wang YT, Huang SW, Liu RL, Jin JY. (2007) Effect of nitrogen application on flavor compounds of cherry tomato fruits. Journal of Plant Nutrition and Soil Science, vol. 170, no. 4, 461-468. https://doi:10.1002/jpln.200700011

57 Kobryń J, Hallmann E. (2005) The effect of nitrogen fertilization on the quality of three tomato types cultivated on rockwool. Acta Hort,.vol. 691, pp. 341-348.Rodriguez A, Leoni S, Bussieres P, Dadomo M, Christou M, Macua IJ, Cornillon P. (1994) The influence of water and nitrogen levels on the quality of the processing tomato grown in European union countries. Acta Hort., vol. 376, pp. 275-278. https://doi.org/10.17660/ActaHortic.1994.376.34

IRSTI 34.29.25; 31.23.17 https://doi.org/10.26577/ijbch.2020.v13.i2.09

T.N. Kobylina[1*], N.M. Mukhitdinov[1], K.T. Abidkulova[1],
N.V. Kurbatova[1], N.O. Kudrina[2], M.B. Alimkulova[1],
Jurate Zaltauskaite[3]

[1] Al-Farabi Kazakh National University, Almaty, Kazakhstan
[2]Central Laboratory for Biocontrol, Almaty, Kazakhstan
[3]Vytautas Magnus University, Kaunas, Lithuania
*e-mail: kobylina.tatyana.n@mail.ru

Anatomic-morphological and phytochemical study of an rare species - *Rheum wittrockii* Lundstr.

Abstract. The article presents the features of the anatomical and morphological structure of the vegetative organs of *Rheum wittrokii* Lundstr. and the results of its qualitative and quantitative phytochemical analyses. The structure of the leaf shows the presence of calcium oxalate druses, which are located mainly under the layer of columnar mesophyll, along the Central part of the leaf blade. Druses in the spongy parenchyma are clearly distinguished and have an almost spherical shape with a peculiar needle-like structure. In the main vein, sections of the sclerenchymic lining are adjacent to the conducting bundle. The covering tissue of the roots has a secondary structure and is represented by a three-layer periderm. In the cells of the main parenchyma of the cortex, numerous calcium oxalate druses are found, which have a round-crystal configuration and are collected in small groups. The vessels of the root xylem are large with ladder and mesh perforation. Features of the main stem parenchyma are its larger, rounded-oblong or oval shape with slightly thickened cell walls. The revealed anatomical features can be used in the case of the diagnosis of medicinal plant raw materials. The study of the chemical composition, the study of biological activity and the development of new herbal medicines is relevant. As a result of studying the chemical composition of the ethanol extract of *Rheum wittrokii* obtained by extracting 96% ethanol, 8 main components were identified. Rhizomes are dominated by chrysophanic acid with an identification probability of 41.4%. The presence of components was found: chrysarobin, chrysophanic acid, emodin-3-methyl ether, emodin-1,3,8-trihydroxy-6-methylanthracene-9,10-dione, which are directly involved in the body's metabolism, providing antioxidant, antiseptic and anti-cancer effects, and also help in the removal of toxins from the body, which has a beneficial effect on the liver, increasing the level of glycogen.

Key words: *Rheum wittrokii* Lundstr., rare species, anatomical and morphological characteristics, phytochemical composition, extracts.

Introduction

The greatest phytochemical interest is the study of the root of this species. The rhizome of an rare species Rheum wittrokii Lundstr. contains two main groups of biological substances. The first group includes tannoglycosides-tannins that have antiseptic, antidiarrheal, and astringent properties. Atroglycosides, the second group, are substances that can enhance intestinal peristalsis. Plant raw materials have good choleretic and laxative properties. In the autumn, raw materials are harvested, the decoction of which is used for anemia and tuberculosis, as well as it contains carbohydrates, organic acids, catechins, anthraquinones [1].

Currently, research on the study of rare plant species that are vulnerable and endangered, have a small habitat and are subject to anthropogenic factors, as well as the possibility of obtaining effective herbal medicines with medicinal properties is of particular relevance [2; 3]. To date, the species composition of the flora of South-Eastern Kazakhstan, its number and location of endemic and rare species is little studied and requires a comprehensive study [4; 5]. More than 6 thousand vascular plants with biologically active substances are found in the flora of Kazakhstan, which require special attention to study the factors of their vital activity: the ecological state of populations, the degree of land degradation that determine the species number, their composition, loca-

tion, geographical distribution, which contributes to the restoration and further existence of the dominant in natural conditions [6].

The flora of Kazakhstan consists of 68 species of trees, 266 species of shrubs, 433 species of semi-shrubs, 2598 species of perennial grasses and 849 species of annual grasses, as well as 515 endemic species, 303 species listed as vulnerable, endangered and rare plants, including *Rheum wittrokii*. The *Polygonaceae* family includes about 30 genera and 800 species that are widely distributed around the globe, especially in the Northern temperate zone. Species of the *Polygonaceae* family are characterized by the presence of tannins in all parts of the plants, especially in the rhizomes, which are used as excellent tanning agents, being a valuable raw material for the tanning and extraction industry [7-10]. Rhubarb varieties are very valuable medicinal herbs containing secondary metabolites that grow in the mountainous and flat-desert regions of Kazakhstan: on the grassy and forest slopes of the mountains. Occurs in Dzhungarian Alatau, Zaili Alatau, Kirghiz Alatau, Kungei and Terskei Alatau, Ketmen ridge, Western Tien Shan [11-13].

Rheum wittrokii Lundstr. - a perennial herb with a juicy, furrowed, hollow inside, stem, 50-100 cm high, with reddish droplets and stripes. Numerous fleshy roots radiate from the powerful short rhizome. The basal leaves are five-and seven-lobed, having a diameter of up to 75 cm, at the top with scattered small villi, on the reverse side along the entire surface densely pubescent with long hairs, and on long, up to 30 cm, cylindrical, often reddish cuttings, collected by a rosette. Stem leaves are ovate-triangular, alternate, up to 10 cm in diameter, with short cuttings. Whitish-pink or red flowers are small, regular, bisexual, collected in numerous paniculate inflorescences and are up to 2 mm long. The fruit is a three-sided, broad-winged and wrinkled, brownish-red nut. *Rheum wittrokii* blooms in the third year of life in June-July and bears fruit in July-August. It grows on grassy and forest slopes of mountains, in the habitat of dark coniferous forests, in open spaces between trees, in infrequent spruce trees and cracks in rock crevices, in the forest, rising to the subalpine belt.

Some chemical components from *Rheum* L. species are pharmacologically important. They are used as a herbal therapeutic agent, in vegetables and for the preparation of natural dyes. More than 250 components, including anthraquinones (emodin, chrysophanol, phizion, aloe-emodin and emodin glycides), antrons, flavonoids, acylglucosides, pyrons stilben, tanning components, etc. are the main biologically active substances of rhubarb, which are widely used in folk medicine: for the treatment of fever, dysentery, blood clotting, laxative, antitumor, and are also used for various skin diseases [14; 15].

The healing potential of rhizome extracts of *Rheum wittrokii* is a promising direction for further study of its biologically active components as sources of necessary compounds for life and its maintenance, including those caused by adverse environmental factors. In the absence of additive effects biologically active compounds of natural origin have a therapeutic effect on the regulation of the main metabolic processes of the body [16].

Materials and methods

Plant raw materials were collected in July 2019, in the flowering phase in the Almaty region (Butakovsky gorge), on the left bank of the Butakovka river, the slope of the South-Eastern exposure with a steepness of 40-450. The soil on which this species grows is mountain black soil. Collection coordinates: N 43010/19//, E 07706/50//, 2183 m above sea level.

The objects of anatomical and morphological research were vegetative organs (leaf blade, root and stem) of *Rheum wittrockii* Lundstr. Raw materials were collected and dried in accordance with the requirements of the State Pharmacopoeia of the Republic of Kazakhstan [17].

The extraction of raw materials was carried out twice. Combined extract concentrated and dried in vacuo. Research was carried out in the Laboratory Ecology of the Biosphere, RSE Al-Farabi KazNU, SSE Center for Physical and Chemical Methods of Research and Analysis, and Laboratory of plant anatomy and morphology (Al-Farabi KazNU).

In laboratory conditions, plant material was recorded in order to study the features of the anatomical structure of the plant. Conservation of plants was carried out by the method of Strasburger-Flemming. The preserving liquid was a mixture of alcohol-glycerine-water in a ratio of 1:1:1. Fixation was performed in 96% ethyl alcohol. Aboveground and underground vegetative organs of the studied species were recorded [18; 19].

Anatomical sections were enclosed in glycerine and balsam. Anatomical preparations were made using a microtome with a TOC-2 freezing device (made in USSR).

Microphotographs of anatomical sections were made using a MC 300 microscope (magnification 10x14, 10x20, 10x40) with a CAMV400/1.3 m video camera (Micros company, Austria).

Anatomical and morphological studies were conducted in accordance with generally accepted methods [20-22].

As part of the phytochemical study, the extraction of biologically active substances of plants was carried out using 96% ethyl alcohol. 10 g of dry, crushed raw material was selected, then 50 ml of alcohol was extracted by infusing at room temperature for 5 hours, then 1.5 ml of the extract was transferred to 2 ml vials and analyzed by chromatographic method with mass spectrometric detection (Agilent 7890B/5977A, USA). The analysis conditions were as follows: sample volume 3.0 µl, sample input temperature 240 °C, without flow division. Separation was performed using a chromatographic capillary column DB-35MS (Agilent, USA) with a length of 30 m, an internal diameter of 0.25 mm and a film thickness of 0.25 microns at a constant velocity of the carrier gas (helium) 1 ml/min. The chromatography temperature is programmed from 40 °C (0 min exposure) to 300 °C with a heating rate of 10 °C/min (15 min exposure). Detection was performed in the SCAN mode m/z 34-750. Agilent MSD ChemStation software (version 1701EA, USA) was used to control the gas chromatography system, record and process of the obtained results and data. Data processing included determination of retention times, peak areas, and processing of spectral information obtained using a mass spectrometric detector. The Wiley 7th edition and NIST'02 libraries were used to decipher the obtained mass spectra (the total number of spectra in the libraries is more than 550 thousand).

Results and discussion

Microscopic studies were performed to determine the morphological and anatomical features of roots, stems and leaves.

It is noted that the leaf blade of wittrock rhubarb has a single-layer upper and lower epidermis in cross-section (Figure 1). The upper epidermis consists of narrow cells of an oblong shape with rare single simple hairs. The lower epidermis consists of rounded and rounded-oblong thin-walled cells, between which there are single stomata. The cells of the upper and lower epidermis are weakly sinuous, connected tightly and covered with a thin layer of cuticle. Under the upper epidermis, the palisade mesophyll is located in two rows, the cells of the spongy mesophyll are located under the columnar mesophyll of the leaf blade and have a loose structure, quite large, with numerous intercellular cells filled with air, elongated and few. In vittrok rhubarb, calcium oxalate druses are noted in the structure of leaf blades, which are located mainly under the layer of columnar mesophyll, along the Central part of the leaf blade. Druses in the spongy parenchyma are clearly distinguished and have an almost spherical shape with a peculiar needle-like structure. The conducting system in the area of the Central part of the leaf blade is represented by two open collateral conducting bundles. One small, and the other larger. The conducting beams are surrounded by a parenchymal lining. In the main vein to the conducting beam adjacent areas sclerenchyma lining. Conducting bundles have a thin lining formed of sclerenchyma cells.

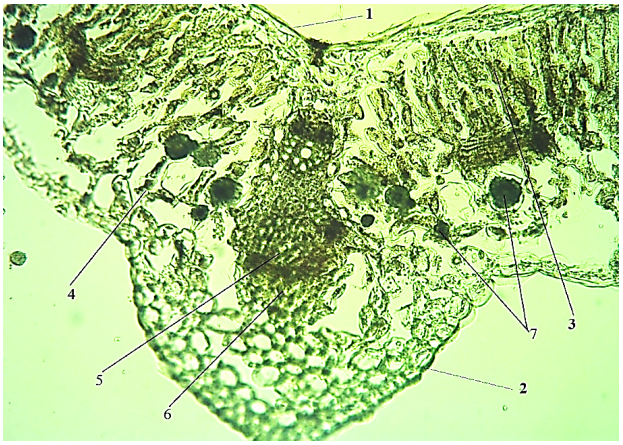

Figure 1 – Cross section of a leaf of Rheum wittrockii (magnification 200).
1-upper epidermis, 2-lower epidermis, 3-columnar mesophyll, 4-spongy mesophyll, 5-central conducting bundle, 6-sclerenchyma cells, 7-calcium oxalate druses

Biometric indicators of the leaf blade of wittrock rhubarb were determined, average measurements of the anatomical structure of the leaf blade were obtained by repeating ten times. Results of the Table 1 show that the cells of the lower epidermis are larger, and the thickness of the columnar mesophyll is expressed better than the thickness of the spongy mesophyll.

When studying the anatomical structure of the root of *Rheum wittrockii*, it was noted that it has a rounded shape and consists of tissues of the central cylinder and primary cortex. From the surface is the periderm (plug). Integumentary tissue of roots secondary structure represented by a three-layer periderm (vellema, phellogen, theloderma). The cork layer consists not only of old flaking layers, but also has new layers consisting of even rows of cells,

regular, elongated rectangular shape in an amount of 3 to 5. Next, after the periderm, is the main parenchyma of the cow part of the root, individual cells of which have numerous starch grains-inclusions of a rounded fine-grained structure. Rounded, loosely located cells of the cow parenchyma have more or less thickened cell walls and irregular shape of the cavities. In the cells of the main parenchyma of the cortex, numerous calcium oxalate druses are found, which have a round-crystal configuration and are collected in small groups. The root of the secondary structure is characterized by the presence of a cambial ring that stands out on the cross section. To the center of the cambium are the elements of the secondary xylem, and to the periphery of the secondary phloem. In the secondary xylem, the primary radial rays of the parenchyma are slightly visible, reaching the center of the root, the primary xylem. The secondary phloem of the root has small breaks, wider to the periphery, evenly spaced along the radius of the root. Xylem vessels are large with stair and mesh perforations. The primary xylem, represented by several vessels, is preserved in the center of the root (Figure 2).

Biometric indicators of the vittrok rhubarb root were determined (Table 2). Table 2 shows the average measurements of the anatomical structure of the root obtained by repeating ten times.

Table 1 – Morphometric indicators of the anatomical structure of the leaf blade.

Thickness, µm				
Epidermis		Mesophyll		leaf blade
Upper	Lower	columnar	spongy	197.55± 14.02
10.06± 0.06	13.11± 0.09	93.23± 0.16	81.15± 0.24	

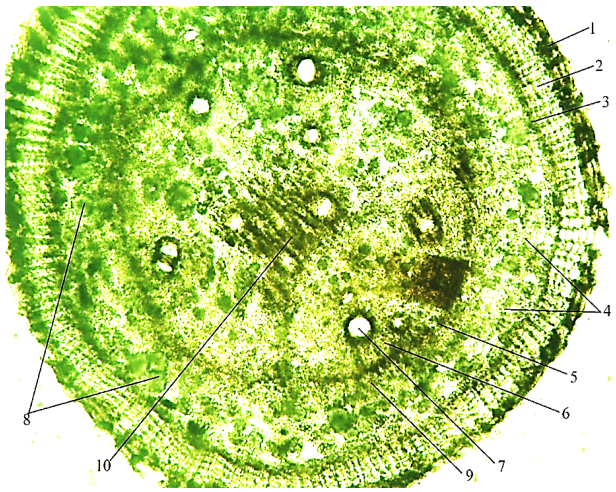

Figure 2 – Cross section of the root of *Rheum wittrockii* (magnification 140).
Note: 1-cork (fellema), 2-phellogen,3-phelloderm, 4-main parenchyma of the cortex,
5-cambial ring, 6-xylem parenchyma, 7-wood vessels (secondary xylem), 8 - calcium oxalate druses,
9 – secondary phloem, 10 – primary xylem.

.

Table 2 – Morphometric indicators of the anatomical structure of the root.

Thickness of the primary crust, µm	Diameter of the central cylinder, µm	Area of xylem vessels, µm^2
120.09± 7.12	161.28± 10.89	86.13± 16.81

It is noted that the diameter of the central cylinder exceeds the thickness of the primary crust.

On the cross section of the stem, it was noted that the shape of the stem is ribbed. Outside the stem is covered with one or two rows of small cells of the epidermis. The cells of the epidermis have an oval, elongated shape. Under the epidermis is the chlorophyll-bearing parenchyma of the primary cortex, consisting of 3-5 rows of loosely arranged isodiametric cells with inclusions.

The cells of the main parenchyma are larger, rounded-oblong or oval in shape with slightly thickened walls. It should be noted that the main part of the central cylinder is occupied by closely spaced vascular-fibrous conducting bundles of the collateral closed type. Each bundle has a distinct sclerenchyma the cover (Figure 3).

In the thickness of the central cylinder, large parenchymal cells are noted. The main biometric indicators of the stem include: the thickness of the primary bark, the diameter of the central cylinder and the area of xylem vessels, whose biometric indicators are shown in Table 3.

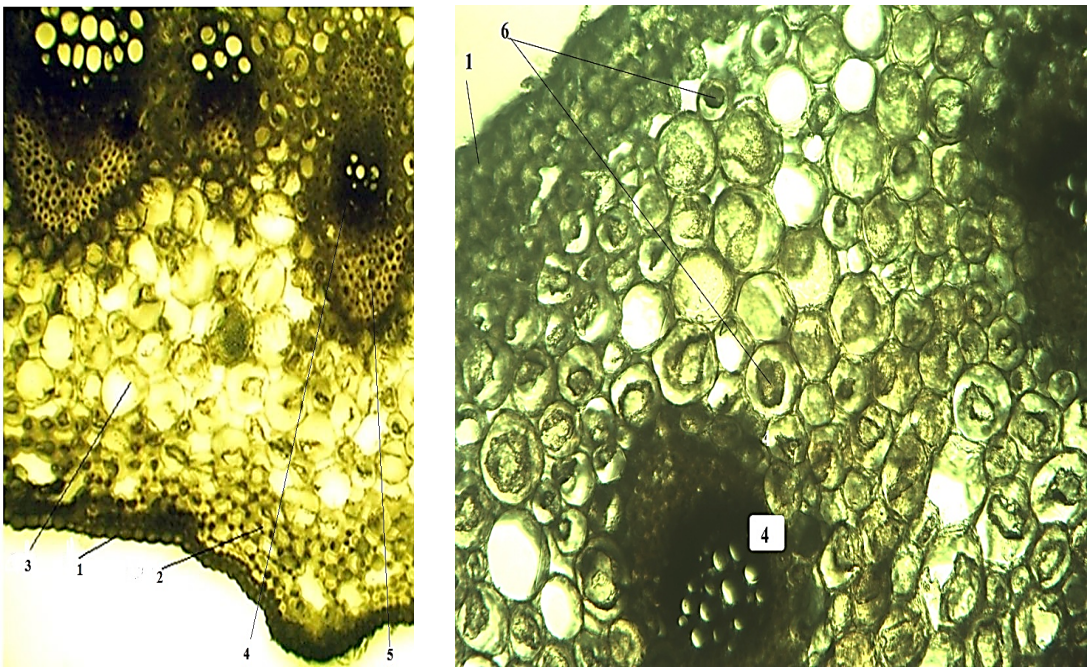

Figure 3 – Cross section of the stem *Rheum wittrockii* (magnification 140).
Note: 1-epidermis, 2-chlorophyll-bearing parenchyma of the primary cortex,
3-rounded cells of the primary cortex, 4-conducting bundle,
5-sclerenchymal lining of the bundle, 6-inclusions.

Table 3 – Morphometric indicators of the anatomical structure of the stem.

Thickness of the primary crust, µm	Diameter of the central cylinder, µm	Area of conducting beams, $x10^{-3}mm^2$
60.18± 3.32	123.17± 9.26	35.72± 6.42

Table 3 shows that the thickness of the primary crust is half the diameter of the central cylinder. Thus, the anatomical study of the leaf blade, root and stem of *Rheum wittrockii* allowed us to determine the features of their structure, as well as to identify additional diagnostic features. As a result of the morphological and anatomical studies of rhubarb wittrockii confirmed the classic structure of the root. Based on the results of morphological and anatomical studies, the criteria for differential diagnosis of the leaf blade, root and stem of *Rheum wittrockii* Lundstr. were determined, which allow for reliable identification of medicinal raw materials.

The next stage of the work was the phytochemical study of this species. Gas-liquid chromatography was used to determine the chemical components

of rhizomes of *Rheum wittrockii*, which allows the analysis, separation and purification of polymers, drugs, proteins, hormones, detergents and other biologically important compounds. When using highly sensitive detectors, the work was carried out with very small amounts of compounds (10^{-11}-10^{-9} g), which is very important. GC-MS chromatogram of the ethanol extract of *Rheum wittrokii* Lundstr. (Figure 4).

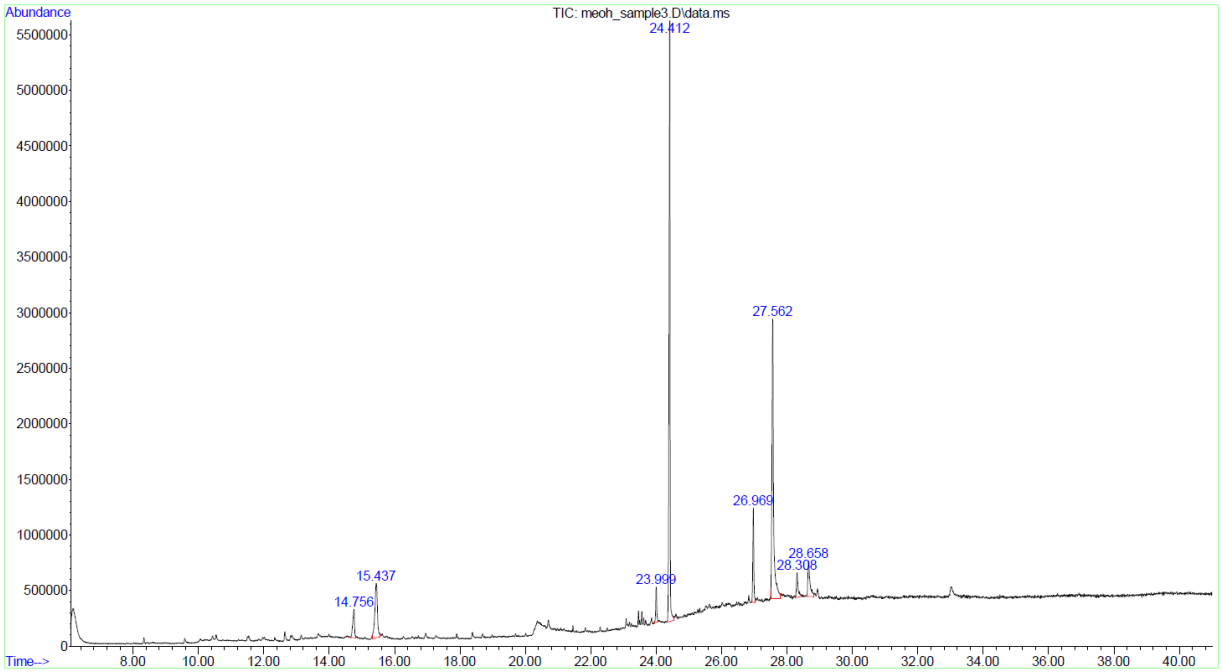

Figure 4 - Chromatogram analysis of *Rheum wittrokii* rhizome extract.

The chromatogram of the analysis of *Rheum wittrokii* rhizome extract (Fig. 4) shows the peak retention time (min) of the following components: sucrose - 14.8, levoglucosan - 15.4, chrysarobin - 24.0, chrysophanic acid - 24.4, emodin-3- methyl ether - 27.0, 4,4'-dimethoxy-2,2'-dimethylbiphenyl - 27.6, emodine 1,3,8-trihydroxy-6-methylanthracene-9,10-dione - 28.3, anthracene octahydrate , 3,9-dimethyl-4-hydroxymethyl-3- [[1-carboxy-2,5,6-trimethyl] heptyl] - 28.7 minutes.

As a result of studying the chemical composition of the ethanol extract *Rheum wittrockii* Lundstr. obtained by extracting 96% ethanol, 8 main components of various chemicals were identified using GC-MS. Chemical analysis of rhizomes allowed to determine useful and medicinal properties with the content of certain components (Figure 5).

Figure 5 determines the chemical content of *Rheum wittrokii* rhizome extract (%), which showed the results: sucrose - 3.2%, levoglucosan - 9.2%, chrysarobin - 2.4%, chrysophanic acid - 41.4%, emodin 3- methyl ether - 6.0%, 4,4'-dimethoxy-2,2'-dimethylbiphenyl - 30.3%, emodine 1,3,8-trihydroxy-6-methylanthracene-9,10-dione - 2.5% , anthracene octahydrate, 3,9-dimethyl-4-hydroxymethyl-3- [[1-carboxy-2,5,6-trimethyl] heptyl] - 4.9%.

Table 4 shows the list and number of biologically active components identified by GC-MS in rhizomes of *Rheum wittrokii*. In the course of a phytochemical study, 8 main compounds of various nature were isolated from the rhizomes of the studied species, according to literature sources: sucrose, laevoglucose, chrysarobin, chrysophanic acid, emodin 3-methyl ether, 4,4'-dimethoxy-2,2'-dimethylbiphenyl, emodin, anthracene octahydrate, 3,9-dimethyl-4-hydroxymethyl-3-[1-carboxy-2,5,6-trimethyl] heptyl], which are shown in table 4. It is obvious that with the probability of identification, the percentage of chrysophanic acid predominates in the rhizomes, which is 41.4%.

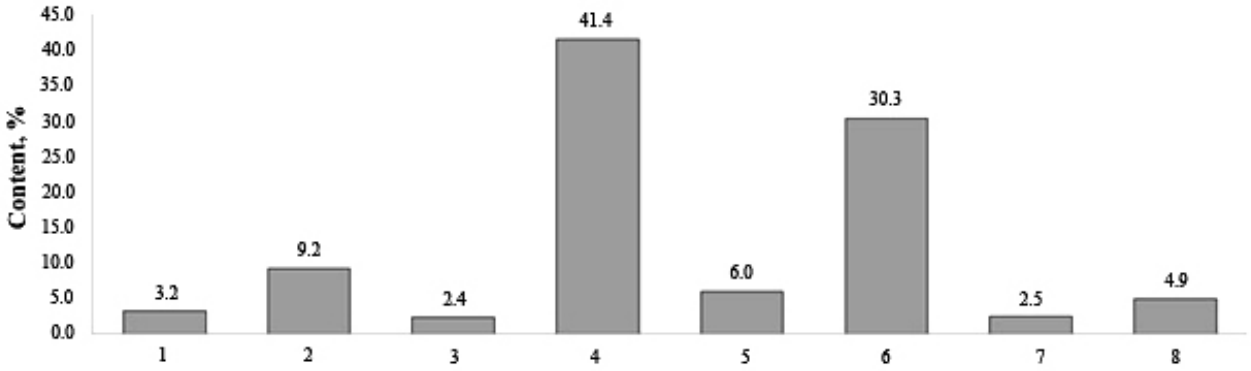

Figure 5 – Content of chemical substances in the extract of rhizomes of Rheum wittrokii (%).
Note: 1- Sucrose, 2 – Levoglucosan, 3 – Chrysarobin, 4 – Chrysarobin,
5 - Chrysophanic acid, 6 - 4,4'-dimethoxy-2,2'-dimethylbiphenyl, 7 - Emodine 1,3,8-trihydroxy-6-methylanthracene-9,10-dione,
8 - Anthracene octahydrate, 3,9-dimethyl-4-hydroxymethyl-3- [[1-carboxy-2,5,6-trimethyl] heptyl]

Table 4 – Results of chromatographic analysis of the extract of *Rheum wittrokii.*

No.	Retention time, min	Compound	Identification probability,%	Percentage,%
1	14.8	Sucrose	71	3.2
2	15.4	Levoglucose	80	9.2
3	24.0	Chrysarobin	69	2.4
4	24.4	Chrysophanic acid	93	41.4
5	27.0	Emodin 3-methyl ether	84	6.0
6	27.6	4,4'-dimethoxy-2,2'-dimethylbiphenyl	76	30.3
7	28.3	Emodin 1,3,8-Trihydroxy-6-methylanthracene-9,10-dione	71	2.5
8	28.7	Anthracene octahydrate, 3,9-dimethyl-4-hydroxymethyl-3-[[1-carboxy-2,5,6-trimethyl] heptyl]	74	4.9

From Table 4 it is seen that the components that make up the rhizomes of *Rheum wittrokii*, such as chrysophanic acid (41.4%), 4,4'-dimethoxy-2,2'-dimethylbiphenyl (30.3%), levoglucosan (9.2%), anthracene octahydrate, 3,9-dimethyl-4-hydroxy-methyl-3-[[1-carboxy-2,5,6-trimethyl] heptyl] (4.9%) are in the largest quantities. The smallest amount was found for emodin 3-methyl ether (6.0%), sucrose (3.2%), emodin 1,3,8-trihydroxy-6-methylanthracene-9,10-dione (2.5%) and chrysarobin (2.4%).

Results of chromatographic analysis of the extract, the activity of some of the studied components of rhizomes of *Rheum wittrokii* Content, % should be distinguished (Table 5).

From Table 5 it should be noted that in the extract of *Rheum wittrokii* rhizomes there are components, such as sucrose used in the treatment of type 2 diabetes mellitus, in the pharmaceutical industry for the manufacture of various medicines. Levoglucosan is an intermediate of the usual distillation of cellulose. Chrysarobin is intended for the treatment of skin diseases (lichen and eczema), is a product of the restoration of chrysophanic acid, has a stable, anti-inflammatory and absorbable effect, can be used for fungal infections of the fingers and feet, pro-inflammatory

and antipruritic, and also relieves cramping in the gastrointestinal tract and biliary tract. Chrysophane acid has an antioxidant effect and is used to treat skin diseases (lichen and eczema). Emodin 3-methyl ether suppresses 26 types of bacteria: *Staphylococcus aureus, Escherichia coli,* green sepsia, streptococcus and dysentery; participates in mutation in an experiment with salmonella TA1535; more strongly inhibits the growth of HeLa cells in cervical cancer, has antibacterial properties, is used as a laxative, etc. Emodin 1, 3, 8-trihydroxy-6-methylanthracene-9, 10-dione inhibits cell proliferation, induces apoptosis and metastasis prophylaxis, and is involved in the death of liver and lung cancer cells.

Table 5 – Activity of Rheum wittrokii rhizome extract.

No.	Components	Formula	Active action	Reference
1	Sucrose	$C_{12}H_{22}O_{11}$	useful in the treatment of type 2 diabetes, in the pharmaceutical industry for the manufacture of various medicines	[23]
2	Levoglucose	$C_6H_{10}O_5$	conventional cellulose intermediate	[24]
3	Chrysarobin (methyldioxyanthranol) chrysarobinum hydroxyl derivatives of anthracene and dihydroanthracene hydrocarbons	$C_{30}H_{26}O_7$	valuable in the treatment of skin diseases (lichen and eczema), it is a product of the restoration of chrysophanic acid, has a stable, anti-inflammatory and resorbing effect, can be used for fungal lesions of the fingers and feet, proinflammatory and antipruritic agent, as well as relieves spasms in the gastrointestinal tract and bile ducts	[25-27]
4	Chrysophanic acid (1,8-dihydroxy-3-methylanthraquinone) or (dioxymethylanthraquinone)	$C_{15}H_{10}O_4$	famous for its antioxidant effect, for the treatment of skin diseases (lichen and eczema)	[28-30]
5	Emodin-3-methyl ether	$C_{16}H_{12}O_5$	destroys 26 types of bacteria: Staphylococcus aureus, E. coli, green sepsis, Streptococcus and dysentery; mutation in the experiment with Salmonella TA1535; stronger inhibition of Hela cell growth in cervical cancer; antibacterial, used as a laxative, etc.	[31-34]
6	Emodin 1,3,8-trihydroxy-6-methylanthracene-9,10-dione	$C_{15}H_{10}O_5$	inhibits cell proliferation, stimulates the induction of apoptosis induction and profilaktiku of metastasis, is involved in cell death of liver cancer and lung cancer	[35–40]

Thus, components such as chrysarobin, chrysophanic acid, emodin 3-methyl ether, emodin-1, 3, 8-trihydroxy-6-methylanthracene-9, 10-dione are directly involved in the metabolism of the body, providing antioxidant, antiseptic and anticancer effects [41; 42]. Based on our results, it can be concluded that *Rheum wittrokii,* as a representative of rare and endangered species, contains in its roots biologically active compounds, which, according to research and literature review, can beneficially affect the human body.

Conclusion

The following morphometric indicators of the leaf blade anatomical structure were found in the medicinal rare plant *Rheum wittrokii*: upper epidermis, lower epidermis, columnar mesophyll, spongy mesophyll, central conducting bundle, sclerenchyma cells, and calcium oxalate druses. The cross section of the stem of *Rh. wittrockii* L. includes: the epidermis, chlorophyll-bearing parenchyma of the primary cortex, rounded cells of the primary cortex, conducting bundle, sclerenchymal lining of the bundle, inclusions. The cross section of the root of *Rheum wittrockii* is characterized by morphological indicators on the anatomy of this plant: cork (fellema), fellogen, felloderm, main bark parenchyma, cambial ring, xylem parenchyma, wood vessels (secondary xylem), calcium oxalate druses, secondary phloem, primary xylem. Thus, morphometric indicators of the anatomical structure of the leaf blade have a thickness of the upper epidermis of 10.06 ± 0.06 μm and the lower epidermis of 13.11 ± 0.09 μm, the thickness

of columnar mesophyll 93.23 ± 0.16 μm and spongy mesophyll 81.15 ± 0.24 μm, and the thickness of the sheet plate itself is 197.55 ± 14.02 μm. Morphometric parameters of the anatomical structure of the root consist of a thickness of the primary cortex of 120.09 ± 7.12 μm, a diameter of the central cylinder of 161.28 ± 10.89 μm, and an area of xylem vessels of 86.13 ± 16.81 μm^2. Morphometric indicators of the anatomical structure of the stem include the thickness of the primary cortex 60.18 ± 3.32 μm, the diameter of the central cylinder 123.17 ± 9.26 μm and the area of the conducting beams 35.72 ± 6.42 x 10^{-3} mm^2.

Phytochemical analysis showed that the root of *Rheum wittrokii* contains carbohydrates, organic acids, catechins, anthraquinones: tannoglycosides and atroglycosides. As is already known, GC-MS (Agilent 6890N/ 5973N, USA) analysis in the study showed the results of chemical compounds, their percentage, retention time can be especially useful in assessing and the likelihood of identifying their chemical characteristics. Components such as chrysophanic acid (41.4%), 4,4'-dimethoxy-2,2'-dimethylbiphenyl (30.3%), levoglucosan (9.2%), anthracene octahydrate, 3,9-dimethyl-4-hydroxymethyl-3-[[1-carboxy-2,5,6-trimethyl] heptyl] (4.9%) are in the greatest quantities. The smallest amount was found for emodin 3-methyl ether (6.0%), sucrose (3.2%), emodin 1,3,8-Trihydroxy-6-methylanthracene-9,10-dione (2.5%) and chrysarobin (2.4%). Thus, 41.4% of the content of ethyl extract of rhizomes of *Rheum wittrokii* contains chrysophanic acid, which indicates an effective antioxidant effect in the treatment of skin diseases (lichen and eczema). Emodin 3-methyl ether is involved in the suppression of 26 types of bacteria: Staphylococcus aureus, E. coli, green sepsis, Streptococcus and dysentery; mutations in the experiment with Salmonella TA1535; in stronger inhibitions of Hela cell growth in cervical cancer; antibacterial, used as a laxative, etc. Emodin 1,3,8-Trihydroxy-6-methylanthracene-9,10-dione inhibits cell proliferation, induces the induction of apoptosis and praphylaxis of metostases, and is involved in the death of liver cancer and lung cancer cells. Chrysarobin is a product of the recovery of chrysophanic acid, has a stable, anti-inflammatory and resorbing effect, can be used for fungal lesions of the fingers and feet, anti-inflammatory and antipruritic agent, and also relieves spasms in the gastrointestinal tract and bile ducts. In the ethyl extract of rhizomes, the presence of chemical components that have great potential in the treatment of many diseases of the body, providing antiseptic, anti-inflammatory, astringent properties that can enhance intestinal peristalsis, which makes it a choleretic and laxative. It also affects the treatment of anemia and tuberculosis, participating in the removal of toxins, which has a beneficial effect on the overall therapeutic state.

References

1 The State Pharmacopoeia of the Republic of Kazakhstan. 2009, no. 2, 802 p. ISBN 9965-759-96-0

2 Dagarova S. S, Sitpayeva G. T. Conservation of Biodiversity of wild Plant of Rheum Wittrockii Lundstr of Kazakhstan. Biosci Biotech Res Asia 2017; 14(1). Available from: http://www.biotech-asia.org/?p=22007

3 Kukenov M.K. Botanical Resource Science of Kazakhstan / M.K. Kukenov. - Almaty: Gylym, 1999. - 176 p. ISBN 9965-473-62-5

4 Borisova M.A., Marakaev O.A. Rare plant species: practice research in nature. - Yaroslavl, 2015. - 64 p. ISBN: 978-0-470-85040-4

5 G. M. Kudabayeva, P. V. Vesselova, M. P. Danilov, B. M. Sultanova, Important Plant Areas of the Peri-North Tien Shan Subprovince as Perspective Protection Areas of Phytobiodiversity, American Journal of Environmental Protection. Special Issue: Applied Ecology: Problems, Innovations. Vol. 4, no. 3-1, 2015, pp. 123-129. doi: 10.11648/j.ajep.s.2015040301.29

6 Holsinger K.E. Demography and extinction in small populations // In: Young A.G., Clarke G.M. (Eds.), Genetics, Demography and Viability of Fragmented Populations. - Cambridge: Cambridge University Press, 2000. - P. 55-74. www.Cambridge University Press. org/9780521783385

7 The Red Book of Kazakhstan. Vol. 2. Part 1. Plants. - Astana, 2014. - 452 p.

8 Chevalier A. Encyclopedia of herbal medicine. DK / Penguin Random House, 2016, p. 127. ISBN: 0-7894-6783-6

9 Mukhitdinov N.M., Ivashchenko A.A., Kurbatova N.V., Abidkulova K.T., Kurmanbaeva M.S., Ametov A.A., Mukasheva K.M. Features of the external and internal structure of the medicinal plant Rheum wittrokii Lundstr in Zailiysky Alatau. Article. International Journal of Applied and Basic Research. Publisher: Publishing House Academy of Natural Sciences (Penza). No. 12. 2017 p. 112-116. ISSN: 1996-3955

10 Gao, L., Xu, X. & Yang, J. Chemical constituents of the roots of Rheum officinale. Chem Nat Compd 49, 603–605 (2013). https://doi.org/10.1007/s10600-013-0689-7

11 Muzychkina R.A., Kurbatova N.V., Korulkin D.Yu. The component composition and biological activity of polyphenolic metabolites of Rumex tianschanicus A. Los. KazNU Bulletin. Biology series. No. 4 (69). 2016. Pp. 22-31. ISSN 1563-0218

12 Shynar S. Dagarova, Gulnara T. Sitpayeva, Jae-Hong Pak & Jung Sung Kim (2017) The complete plastid genome sequence of Rheum wittrockii (Polygonaceae), endangered species of Kazakhstan, Mitochondrial DNA Part B, 2:2, 516-517, DOI: 10.1080/23802359.2017.1361359

13 Pandith, S.A., Dar, R.A., Lattoo, S.K. et al. Rheum australe, an endangered high-value medicinal herb of North Western Himalayas: a review of its botany, ethnomedical uses, phytochemistry and pharmacology. Phytochem Rev 17, 573–609 (2018). https://doi.org/10.1007/s11101-018-9551-7

14 Li YX, Gong XH, Li Y, et al. The Influence of Aconitum carmichaelii Debx. on the Pharmacokinetic Characteristics of Main Components in Rheum palmatum L. Phytother Res. 2015;29(8):1259-1264. doi:10.1002/ptr.5369

15 Diaz-Muñoz G, Miranda IL, Sartori SK, de Rezende DC, Alves Nogueira Diaz M. Use of chiral auxiliaries in the asymmetric synthesis of biologically active compounds: A review. Chirality. 2019;31(10):776-812. doi:10.1002/chir.23103

16 Thomford NE, Senthebane DA, Rowe A, et al. Natural Products for Drug Discovery in the 21st Century: Innovations for Novel Drug Discovery. Int J Mol Sci. 2018;19(6):1578. Published 2018 May 25. doi:10.3390/ijms19061578

17 The State Pharmacopoeia of the Republic of Kazakhstan. 2008, No. 1, 591 p.

18 Prozina M.N. Botanical microtechnics. - M., 1960 .-- 208 p.

19 Permyakov A.I. Mikrotehnika - M., 1988. - S. 11-18, 28-29. ISBN 5-211-00683-6: 10 к

20 Barykina R.P., Veselova T.D., Devyatov A.G. et al. Handbook of Botanical Microtechnology (Fundamentals and Methods). - M., Moscow State University, 2004. - 312s. ISBN 5-211-06103-9.

21 G.G. Fourst. Methods of anatomical and histochemical studies of plant tissues. Moscow: Nauka, 1979. - 154 p.

22 Vekhov V.N., Lotova L.I., Filin V.R. Workshop on the anatomy and morphology of higher plants. - Moscow: Moscow State University, 1980. - 560 s.

23 The State Pharmacopoeia of the Russian Federation of the XIII edition. 2016 (Order of the Ministry of Health of Russia no. 771, 2015). FS.2.1.0034.15 Sucrose.

24 Bacik JP, Klesmith JR, Whitehead TA, et al. Producing glucose 6-phosphate from cellulosic biomass: structural insights into levoglucosan bioconversion. J Biol Chem. 2015;290(44):26638-26648. doi:10.1074/jbc.M115.674614

25 Jeong HJ, Kim HY, Kim HM. Molecular mechanisms of anti-inflammatory effect of chrysophanol, an active component of AST2017-01 on atopic dermatitis in vitro models. Int Immunopharmacol. 2018;54:238-244. doi:10.1016/j.intimp.2017.11.019

26 Matsuda H, Morikawa T, Toguchida I, Park JY, Harima S, Yoshikawa M. Antioxidant constituents from rhubarb: structural requirements of stilbenes for the activity and structures of two new anthraquinone glucosides. Bioorg Med Chem. 2001;9(1):41-50. doi:10.1016/s0968-0896(00)00215-7

27 Onoda T, Li W, Sasaki T, Miyake M, Higai K, Koike K. Identification and evaluation of magnolol and chrysophanol as the principle protein tyrosine phosphatase-1B inhibitory compounds in a Kampo medicine, Masiningan. J Ethnopharmacol. 2016;186:84-90. doi:10.1016/j.jep.2016.03.063

28 Choi JS. Chrysophanic Acid Induces Necrosis but not Necroptosis in Human Renal Cell Carcinoma Caki-2 Cells. J Cancer Prev. 2016;21(2):81-87. doi:10.15430/JCP.2016.21.2.81

29 Fei Y, Wang J, Peng B, et al. Phenolic constituents from Rheum nobile and their antioxidant activity. Nat Prod Res. 2017;31(24):2842-2849. doi:10.1080/14786419.2017.1303691

30 Vysocina (Vysocina) G. (Galina) I. (Ivanovna). Antrakhinones and biological activity of species of the genus Rheum L. (Poligonatseva) (Review) // Chemistry of plant raw materials, 2018. No. 4. P. 29-41. URL: http://journal.asu.ru/cw/article/view/3785

31 Huang Q, Shen HM, Ong CN. Inhibitory effect of emodin on tumor invasion through suppression of activator protein-1 and nuclear factor-kappaB. Biochem Pharmacol. 2004;68(2):361-371. doi:10.1016/j.bcp.2004.03.032

32 Huang Q, Shen HM, Ong CN. Emodin inhibits tumor cell migration through suppression of the phosphatidylinositol 3-kinase-Cdc42/Rac1 pathway. Cell Mol Life Sci. 2005;62(10):1167-1175. doi:10.1007/s00018-005-5050-2

33 Tikhomirov AS, Shtil AA, Shchekotikhin AE. Advances in the Discovery of Anthraquinone-Based Anticancer Agents. Recent Pat Anticancer Drug Discov. 2018;13(2):159-183. doi:10.2174/1574892813666171206123114

34 Tutin, F., Clewer HWB. The constituents of rhubarb. J. Chem. Soc., Trans. 1911,99 , 946-967. https://doi.org/10.1039/CT9119900946

35 Ramana L.V., Apparato K.S., Rao B.N., Rao M.S. New phenolic constituents from the bark of Valsurian tripholyate. J. Pharmacogn. Phytochem. 2017; 6: 1314–1316

36 Fuyo M., Venkatachalam M., Girard-Valenciennes E., Caro J., Dufos L. Antraquinones and their derivatives from fungi of marine origin: structural diversity and individual biological activities. Mar. Drugs. 2016; 14: 64. https://doi.org/10.3390 / md14040064

37 Malik EM, Müller CE. Anthraquinones As Pharmacological Tools and Drugs. Med Res Rev. 2016;36(4):705-748. doi:10.1002/med.21391

38 Zhang B, Ji J, Liu X, et al. Rapid adsorption and enhanced removal of emodin and physcion by nano zirconium carbide. Sci Total Environ. 2019;647:57-65. doi:10.1016/j.scitotenv.2018.07.422

39 Sanders B, Ray AM, Goldberg S, et al. Anti-cancer effects of aloe-emodin: a systematic review. J Clin Transl Res. 2017;3(3):283-296. Published 2017 Sep 7.

40 Huang D, Ou B, Prior RL. The chemistry behind antioxidant capacity assays. J Agric Food Chem. 2005;53(6):1841-1856. doi:10.1021/jf030723c

41 Rajkumar V, Guha G, Ashok Kumar R. Antioxidant and Anti-Cancer Potentials of Rheum emodi Rhizome Extracts. Evid Based Complement Alternat Med. 2011;2011: 697986. doi:10.1093/ecam/neq048

42 Li Y, Jiang JG. Health functions and structure-activity relationships of natural anthraquinones from plants. Food Funct. 2018;9(12):6063-6080. doi:10.1039/c8fo01569d

IRSTI 34.23.35 https://doi.org/10.26577/ijbch.2020.v13.i2.10

O.A. Iksan[1,2*], I.A. Kisselev[1], A.A Garshin[1,2], L.A. Skvortsova[1], Zh.A. Zhaniyazov[1], M.A. Alpysbes[3], Charleston W. K. Chiang[4], L.Z. Musralina[1], G.S. Zhunussova[1], E.M. Khussainova[1]

[1]Institute of General Genetics and Cytology, Almaty, Kazakhstan
[2]Al-Farabi Kazakh National University, Almaty, Kazakhstan
[3]Eurasian National University by L.N. Gumilyov, Nur-Sultan, Kazakhstan
[4]University of Southern California, Los Angeles, USA
*e-mail: o.ixan@mail.ru

Analysis of the Kazakh tribe Baiuly based on the distribution of the Y-chromosome haplogroups

Abstract. A haplogroup is a group of similar alleles that have a common ancestor in which a mutation has occurred, inherited by all descendants. Haplogroups, particularly from the Y-chromosome (Y-DNA), is widely used in population genetics and genetic genealogy, a science that studies the genetic history of mankind. Recent studies of the Y-chromosome of modern Kazakhs have demonstrated the diversity of the Kazakh gene pool. During the expedition carried out in 2014-2016, clinical material was collected from varios regions of Kazakhstan, representing samples of peripheral blood and buccal scrapings. All representatives of Kazakh nationality were familiarized with informed consent. In total 1623 respondents participated in the study, 169 of whom were representatives from Baiuly tribe of Junior zhuz. We analyzed the provided samples and found that the Baiuly is characterized by 10 haplogroups, the most prevailing of which is the C2 haplogroup (85%).

Key words: Y-chromosome, haplogroup, haplotype, kazakh, junior zhuz, Baiuly tribe.

Introduction

Historically, Kazakhs were formed by a combination of previously isolated or differentiated nomadic tribes belonging to the Golden Horde. Kazakh tribes were geographically divided into three tribal associations – Senior, Middle and Junior zhuzes. Each of which is characterized by its own unique tribal composition and occupied territory [1]. Nowadays, many modern representatives of previously nomadic ethnic groups, including Kazakhs, have retained knowledge of their tribal affiliation as part of their tradition and culture.

According to the latest estimates of Professor B. Rakishev, carried out in 2013, the smallest of the three Kazakh zhuzes is the Junior Zhuz, numbering 2,521,900 people. The junior zhuz is made up of three main tribes – Baiuly, Alimuly and Zhetiru. The Baiuly tribe is the most numerous tribe in the Junior Zhuz and with 1,120,000 people, it is the third in size among all Kazakh tribes after the Argyn and Dulat tribes [2].

At the moment, the Baiuly tribe mainly inhabits the western part of Kazakhstan, namely in the Mangistau, Atyrau and West Kazakhstan regions, as well as in the border regions of Russia, such as the Astrakhan region or Orenburg. Due to the small number of sources and inconsistent accounts, many questions remain regarding the origin of Kazakh tribes. The formation of Kazakh zhuzes is also not recorded in written history, which contributed to existence of various versions of the Kazakh origin among historians and ethnographers.

In the encyclopedia of Brockhaus and Efron, published from 1890 to 1916: “Baiuly are one of the three generations that make up the Junior Kazakh Horde. According to Kazakh legend, the ancestor of this generation is Kadyrkazhi (Kadyr-Hajja), the son of Alshin, the founder of the Junior Horde. “Baiuly” (Kadyrkazhi) had 12 sons who were the founders of the 12 tribes of Baiuly dynasty. The names of the tribes of the Baiuly dynasty: Berish, Sherkesh, Maskar, Adai, Zhapas (Zhappas), Ysyk, Essentemir, Baibakty, Alasha, Tana, Kyzylkurt and Taz”. How-

ever, there are other facts in the historical literature [3].

According to the genealogy, Baiuly became a member of the Junior Zhuz and joined to the Alshin union. According to some reports, the Baiuly tribe was once located on the banks of the Bai-Taiga (rich taiga), which covers an area of 600 square kilometers in the upper reaches of the Alash river (Figure 1). The people of this taiga, with rich wildlife, where hunting is practiced, probably joined the Jochi army under the name of Bai. The name «Baiuly» first appears in historical documents in 1561. On June 23 same year, the bi of Nogai Horde Smail, in a letter to the Russian Tsar Ivan the Terrible, called Baiuly as ulus [4].

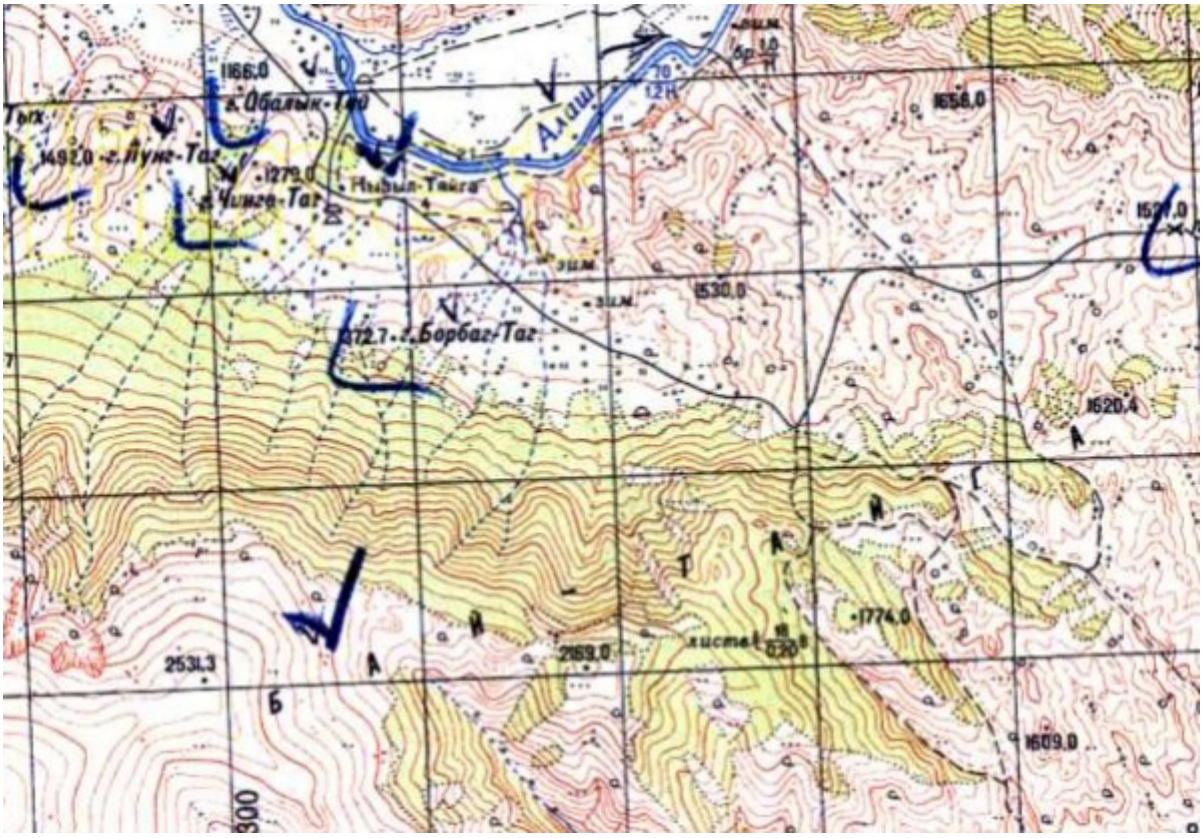

Figure 1 – Bay-taiga region in the upper reaches of the Alash River, which in ancient times was the habitat of the Bayuly tribe [5]

In addition to the study of historical text, another important approach to study the formation of any ethnic groups, tribes or tribes is through population genetic research of the ancient and modern population using modern methods of physical anthropology and molecular genetics.

Research on the Y-chromosome is the most relevant to the current study here. Because of haploidy, Y-chromosome is transmitted strictly through the paternal line and does not undergo recombination. As a result, the Y chromosome haplogroups are very effective markers that can be used to study migration events in the history of certain peoples and the formation of an ethnic group as a whole. Such studies have been carried out in many populations around the world. At this time, there is an active accumulation of information on various markers of the Y-chromosome in Kazakh tribes [6-8]. However, the haplogroup of the Baiuly tribe has not been sufficiently studied.

Therefore, the purpose of this work was to study the composition of the gene pool of the Baiuly tribe using materials from the Population Genetics Laboratory of the Institute of General Genetics and Cytology.

Materials and methods

The study used biomaterials of the modern population of Kazakhstan (DNA, blood and buccal scrapings) stored in the Genbank of the Laboratory of Population Genetics of the Institute of General Genetics and Cytology. In total, 1623 volunteers participated

in the study, of which 169 people are representatives of the Baiuly tribe. The main biomaterial was collected during the expedition in 2014-2016 from Kazakh nationals with voluntary informed consent across various regions of the Republic of Kazakhstan. The ethnic and tribal affiliation of the volunteers was determined by a detailed individual questionnaire.

DNA was extracted from buccal scrapings and frozen (-20 °C) peripheral blood samples containing EDTA as an anticoagulant agent. The QIAamp DNA Mini Kit (Qiagen, Germany) and the GeneJET Genomic DNA Purification Kit (Thermo Scientific, USA) were used for extracting genomic DNA.

Quantitative and qualitative assessment of the extracted DNA was performed using a DNA photometer (Biofotometer Plus, Eppendorf, Germany) and electrophoretic analysis using EV265 Power Supply (Consort, India).

Genotyping of 17 polymorphic STR loci (DYS19, DYS389I, DYS389II, DYS390, DYS391, DYS392, DYS393, DYS385a, DYS385b, DYS437, DYS438, DYS439, DYS448, DYS456, DYS458, DYS448, DYS456, DYS458, DYS635, multi-GATA format) by PCR using the enzymatic amplification system of the AmpFlSTR YfilerTM kit (Life Technologies, USA). Amplification products were separated and determined using an ABI PRISM 310 genetic analyzer (Applied Biosystems, USA). Alleles were identified using the GeneMapperID ID-X v1.4 software (Thermo Scientific, USA) based on the allelic ladders included in the sets.

Previously, haplogroups were identified using Whit Athey's online predictors (http://www.hprg.com) and NEVGEN (http://www.nevgen.org/) based on microsatellite haplotype data. Then the samples were tested for 15 single nucleotide polymorphisms (M231, M217, M215, M17, M285, M242, M343, M172, M122, P37.2, M61, P15, M253, M479 and M267) to clarify the haplogroups of the Y chromosome. Analysis of polymorphisms was performed using PCR with subsequent restriction and analysis of the length of restriction fragments (PCR-RFLP). The primer sequences and reaction conditions are shown in Table 1.

Table 1 – The primer sequences and reaction conditions

Haplogroup	Marker(1)	Primer sequence 5'-3'	Fragment Size (bp)	Mutation	Mutated position (nt)	Enzyme	Allele Fragments (bp)
C2	M217	f tgaaggagaatgaaaaagttgggtggc r agcaaaagataattgttccagggt	352	A→C	327	BanI	(A)352 (C)327/25
N	M231	f attatcctggaaaatgtgggctcg r tccgattcctagtcacttggtt	326	G→A	326	TaqI	(G)221/105 (A)326
E1b1b	M215	f gtaaaactcagatatatacatcccatg r aaaaaaaaagaatcactatcttaacg	386	A→G	222	Bse1l	(A)386 (G)222/164
R1a1	M17	f ctggtcataacactggaaatc f tgaacctacaaatgtgaaact	168	4G→3G	DdeI	MluI	(4G)168 (3G)24/144
Q	M242	f aactcttgataaaccgtgctg r tccaatctcaattcatgcctc	366	C→T	180	Alw21I	(C)187/179 (T)366
G2a	P15	f gagttttctaacagggcgtaaca r caactttcatctgccttcagac	155	C→T	133	HpyCH4IV	(C)134/23 (T)157
I1	M253	f gcaacaatgagggttttttg r cagctccacctctatgcagttt	400	C→T	283	HincII	(C)280/120 (T)400
I2	P37.2	f cgtctatggccttgaaga r tccgaaaatgcagacttt	447	T→C	135	HpyCH4III	(T)447 (C)311/136
J2	M172	f aaattaggagccagatgacc r aataataattgaagacctttgagt	176	T→G	151	HinfI	(T)176 (G)151/25
L	M61	f attggattgatttcagccttc r attttattttctgtgttccttgc	190	C→T	98	TaqI	(C)97/93 (T)190
R1b	M343	f gcagagtgccctcgtggt r acctggaaccagtgctcctt		A→G		Hpy8I	

Continuation of table 1

Haplogroup	Marker(1)	Primer sequence 5'-3'	Fragment Size (bp)	Mutation	Mutated position (nt)	Enzyme	Allele Fragments (bp)
G1	M285	f ggatggacaaggtaagacttttca r ctgttgcccaggctagtgtc	371	G→C	371	RsaI	(G)175/196 (C)371
O2	M122	f tagaaaagcaattgagatactaattca r gcgatgctgatatgctagttcag	122	A→G	73	Hin1II (NlaIII)	(A)100/22 (G)122
J1	M267	f acgtcacccatctcaacatc r aaagaatgtctccccatgagg	306	T→C	189	DdeI	(T)158/69/49/3 (C)207/69/30
R2	M479	f gatactttatcaggcttacttc r cgattctgagagatttggtt	323	C→T	107	HphI	

Results and discussion

The study of the haplotype diversity of the Y chromosome in the Kazakh population belonging to the Baiuly tribe (Junior Zhuz) revealed 10 haplogroups, of which 8 were identified as a result of testing single nucleotide polymorphisms, and 2 haplogroups (O1b2 and T) were determined by the NevGene predictor using the microsatellite haplogroup. Analysis of the spectrum of Y-chromosome haplogroups in the Baiuly tribe showed the presence of a major haplogroup C-M217, which makes up 85% of their gene pool. The remaining 15% of the Bayuly tribe gene pool is represented by the sector of 9 identified haplogroups, but their percentage is extremely small, where each of them is less than 5% of the total composition of haplogroups (Figure 2).

Haplogroup C-M217, also known as C2 (and previously as C3), is the most frequently occurring branch of the wider Y-chromosome DNA haplogroup C (M130) [9]. It is found mostly in central Asia, Eastern Siberia and at is present at significant frequencies in part of East Asia and Southeast Asia including some populations in the Caucasus and Middle East. It is assumed that haplogroup C-M217 originated approximately 7,100 – 16,700 years ago in eastern or central Asia. The closest phylogenetic relatives are found in the vicinity of South Asia, East Asia, or Oceania.

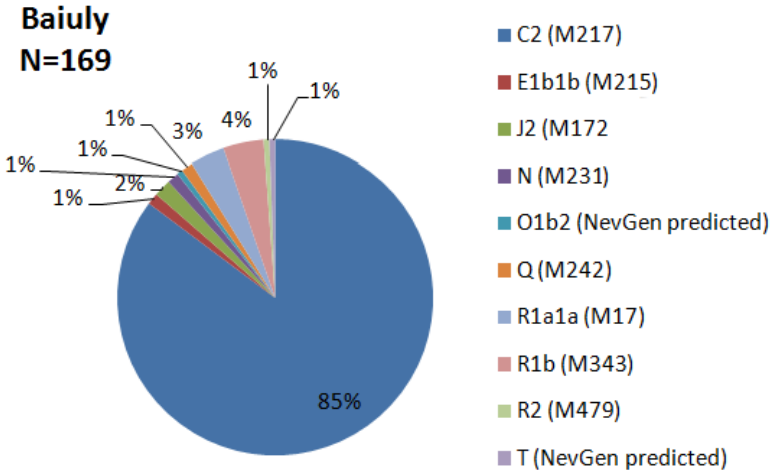

Figure 2 – Diagram of distribution of the Y-chromosome haplogroups in the Kazakh tribe Baiuly

The haplogroup C-M217 is now found at high frequencies among Central Asian peoples, indigenous Siberians, and some Native peoples of North America. In particular, males belonging to peoples such as the Buryats, Evenks, Kalmyks, Kazakhs, Mongolians, and others have high levels of M-217 [10-17]. Among Kazakhs from different regions of Kazakhstan, the total occurrence of variants of hap-

logroup C2 on average reaches 80% [18-22]. One particular haplotype within Haplogroup C-M217 (star-cluster C2*(C2*-ST)) has received a great deal of attention, because of the possibility that it may represent direct patrilineal descent from Genghis Khan [23], though that hypothesis is controversial. In a recent study [24] of Y-chromosomes of more than 800 people, carriers of the "star-cluster" C2 *, showed that its origin and distribution in Eurasia is more likely associated with the ancient Mongol-speaking tribes than with Genghis Khan. According to the data, the estimated age of the C2 * – ST star cluster was 2576 years, preceding the rise of the Great Mongol Empire [25]. The authors hypothesize that the C2 * -ST line originated in the northern region of the Greater Khingan and spread during the dispersal of ancient Mongolian-speaking populations. Thus, this is the initially dominant haplogroup of the "proto-Mongols". The highest frequency of C2 * -ST was noted in several populations of Kazakhs in South-East Kazakhstan, followed by populations of North-West China, Mongolia, Buryatia and Uzbekistan. In Kazakhstan, with a frequency of more than 50%, C2 * -ST occurs in tribal groups of the Elder Zhuz and the Kerey tribe of the Middle Zhuz [14]**, [20]**.

After haplogroup C2-M217, the second most prevalent component of the Y-chromosome gene pool of the Kazakh tribe Baiuly (about 8%) is represented by three variants of haplogroup R: R1b (M-343) – 4.1%, R1a1a (M-17) – 3.6% and R2 (M-479) – 0,6%.

Haplogroup R1b arose from a mutation of the haplogroup R1 that occurred in a man who lived about 22,800 years to the present day (the date was determined from SNPs by YFull [26]). The last common ancestor of R1b carriers lived 20.4 thousand years ago [21].

A number of modern geneticists believe that R1b originated in Central [27] or Western Asia [28] presumably 16,000 years ago [29]. At first, the hypothesis was put forward that R1b is indigenous to Western Europe, the geographical location where the haplogroup is most prevalent. Subsequently, it was shown that R1b haplotypes have greater variety of small side branches in Anatolia and the Caucasus than in Europe [30].

As was mentioned R1b is the most common haplogroup in Western Europe, reaching over 80% of the population in Ireland, the Scottish Highlands, western Wales, the Atlantic fringe of France, the Basque country and Catalonia. It is also common in Anatolia and around the Caucasus, in parts of Russia and in Central and South Asia. Besides the Atlantic and North Sea coast of Europe, hotspots include the Po valley in north-central Italy (over 70%), Armenia (35%), the Bashkirs of the Urals region of Russia (50%), Turkmenistan (over 35%), the Hazara people of Afghanistan (35%), the Uyghurs of North-West China (20%) and the Newars of Nepal (11%). R1b-V88, a subclade specific to sub-Saharan Africa, is found in 60 to 95% of men in northern Cameroon [31]. It is also found in Central Asia, Eastern Europe, North Africa, Western Asia. After the migration of Europeans to America and Australia, it makes up a significant share there as well.

R1b is found in almost all kazakh tribes, with predominance in the Kypshak tribe of the Middle zhuz [32].

The haplogroup R1a is a Y-chromosomal haplogroup common in Central and Eastern Europe, Central and South Asia, South Siberia and Scandinavia [33,34].

R1a arose about 22 thousand years ago [35] (according to other sources – about 25 thousand years ago [29**]**) from a mutation of the haplogroup R1 that occurred in a man who lived about 22 800 years ago (the date was determined from snips by YFull [36]) presumably in Asia.

While R1a arose about 22,000 to 25,000 years ago, its subclass (R1a1a1) diversified around 5800 years ago [29**]**. The place of origin of the subclade plays a role in the debate about the origin of the Proto-Indo-Europeans.

There are different hypotheses about timing and origin of haplogroup R1a. According to recent studies [37], R1 haplogroup and its subclade R1a resulted from a series of mutations on the root R haplogroup. The time of occurrence is approximately after the last glacial maximum. The exact place of origin of the haplogroup R1a is currently unknown, but could include geographic regions such as Pakistan, Northwest India, the Balkans as these regions have the greatest genetic diversity of this haplogroup. An alternative hypothesis is that the haplogroup R1a came to the Balkans from migratory flows coming from the Eurasian steppes, and due to the fact that migrations occurred in waves, a diversity of mutations was provided. In South Asia, for 10,000 years, the density and number of population are the largest on the planet, and therefore the diversity of the haplogroup is also great. Based on this, geneticists suggest that the R1a haplogroup could have arisen either in Central Asia or in southern Russia – in Siberia [33].

In Kazakhstan R1a also is found in representatives of almost all kazakh tribes, but with a predominance in the Kozha tribe [16]

The rest of the haplogroups of the Y-chromosome were found in the sample of representatives of

the Baiuly tribe with a frequency of less than 2%. Thus, the genetic portrait of the Kazakh tribe Baiuly, at least though the male linage, is determined by a very high contribution of the Central Asian (proto-Mongolian) component (haplogroup C-M217) and a small presence of a "paleo-European" substrate (variants of haplogroup R), which prevailed in Central Asia during the Scythian-Sarmatian period.

Conclusion

In this study, we have characterized for the first time the gene pool of the Kazakh tribe Baiuly. Our study was based on a single extensive panel (17 STR loci, 15 SNP) of Y-chromosome markers in a sample of 169 people. For representatives of this tribe, the major haplogroups are C2-M217, as well as R1b – M343, typical for the peoples of the countries of Western and Central Europe [38]. In general, this tribe has a fairly high level of genetic diversity.

The information we have uncovered about the ethnogenesis of the Baiuly tribe is important for its people given the increasing ethnic self-awareness, the strengthening of national culture and language, and the growing interest in the history of their people. In addition, the results are important for understanding the ethnogenesis of Kazakhs, which are relevant for anthropologists, archaeologists, linguists, historians, or ethnographers interested in the reconstruction of the history of the people of Kazakhstan. This study lays the foundation for subsequent large-scale studies of the Baiuly tribes with its unique history, including genome-wide analysis.

Acknowledgments

We thank all sample donors for their contributions to this work. We would like to thank our colleagues from the Laboratory of Molecular Genetics (Institute of General Genetics and Cytology, Almaty, Kazakhstan): L. Djansugurova for helpful comments and discussions, B. Bekmanov, E. Kuzovleva, A. Amirgaliyeva, G. Abylkassymova, A. Seisenbayeva, S. Abdikerim, Nurzhibek, O. Sapargali for laboratory and sampling assistance. This research has been funded by the Science Committee of the Ministry of Education and Science of the Republic of Kazakhstan (Grant No. BR05233709).

References

1 Vostrov, V.V. and Mukanov, M.C., (1968) Rodoplemennoi sostav i rasselenie kazakhov (konets 19–nachalo 20 vekov) (Tribal Composition and Resettlement of the Kazakhs (Late 19th–Early 20th Centuries), Almaty: Nauka.

2 Https://stan.kz/argyn-men-dulat-kazakstan-dagy-en-sany/

3 Kazakh-Russian relations in the XVI-XVIII centuries. A., (1961) [Kazakhsko-russkiye otnosheniya v XVI–XVIII vv. A.]. 406-p.

4 History of Kazakhstan in Russian sources of the XVI-XX centuries. [Istoriya Kazakhstana v russkikh istochnikakh KHVI- XX vekov.] I-volume. (2005) Almaty, Dyk-Press, lived, 126 p.

5 Fig. Serik Dauletov. (2015) Alshyn zhejiresi (New vision): /Historical research/. Taraz. 65 p. ISBN 978-601-06-3257-8

6 A. Agdzhoyan, Yu. M. Yusupov, Yu. V. Bogunov, M.B. Lavryashina, I. M. Tazhigulova, A. R. Akilzhanova, Zh. Sh. Zhumadilov, O. P. Balanovsky, E. V. Balanovskaya. Genesis of the largest tribal group of Kazakhs – the Argyns – in the light of population genetics. [Genezis krupneyshey rodoplemennoy gruppy kazakhov – argynov – v svete populyatsionnoy genetiki]. Moscow University Bulletin. Series XXIII ANTHROPOLOGY No. 4/2016: 59-68 p.

7 Akerov T.A. Naimans in the XII-XIV centuries. (aspects of origin and ethnopolitical ties) (Russian),[Naymany v XII–XIV vv. (aspekty proiskhozhdeniya i etnopoliticheskikh svyazey)] http://kghistory.akipress.org

8 ASHIRBEKOV, E. Et al. (may 2018) Analysis of the zhuz organization of Kazakh tribes based on the distribution of Y-chromosome haplogroups. [Analiz zhuzovoy organizatsii kazakhskikh plemen na osnove raspredeleniya gaplogrupp Y-khromosomy.] Experimental Biology, [S.l.], v. 73, n. 4, pp. 81-89. ISSN 2617-7498. DOI: https://doi.org/10.26577/EB-2017-4-1304

9 ISOGG, 2015 "Y-DNA Haplogroup C and its Subclades – 2015" (15 September 2015).

10 Lell JT, Sukernik RI, Starikovskaya YB, et al. (January 2002). "The dual origin and Siberian affinities of Native American Y chromosomes". Am. J. Hum. Genet. 70 (1): pp. 192–206. Doi:10.1086/338457. PMC 384887. PMID 11731934.

11 Hammer MF, Karafet TM, Park H, et al. (2006). "Dual origins of the Japanese: common ground for hunter-gatherer and farmer Y chromosomes". J. Hum. Genet. 51 (1): 47–58. Doi:10.1007/s10038-005-0322-0. PMID 16328082.

12 Di Cristofaro J, Pennarun E, Mazières S, Myres NM, Lin AA, et al. (2013). "Afghan Hindu Kush: Where Eurasian Sub-Continent Gene Flows Converge". PLOS ONE. 8 (10): e76748. Bibcode:2013ploso...876748D. Doi:10.1371/journal.pone.0076748. PMC 3799995. PMID 24204668.

13 Malyarchuk B, Derenko M, Denisova G, et al. (2010). "Phylogeography of the Y-chromosome haplogroup C in northern Eurasia". Annals of Human Genetics. 74 (6): 539–546. Doi:10.1111/j.1469-1809.2010.00601.x. PMID 20726964.

14 Boris Malyarchuk, Miroslava Derenko, Galina Denisova, Sanj Khoyt, Marcin Wozniak, Tomasz Grzybowski, and Ilya Zakharov, (2013) "Y-chromosome diversity in the Kalmyks at the ethnical and tribal levels." Journal of Human Genetics 58, pp. 804–811; doi:10.1038/jhg.2013.108; published online 17 October 2013.

15 Natalia Balinova, Helen Post, Alena Kushniarevich, Siiri Rootsi, et al. (2019), "Y-chromosomal analysis of clan structure of Kalmyks, the only European Mongol people, and their relationship to Oirat-Mongols of Inner Asia." European Journal of Human Genetics. Https://doi.org/10.1038/s41431-019-0399-0

16 Wells RS, Yuldasheva N, Ruzibakiev R, et al. (August 2001). "The Eurasian heartland: a continental perspective on Y-chromosome diversity". Proc. Natl. Acad. Sci. U.S.A. 98 (18): 10244–9. Bibcode:2001PNAS...9810244W. Doi:10.1073/pnas.171305098. PMC 56946. PMID 11526236.

17 Karafet T, Xu L, Du R, et al. (September 2001). "Paternal population history of East Asia: sources, patterns, and microevolutionary processes". Am. J. Hum. Genet. 69 (3): 615–28. Doi:10.1086/323299. PMC 1235490. PMID 11481588.

18 Serikbai Abilev, et al. (Published February 2012) The Y-chromosome C3* Star-Cluster Attributed to Genghis Khan's Descendants is Present at High Frequency in the Kerey Clan from Kazakhstan. // Human Biology. DOI: 10.3378/027.084.0106

19 Zhabagin M.(2013) Gene pool of the tore genus in the context of the general structure of the kazakh and mongols (according to the data on the Y-chromosome polymorphism), [genofond roda tore v kontekste rodovoy struktury kazakhov i mongolov (po dannym o polimorfizme Y-khromosomy)]. // X Congress of Ethnographers and Anthropologists of Russia: Abstracts. Moscow, July 2-5,.: ISBN 978-5-4211-0087-4

20 M.K. Zhabagin et al. (2014). Relationship of y-chromosome variability and general structure: general pool of steppe aristocracy and spirituality of kazakh, svyaz' izmenchivosti y-khromosomy i rodovoy struktury: genofond stepnoy aristokratii i dukhovenstva kazakhov.. Moscow university bulletin. Series xxiii anthropology № 1/2014: pp. 96–101

21 Zhabagin, et al. (2017). The Connection of the Genetic, Cultural and Geographic Landscapes of Transoxiana. Scientific Reports, 7(1). Doi:10.1038/s41598-017-03176-z

22 Ashirbekov, et al. (2018). Molecular Genetic Analysis of Population Structure of the Great Zhuz Kazakh Tribal Union Based on Y-Chromosome Polymorphism. Molecular Genetics, Microbiology and Virology, 33(2), pp. 91–96. Doi:10.3103/s0891416818020040

23 Zerjal T, Xue Y, Bertorelle G, et al. (March 2003). "The genetic legacy of the Mongols". Am. J. Hum. Genet. 72 (3): 717-21. Doi:10.1086/367774. PMC 1180246. PMID 12592608. As pdfarchived 10 July 2012 at the Wayback Machine

24 Lan-Hai Wei et al. Whole-sequence analysis indicates that the Y chromosome C2*-Star Cluster traces back to ordinary Mongols, rather than Genghis Khan // European Journal of Human Genetics

25 Wei LH, Yan S, Lu Y, et al. (2018) Whole-sequence analysis indicates that the Y chromosome C2*-Star Cluster traces back to ordinary Mongols, rather than Genghis Khan. Eur J Hum Genet.;26(2):230-237. Doi:10.1038/s41431-017-0012-3

26 Https://www.yfull.com/tree/r1b/

27 Variations of R1b Ydna in Europe: Distribution and Origins.

28 International Society of Genetic Genealogy (ISOGG) – Y-DNA Haplogroup R and its Subclades – 2009

29 Klyosov, A. (2012). Ancient History of the Arbins, Bearers of Haplogroup r1b, from Central Asia to Europe, 16,000 to 1500 Years before Present. Advances in Anthropology, 2, pp. 87-105. Doi: 10.4236/aa.2012.22010.

30 Origins, age, spread and ethnic association of European haplogroups and subclades (англ.). Eupedia, your guide to Europe in English (last update: March 2010).

31 Https://www.eupedia.com/europe/Haplogroup_r1b_Y-DNA.shtml#migration_map

32 Zhabagin M. (2017) Analysis of the relationship of y-chromosome polymorphism and the pendant structure in the kazakh population [analiz svyazi polimorfizma y-khromosomy i rodoplemennoy struktury v kazakhskoy populyatsii]. // Dissertation for the degree of candidate of biological sciences – 03.02.07 – genetics. Moscow.

33 Underhill, Peter A.; et al. (26 March 2014). "The phylogenetic and geographic structure of Y-chromosome haplogroup r1a". European Journal of Human Genetics (published January 2015). 23 (1): pp. 124–131. 10.1038/ejhg.2014.50. PMC 4266736. PMID 24667786.

34 Underhill, PA; Myres, NM; Rootsi, S; Metspalu, M; Zhivotovsky, LA; King, RJ; Lin, AA; Chow, CE; et al. (2009). Separating the post-Glacial coancestry of European and Asian Y chromosomes within haplogroup r1a. European Journal of Human Genetics (published April 2010). 18 (4): pp. 479-484. 10.1038/ejhg.2009.194.

35 Sharma, S; Rai, E; Sharma, P; Jena, M; Singh, S; Darvishi, K; Bhat, AK; Bhanwer, AJ. Et al. (2009). «The Indian origin of paternal haplogroup R1a1(*) substantiates the autochthonous origin of Brahmins and the caste system». Journal of Human Genetics. 54(1): pp. 47-55

36 https://www.yfull.com/tree/r1a/

37 https://www.eupedia.com/europe/Haplogroup_r1a_Y-DNA.shtml

38 Anatole Klyosov. (2012) Ancient History of the Arbins, Bearers of Haplogroup r1b, from Central Asia to Europe, 16,000 to 1500 Years before Present. Advances in Anthropology Vol. 2(No. 2):87-105. DOI: 10.4236/aa.2012.22010

IRSTI 31.27.17; 31.27.19 https://doi.org/10.26577/ijbch.2020.v13.i2.11

M. Irfan[1*], J. Bakhtawar[1], S. Sadia[1],
H.A. Shakir[2], M. Khan[2], S. Ali[3]

[1]Department of Biotechnology, University of Sargodha, Sargodha, Pakistan
[2]Department of Zoology, University of the Punjab new campus, Lahore, Pakistan
[3]Department of Zoology, Government College University, Lahore, Pakistan
*e-mail: irfan.ashraf@uos.edu.pk, irfan.biotechnologist@gmail.com

Utilization of fruit wastes for enzyme production in submerged fermentation

Abstract. This study was aimed at production of cellulase, amylase, tannase and ethanol by co-culturing of *Bacillus megaterium* and *Saccharomyces cerevisiae* using fruit waste as the sole substrate in submerge fermentation. Maximum amylase production (1.208 ± 0.14 IU/mL) was observed in fresh melon peel substrate after 48 h of fermentation. Maximum filter paper activity (0.645 ± 0.02 IU/mL) and tannase production (0.25 ± 0.01 IU/mL) was obtained from rotten peach after 24 h of fermentation. Sweet lemon peels yielded highest carboxymethyl cellulase production (0.435± 0.02 IU/mL) after 24 h of fermentation. Maximum reducing sugars (2.537± 0.07 mg/mL) and total sugars (17.703 ± 0.13 mg/mL) liberation was observed from sweet lemon peels after 24h of fermentation. Maximum ethanol production (0.56 ± 0.03 mg/mL) was also found from sweet lemon peel after 72h of fermentation. Findings of this study showed that sweet lemon peels had potential for production of biologically active compounds via microbial fermentation.
Key words: Fruit waste, *Bacillus megaterium, Saccharomyces cerevisiae,* bioethanol, sugars, amylase, tannase, cellulase.

Introduction

Disposal of massive food, fruits and vegetables waste (FVW) is currently an alarming matter; because of emitting significant amount of greenhouse gases. Hence it has been proved to be a reason of soil and water pollution. About 4.14 tons of CO_2 is counted to be released by per ton of wood waste. Despite that, food and vegetable wastes also seem to be rich in carbohydrates, proteins, fats, antioxidants, some biologically active compounds, natural colorants and in moisture. Due to the biochemical features and size of FVWs, numerous studies have been carried out to get valuable yields by transforming global FVWs [1]. Studies based on microbial processing provide new perspectives by producing organic acids, enzymes, flavoring materials, biomethane, food colorants and bioethanol from FVWs via microbial applications [1].

Enzymes are mostly proteinaceous in nature and found in all living systems in order to catalyze variety of reactions. In production of wine, cheese, beer, bread, vinegar and manufacturing supplies like linen and leather enzymes are substantially being used in the form of plant or bacterial extracts. But the major issue associated with enzymes usage in industrial processes is their cost. Wide ranging enzyme production is a matter of high budget utilization and application in manufacturing processes will ultimately affect the prices of the final product. Though, raw materials are contributing 28% of functioning cost. Lignocellulosic material is being used from many decades as a source of inexpensive carbohydrates and can be used as raw matter to produce great valuable yields like organic acids, enzymes, bioethanol, and biodegradable plastics. Processed waste produced via food industries is uneatable and has lignocellulosic nature. Lignocellulose is composed of lignin, cellulose, and hemicellulose, some traces of salts, pectin, minerals, and ash [2].

Lignocellulose is recalcitrant due to its complex structure so we cannot use it directly for microbial processing. Though, lignocellulose is subjected to enzymatic hydrolysis and pretreatment to release fermentable sugars which are utilized for growth and sustenance of enzymes producing microbes [3]. Lignocellulolytic enzymes are being considered very important because of broad range of demand in paper and pulp, detergent, textile, and bioethanol industries. Currently cellulosic-bioethanol is commonly used as

a carbon-neutral technology along with a source of renewable energy. So cellulolytic enzymes demand is increasing day by day [1]. Transformation of lignocellulosic matter into significant products like biofuels has a noteworthy global outcome. Lignocellulosic material has a significant role in biofuels production and dropping the world's reliance in overwhelming fossils fuel [4].

Amylolytic enzymes are used to hydrolyze oligosaccharides, polysaccharides, and starch into simple sugars, such as maltose, fructose, and glucose having low molecular weights. The starches are composed of two foremost elements, amylose that is a linear chain of unbranched D-glucose remains linked through α 1-4 bond plus amylopectin, which is well branched D-glucose remains linked by α 1-6 bond. The amylases might be categorized into exo and endoamylases on the basis of their approaches of hydrolysis. Prevailing number of exoamylases attacks α 1-4 bonds, but some of them like glucoamylase can target both α 1-4 and α 1-6 bonds in order to yield simple sugars like glucose and maltose [5].

Endoamylase cleaves α 1-4 bond in starch, while does not interrupt α 1-6 bond in amylo-pectin and its correlated complex polysaccharides. Best illustration of α-amylase is endoamylase due to production of varying fragments of oligosaccharides by starch. Glucoamylase only targets non-reducing ends while α -amylase acts on random locations in starch [6].

Tannase (tannin-acyl-hydrolase) is acknowledged for hydrolyzing tannin to glucose and gallic-acid which is a substrate used for the manufacturing of trimethoprim and propylgallate. Tannin is considered to be forth utmost plentiful plant component after celluloses, hemicelluloses, and lignin. Tannase can be used to reduce a stringency of the products so commonly it is used in beverage and food industries, beside that it is valuable in dropping tannic-acid absorption in tannery effluents [1]. All these enzymes had potential application in various industries. This study was designed to produce valuable products (enzymes) from rotten fruits and fruit waste by co-culturing of *Bacillus megaterium* and *Saccharomyces cerevisiae* in submerged fermentation.

Materials and methods

Objects. Microbial strains (*Bacillus megaterium* and *Saccharomyces* cerevisiae) were attained from the microbial collection of Biotechnology laboratory of the Department of Biotechnology, University of Sargodha, Pakistan. *B. megaterium* was revived on nutrient agar (Oxoid, UK) slants and *S. cerevisiae* was revived on potato dextrose agar (Oxoid, UK) slants.

Inoculum preparation. The *Bacillus* culture was taken on loop from nutrient agar slants. Furthermore, it was maintained in sterile nutrient broth vials and harvested for 24 h. The cloudy appearance of *B. megaterium* growth predicted that the successful inoculum was ready to use as stock. *S. cerevisiae* was maintained as stock culture on potato dextrose agar (Oxoid, UK) slants.

Fermentation technique. Submerged fermentation was conducted in Erlenmeyer flasks of 250 mL capacity containing 15 mL fermentation media comprised of 2% of substrate separately in each flask and sterilized at 121 °C and 15 Psi for 15 min. Inoculation was carried out in a sterilized environment with 1% of each 24 h old vegetative culture of *B. megaterium* and *S. cerevisiae*. After that inoculated flasks were placed on shaking incubator at 35°C with shaking rate of 120 rpm for 72 h and samples were collected after 24 h, 48 h and 72 h. After each sampling, the sample was centrifugated at 10,000 x g for 10 min at 4°C. The obtained supernatant was further employed for analysis.

Cellulase assay. Carboxy methyl cellulase (CMCase) and filter paper activity (FPase) was done as explained in our previous reports [7]. Estimation of CMCase activity was carried out by adding 0.5 mL of crude enzyme with 0.5 mL of 1% CMC (prepared in 0.05 M citrate buffer having pH 5) and reaction was incubated for 30 min at 50 °C. While for FPase 500 µL of crude enzyme was added up in a test tube having Whatman No.1 filter paper strips (1x 6 cm) and 0.5ml of 0.05 M Sodium Citrate Buffer (pH 5). Mixture was further incubated at 50°C for 30 min. After incubation 1.5 mL DNS (Sigma, USA) was added in test tubes to stop the reaction and boiled in a water bath for 10 minutes and absorbance was taken at 540nm. Glucose was utilized as standard.

Amylase assay. Activity of α-amylase was calculated using amylase assay conditions [8]. Reaction mixture having 0.5 mL of crude enzyme and 0.5mL of 1% starch solution (pH 7) incubated at 60°C for 30 min. After that 1.5mL of 3,5 dinitro-salicylic acid (DNS) reagent was added to stop the reaction and the mixture was kept in boiling water bath for 10 min. After the cooling of mixture, optical density was recorded at 540 nm. Maltose was taken as a standard.

Tannase assay. Tannase activity was calculated by method described by Miller [9]. The enzyme solution volume was taken 1 mL which was added with 1mL tannic acid reagent as substrate. Reagent was prepared in 0.5% tannic acid in acetate buffer. The reactants were incubated for 30 min at 37°C and then placed for 15 min boiling in water bath to stop the en-

zyme substrate activity. From this enzyme-substrate system, 1 mL was taken in test tube and 3 mL of dinitro-salicylic acid (DNS) reagent was added in test tubes and the mixture again boiled for 10 min. After boiling, solution with 10ml distilled water was diluted and absorbance was recorded at 540 nm via above mentioned method against blank solution. Each reaction was carried out in triplicate.

Analytical methods. Estimation of reducing sugars released by the hydrolytic action of enzymes was carried out by using dinitro-salicylic acid (DNS) method [9], by taking 0.5 mL sample with 1.5 mL DNS (Sigma, USA). Boiling was carried out at 100°C for 10 min and OD was measured at 540 nm. Total sugars were estimated through phenol sulfuric acid method [10], by taking 0.5 mL sample, 25 mL H_2SO_4 and 0.5 mL phenol. It was kept under room temperature only for 30 min, after that optical density was measured using spectrophotometer at 490nm. Ethanol was measured by HPLC as described by Irfan et al [11]. BioRad Aminex HPX 87H column (250 mm 9 4.6 mm) was used having mobile phase of 5mM H_2SO_4, 0.7 mL/min flow rate and 60°C column temperature. Each sample was passed from sterile membrane filter of 0.2 µl and analysis was done by using 20µl injection volume.

Statistical analysis. The whole data generated from experiments was analyzed statistically using Microsoft excel program (version 2016) and values presented as mean of triplicates.

Results and discussion

Three kinds of fruit wastes were used comprising of fresh melon peel, rotten peach, and sweet lemon peel. Each of the fruit waste medium was inoculated with co-culture of *Bacillus megaterium* and *Saccharomyces cervisae* and incubated for 3 days. After 24, 48 and 72 h, sample was taken and enzyme assays for CMCase, Fpase, amylase, tannase and total sugar, reducing sugar and ethanol were conducted.

Using the fresh melon peel as a substrate, highest enzyme activities of amylase (1.208 ± 0.14 IU/mL), tannase (0.18± 0.01 IU/mL) and CMCase (0.078± 0.01 IU/mL) was observed after 48 h of fermentation. Highest FPase activity (0.43± 0.03 IU/mL) was observed after 24 h of fermentation (Figure 1). Minimum CMCase, amylase and tannase activities were observed with 24 h of fermentation indicating the importance of the fermentation period.

Maximum reducing sugar0.047± 0.001 mg/mL was obtained after 48 as well 72 h of fermentation by using fresh melon peels, while maximum total sugar 0.335 ± 0.004 mg/mL was estimated after 24 h of fermentation time. No ethanol production was evaluated after 24 h, and 0.14 ± 0.01 mg/mL was experienced after72 h of fermentation period (Figure 2).

When rotten peach was used as substrate for fermentation, the maximum evaluated enzyme production of FPase (0.645± 0.02 IU/mL), amylase (0.45± 0.01 IU/mL), tannase (0.25± 0.01 IU/mL) and CMCase (0.057 IU/mL) was obtained after 24 h of fermentation time (Figure 3). By increasing the fermentation period up to 48 or 72 h minimum enzyme activity was noted.

Reducing sugar estimated from rotten peach was 0.013 ± 0.001mg/mL, which remained same after 48 and 72 h of fermentation. Maximum total sugar production 1.87± 0.05 mg/mL was optimized after 48 and 72 h of fermentation. Ethanol production by using rotten peach was 0.051± 0.001 mg/mL appeared after 48 and 72 h of fermentation, while 24h of fermentation period gave minimum ethanol production (Figure 4).

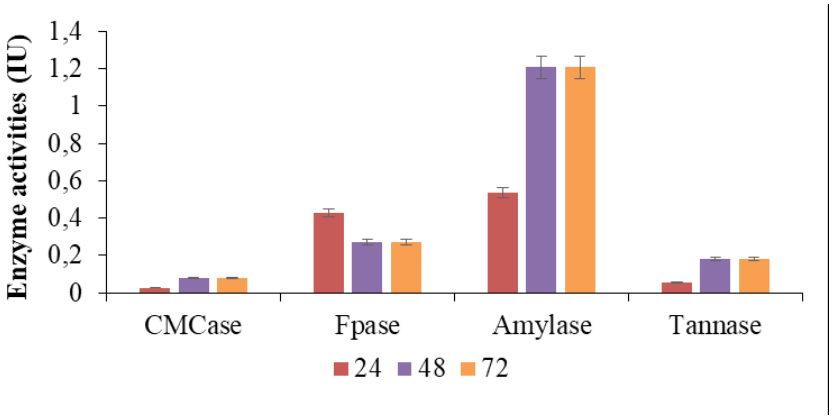

Figure 1 – Enzymes production from fresh melon peels in submerged fermentation

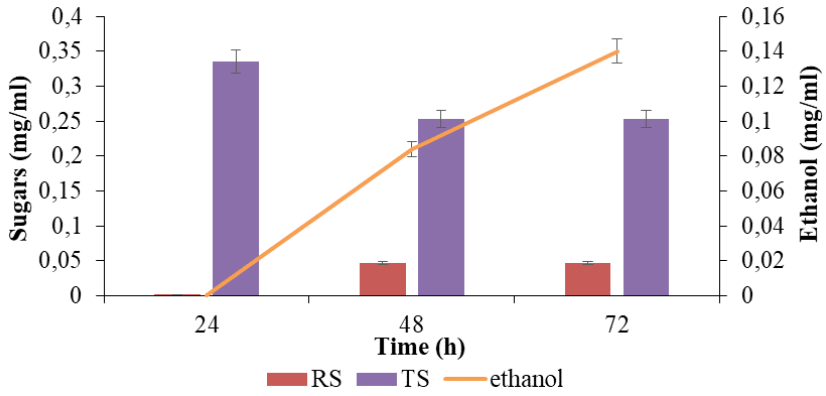

Figure 2 – Reducing sugars (mg/mL), total sugars (mg/mL) and ethanol (mg/mL) produced in submerged fermentation using fresh melon peels

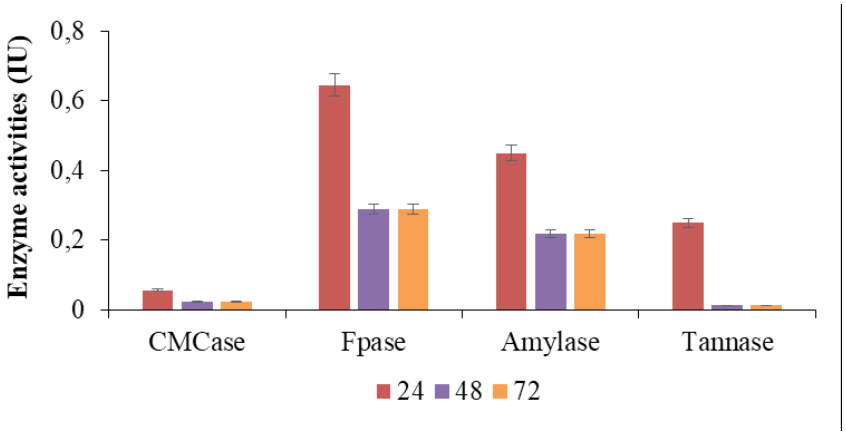

Figure 3 – Enzymes production from rotten peach in submerged fermentation

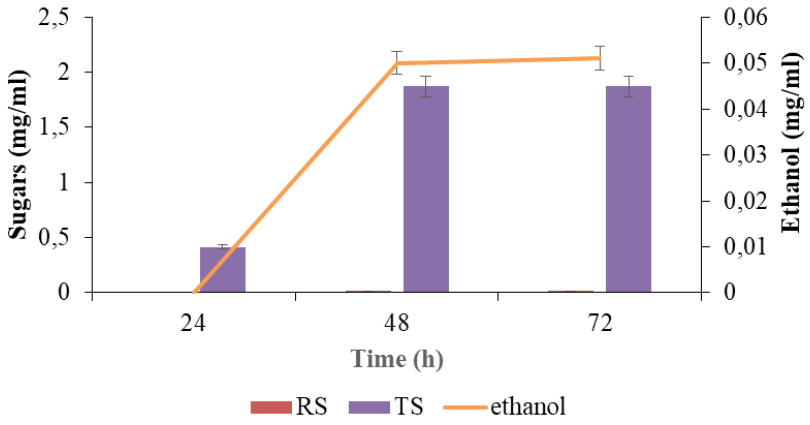

Figure 4 – Reducing sugars (mg/mL), total sugars (mg/mL) and ethanol (mg/mL) produced in submerged fermentation using fresh rotten peach

Sweet lemon peel also exhibited potential for enzyme production. The maximum production of amylase (0.529± 0.03 IU/mL), CMCase (0.435 ± 0.02 IU/mL) and FPase (0.295± 0.01 IU/mL) was examined after 24 h of fermentation, while after increasing fermentation period up to 72 h minimum amylase, CMCase and FPase activities were observed. Tannase production was noted maximum after 48 h of fermentation, which remained same even after 72 h of fermentation (Figure 5).

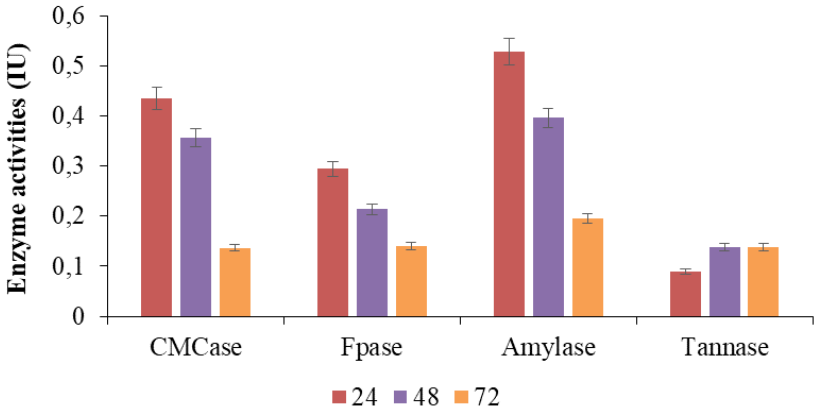

Figure 5 – Enzymes production from sweet lemon peels in submerged fermentation

Reducing sugar and total sugar for the sweet lemon peels were observed to be 2.537± 0.07 mg/mL and 17.703± 0.13 mg/mL respectively after 24h of fermentation time, by increasing fermentation time to 48 or 72h a decline in reducing and total sugar was experienced. Maximum ethanol production for this substrate was 0.56± 0.03 mg/mL estimated after 72 h of fermentation (Figure 6), while 24h gave minimum ethanol yield.

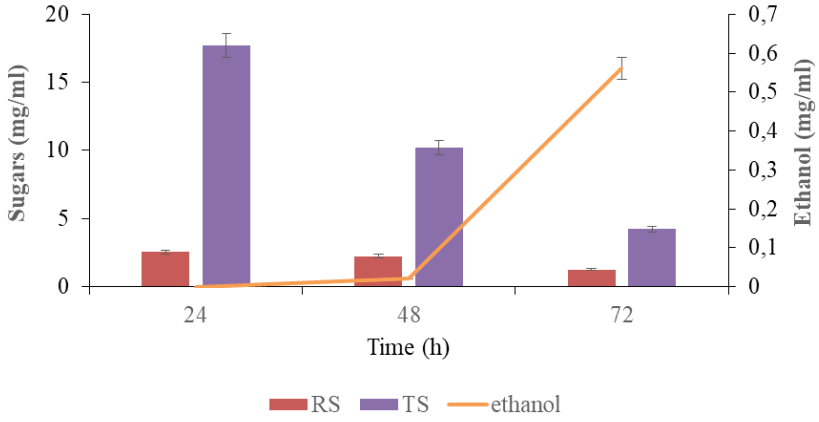

Figure 6 – Reducing sugars (mg/mL), total sugars (mg/mL) and ethanol (mg/mL) produced in submerged fermentation using sweet lemon peels

Norsalwani and Norulaini, [12] reported maximum cellulase activity of 2.65 FPU/ml, produced by palm kernel cakes as substrate. Co-culturing of *Cellulomonas carte, B. megaterium, P. putida* and *Pseudomonas fleuroscence* on banana solid waste exhibited maximum β, D glucosidase activity of 0.602 U/mL on 25th day and FPase of 0.178 U/mL on 20th day of fermentation [13]. In a study, decayed fruit waste was taken and novel cellulase producing actinomycetes were isolated and highest enzyme production was observed using fruit waste media as our carbon source [14].

Commonly fungi are known for the production of tannase but some bacterial species like *Lactobacillus* sp. and *Bacillus sp*. were also well known for the production of tannase [15]. A recent study revealed that *Klebsiella oxytoca* had potential of tannase production using peels of *Citrus limetta* in solid state fermentation [16]. Although the findings reported in earlier reports differed with the present study due to substrate, microorganism, and culturing technique.

In a recent study by Cyprian et al [17], maximum concentration of amylase 259.00 ± 1.23 U/mL was reported to be obtained by using Banana waste. It was reported that fermentation period plays an important role in amylase production by using fruit waste. Moreover, decline in amylase production may be caused due to nutrients exhaustion or denaturation of enzyme. Hence short duration of fermentation period may lead to cost effective amylase production. Oshoma et al [18] has reported that Banana peel has a potential of producing amylase due to its easy availability and cost effectiveness. It was further reported that maximum amylase yield can be obtained after 96 h of fermentation. After this period amylase activity gradually decreases due to depletion of nutrients required for microbial growth and amylase production [18]. In a study done for amylase estimation, maximum yield of amylase was reported by using solid waste of banana with microbial strain of *Bacillus subtilis* [19]. Mango kernel was used as a substrate under optimized conditions with microbial strain of *Fusarium solani* and 0.889 U/g of amylase was successfully produced [20]. α-amylase production was optimized to be 8.26 U/mL in submerged fermentation after 5 days of fermentation by *Streptomyces sp.* using orange waste as a sole carbon source [21]. In another study amylase production was experienced with brewer's spent grain hydrolysate as substrate using Catabolite-repressed strain of *Bacillus subtilis KCC103* through submerged fermentation [22]. Cassava waste has also been utilized for amylase production by *Bacillus* sp. [23].

Zabed et al [24] has reported that *S. cerevisiae* can be employed for ethanol production using fruit and vegetable waste materials and the pH was maintained in the range of 4.0-5.0. In a recent study, it has been reported that maximum bioethanol yield can be obtained by using pineapple waste if fermentation is carried out under low pH range of 3.0-4.0 [25,26]. *S. cerevisiae* has proved to be much better in pineapple waste as compared to other fruit and vegetable wastes. Another study reveals that bioethanol production from Orange peel and Banana was around 2 and 3% [27]. Strain of *S. cerevisiae* with the cashew apple juice has also shown bioethanol production [28]. Banana peel and Apple pomace produced 38% of ethanol yield by *S. cerevisiae* after the 36 h of fermentation [29]. Recent study reported that mango waste yield maximum amylase activity using *Bacillus* sp. in submerged fermentation [30]. Fruit waste of longan had potential of bioethanol production in submerged fermentation [31]. Banana peels has been reported as potential substrate for ethanol production by *Klebsiella* sp. SWET4 [32]. So, these studies have shown that the fruit waste could be utilized as a potential substrate for the production of enzymes and bioethanol.

Conclusion

Results of this study showed that a huge amount of fruit wastes that are being thrown in open places could be utilized for the production of valuable products through microbial fermentation. Sweet lemon peels were found to be the best substrate for the production of cellulases (CMCase 0.435 ± 0.02 IU/mL and FPase 0.295± 0.01 IU/mL) and amylase (0.529± 0.03 IU/mL) in submerged fermentation after 24h. Maximum ethanol production was obtained by sweet lemon peels after 72h of fermentation.

Acknowledgement

The authors would like to acknowledge the Department of Biotechnology, University of Sargodha, Pakistan for providing facilities to conduct this work.

References

1 Panda S.K., Mishra S.S., Kayitesi E., Ray R.C. (2016). Microbial-processing of fruit and vegetable wastes for production of vital enzymes and organic acids: Biotechnology and scopes. Environ. Res. vol. 146, pp. 161-172.https://doi.org/10.1016/j.envres.2015.12.035

2 Ravindran R., Jaiswal A. (2016). Microbial enzyme production using lignocellulosic food industry wastes as feedstock: a review.Bioengineering. vol.3, no. 4, pp. 30.https://doi.org/10.3390/bioengineering3040030

3 Meng X., RagauskasA.J. (2014). Recent advances in understanding the role of cellulose accessibility in enzymatic hydrolysis of lignocellulosic substrates. Curr. Opin. Biotechnol. vol. 27, pp.150-158. https://doi.org/10.1016/j.copbio.2014.01.014.

4 Pocan P., Bahcegul E., Oztop M.H., Hamamci H. (2018). Enzymatic hydrolysis of fruit peels and other lignocellulosic biomass as a source of sugar.

Waste biomass valorization.vol.9, no.6, pp.929-937. https://doi.org/10.1007/s12649-017-9875-3

5 Kar S., Ray R.C. (2008). Partial characterization and optimization of extracellular thermostable Ca2þ inhibited α-amylase production by Streptomyces erumpens MTCC 7317. J. Sci. Ind. Res. vol. 67, pp. 58-64.

6 Horvathova V., Janecek S., Sturdik E. (2000). Amylolytic enzymes: their specificities, origins and properties. Biol. Bratisl. vol. 55, no. 6, pp. 605-615.

7 Irfan M., Gulsher M., Abbas S., Syed Q., Nadeem M., Baig S. (2011). Effect of various pretreatment conditions on enzymatic saccharification. Songklanakarin J. Sci.Technol. vol. 33, no. 4, pp. 397-404.

8 Irfan M., Nadeem M., Syed Q., Shakir HA., Qazi JI. (2016). Study on Some Properties of Calcium-dependent a-Amylase from Bacillus subtilis through Submerged Fermentation of Wheat Bran. Chem. Biochem. Eng. Q. vol.30, no. 4, pp. 429-437. https://doi.org/10.15255/CABEQ.2016.831

9 Miller G.L. (1959). Use of Dinitrosalicylic Acid Reagent for Determination of Reducing Sugar. Anal. Chem. vol. 31, no.3, pp.426-428.https://doi.org/10.1021/ac60147a030

10 Dubois M., GillesKA., HamiltonJK., RebersPA and SmithF. (1956). Colorimetric method for determination of sugars and related substances. Anal. Chem. vol.28, pp. 350-356.https://doi.org/10.1021/ac60111a017

11 Irfan M., AsgharU., Nadeem M., NeloferR., Syed Q., ShakirHA, Qazi JI. (2016). Statistical optimization of saccharification of alkali pretreated wheat straw for bioethanol production. Waste Biomass Valor. vol. 7, no. 6, pp. 1389-1396.https://doi.org/10.1007/s12649-016-9540-2

12 Norsalwani T.L.T., Norulaini N.A.N. (2012). Utilization of lignocellulosic wastes as a carbon source for the production of bacterial cellulases under solid state fermentation. Int. J. Env. Sci. Dev. vol.3, no. 2, pp. 136-140.https://doi.org/10.7763/IJESD.2012.V3.203

13 Dabhi B.K., Vyas R.V., Shelat H.N. (2014). Use of banana waste for the production of cellulolytic enzymes under solid substrate fermentation using bacterial consortium. Int. J. Curr. Microbiol. App. Sci. vol. 3, no.1, pp. 337-346.

14 Rathnan R.K., Ambili A. (2011). Cellulase enzyme production by Streptomyces sp. using fruit waste as substrate. Aust. J. Basic Appl. Sci. vol.5, no. 12, pp.1114-1118.

15 Aguilar-Zarate A.P., Hernandez C.M.A., Montanez J.C., Cerda B.R.E., Aguilar C.N. (2014). Bacterial tannases: production, properties and applications. Rev. Mex. Ing. Quim.vol.13, no. 1, pp. 63-74.

16 Shakir HA., Fatima K., Irfan M., Khan M., Ali S., Saeed S., Qazi JI. (2020). Citrus limetta (Musambi) Peels: An efficient cheap substrate for tannaseproduction in solid state fermentation. Pak. J. Biotechnol. vol. 17, no. 2, pp. 53-61.https://doi.org/10.34016/pjbt.2020.17.2.53

17 Cyprian, E. O., Henrietta, O. O., Eguakun-Owie, S. O., & Omonigho, S. E. (2017). Fruit Wastes as Substrate for the Production of Amylase by Aspergillus niger. Trop. J. Nat. Prod. Res. Vol. 1, no. 4, pp. 182-185.https://doi.org/10.26538/tjnpr/v1i4.9.

18 Oshoma, C. E., Eguakun-Owie, S. O., &Obuekwe, I. S. (2019). Utilization of Banana Peel as a Substrate for Single Cell Protein and Amylase Production by Aspergillusniger. African Scientist. Vol.18, no.3, pp, 143-150.

19 Unakal C., Kallur R.I.,Kaliwal B.B. (2012). Production of α-amylase using banana waste by Bacillus subtilis under solid state fermentation. Eur. J. Exp. Biol. vol. 2, no. 4, pp.1044-1052.

20 Kumar D., Yadav KK., Muthukumar M., Garg N. (2013). Production and characterization of α-amylase from mango kernel by Fusariumsolani NAIMCC-F02956 using submerged fermentation. J. Env. Biol. vol. 34, pp.1053-1058.

21 MahmoudK. (2015). Statistical optimization of cultural conditions of a halophilic alpha-amylase production by halophilic Streptomyces sp. grown on orange waste powder. Biocatal. Agric. Biotechnol., vol.4, no.4, pp.685-693.https://doi.org/10.1016/j.bcab.2015.08.011

22 Rajagopalan G and Krishnan C. (2008). α-Amylase production from catabolite derepressed-Bacillus subtilis KCC103 utilizing sugarcane bagasse hydrolysate. Bioresour. Technol. vol.99, no.8, pp. 3044-3050.https://doi.org/10.1016/j.biortech.2007.06.001

23 Selvama K., Selvankumarb T., Rajiniganthb R., Srinivasanb P., Sudhakarb Ch., Senthilkumara B., and Govarthanan M. (2016). Enhanced production of amylase from Bacillus sp. using groundnut shell and cassava waste as a substrate under process optimization: waste to wealth approach. Biocatal. Agric. Biotechnol. vol. 7, pp. 250-256.https://doi.org/10.1016/j.bcab.2016.06.013

24 Zabed H, FaruqG, SahuJN, AzirunMS, HashimR, and NasrulhaqBoyceA(2014). Bioethanol production from fermentable sugar juice. Sci. World. J. pp, 1-13. https://doi.org/10.1155/2014/957102

25 Hossain A.B.M.S.,& FazlinyA.R. (2010). Creation of alternative energy by bio-ethanol production from pineapple waste and the usage of its prop-

erties for engine.Afr. J. Microbiol. Res.vol.4, no.9, pp.813-819.https://doi.org/10.5897/AJMR.9000206

26 Khandaker, M. M., Abdullahi, U. A., Abdulrahman, M. D., Badaluddin, N. A., & Mohd, K. S. (2020). Bio-ethanol production from fruit and vegetable waste by using saccharomyces cerevisiae. In Bioethanol. IntechOpen.https://doi.org/10.5772/intechopen.94358

27 Shilpa C.,Chanchal G.M. (2013). Alcohol Production from Fruit and Vegetable Waste. Int. J. Appl. Eng. Res.vol.8, no.15, pp.1749-1756.

28 Neelakandan T., Usharani G. (2009). Optimization and production of bioethanol from cashew apple juice using immobilized yeast cells by Saccharomyces cerevisiae. Am. Eurasian J. Sci. Res.vol.4, pp. 85-88.

29 Borah D., Mishra V. (2011). Production of biofuel from fruit waste. Int. J.Adv. Biotechnol. Res. vol. 11, pp. 71-74.

30 Saleh F., Hussain A., Younis T., Ali S., Rashid M., Ali A., Mustafa G., Jabeen F., Al-Surhanee AA., Alnoman M.M., Qamar S. (2020). Comparative growth potential of thermophilic amylolytic Bacillus sp. On unconventional media food wastes and its industrial application. Saudi J. Biol. Sci. vol. 27, pp. 3499-3504. https://doi.org/10.1016/j.sjbs.2020.09.045.

31 Nguyen TVT., Unpaprom Y., Manmai N., Wangchai K., Ramaraj R. (2020). Impact and significance of pretreatment on the fermentable sugar production from low-grade longan fruit wastes for bioethanol production. Biomass Conv. Bioref https://doi.org/10.1007/s13399-020-00977-7.

32 Sarkar D., Prajapati S., Poddar K., Sarkar A. (2020). Ethanol production by Klebsiella sp. SWET4 using banana peel as feasible substrate. Biomass Conv. Bioref. https://doi.org/10.1007/s13399-020-00880-1.

IRSTI 34.49.19 https://doi.org/10.26577/ijbch.2020.v13.i2.12

E.S. Jafarov*, M.Z. Velijanova

Institute of Radiation Problems, NAS of Azerbaijan, Baku, Azerbaijan
*e-mail: elimkhan.jafarov@gmail.com

Study of the adaptive reaction to salt stress of *Cicer arietinum* L., grown from seeds exposed to presowing γ – irradiation

Abstract. It was found that γ-irradiation under certain conditions accelerates the growth and development of plants, improves their productivity and quality characteristics. Based on this, in the presented article, we tried to determine the range of the seed irradiation dose, which helps to reduce the negative effect of salt. For this, a fairly wide range of both the radiation dose and the salt concentration was used. The response of the plant to salt stress was determined on the basis of changes both in a biometric parameters, and in the content of malondialdehyde (MDA), proline, and total protein. According to the results, the main biometric indices increased markedly in chickpea upon pre-sowing irradiation at doses of 1-5 Gy and germination under normal conditions. The maximum increase in individual indices was found at a dose of 5 Gy. In the case of non-irradiated seeds grown under salt conditions, even a low concentration (1 mmol) of salt led to inhibition of the plant development. Seedlings, germinated from seeds irradiated in the dose range from 5 to 100 Gy, were shown to grow normally even at high salt concentrations. At a stimulating dose of 5 Gy, an increase in salt concentration from 1 to 50 mmol led to a gradual increase in MDA levels in the leaves. An increase in salt concentrations in the range of 1-200 mmol also led to a marked increase in the proline content. Under high concentrations (from 10 to 200 mmol) of salt, seed irradiation led to a sharp decrease in the total protein content. Irradiation of seeds at doses of 5- 100 Gy is assumed to reduce the effects of salt stress to some extent. At high salt concentrations, proline plays a significant role in protecting the plant from salt stress.

Key words: *Cicer arietinum* L., presowing γ-irradiation, salt stress, biometric indices, malondialdehyde, proline, total protein.

Introduction

It is generally known that seeds during their germination are quite susceptible to the action of various environmental factors [1-3]. This attribute facilitated the use of various physical or chemical agents prior to sowing, primarily focused on increase in productivity of agricultural plants [4].

At the present time, due to its relative simplicity and cheapness, pre-sowing γ-irradiation of seeds has become the most used seed treatment method. The results of previous studies have shown that pre-sowing γ-irradiation of seeds allows increasing the economic efficiency of crop cultivation, which is reflected in acceleration of plant productivity, reduction of the vegetation period and cost price of production.

For example, in their studies, Singh et al. [5] showed that an irradiation treatment, in general, causes an improvement in plant growth and yield characteristics, such as shoot and root mass, root length and surface area, leaf area and chlorophyll Soil Plant Analysis Development (SPAD) index, tiller number and grain yield. The study concludes that γ-irradiation at a low dose (25 Gy or lower) stimulates, while a high dose (100 Gy and above) inhibits plant growth and development of wheat. The adverse effect at 100 Gy and more are explained by the author by the low efficiency of carbon and nitrogen assimilation and plant assimilation of mineral nutrients, which are a determining factor in plant health.

Jae-Sung Kim et al. investigated the effect of small doses of γ-rays on the germination rate and the germination physiology of the seeds of Welsh onion (*Allicm fistulosum* L.) and spinach (*Spinacia oleracea* L.). The authors showed that the germination rate of the irradiated group was significantly higher than that of control; most notably in the irradiation groups of 1 or 2 Gy prior to sowing of spinach seeds. On the Welsh bulb, the germination rate of the 1 Gy irradiation group increased by 17% as compared to control [6].

Subhan et al. investigated the effect of γ- radiation at the rate of 10, 20 and 30 krads on growth and

yield of barley. Irradiation had positive effects on grain yield with maximum production at the rate of 10 krads of γ- rays [7].

The influence of γ- radiation in doses of 100, 200, 300 and 400 Gy on the germination and physiological characteristics of wheat seedlings was studied by Borzouei et al. [8]. The authors showed that the mean germination time, the length of the roots and shoots, as well as the dry weight of the seedling decreased with increasing radiation dose. However, the proline content in a dose of 100 Gy increased approximately 2 times in comparison with the control. According to the authors, the positive regulation of some physiological characteristics and the growth of wheat seedlings after treatment with γ- radiation can be used to combat diseases such as drought and salt stress.

Brazilian scientists Ramabulana et al. have found that ionizing radiation causes metabolites, glucomorin and its derivatives in *Moringa oleifera* with various biological activities in plants. In their opinion, these molecules can be considered as components of the inducible defense mechanism of a plant from oxidative stress [9].

Another study examined the effect of low dose γ- radiation on improving the drought resistance of a local Iranian rice variety. The results showed that under stressful conditions, preliminary treatment of seeds with γ-irradiation cause a significant increase in callus growth compared to those of controls [10].

Pre-sowing irradiation of seeds is not only an agricultural method for increasing yield, but it is also used to improve the quality characteristics of agricultural plants [11]. For example, there was an increased sugar content in sugar beet, protein in cereal plants, starch in potato, useful alkaloids in medicinal plants, and vitamins in fruit and vegetable crops [12,13]. There was also an increase in the content of proline and chlorophyll in wheat seedlings grown from γ-irradiated seeds at a dose of 100 Gy [4], an increase in the concentration of soluble sugars, proteins and proline in soybeans, grown from seeds subjected to pre-sowing γ-irradiation at a dose of 20 Gy [14].

Ionizing radiation is suggested to activate intracellular defense systems, thereby leading to stimulation of physiological processes through a complex chain of signaling pathways [15].

There is another opinion, according to which the stimulating effect of γ-irradiation of seeds at small doses is the result of a phytohormonal balance change [16].

It was established that pre-sowing treatment of seeds with γ- irradiation was not inferior in results (sometimes are even superior) to the chemical treatment of seeds [17] and human lymphocytes exposed to low doses of ionizing radiation become insensitive to both high doses of radiation and chemical mutagens that cause double-stranded DNA break [18].

Another interesting fact is that it was found that high concentrations of NaCl cause a decrease in plant growth, the content of photosynthetic pigments, the total content of soluble protein, the content of nucleic acids, and yield characteristics. At the same time, lipid peroxidation and the content of non-enzymatic antioxidants such as anthocyanin, ascorbic acid and α-tocopherol are also increased [19-21]. However, irradiation of seeds with γ- rays mitigates the adverse effect of salt stress compared to non-irradiated seeds [19].

It should be noted that, despite the complete suppression of metabolism, the genetic program of plant development is preserved in the seed [22]. Therefore, when seeds are in the aquatic environment, it contributes to the proceeding of metabolic reactions. However, energy is consumed in the course of these reactions. The energy of ionizing radiation absorbed by seeds was shown to be able to accelerate the transition of the deeply repressed genome of embryonic cells to active state and, thereby, reduce the harmful effects of the stressor [23-25].

The radiation energy in stimulating doses may be sufficient to accelerate the implementation of the genetic program of plant development without changing it, which will result in the reduction of the maturation time, an increase in yield and an improvement in its qualitative characteristics.

Hanafy Ahmed et al. [26] show an increase in the resistance of *Ambrosia maritima* L. to salt stress, the seeds of which were subjected to pre-sowing γ- irradiation. The authors found that irradiation of plant seeds with 40 or 80 Gy increased plant tolerance to salinity comparing to control, concerning plant height, fresh and dry weights, photosynthetic pigments. It was noticed that radiation alleviates the adverse effect of salinity by increasing total sugar and total soluble phenols in shoots of damsissa plants.

Kumar et al. [27] carried out a more detailed study of the effect of pre-sowing γ- radiation of seeds on salt tolerance. The authors tried to establish the role of pre-sowing γ- radiation of seeds at 2.5, 5, 10, 20, 50, and 100 Gy on the growth of pigeon peas, seed yield and seed quality under salt stress at 0, 80 and 100 mM NaCl. Irradiated plants showed better results than non-irradiated plants, even with increasing salinity. Seed yield and protein and iron content were also positively influenced by low-dose γ- radiation under NaCl stress.

Kumar et al. [28] also showed that a low dose of γ-radiation leads to accelerated growth and a number

of other physiological signs in non-leguminous and leguminous crops. As a result, plants become more salt tolerant. The relationship between γ- radiation of seeds and the response to salinization stress may be associated with the favorable maintenance of gas exchange characteristics, antioxidant enzyme activity, membrane stability, and proline and glycine betaine contents. According to the authors, one or more of these mechanisms can simultaneously contribute to the salt tolerance of agricultural plants.

In the present work, by studying the defense reactions, namely, we tried to find out the role of presowing γ-irradiation of seeds in the development of chickpea under high salinity conditions. The reaction of the plant was assessed by estimating changes in both biometric indices and in the content of MDA, proline and total protein.

A quite wide range of irradiation doses (from 1 to 200 Gy) and salt concentrations (from 1 to 200 mmol) was used. The effects of irradiation and salt were studied both individually and in combination.

Materials and methods

*Object of the study***.** Chickpea (*Cicer arietinum* L.) is an annual plant, which belongs to *Fabaceae* family. The variety of chickpea Uqu nene was chosen. The choice of peas as an object of research is because the local variety of peas "Uqu nene" has been released in Azerbaijan. The variety is patented by the Ministry of Agriculture of the Republic of Azerbaijan (number and time of patent filing – No. 00278, 02/14/2019), and the patent holder of the variety is the Azerbaijan Scientific Research Institute of Agriculture [29]. A characteristic feature of this variety is that it grows normally in the soil and climatic conditions of the Republic. In addition, peas are one of the main elements of the human diet. The increase in the size of saline lands all over the world (including in Azerbaijan) prompted the study of the influence of salt on the development and quality indicators of this variety.

Equipment – RUXUND installation with a ^{60}Co γ-radiation source, spectrophotometer JENWEY – 6_7 Series (UK), centrifuge HIMAC-CT 15 RE (UK), dielectric separator SDL-1 (Kropotkin Plant MiSSP-SOVPLAST, Inc., Russia), grain moisture meter Fauna-M (LLC firm Lepta, Russia), thermostat (Lasers and Equipment Co., Russia), chamber – phytotron – FED 53 (Binder, Germany) for growing seedlings.

Plant growth conditions. Considering that the development of plants significantly depends on seed moisture, seeds with the moisture content of 16-17% were selected for experiments. Seed samples were separated by an electric separator SDL-1 (Kropotkin Plant MiSSP-SOVPLAST, Inc., Russia) and the moisture content was measured by the dielcometer Fauna-M (LLC firm Lepta, Russia). Using a ^{60}Co irradiation source (Rosenergoatom Concern, Russia), seeds were exposed to pre-sowing γ-irradiation (the irradiation dose in all cases was 0.048 Gy/s). For this, the seeds were placed in paper packets (30 seeds into each packet) with a surface area of 20 cm^2. To study the dose-response relationship, doses of 1, 5, 10, 50, 100 and 200 Gy were applied.

Both irradiated at doses of 1, 5, 10, 50, 100 and 200 Gy, and non-irradiated seeds were grown in the dark (thermostat, 300 K) in a 9 cm-diameter plastic Petri dishes (15 seeds per Petri dish). 4 days later, seedlings, both test and control, were placed in dishes filled with tap water and placed in a growth chamber (temperature, humidity presented below) in conditions of hydroponics. In order to create salt stress, NaCl in concentrations of 1, 5, 10, 50, 100, and 200 mM was added to dishes with water before planting seedlings.

The experiments were carried out in three different variants:

1 – seeds irradiated at different doses were grown in an aqueous medium without salt;

2 – non-irradiated seeds were grown in saline solutions with different concentrations of NaCl;

3 – seeds irradiated at different doses were grown in different concentrations of salts.

In all cases, conditions were created that were similar to the natural ones. While grown in the thermostat, seeds were exposed to 12/12 day-night period (by wrapping the Petri dishes in dark paper). The temperature and humidity in the growth chamber where seedlings were grown during the day was 23 ± 1°C and 55 %, and at night 15 ± 1°C and 70 %, respectively. To provide the necessary lighting conditions, a fluorescent lamp (37.6 W/m^2) was used.

*Estimation of malondialdehyde content***.** The malondialdehyde (MDA) content, as a product of lipid peroxidation, was determined by thiobarbituric acid reaction [30]. After recentrifugation at 12,000 g for 10 min, the absorbance of supernatant was recorded at 532 and 600 nm. The value for non-specific absorption at 600 nm was subtracted. The concentration of MDA was calculated using the formula:

$$C_{MDA} = (D_1 - D_2) \cdot V_2 / \varepsilon \cdot I \cdot V_1,$$

where: D_1 and D_2 – optical densities at 532 and 600 nm, respectively; ε – coefficient of absorbance (155 mM^{-1} cm^{-1}); V_1 – the total and V_2 – the final volume of the ditch in cm^{-3}; I – the length of the ditch in cm.

MDA concentration was estimated in mmol/L per 1 g of dry weight.

Estimation of proline content. The content of free proline in fresh plant material was determined using the method of Bates et al. [31]. The plant material was homogenized in 3% sulfosalicylic acid. The homogenate was filtered and centrifuged for 15 min at 1,000 g. The ninhydrin reagent prepared without heating (1.25 g of ninhydrin, 30 mL of glacial acetic acid, 20 mL of 6 M H_3PO_4 solution) and 2.0 mL of glacial acetic acid were added to the filtrate. The reaction mixture was incubated for 1 h on a water bath at 100^0C and then it was quickly cooled to the room temperature. After cooling, 4 mL of toluene was added to each tube, shaken for 30 s and settled. After 15 min, the upper toluene layer, into which all the dye passed, was separated from the aqueous phase. The color intensity was measured using a spectrophotometer JENWEY – 6_7 Series (UK), at a wavelength of 520 nm against toluene.

The proline content was determined from a calibration curve constructed using a set of standard solutions in 3% sulfosalicylic acid. The data obtained were expressed in μmol of proline per 1 g of fresh weight.

Estimation of the total protein content. The method developed by Sedmak and Grossberg [32] was used to determine the protein content in leaf samples. For this purpose, a 0.12% Sedmak solution (0.6 g of Coomassie brilliant blue G-250 + 500 mL of $HClO_4$) and a diluted leaf extract solution (10 mL of leaf extract diluted with 90 μL of dH_2O) were prepared. The Sedmak solution (750 μL), glycerol-water solution (1:1) (750 μL) and homogenization buffer (40 μL) were added to the leaf extract solution (10 μL). The optical density of the resulting mixture was determined at 610 nm, and the protein concentration was established using a calibration curve constructed on the basis of known optical densities. To build the calibration curve, bovine serum albumin (Reanal, Hungary) was used as a standard.

The total protein content was determined by the formula:

$$m = A \cdot E / H,$$

where: A – the protein concentration determined by the calibration curve; E – the dilution coefficient; H – the plant material mass.

Study of biometric parameters and germination. For 4-day-old seedlings the number of seeds germinated at a certain time was determined by conventional method (manual counting). For 2-week-old seedlings some biometric parameters (sprout length, main root length, the number of rootlets, number and size of leaves, number, and average length of internodes) along with MDA level, proline and total protein content in the leaves were estimated.

The experiments on biometric parameters were carried out in three biological replicates. In all cases, the results were almost the same (results of one of them are presented in Table 1 and shown on Figure 1). The experiments were also carried out in three analytical replicates. To evaluate the experimental data, parametric statistical methods were used, and to assess the reliability of the difference between the experimental data and the control, the Student's criterion was used [33]. In this case, the average statistical error of analytical replication was approximately 15 – 20%, and the differences between the experimental data and the control became significant at $| t | > 2$ ($p < 0.05$).

Results and discussion

Biometric indices of chickpea seedlings germinated from seeds subjected to pre-sowing γ – irradiation. It should be noted that the method of pre-sowing irradiation of seeds, leading to radiation-induced stimulation of plant growth and development, was actively developed at the end of the last century [12]. However, researchers continue to obtain guaranteed improvement in product quality. This is attributed to the fact that over the past years the set of regionalized varieties and crops has almost completely changed. A need arises to determine the optimal dose range for each crop and regionalized variety, since the economic effect of pre-sowing irradiation depends on it [34]. Considering this, we compared biometric parameters of the plant, such as the length of the sprout, length of the main root, number of rootlets, number and size of leaves, number, and average length of internodes for assessment of the reaction of chickpea seeds to irradiation in the dose range of 1-200 Gy.

The general view of chickpea seedlings grown from irradiated seeds under normal conditions is shown in Figure 1a and the data determined for its biometric indices is presented in Table 1.

Biometric observations have shown that plants grown from irradiated seeds in the dose range of 5-10 Gy significantly exceeded control in growth intensity. In this case, there was an increase in both length of stems and root. In this dose range, the number and average length of internodes also increased. The maximum increase in individual indices (about 20%, compared to control) was observed at a dose of 10 Gy, while relatively larger doses inhibited plant growth and development.

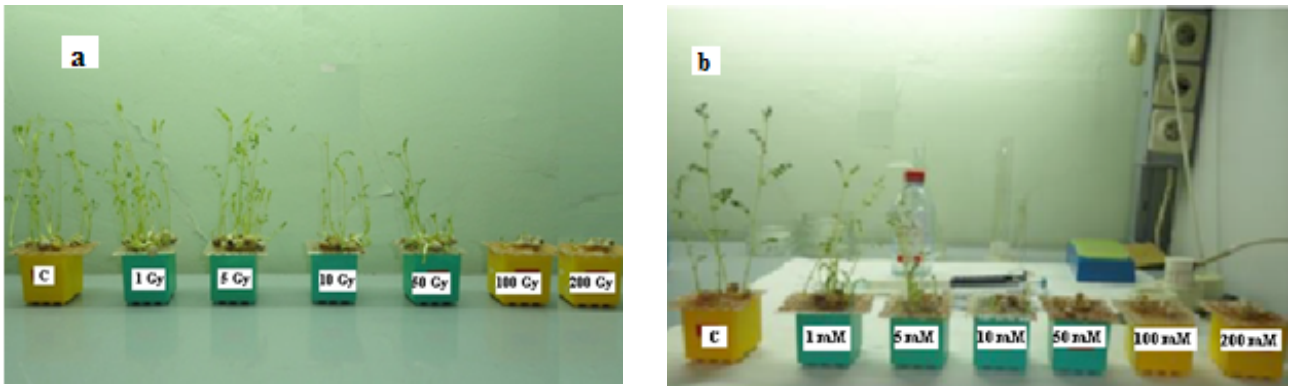

Figure 1 – Visibility of chickpea seedlings growing from:
a – irradiated seeds under normal conditions; b – non-irradiated under salt conditions.

Table 1 – Dependence of the biometric indices of chickpea on the irradiation doses of seeds

Irradiation doses, Gy	Sprout length, см	Number of leaves	Number of internodes	Average length of internodes, cm	Main root length	Number of rootlets	Leaf surface area, cm^2
C	18-19	13	8	2.2 – 2.3	7-8	10	48
1	19-20	14	9	2.2 – 2.3	7-8	12	46
5	20-21	15	9	2.3 – 2.4	9-10	10	50
10	20-21	15	8	2.2 – 2.3	8-9	11	46
50	17-18	10	6	2.1 – 2.2	5-6	10	44
100	13-14	8	6	2.1 – 2.2	3-4	10	42
200	13-14	7	6	2.0 – 2.1	3-4	9	42

Approximately same results were obtained for wheat. It was shown that low doses (25 Gy and lower) of γ- radiation contribute to the development of the plant, which manifests itself in an increase in the basic biometric parameters [5]. Moreover, high doses inhibit the growth and development of wheat [8].

The irradiated seeds of Welsh onion (*Allicm fistulosum* L.) and spinach (Spinacia oleracea L.) at low doses (1-2 Gy) also showed high germination rate compared to control [6]. Kumar et al. [28] also showed that a low dose of γ-radiation leads to increased growth and several other physiological attributes in non-legume and legume crops.

The studied seeds of the chickpea were characterized by high germination (87-92%). Interestingly, the studied range of this parameter was practically independent of the irradiation dose.

The number of rootlets was also practically independent of the irradiation dose.

A different picture was observed for the length of the roots. Irradiation in the dose range of 1 to 10 Gy stimulated root development.

Based on the results of studying the growth and development of the chickpea plant, we can conclude that the stimulating dose for seeds was in the range of 5 – 10 Gy. Wherein, irradiation doses of more than 10 Gy were found to negatively affect the growth and development of this plant.

Biometric indices of chickpea seedlings grown in salt solutions at various concentrations of NaCl. High salinity is known to be one of the main abiotic factors in some places leading to the destruction of the ionic balance of the soil. In this case, plants are exposed to even greater salt concentrations, which inevitably leads to violation of the metabolism of plant cells. In particular, it was found that salt stress leads to the destruction of the biological structure of membranes, chloroplasts, and mitochondria [35]. As a result, their biological functions are disrupted, and the electron transfer rate decreases leading to the decreased productivity of cultivated plants and reduced biodiversity of wild plants [35].

According to the results of our experiments, germination of chickpea seeds strongly depends

on salt concentration (Figure 1b). Its significant decrease was noted with increasing NaCl concentrations. For instance, about 90 % germination rate was observed for the control variant, whereas at 1 mmol, 5 mmol, 10 mmol and 50 mmol concentrations of NaCl the approximate germination was, respectively, 80%, 70%, 50%, and 20%. The seeds did not grow at higher concentrations of NaCl, namely 100 and 200 mmol. Biometric indices of chickpea grown at various concentrations of NaCl are presented in Table 2.

According to the results, salt stress has a more dramatic effect on the plant development. Even low salt concentration (1 mmol) leads to the inhibition of the plant development. Further increase in the concentration of salt from 1 mmol to 10 mmol has more inhibitory effects: plant growth practically stopped at 10 mmol concentration.

Table 2 – Dependence of the biometric indices of chickpea on the concentration of NaCl

Concentrations of NaCl, mmol	Sprout length, см	Number of leaves	Number of internodes	Average length of internodes, cm	Main root length	Number of rootlets	Leaf surface area, cm^2
C	18	13	8	2.2 – 2.3	7-8	11	47
1	15	9	6	1.8 – 1.9	7-8	12	26
5	11	5	5	1.3 – 1.4	5-6	11	11
10	5	2	2	0.4 – 0.5	3-4	10	0,7
50	2	-	-	-	2-3	8	-
100	-	-	-	-	1-2	8	-
200	-	-	-	-	-	-	-

At 1-10 mmol concentrations of NaCl, biometric indices, such as the leaf size, the length of the main root, the number and the average length of internodes also decrease in addition to the plant growth. The number of rootlets remains practically unchanged.

It is known that salt stress is one of the main environmental factors that reduce plant productivity. Plants under stress survive due to the functioning of protective mechanisms [36]. Zhani et al. [37], using five Tunisian varieties of chili peppers (*Capsicum frutescens* L.) as an example, showed that increased salt stress for all varieties negatively affects basic biometric parameters, such as length, fresh and dry root mass, amount, and surface area of leaves. The authors note that in response to salt stress in the leaves of the studied plants, proline biosynthesis is activated.

A significant slowdown in growth and development with an increase in the concentration of NaCl was also demonstrated for seedlings of *Jatropha curcas* L. [21].

Salt stress resulted in the decrease of total fresh and dry weight by 41.75% and 53.62%, respectively [38].

NaCl induced significant differences in quantities of proteins and enhanced activities of superoxide dismutase (SOD), catalase (CAT) and peroxidase (POX) [39]. The authors suggest that an increase in antioxidant enzyme activity may be a response to cellular damage caused by NaCl. According to them, an increase in the activity of these enzymes could not stop the harmful effect of NaCl, but it reduced the severity of stress and, thus, allowed *Excoecaria agallocha* to grow in the salty habitat of mangroves.

Change in biometric indices of chickpea seedlings grown from irradiated seeds at various concentrations of NaCl. The effects of salt stress on the development of chickpea grown from seeds subjected to pre-sowing γ-irradiation are presented on Figure 2.

According to the results, when 1 Gy dose pre-irradiated seeds germinated under salinity, the normal development of the seedlings was delayed. This was more pronounced at NaCl concentrations of 50 mmol or more.

It is interesting that when seeds were irradiated in doses of 5-100 Gy, seedlings grew normally even at high concentrations of salt.

These results attract the most attention. Phenomenon called cross-adaptation has been confirmed by some researchers [40-42]. According to this phenomenon, the adaptation of a plant to the effects of any environmental factor increases its tolerance to the effects of another environmental factor. We assume that our results are completely consistent with these conclusions.

Considering that in real conditions, plants are simultaneously exposed to the combined effects of several environmental factors, and these actions can be antagonistic, additive, or synergistic, our results on the combined effects of irradiation and salt stress on plants are explainable from this point of view.

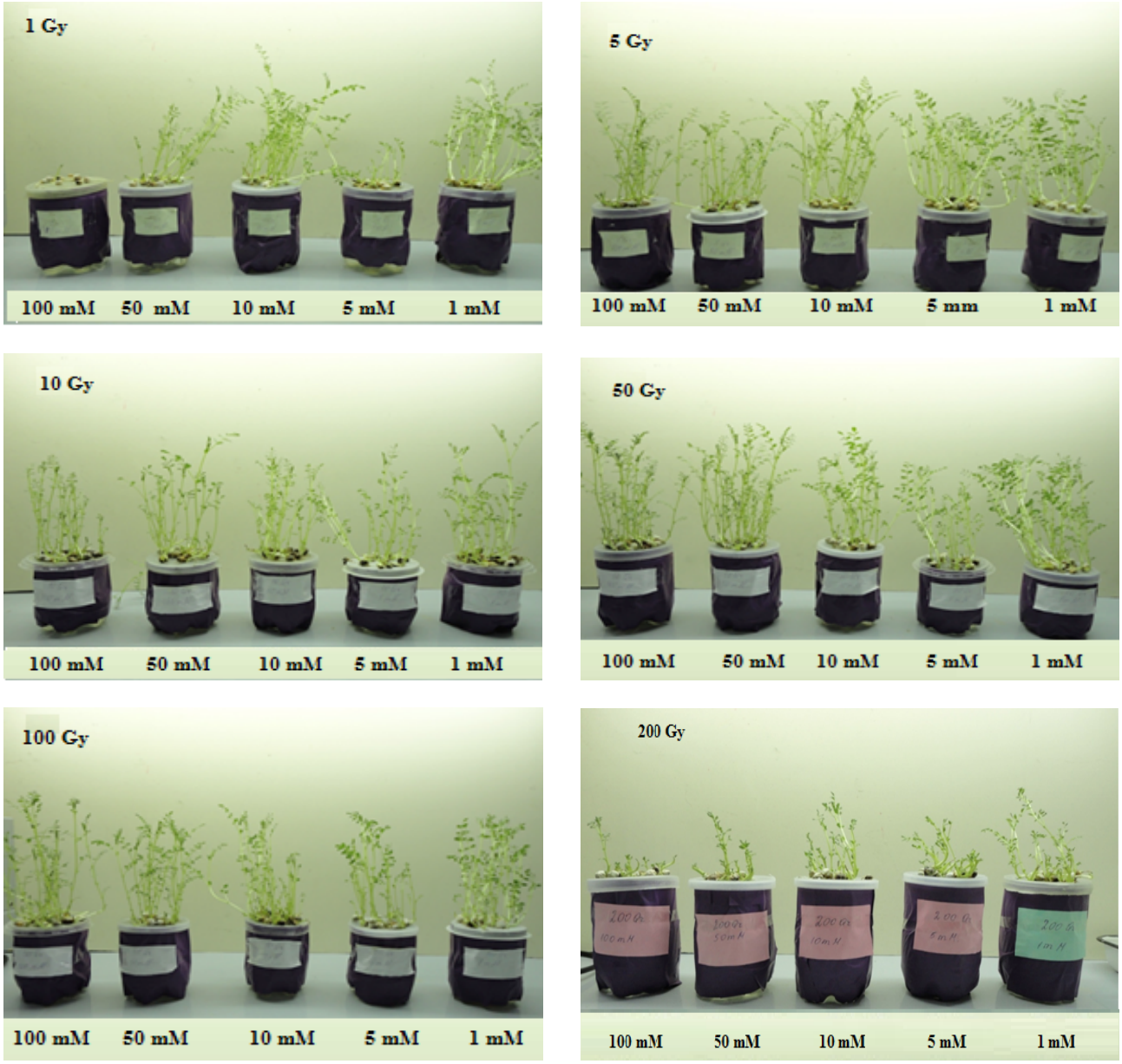

Figure 2 – Biometric indices for chickpea grown from seeds exposed to pre-sowing γ –irradiation under salt stress

Increasing the resistance of plants to salt stress, the seeds of which were subjected to pre-sowing γ-radiation, is shown in many works. For example, in the case of damssisa plants (*Ambrosia maritima* L.) it was shown that irradiation of seeds at doses of 40 (or 80 Gy) significantly increases the resistance of plants to salinization compared to control [26].

It is interesting to note that pre-sowing seed irradiation positively affects the biometric parameters in drought conditions [43]. This suggests the identity of the role of pre-sowing irradiation of seeds under stressful conditions of various kinds.

Kumar et al. [27] showed that irradiation of pea seeds at relatively low doses leads to an increase in

the salt tolerance of the plant. At the same time, irradiated plants show better results than non-irradiated ones, even with an increase in salinity.

Wang et al. [44] showed that γ-irradiation with a dose of 50 Gy has a beneficial effect on seedlings of highland barley under stress conditions with lead/ cadmium. Moreover, seedlings irradiated at a dose of 50 Gy have a lower content of hydrogen peroxide and MDA under stress compared with seedlings without prior irradiation. Moreover, proline levels in γ-irradiated seedlings at 50 Gy were significantly higher than in non-irradiated seedlings under stress conditions with lead/ cadmium. The authors suggest that γ- radiation, to some extent, reduces the toxic effects of heavy metals on crops.

From the large amount of data available on transcript-profiling studies in plants subjected to drought and salt it is becoming apparent that plants perceive and respond to these stresses by quickly altering gene expression in parallel with physiological and biochemical alterations [35]

Brazilian scientists Ramabulana et al. have found that ionizing radiation causes production of glucomoringin and its derivatives in *Moringa oleifera*. These molecules can in turn be regarded as components of the inducible defense mechanism of the plant against the effects of oxidative stress [9].

Effect of salt stress on the content of MDA in chickpea grown from the seeds exposed to pre-sowing γ-irradiation. The mechanisms of the effects of irradiation on biological objects are known to be associated either with chemical transformations in the cells (indirect effect) [45], or with direct effects on DNA (target theory) [46]. The mechanism of indirect action is based on the interaction of ionizing radiation with water molecules and the reactions caused by various ions and free radicals, which are formed as a result of such effects. Mechanisms of direct exposure are associated with the direct effect of ionizing radiation on DNA and RNA, which play the role of a target in the cell [46]. It should be noted that the interaction of free radicals with lipids of the cell membranes takes place. As a result of this interaction, the oxidation of lipids by the radical chain mechanism occurs [47]. The oxidation and damage of membranes were shown to cause the formation of several final products including MDA [47,48] and the degree of structural damage was determined by the level of this product.

The results of our studies regarding the effect of salt stress (at various NaCl concentrations) on the dynamics of changes in the MDA content in leaves of chickpea, grown from the seeds exposed to pre-sowing γ – irradiation are presented in Figure 3.

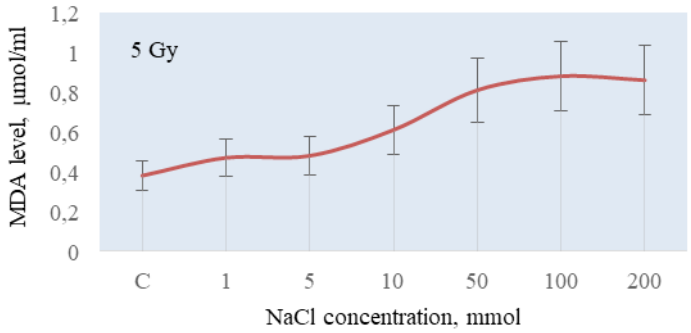

Figure 3 – The dynamics of changes in the MDA content under the combined conditions of radiation and salt stresses.

In this case, the dose of seed irradiation was 5 Gy. This dose was selected for the following reason: firstly, it is a stimulating dose for chickpea growing under normal conditions, and secondly, the biometric indices at irradiation doses of 10, 50, and 100 Gy under all concentrations of salt are almost identical to those obtained at 5 Gy (Figure 2).

According to the results, with increasing salt concentrations from 1 to 50 mmol, the MDA content gradually increased in chickpea seedlings, germinated from the seeds exposed to pre-sowing irradiation at a dose of 5 Gy. However, a further increase in the salt concentration from 50 to 200 mM did not lead to a noticeable increase in the MDA content.

Salt stress can be assumed to manifest itself at 1 mmol concentration of NaCl. A further increase in salt concentration, i.e., an increase in the intensity of salt stress, causes an increase in the structural dis-

mantling of membrane lipids, which is accompanied by a noticeable increase in the content of MDA. The increase in the content of MDA, i.e., structural dismantling of membrane lipids continued till 50 mmol concentration of salt (MDA content in the 50 mmol NaCl solution is approximately 1.5 times higher compared to control). However, at higher concentrations of NaCl (greater than 50 mmol), further oxidation and damage to lipid membranes did not occur.

At salt concentrations of 1 to 10 mM, the MDA content does not increase significantly. A marked increase occurs at concentrations from 10 to 50 mM NaCl.

Similar results were obtained for barley under the action of heavy metals [44], where γ- irradiation with a dose of 50 Gy demonstrated a beneficial effect on seedlings of highland barley under stress conditions with lead/ cadmium. Moreover, seedlings irradiated at a dose of 50 Gy have a lower content of H_2O_2 and MDA under stress compared with seedlings without irradiation.

Our previous research showed that for non-irradiated chickpea grown at 50 mmol NaCl, the MDA content exceeded the control level by about 2.1 times [49].

Based on these data, it can be assumed that irradiation of seeds in stimulating doses to some extent prevents the lipid peroxidation of cell membranes of chickpea, grown at low concentrations of NaCl (1-50 mmol NaCl). Therefore, salt stress does not significantly damage the membranes, and as a result, a large amount of MDA does not form.

However, at higher concentrations of NaCl, the nature of the action of salt stress, i.e., the dynamics of changes in the content of MDA changes. In this case, pre-sowing irradiation of seeds does not allow the further development of the reaction of lipid oxidation, and the content of MDA remains almost constant.

Effect of salt stress on the proline content in leaves of chickpea, grown from the seeds exposed to pre-sowing γ-irradiation. The response of plants to the damaging effects of the stressor is known to lead mainly to increased development of reactive oxygen species, which is usually accompanied by an increase in the activity of antioxidant enzymes. Low molecular weight antioxidants, including proline, have protective effect on the plant [50]. An understanding of the molecular mechanisms of plant responses to various abiotic stresses gives hope that genetically modified crops will cope better with these stresses.

Kadhimi et al. [43] showed that pre-sowing γ-irradiation, having a positive effect on the growth and development of rice under drought conditions, contributes to an increase in proline content. Zhani et al. [37] also demonstrated the activation of proline biosynthesis for *Capsicum frutescens* L. under conditions of salt stress. Borzouei et al. [8] showed that with γ-irradiation the proline content for wheat can increase up to two times.

Concentration-dependent changes in the proline content in freshly picked chickpea leaves are presented in Figure 4.

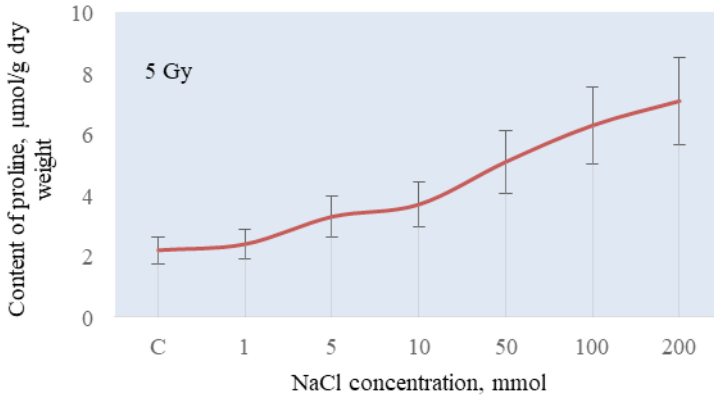

Figure 4 – The dynamics of changes in the proline content under the combined conditions of radiation and salt stresses

According to the results of our studies, there is a concentration-dependent dynamic of changes in the content of proline. In other words, an increase in the salt concentration in the studied range (1-200 mmol) leads to a marked increase in the proline content. However, the levels of these changes at various con-

centrations are not the same. More precisely, while at low concentrations (1-10 mmol) of salt, the dynamics of changes is more monotonous and the scale of changes is not large, then at high concentrations (50-200 mmol), changes in the proline content are larger.

A significant increase in proline content under stressful conditions (including salt stress) is indicated for many plants. An increased proline content under stress conditions was reported previously by Kishor et al. [51] and Kolupaev et al. [52]. Proline accumulation under abiotic stress, depending on the type and degree of stress amounts to several millimolar concentrations [53]. Proline accumulation is believed to be caused by *de novo* synthesis or a decrease in its degradation, or both [54].

It has been established that for many plants under conditions of salt stress and drought, due to an increase in synthesis and/ or a decrease in degradation, the proline content reaches up to 80% of the amino acid pool (under normal conditions, it is 5%) [55,56].

It should be noted that genes encoding the majority of enzymes associated with proline synthesis and degradation were cloned and partially characterized. However, factors regulating the expression of these enzymes have not been identified [51].

Several attempts have been made to increase the level of proline accumulation in plants by transferring genes that activate its biosynthesis pathways. For example, tolerance to abiotic (in particular, salt) stress, as well as improved growth and development were observed in various transgenic plants, which were characterized by an increased content of proline [51].

A significant increase in proline content under stressful conditions (including salt stress) is indicated for many plants. Proline accumulation is associated with both an increase in synthesis and a decrease in its degradation [37,51]. Similarly, a decrease in the level of accumulated proline in the rehydrated plants is due to both down regulation of proline biosynthetic pathway enzymes and upregulation of proline degrading enzymes [51].

Effect of salt stress on the total protein content in leaves of chickpea, grown from the seeds exposed to pre-sowing γ – irradiation. The main goal of cultivating cereals and leguminous crops is, first of all, to increase the content of proteins, carbohydrates, lipids, vitamins, etc. [57]. Therefore, researches on the effect of various factors on the qualitative and quantitative composition of agricultural plants are still relevant. Ionizing radiation has a special place among these factors. Although the chemical composition of plants, which determines their quality, is formed in the process of evolution, variability is also inherent in it. Under the influence of external factors, both quantitative and qualitative changes in the chemical composition of plants can occur. The creation of new, more tolerant to environmental conditions and more productive plant genotypes is conditioned by this circumstance. Moreover, the ability of plant cells to respond to adverse effects ensures their existence also in severe environmental conditions [58].

There are facts according to which the nature of protein biosynthesis also changes, metabolic processes and physiological functions of the organism as a whole are disrupted [59,60].

In the leaves of seedlings germinated from seeds exposed to pre-sowing irradiation and grown at 1-10 mmol NaCl concentrations, the total protein content was approximately the same as in the control sample (Figure 5). However, under high salt concentrations (10-200 mmol), seed irradiation led to a sharp decrease in the total protein content.

It should be noted that different dependence is characteristic of non-irradiated chickpea seeds grown under salinity. At low NaCl concentrations (up to 1 mmol NaCl), changes in the protein content were not observed. A significant change in the protein content occurred at NaCl concentrations higher than 1mmol. At these concentrations, salt stress was accompanied by a significant decrease in the total protein content [61].

The comparison of the results of our current and previous researches shows that the irradiation of seeds in stimulating doses relative to the total protein content, to some extent expands the field of plant tolerance to salt stress. In other words, irradiation of seeds at a dose of 5 Gy prevents the destruction of proteins in the range of NaCl concentrations from 1 to 10 mmol. Because, under such severe conditions, the total protein content remains almost constant and does not differ from the content of the control sample. It is seen that pre-sowing irradiation of seeds at a dose of 5 Gy, to some extent, facilitates the effect of salt at its low concentrations. Since, in contrast to high concentrations, in this case, the total protein content does not undergo a large-scale decrease.

It should be noted that our results on the total protein content for chickpeas do not differ from the results obtained for pigeon peas. For two genetically diverse varieties of pigeon peas (Pusa-991 and Pusa-992), pre-sowing γ- radiation at low radiation doses (<0.01 kGy) gave a positive effect. In other words, low-dose γ- radiation in this case also had a positive effect on protein content under stress NaCl [27].

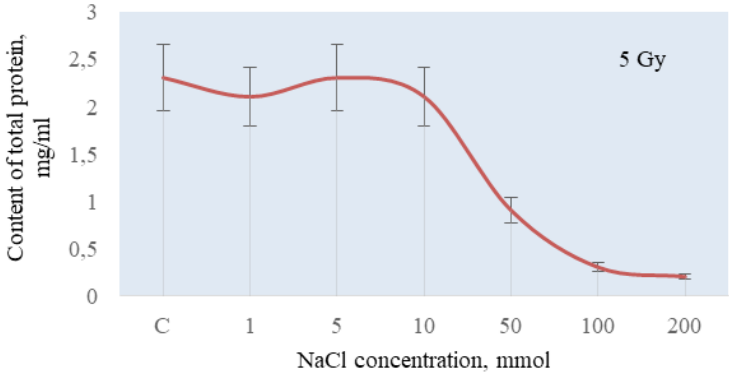

Figure 5 – The dynamics of changes in the total protein content under the combined conditions of radiation and salt stresses.

Conclusion

The results of our research have shown that:

- a significant increase in the main biometric indices is observed in chickpea seeds irradiated at doses of 5-10 Gy and grown in normal conditions. The maximum increase in individual indices (about 20% compared to control) is detected at a dose of 10 Gy. Negatively affecting, irradiation doses higher than 10 Gy, inhibit plant growth and development;

- for non-irradiated chickpea seeds grown under salinity conditions, even a small concentration (1 mmol) of salt leads to an inhibition of the development of this plant (salt stress is manifested at 1 mmol NaCl). A further increase in the concentration from 1 to 10 mmol impedes the development even more, and at concentrations above 10 mmol, plant development practically stops. At salt concentrations in the range of 1-10 mmol, in addition to growth, biometric indices of plants, such as number and size of leaves, length of the main root, number and average length of internodes also decrease;

- seedlings germinated from seeds irradiated in doses of 5-10 Gy grow normally even at high concentrations of NaCl;

- at stimulating doses increase in salt concentration from 1 to 50 mmol leads to a gradual increase in the MDA content in the leaves. However, further increase in salt stress does not lead to a marked increase in the content of the product of membrane lipid peroxidation;

- an increase in the NaCl concentration in the range of 1-200 mmol, at stimulating doses leads to a noticeable increase in the proline content. The scale of the changes at different salt concentrations is not the same. More precisely, while at low salt concentrations (1-10 mmol) the dynamics of changes is more monotonous and the changes are not large, at high concentrations (50-200 mmol), changes in the proline content are more significant, which proves its positive role in protecting plants from salt stress;

- irradiation of seeds at stimulating doses relative to the total protein content, to some extent expands the degree of plant tolerance to salt stress. In other words, when NaCl concentrations range from 1 to 10 mmol, irradiation of seeds at a stimulating dose prevents the destruction of proteins, the total protein content remains almost constant and does not differ from its content in control. However, at high salt concentrations (from 10 to 200 mmol), seed irradiation leads to a sharp decrease in the total protein content.

In general, the results showed that irradiation of seeds in doses from 5 to 10 Gy, to some extent, reducing the effects of salt stress, can partially balance the destructive consequences of excess salt.

We suggest that pre-sowing treatment of seeds with low doses of γ- irradiation (from 5 to 10 Gy) can be used to increase tolerance to salt stress and minimize yield loss caused by excess salt. This perspective method can serve as a useful tool for promotion of agriculture in areas with low salinity.

References

1 Shanko D., Jateni G., Debela A. (2017). Effects of Salinity on Chickpea (Cicer arietinum L.) Landraces During Germination Stage. J. Biochem. Mol. Biol. vol..3, no.2:9, pp.1-5. doi:10.21767/2471-8084.100037.

2 Liu R., Wang L., Tanveer M., & Song J. (2018). Seed Heteromorphism: An Important Adaptation of Halophytes for Habitat Heterogeneity. Frontiers in plant science. vol.9:1515, pp.1-10. doi. org/10.3389/fpls.2018.01515.

3 Footitt S., Walley P. G., Lynn J. R., Hambidge A. J., Penfield S., & Finch-Savage W. E. (2020). Trait analysis reveals DOG1 determines initial depth of seed dormancy, but not changes during dormancy cycling that result in seedling emergence timing. The New phytologist. vol. 225(5), pp. 2035–2047. doi. org/10.1111/nph.16081.

4 Bozhkov A. I., Kovalova M. K., Azeez Z. A., Goltvjansky A. V. (2020). The effect of pre-sowing seed treatment on seedlings growth rate and their excretory activity. Regulatory Mechanisms in Biosystems. vol. 11(1), pp. 60-66. doi:10.15421/022008.

5 Singh B., Ahuja S., Singhal R.K., Venu Babu P. (2013). Effect of γ- radiation on wheat plant growth due to impact on gas exchange characteristics and mineral nutrient uptake and utilization. J Radioanal Nucl Chem. vol. 298, no.1, pp. 249-257, doi: 10.1007/s10967-012-2342-5.

6 Jae-Sung K., Eun-Kyung L., Myung_H.B.K., Dong_Hee K., Young_B. L. (2000). Influence of low dose γ – radiation on the physiology of germinative seed of vegetable crops. Korean J. of Environmental Agriculture. vol.19, no.1, pp. 58-61.

7 Subhan F., Anwar M., Ahmad N., Gulzar A., Siddiq A. M., Rahman S., Ahmad I. and Rauf A. (2004). Effect of Γ- Radiation on Growth and Yield of Barley under Different Nitrogen Levels. Pakistan Journal of Biological Sciences. vol.7, no.6, pp. 981-983, doi: 10.3923/pjbs.2004.981.983.

8 Borzouei A., Kafi M., Khazaei H. (2010). Effects of γ- radiation of germination and physiological aspects of wheat (Triticum aestivum L.) seedlings. Pakistan Journal of Botany,

vol. 42, no.4, pp. 2281-2290.

9 Ramabulana T., Mavunda R. D., Steenkamp P. A., Piater L. A., Dubery I. A., Ndhlala A. R., Madala N. E. (2017). γ- radiation treatment activates glucomoringin synthesis in Moringa oleifera. Brazilian J. of Pharmacognocy (Revista Brasileira de Farmacognosia). vol. 27, no.5, pp. 569-575. doi. org/10.1016/j.bjp.2017.05.012

10 Falahati A., Kazemitabar S.K., Bahrami A.R., Lahouti M., Rahimi M.F. (2007). The study of γ- irradiation effects on drought tolerance in rice (Oryza sativa L.). Indian Journal of Crop Science. vol. 2, no.1, pp. 155 – 158.

11 Ahuja S., Kumar M., Kumar P., Gupta V. K., Singhal R. K., Yadav A., Singh B. (2014). Metabolic and biochemical changes caused by γ- irradiation in plants. Journal of Radioanalytical and Nuclear Chemistry. vol. 300, no.1, pp. 199–212.

12 Kuzin A.M. (1997). The stimulating effect of ionizing radiation on biological processes. M.: Atomizdat, 132 p.

13 Levin V.I. (2000a). Agro ecological effects of exposure to plant seeds of electromagnetic fields of various modalities: Ph.D. Thesis. Moscow. 36 p.

14 Moussa H.R. (2011). Low Dose of Γ- irradiation enhanced drought tolerance in soybean. Acta Agronomica Hungarica. vol. 59, no.1, pp. 1–12. doi. org/10.1556/AAgr.59.2011.1.1.

15 Stark M. (2008). Hormesis. Adaptation, and the Sandlipe Model. Critical Reviews in Toxicology. vol. 38, pp. 641–644. doi. org/10.1080/10408440802026422.

16 Wi S.G. (2007). Effects of γ- irradiation on morphological changes and biological responses in plants. Micron. vol. 38, no.6, pp. 553–564. doi: 10.1016/j.micron.2006.11.002.

17 Levin V.I. (2000b). Agroecological aspects of presowing treatment of seeds of agricultural crops with γ- rays (ed. by N.P. Kuznetsov). Moscow: VNII "Agroecoinform". 221 p.

18 Wolff S., Afzal V., Wiencke J.K., Olivieri G., Michaeli A. (1988). Human lymphocytes exposed to low doses of ionizing radiations become refractory to high doses of radiation as well as to chemical mutagens that induce double-strand breaks in DNA. Int. J. Radiat. Biol. Phys. Chem. Med. vol. 53, no.1, pp. 39-48.

19 Mohammed Abdel Haleem M.A., Mohamed Heba I., Zaki Laila M., Mogazy Asmaa M. (2012). Pre-exposure to γ- rays alleviates the harmful effect of salinity on cowpea plants. J. of Stress Physiology and Biochemistry. vol.8, no.4, pp. 199-217.

20 Hassanein R. A., Hashem H. A. and Khalil R. R. (2012). Stigmasterol treatment increases salt stress tolerance of faba bean plants by enhancing antioxidant systems. Plant Omics Journal. vol. 5, no.5, pp. 476-485.

21 Gao S., Ouyang C., Wang S., Xu Y., Tang L., Chen F.. (2008). Effects of salt stress on growth, antioxidant enzyme and phenylalanine ammonia-lyase activities in Jatropha curcas L. seedlings. Plant Soil and Environment., vol. 54, no. 9, pp. 374–381. doi. org/10.17221/410.

22 Penfield S., King J. (2009). Towards a systems biology approach to understanding seed dormancy and germination. Proc.R. Soc. B. vol.276, pp. 3561-3569, doi.org/10.1098/rspb.2009.0592.

23 Kuzin A.M., Kaushansky D.A. (1981). Applied Radiobiology. M.: Energoizdat. 224 p.

24 Rania S. H., Samia A. A. (2018). Physiological and molecular studies on the effect of γ- radiation in fenugreek (Trigonella foenum-graecum L.) plants. J. of genetic engineering and biothechnology. vol.16, pp. 683-692.

25 Dar, T. A., Uddin M., Khan M. Masroor A., Ali A., Mir S. R., Varshney L. (2015). Effect of Co-

60 γ- irradiated chitosan and phosphorus fertilizer on growth, yield and trigonelline content of Trigonella foenum-graecum L., Journal of Radiation Research and Applied Sciences. vol.8, pp. 446-458. doi.org/10.1016/j.jrras.2015.03.008.

26 Hanafy Ahmed A. H., Ghalab A. R. M., Hussein O. S. and El-Hefny A. M. (2011). Effect of γ-Rays and Salinity on Growth and Chemical Composition of Ambrosia maritima L. Plants. J. Rad. Res. Appl. Sci., vol.4, no. 4A, pp.1139 – 1162.

27 Kumar P., Sharma V., Atmaram C. K., Singh B. (2017a). Regulated partitioning of fixed carbon (14C), sodium (Na+), potassium (K+) and glycine betaine determined salinity stress tolerance of γ- irradiated pigeonpea [Cajanus cajan (L.) Millsp]. Environ. Sci. Pollut. Res. vol.24, no.8, pp. 7285–7297.

28 Kumar P., Sharma V., Yadav P. and Singh B. (2017b). γ- Ray Irradiation for Crop Protection Against Salt Stress. Defence Life Science Journal. vol.2, no.3, pp. 292-300.

29 STATE REGISTER of selection achievements which are protected and given permission to use for the production of agricultural product in Republic of Azerbaijan. Baku, 2020.

30 Ohkawa H., Ohishi N., Yagi K.Ohkawa. (1979). Assay for lipid peroxides in animal tissues by thiobarbituric acid reaction. Anal Biochem. vol. 95, no.2, pp. 351-358, doi.org/10.1016/0003-2697(79)90738-3.

31 Bates L. S., Waldren R.P., Teare I.D. (1973). Rapid determination of free proline for water – stress studies. Plant and Soil. vol.39, no.1, pp. 205-207. doi.org/10.1007/BF00018060.

32 Sedmak J.J., Grossberg S.E. (1977). A rapid, sensitive, and versatile assay for protein using Coomassie Brilliant Blue G-250. Analytical Biochemistry. vol. 79, no.1-2, pp. 544-552, doi: 10.1016/0003-2697(77)90428-6.

33 Lakin G.F. (1990). Biometrics [Biometriya]. Moskow, Vysshaya shkola, 352 p.

34 Churyukin R.S., Geraskin S.A. (2013). The effect of irradiation (60Co) of barley seeds on the development of plants in the early stages of ontogenesis. Radiation and risk. vol. 22, no.3, pp. 80-92.

35 Chaves M.M., Flexas J., Pinheiro C. (2009). Photosynthesis under drought and salt stress: regulation mechanisms from whole plant to cell. Ann. Bot. vol.103, pp. 551–560. doi.org/10.1093/aob/mcn125.

36 Becana M., Moran J. F., Iturbe-Ormaetxe, I. (1998): Iron dependent oxygen free radical generation in plants subjected to environmental stresses: toxicity and antioxidants. Plant Soil. vol. 201, pp. 137–147. doi.org/10.1023/A:1004375732137.

37 Zhani K., Mariem B.F., Fardaous M., Cherif H. (2012). Impact of salt stress (NaCl) on growth, chlorophyll content and fluorescence of Tunisian cultivars of chili pepper (Capsicum frutescens L.). J. Stress Physiol Biochem. vol.8, no.4, pp. 236-252.

38 Yarsi G., Altuntas O., Sivaci A. and Dasgan H. Y. (2017). Effects of Salinity Stress on Plant Growth and Mineral Composition of Grafted and Ungrafted Galia C8 Melon Cultivar. Pak. J. Bot., vol.49, no.3, pp. 819-822.

39 Umesh R. P., Panneerselvam R. (2012). Changes of Protein Content, Activity and Active Isoforms of Antioxidative Enzymes in Excoecaria agallocha under Salt Stress. Inter. J. of Research in Plant Science. vol.2, no.4, pp. 62-66.

40 Kuznetsov Vl.V., Khydyrov B.T., Roshupkin B.V., Borisova N.N. (1990). General systems of cotton resistance to salinization and high temperature. Plant Physiology. vol.37, pp. 987-996.

41 Zhu Y., Qian W., Hua J. (2010). Temperature Modulates Plant Defense Responses through NB–LRR–Proteins. PLOS Pathogens. vol.6, pp. 1-12. doi.org/10.1371/journal.ppat.1000844.

42 Wang Y., Bao Z., Zhu Y., Hua J. (2009). Analysis of Temperature Modulation of Plant Defense against Biotrophic Microbes. Mol, Plant Microbe. Interact. vol.22(5), pp. 498-506. doi:10.1094/MPMI-22-5-0498.

43 Kadhimi A. A., Zain C. R. C. M., Alhasnawi A. N., Isahak A., Ashraf M. F., Mohamad A., Doni F. and Wan Yusoff W. M. (2016). Effect of Irradiation and Polyethylene Glycol on Drought Tolerance of MR269 Genotype Rice (Oryza sativa L.). Asian J. of Crop Science. pp. 1-8. doi: 10.3923/ajcs.2016.52.59.

44 Wang X., Ma R., Cui D., Cao Q. (2017). Physio-biochemical and molecular mechanism underlying the enhanced heavy metal tolerance in highland barley seedlings pre-treated with low-dose γ-irradiation. Scientific Reports. vol.7, p. 14233. doi: 10.1038/s41598-017-14601-8.

45 Margulis M.A., Margulis I.M. (2005). On the mechanism of the biological effect of ionizing radiation. Journal of Physical Chemistry. vol.79, no. 6, pp. 1142-1151.

46 Tsytsugina V.G., Floru H., Polikarpov G.G. (2005). Multi-aberrant cells and pycnosis of nuclei in aquatic organisms from an area with a high content of radionuclides. Marine Ecological Journal. vol.4, no.1, pp. 84-90.

47 Montiller J.L., Cacas J.L. (2004). The upstream oxylipin profile of Arabidopsis thaliana: A tool to scan for oxidative stresses. Plant J., vol.40, pp. 439-450.

48 Miller R., Suzuki N., Cifici-Yilmaz S., Mittler R. (2010). Reaktive oxygen species homeostasis and signaling during drought and salinity stresses. Plant Cell Environ., vol.33, pp. 453-467. doi: 10.1111/j.1365-3040.2009.02041.x. Epub.

49 Velijanova M.Z., Orujeva J.R., Jafarov E.S. (2018). Effect of salt stress on the content of malondialdehyde in chickpea leaves (Cicer arietinum L.), the seeds of which were exposed to γ-radiation at different doses before sowing. Proceedings of Inter. Conf. "Radiation technologies in agriculture and food industry: current state and prospects". Obninsk, 2018. pp.65-68.

50 Ozden M., Demirel U., Kahraman A. (2009). Effects of proline on antioxidant system in leaves of grapevine (Vitis vinifera L.) exposed to oxidative stress by H2O2. Scientia Horticulturae. vol. 119 (2), pp. 163-168. doi.org/10.1016/j.scienta.2008.07.031.

51 Kavi Kishor P. B., Sangam S., Amrutha R. N., Sri Laxmi P., Naidu K. R., Rao K. R. S. S., Rao S., Reddy K. J., Theriappan P. and Sreenivasulu N. (2005). Regulation of proline biosynthesis, degradation, uptake and transport in higher plants: Its implications in plant growth and abiotic stress tolerance. Current science, vol.88, no.3, pp. 424-438.

52 Kolupaev Yu.E., Wayner A.A., Yastreb T.O. (2014). Proline: physiological functions and regulation of the content in plants under stressful conditions. Bulletin of the Kharkov National Agrarian University. Biology Series. vol. 2, no.32, pp. 6-22.

53 Delauney A.J. and Verma D.P.S. (1993). Proline biosynthesis and osmoregulation in plants. Plant J. vol.4, pp. 215-223. doi.org/10.1046/j.1365-313X.1993.04020215.x.

54 Hare P. D., Cress W. A. and Van Staden J. (1998). Dissecting the roles of osmolyte accumulation during stress in plants. Plant Cell Environ. vol. 21, no.6, pp. 535-553. doi.org/10.1046/j.1365-3040.1998.00309.x.

55 Kavi Kishor P.B. (1988). Effect of salt stress on callus cultures of Oryza sativa L. J.Exp. Bot. vol.39, pp. 235- 240. doi.org/10.1093/jxb/39.2.235.

56 Kohl D. H., Kennelly E. J., Zhu Y., Schubert K. R. and Shearer G. (1991). Proline Accumulation, Nitrogenase (C2 H2 reducing) Activity and Activities of Enzymes related to Proline Metabolism in Drought-Stressed Soybean Nodules. J. Exp. Bot. vol.42, no.240, pp. 831-837.

57 Bukharina I.L., Lyubimova O.V. (2009). Plant biochemistry (Educational-methodical manual). Izhevsk, 51 p.

58 Plant life under Changing Environment. Responses and management (Ed.-s: D. Tripathi, V. Sigh, D. Chauhan et al.). 1 st Edition. Academic Press. 2020, 1012 p.

59 Grodzinsky D.M., Kolomiyets K.D., Kutlakhmedov Yu.A. (1991). Anthropogenic radionuclide anomaly and plants (Ed. D. M. Grodzinsky) Kiev: Lybid. 160 p.

60 Kosakivska I.V. (2003). Physiological and biochemical bases of plant adaptation to stress. K.: Stal. 191 p.

61 Velijanova M.Z., Orujeva J.R., Jafarov E.S. (2019). Influence of pre-seeding γ – irradiation of seeds on the content of the total protein in Cicer arietinum L., growing in the conditions of salt stress. Proceedings of Inter. Conf. Nuclear and Radiation Technologies in Medicine, Industry and Agriculture. Almaty – 2019, Republic of Kazakhstan, pp. 227-228.

IRSTI 76.29.34 https://doi.org/10.26577/ijbch.2020.v13.i2.13

A.K. Martusevich[1,2*], O.B. Zhdanova[3,4]

[1]Privolzhsky Research Medical University, Nizhny Novgorod, Russia
[2]Nizhny Novgorod State Agricultural Academy, Nizhny Novgorod, Russia
[3]Institute of Parasitology – Branch of Scientific Center "All-Russian Institute of Experimental Veterinary named after Ya.R. Kovalenko and K.I. Skryabin", Moscow, Russia
[4]Kirov State Medical University, Kirov, Russia
*e-mail: cryst-mart@yandex.ru

Dynamics of some physical and chemical properties of biological fluids in surgical treatment of alveolar hydatid disease of liver

Abstract. The aim of the current work was to clarify the dynamics in crystallogenic and initiating activity of patients' biological fluids in alveococcosis during surgery and in the late postoperative period. The material of the study included samples of saliva of 22 patients treated for alveococcosis. Sampling of biological fluids was managed at the admission and prior to discharge from the hospital. Subsequently slides were prepared using teziocrystalloscopy technique that combines the study of the crystal forming activity of mixed saliva (classical crystalloscopy) and its initiating properties considering 0.9% sodium chloride solution as basis substance (comparative teziography). Criterial evaluation of the results of crystalloscopic and tezigraphic tests was carried out using own system of parameters. The data of visual morphometry of microslides of dehydrated saliva was supplemented with spectrophotometric analysis of crystalloscopic and tezigraphic facies performed on PowerWave XS microplate spectrophotometer (USA) at wavelengths of 300, 350 and 400 nm. It was noted that surgical treatment leads to partial normalization of physical and chemical parameters and composition of patient's biological fluids during hospital discharge.
Key words: alveococcosis, alveolar hydatid disease, surgical treatment, saliva, crystallization.

Introduction

Significantly large group of patients with focal liver diseases was considered to be radically "inoperable" based on the data of exploratory laparotomy and palliative invasions [1-5].

Recently, in repeated operations on liver, doctors limited themselves to excision or curettage of fistulas, dissection of purulent cavities and injecting parasitotropic drugs [6-9]. There seems to be a real possibility to perform repeated radical operations on patients previously considered as "inoperable" [2-5, 9-11].

It is generally assumed that the first radical dissection of liver after exploratory laparotomy due to alveococcosis was performed by S.S. Yudin (1929) [1]. According to Merzlikin et al. (2011) and Błaszkowska, Góralska (2016), the development of surgery contributed to the fact that the majority of patients with focal liver lesions were not operated in specialized medical institutions [8,9]. Simultaneously, many of them due to technical complications and incorrect assessment of the operability of the lesion focus are limited to palliative surgery or exploratory laparotomy, thus dooming patients on disability and poor outcome [1, 4, 10-12].

Since 1964, a number of works of Russian surgeons dedicated to repeated operations, mainly on the liver alveococcosis, has been published [1-5]. Papers of Zhuravlev V.A. and other researchers showed that there is a serious problem of providing a radical means to "inoperable" patients with focal lesions of the liver, which occurred in parallel with advent of different skills in surgical treatment of patients with focal lesions of the liver [1-4, 8, 12-14].

On the other hand, it is important to support the full diagnostic guiding of alveococcosis surgery. The use of modern instrumental methods for study of liver morphology (X-ray diagnostics with contrasting, CT and magnetic resonance imaging, ultrasonography) enables evaluating with a high degree of accuracy the nature, depth and severity of structural damage of the organ associated with the development of the disease [10, 13, 15-19]. Intensity of the immune response to the presence of the parasite can be verified using latex agglutination reactions, and a specific ELISA alveococcosis diagnosticum [20]. Furthermore, alveococcus scolexes in some cases

can be found in the sputum. At the same time, the features of the metabolic changes, including changes in the physical and chemical properties of biological fluids in alveococcosis, surgical treatment of it as well as treatment within postoperative period were insufficiently studied previously. In this regard, we have shown that the presence of alveococcus significantly and directionally changes the crystallogenic properties of biological substrates, and the nature of this transformation leads to similar shifts in crystallostasis of saliva and urine [21-23]. In connection with the above, clarifying the dynamics of crystallogenic and initiating activity of patients' biological fluids in alveococcosis during surgery and in the late postoperative period, designating current research, has a great scientific and practical interest.

Materials and methods

Samples of saliva of 22 patients treated for alveococcosis at the Kirov Zonal Centre of Liver and Biliary Tracts were studied. The diagnosis was verified with standard instrumental (ultrasound, CT and/or MRI) and laboratory (latex agglutination, ELISA) tests. All the patients have successfully undergone surgery (partial hepatectomia, lobectomia, hemihepatectomia).

Sampling was managed at the admission and prior to hospital discharge. Within 3 hours before the study, patients did not engage in physical activity, neither they were in a state of psycho-emotional stress. Before collection of biological fluids, patients rinsed their mouths thoroughly with approximately 100 mL of dH_2O for 5 min. Afterwards 1 mL of oral fluid was collected by spitting into clean and dry test tubes.

Subsequently slides were prepared using teziocrystalloscopy technique that combines the study of the crystal forming activity of mixed saliva (classical crystalloscopy) and its initiating properties considering 0.9% sodium chloride solution as basis substance (comparative teziography) [21-23].

Criterial evaluation of the results of crystalloscopic and tezigraphic tests was carried out, using own system of parameters [21, 23]. It allows estimating specialties of crystallization (initiation potential – in teziography) of the biological substrate, severity of the individual zones of the facia, degree of destruction of crystalline and amorphous components, the uniformity of their distribution on the texture of the sample, etc.

The data of the visual morphometry of microslides of dehydrated saliva was supplemented with spectrophotometric analysis of crystalloscopic and teziographic facias, performed on PowerWave ™ XS microplate reader (BioTek, USA) at the wavelengths of 300, 350 and 400 nm. To neutralize the influence of the characteristics of glass to the results of spectrometric studies of biological crystals we calculated the level of optical density of facies by subtracting the optical density of pure glass from the total value of the indicator.

The study was approved by the local ethical committee of Kirov State Medical University (19.09.2016, No. 16).

Statistical data analysis was done using the Microsoft Excel 2007 spreadsheets along with Primer of biostatistics version 4.03 program.

Results and discussion

Considering that saliva is the most convenient noninvasive marker of modification of physical and chemical properties and composition of the blood and also biological substrates secreted in the digestive tract. Last one is locus morbi of alveococcosis and therefore advantageously reflects its functional and metabolic status, consequently current analysis of crystallogenic activity of the biological fluid was of particular scientific and practical interest. Based on the studies it was found that the dynamics of varying parameters is observed in all major morphometric parameters of crystalloscopic facies of patients' saliva (Figure 1).

In particular, the multidirectional changes recorded in respect of the indicators of dehydration structuring of biological medium – the structure index (SI) and crystallizability (Cr) of biological substrate components. So, initially in patients with alveococcosis on the slides of oral fluid there are more complex by the nature of the organization elements, fern-like, dendrite crystals with branching order of 3.4 or higher, which is reflected in the growth of structure in relation to the level of the index microslides of saliva of nearly healthy people ($p<0.05$). The enlargement of the main structural elements of the saliva facies of patients with alveococcosis leads to a decrease in the density of the crystals (Figure 2), being registered as a parameter "crystallizability" ($p<0.05$). In turn, the pathological character of the detected shifts of crystalogenic potential of considered patients is clearly manifested in the dynamics of facies destruction, reaching almost 2 relative units (rel.un.), which corresponds to the formation of severe disturbance of crystal elements formation while maintaining their differentiation by types.

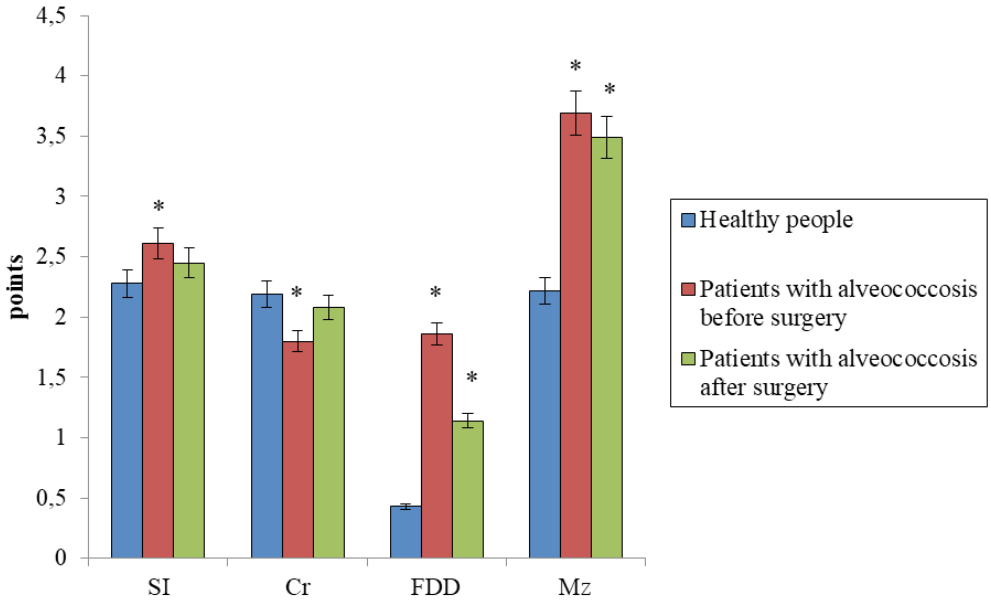

Figure 1 – The result of parametric analysis of own crystallization of patients' saliva during surgical treatment of alveococcosis (SI – structure index, Cr – crystallizability, FDD – facia destruction degree, Mz – clearity of marginal zone; "*" – value of statistical differences to the level of healthy people is $p<0.05$)

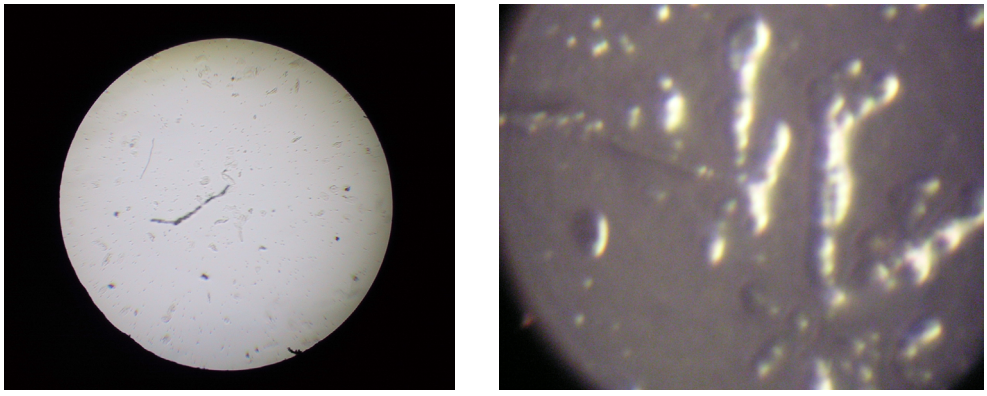

A. In healthy person

B. In patient with alveococcosis

Figure 2 – Crystallosopic facias of the saliva of healthy person and patient with alveococcosis (magnification x56)

It is known that in the pathogenesis of alveococcosis not only mechanical properties of the developing liver and other organs of the parasite, but the immunological reactions to its presence are manifested. Therefore, in the blood, and to a lesser extent in other biological substrates an increased concentration of immunoglobulins was noted that leads to an increase in their protein levels. Data for markers of metabolic shifts in saliva crystallogram serves as a manifestation of the marginal zone of the slides (parameter Mz), where the protein macromolecules of dehydration are concentrated. It was found that this index in patients with alveococcosis is registered on high value, and it is significantly below normal level ($p<0.05$). In general, prior to the surgery crystallogenic properties of saliva significantly differ from crystalloscopic "pattern" of a healthy person.

Within the early postoperative period crystallogenic properties of studied biological fluid are transformed significantly (Figure 1). Thus, there is almost complete normalization of the parameters characterizing the complexity and density of

structure-building crystal elements (SI and Cr, respectively). It should be noted that both of these parameters do not significantly vary in relation to control (pre-surgery) level, while greatly differ from the baseline ($p<0.05$). The main parameter describing the "correctness" of crystallogenesis – the facia destruction degree (FDD) – is also reduced significantly compared with the preoperative crystalloscopic "pattern" ($p<0.05$) but does not reach the physiological level.

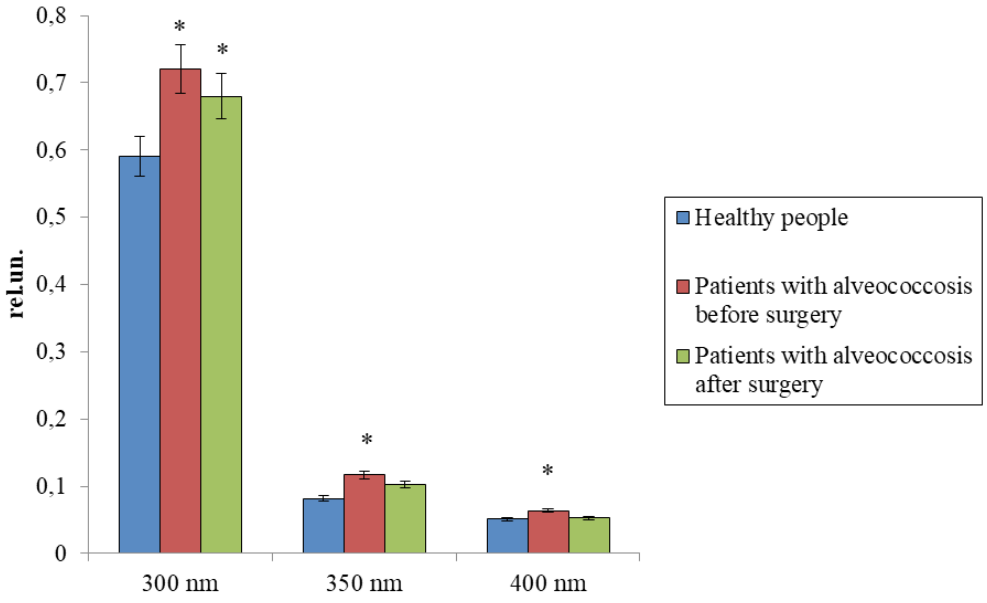

Figure 3 – Spectrometric analysis of saliva crystalloscopic facias of patients with alveococcosis during surgery ("*" – value of statistical differences to the level of healthy people is $p<0.05$)

It is interesting that the severity of the marginal zone of saliva microslides after the operation changes at a minimum degree. This trend is perhaps related to the persistence of high concentrations of anti-alveococcus antibodies in the blood and, therefore, in other biological fluids. This, in turn, has a corresponding impact on the parameter Mz, being directly dependent on the level of a protein. Upon completion of surgery partial normalization of crystallogenic properties of saliva is observed in patients with alveococcosis.

Such data is fully confirmed by a verifying method – spectroscopic study of crystalloscopic facies (Figure 3). Considering the fact that the prevalent trend of the shifts of crystallogenic properties of saliva in alveococcosis is enlargement of crystal elements along with the complexity of their construction, the increase of the optical density of the sample as a whole, for all wavelengths used in the preoperative period, seems to be logical from control values ($p<0.05$). The presence of such shifts was first shown in this study.

After the surgery, the level of the total optical density of crystalloscopic facies of saliva decreases but remains significantly higher than the values which are typical for healthy individuals (Figure 3). It should be noted that this dynamic is most clearly seen in the spectroscopic study at $\lambda = 300$ nm, but is less pronounced at $\lambda = 350$ nm, and at the maximum $\lambda = 400$ nm, as a result of rather low absolute values, it is almost eliminated.

Analysis of the initiating properties of saliva of the considered cohort of patients during surgery (Figure 4) demonstrated initially significantly higher level of the basic indicator of the initiating potential of biological fluid – tezigraphic index (TI), when compared to healthy subjects ($p<0.05$). Upon completion of surgical treatment, this parameter is moderately decreased, but these changes are not even statistically significant. A similar pattern was registered respectfully to the complication marker of structure-building elements – crystallinity (C). However, the postoperative level of the indicator does not significantly differ from both the pre-surgery and normal tezigraphic pattern of saliva. The minimal variation among the basic tezigraphic indicators (Figure 4) is uncovered for the belt coefficient (BC), which is the

criterion of scattering of molecular weight of biological substrate components.

The effectiveness of surgical treatment is most clearly manifested in the dynamics of the principal tezigraphic criterion of "correctness" of the processes of structure formation – the facia destruction degree, as well as the clearity of the marginal zone of the slides (Figure 4). These figures after the completion of surgery were significantly reduced relative to the preoperative level, but without reaching the structures which are typical for healthy individuals ($p<0.05$). This trend is an indirect evidence of the safety of alveococcus-associated metabolic shifts of the composition and physical-chemical properties of biological fluids and after performing radical surgery.

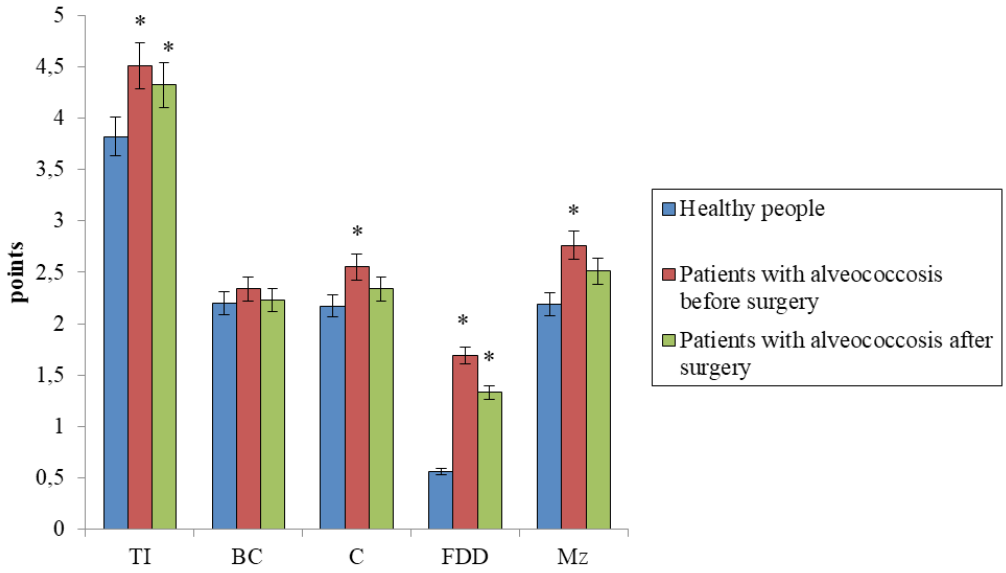

Figure 4 – The data of tezigramms parametric analysis of saliva during surgical treatment of alveococcosis (TI – teziographic index, BC – belt coefficient, C – crystallinity, FDD – facia destruction degree, Mz – clearity of marginal zone; "*" – value of statistical differences to the level of healthy people is $p<0.05$)

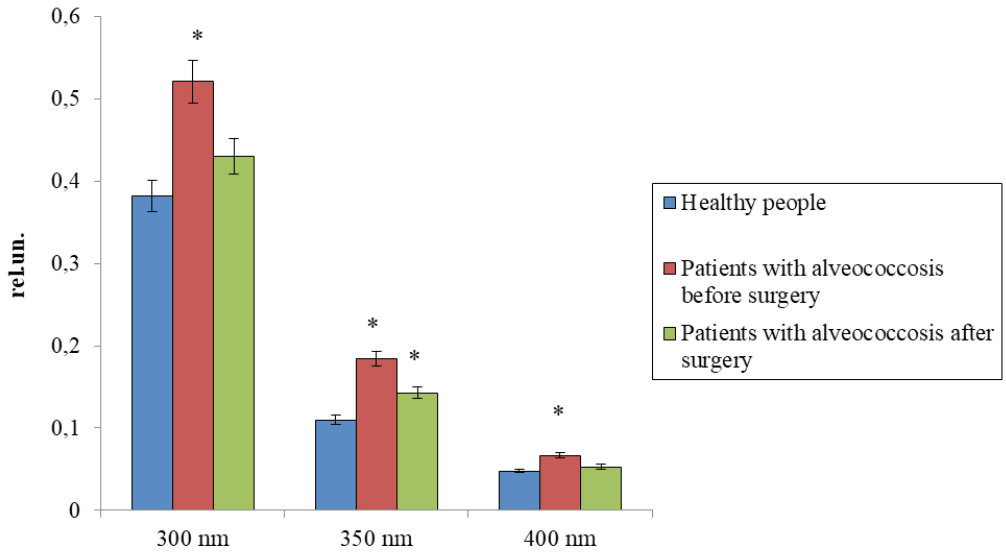

Figure 5 – Results of spectrometry of saliva tezigraphic facias of patients with alveococcosis during surgery ("*" – value of statistical differences to the level of healthy people is $p<0.05$)

These variations are fully verified by the results of spectroscopic study of tezigraphic facies of patients' saliva in the dynamics of surgical treatment (Figure 5). In this case the dynamics of the total optical density of tezigrams is evident at all wavelengths used.

Acknowledgment

Authors thank Dr. Vladimir Yanchenko (from Kirov State Medical University, Russia) for advance in patients' selection.

Conclusion

Conducted crystalloscopic studies allowed us to establish that in alveococcosis of the liver there are significant transformations of the crystallogenic properties of saliva. They are manifested in an increase in the structure index, the severity of the sample marginal zone and the degree of destruction of individual structures, as well as in a decrease in crystallizability. Such shifts lead to an increase in the optical density of facias. After surgical treatment, most of the parameters are normalized, while only the degree of facias destruction and the clarity of the marginal zone of the samples are preserved at elevated values. At the same time, the optical density of micro-preparations remains elevated only at a wavelength of 350 nm. Identification of such dynamics of crystalloscopic indicators allows us to consider them as an additional indicator of the effectiveness of treatment of alveococcosis of the liver. Further verification of the diagnostic information content of the technology used by us can become the basis for developing a method for rapid testing of the usefulness of liver resection in alveococcosis. In addition, our data complement the understanding of the metabolic changes that are formed in the body of patients with alveococcosis of the liver.

References

1 Alperovich B.I. (1997) Alveokokkoz [Alveococcosis]. Yakutsk. 254 p.

2 Panteleev V., Nartaylakov M., Mustafin A. et al. (2019) Surgical treatment of liver echinococcosis and alveococcosis. Infez Med. vol. 27, no. 4, pp. 422-428.

3 Novozhilov A.V., Movsisyan M.O., Grigoriev S.E., Magolina O.V., Kleimenova N.S. (2019) Kombinirovannaya levaya gemigepatektomiya v lechenii mul'tiorgannogo al'veokokkoza [Combined left hemihepatectomy for multiple organ alveococcosis]. Khirurgiia (Mosk). no. 9, pp. 52-57. doi: 10.17116/hirurgia201909152.

4 Veronsky G.I. (1997) Surgical treatment of liver alveococcosis. Annals of surgical hepatology, no. 2, pp. 15-19.

5 Zhuravlev V.A. (1997) Liver alveococcosis. Annals of surgical hepatology, no. 2, pp. 9-14.

6 Gawor J. (2011) Potential risk factors for alveolar echinococcosis in humans in Poland. Przegl. Epidemiology. vol. 65, no. 3, pp. 465-470.

7 Kogan E.A., Nekrasova T.P., Lerner Y.V., Kukleva A.D. (2020) Sochetanie al'veokokkoza pecheni i gepatotselliuliarnoĭ kartsinomy (sektsionnoe nabliudenie) [Liver alveococcosis concurrent with hepatocellular carcinoma (autopsy observation)]. Arkh Patol. vol. 82, no. 1, pp. 47-51. doi: 10.17116/patol20208201147.

8 Merzlikin N.V., Alperovich B.I., Paramonova M.M. (2011) Repeated operations in localized liver diseases. Surgery. no. 8, pp. 51-57.

9 Błaszkowska J, Góralska K. (2016) Clinical cases of parasitoses and fungal infections important from medical point of view. Ann Parasitol. vol. 62, no. 4, pp. 255-265. doi: 10.17420/ap6204.61.

10 Dybicz M., Borkowski P.K., Padzik M., Baltaza W., Chomicz L. (2018) Molecular determination of suspected alveolar echinococcosis requiring surgical treatment in human cases from Poland. Ann Parasitol. vol. 64, no. 4, pp. 339-342. doi: 10.17420/ap6404.169.

11 Pielok Ł., Karczewski M., Cierach W. et al. (2020) Portal hypertension as a result of the incomplete surgically treated advanced alveolar echinococcosis: a case description. BMC Gastroenterol. vol. 20, no. 1, pp.176. doi: 10.1186/s12876-020-01320-0.

12 Scripenco O.G., Shatveryan G.A., Bagmet N.N. (2012) Liver alveococcosis: retrospective analysis of treatment of 51 patients. Surgery. no. 12, pp. 4-13.

13 Stefaniak J. (2007) Guidelines for diagnosis and treatment of liver alveococcosis caused by Echinococcus multilocularis. Wiad. Parazytologia. vol. 53, no. 3, pp. 189-194.

14 Tumolskaya N.I. (2010) Cases of alveococcosis in humans in European part of Russia. Medical parasitology and parasitic diseases. no. 3, pp. 45-47.

15 Cheremisinov O.V. (2003) Possibilities of radiological and magnetic resonance tomography in diagnostics of liver alveococcosis. Medical visualization. no. 4, pp. 46-52.

16 Gossios K.J. (1997) Uncommon locations of hydatid disease: CT appearances. European Radiology. vol. 7, no. 8, pp. 1303-1308.

17 Imankulov S.B., Fedotovskikh G.V., Zhampeissov N.K. et al. (2015) Treatment of liver alveo-

coccosis with high-intensity focused ultrasound. Ultrason Sonochem. vol. 27, pp. 707-711. doi: 10.1016/j.ultsonch.2015.05.022.

18 Patkowski W., Kotulski M., Remiszewski P. et al. (2016) Alveococcosis of the liver – strategy of surgical treatment with special focus on liver transplantation. Transpl Infect Dis. vol. 18, no. 5, pp. 661-666. doi: 10.1111/tid.12574.

19 Tsitouridis I., Dimitriadis A.S. (1997) CT and MRI in vertebral hydatid disease. European Radiology. vol. 7, no. 8, pp. 1207-1210.

20 Wnukowska N., Salamatin R., Gołab E. (2011) Human echinococcosis in Poland in 2003-2010 according to the serological tests results of NIPH-NIH. Przegl Epidemiology, vol. 65, no. 3, pp. 455-458.

21 Martusevich A.K., Grishina A.A., Bochkareva A.V. (2010) Crystallodiagnostics of some animals' helmintosis. Asian Pacific Journal of Tropical Medicine. vol. 3, no. 3, pp. 176-179.

22 Martusevich A.K., Zhdanova O.B., Yanchenko V.A. (2006) Pathogenic significance of biological fluids crystallization in alveococcosis. Annals of surgical hepatology. vol. 11, no. 3, pp. 50-51.

23 Martusevich A.K., Zhdanova O.B., Napisanova L.A. (2012) Biocrystalomics in parasitology: state-of-the-art, possibilities and perspectives. Russian Journal of Parasitology. no. 4, pp. 77-88.

IRSTI 31.19.15 https://doi.org/10.26577/ijbch.2020.v13.i2.14

I.Yu. Silachyov

Institute of Nuclear Physics, Almaty, Kazakhstan
e-mail: silachyov@inp.kz

Neutron activation analysis of rare earth raw material using a planar detector and thorium as an internal standard

Abstract: The application of comparator instrumental neutron activation analysis (INAA) combined with the internal standard method and counting of the induced activity by a planar type HPGe detector was considered to determine eleven lanthanides by the long-lived radionuclides in some types of rare earth and rare metal ores. The enhanced thorium contents of these objects made possible to use it as an internal standard in comparator INAA. Thorium mass fractions of the samples were determined by the method of instrumental gamma-spectrometry with the relative standard uncertainty less than 4% (P = 0.68). Four samples of geological reference materials (rocks, including a uranium-bearing rock) certified for rare earth element (REE) contents were used to verify accuracy of the method. The proposed variant of comparator INAA was shown to insure accuracy of routine analysis of the corresponding geological objects for REE contents by the III category of precision according to the industrial standard OST 41-08-221-04 (Russian Federation). To test the method twenty thorium-enriched samples from Shock-Karagai rare earth deposit (North Kazakhstan) and several similar rare metal ore samples were analyzed for lanthanide contents.

Key words: lanthanides, neutron activation analysis, internal standard.

Introduction

Instrumental neutron activation analysis (INAA) proved itself as one of the most effective methods of geological sample analysis for element contents long ago [1]. Despite the continued dynamic development of the alternative methods of elemental analysis [2] INAA is still widespread to solve a range of geochemical tasks from rock characterization [3-6] to identification of metallogenic provinces [7].

One of the most important INAA applications in geochemistry should be associated with the solution of such a difficult problem as individual lanthanide analysis [8-12]. Different investigators repeatedly emphasized undoubted advantages of INAA comparing with the other up-to-date instrumental methods of rock analysis for lanthanide contents [4, 13-15]. INAA is mostly known to get the benefit from rare earth element (REE) determination at the levels far lower their Clarke (crust average) contents, from the absence of sample decomposition and hence the need of chemical blank evaluation, clear and generally minimal matrix effect, insignificant spectral interferences and reasonable cost of the analysis. Typical rocks being analyzed by INAA, corrections for uranium fission products are usually small, and neutron flux self-shielding by major elements is practically absent.

In the case of REE analysis, main disadvantage of INAA by the long-lived radionuclides consists in its long duration, no less than 30 days after sample irradiation, to guarantee complete decay of ^{153}Sm (a spectral interference of ^{153}Gd).

All the long-lived radionuclides – the products of lanthanides activation – are characterized by rather low-energy analytical gamma-lines the most high-energy of which belongs to ^{40}La (328.8 keV). This makes possible to use in INAA a planar type semiconductor detector distinct from a coaxial one in higher detection efficiency of low-energy gamma radiation, far better energy resolution, and lower background of Compton continuum [10]. Moreover, gadolinium content being determined by radionuclide ^{161}Tb (25.7 keV), analysis can be carried out 1–2 weeks earlier.

Soon after becoming commercially available, high purity (HP) Ge planar type detectors found their broad application to analyze rocks [16, 17], chondrites [18], river sediments [19], etc. for REE contents by INAA. After getting access to the high-effective coaxial detectors with HPGe crystals of big volumes (≥200 cm^3), taking into account their higher cost, the planar type detectors were

continually used as additional ones to determine a wide range of elements including lanthanides in chondrites [20], rock reference materials [21], to study continental shelf sediments [22] and so on.

Widespread and convenient k_0-method as a variant of comparator INAA had long been recognized for concentration standardization [23]. Although it doesn't need certified reference materials (CRMs) to calibrate gamma spectrometers, k_0-method is not deprived of some drawbacks because the comparator (an Au-containing sample) is used as an external standard [13]. All the advantages of comparator INAA can be realized only by joint application of the internal standard method [24] and an independent method to analyze the element used as the comparator [25].

Iron is often selected as the internal standard to implement comparator INAA of different rock samples [26], while its content can be conveniently determined by X-ray fluorescence method (XRF) [13, 25]. A planar type detector measures ^{59}Fe count rate by the 192.3 keV gamma-line with 3.1% of the quantum yield. Insufficient intensity of this line restricts application of iron as the internal standard within its content of the samples no less than ≈5%. Other comparators being used, particularly – thorium the enhanced contents of which often accompany REE deposits [27], the range of the objects accessible for analysis could be substantially expanded.

In this work comparator INAA using a planar type detector was tried to analyze eleven lanthanides in the thorium-enriched objects such as REE and rare metal ores. Instrumental gamma-spectrometry (IGS) was used to measure thorium content of the samples since this method usually provides the higher precision of thorium determination than XRF.

Materials and methods

To implement INAA about 100 mg of the investigated rock samples ground to the particle size ≈0.07 mm were sealed in plain double polyethylene bags (approximately 1 mm of the sample thickness) and stacked up in aluminium foil. Every package prepared for a separate irradiation included ten assays and a zirconium monitor of the neutron flux (10 mg of ZrO_2) placed in the middle. Package length was about 10 mm.

All the packages were irradiated for 2.5 h in the position № 4 inside the peripheral vertical channel № 10-6 of the light-water research reactor WWR-K (Almaty, Kazakhstan) by the thermal neutron flux density 8.9×10^{13} cm^{-2} s^{-1}; the fast neutron flux density amounted to 6.0×10^{12} cm^{-2} s^{-1} [28]. The selected time of activation was based on the previous experience of typical rock sample investigations using the same facilities. To reduce the influence of the gradient of neutron spectrum composition, the packages were oriented along the channel axis. In this case the radial component of the gradient (8.5% per 1 cm) was the same for all irradiated assays and the axial one (1.2% per 1 cm) can be neglected.

Gamma-spectrometric measurements of the studied assays were conducted several times: after 6–7 days of decay (to determine La, Sm, and Ho), 12–13 days (to determine Nd, Lu, and Gd), and after 3 weeks (to determine Ce, Eu, Tb, Yb, Tm). Counting time was about 30 min, 40 min, and 1 h, correspondingly. The distance from the assay bags to the detector cap amounted to 40 mm ("far" geometry) for the first counting and 10 mm for the others two. The irradiated samples were counted by a planar HPGe detector GLP36360 with the crystal dimensions 36×13 mm and an energy resolution of 585 eV at the 122 keV peak of ^{57}Co connected to an ORTEC multi-channel analyzer DSPEC LF. MAESTRO software by ORTEC was used for the spectra collection. Detector calibration for relative detection efficiency $\varepsilon(E)$, where E is a gamma-ray energy, was made with the help of a multi-gamma ray standard MGS-1 (^{152}Eu, ^{154}Eu, ^{155}Eu) and an isotopic source ^{133}Ba, both by Canberra. $\varepsilon(E)$ values were evaluated in the interval from the weighted energy 30.85 keV of Cs$K\alpha_1$ and Cs$K\alpha_2$ X-ray lines (^{133}Ba) to 411.12 keV (^{152}Eu). A fourth power polynomial was used to fit the calibration curve.

Spectra treatment was carried out by "AnalGamma" software developed in the Institute of Nuclear Physics. The software approximates a part of gamma-ray spectrum in the treatment window by Gaussian curves and a flat background and calculates peak count rates in cps. Partly overlapping peaks can be reliably resolved. Quality of the approximation is checked by the χ^2 test.

Main nuclear parameters of the analytical gamma-lines of the radionuclides used to determine lanthanide content (including thorium as the internal standard) and the accounted interferences are presented in Table 1. If more than one line can be used for analysis preference was given to the cases of higher count rate (taking account of the detection efficiency) and minor peak overlapping. Thus, the same gamma-lines as the usually recommended

ones (e.g. [10]) were used for ^{152}Eu and ^{177}Lu counting. The part of ^{177}Lu count rate resulted from ^{176}Yb by the (n, γ) reaction was evaluated using the basic equation of activation [10]. With the Yb to Lu relation corresponding to their Clarke contents ^{176}Yb contribution to ^{177}Lu activity after 2.5 h of irradiation is ≈1.7% and can be neglected. The low-energy ^{153}Sm gamma-line was selected to avoid spectral interference by ^{233}Pa due to the thorium high contents. The same reason prevailed in the case of terbium determination by ^{160}Tb; the latter is accounted for a ^{233}Pa gamma-line only if thorium content exceeds that of terbium by more than one order of magnitude. The most intensive gamma-line of ^{169}Yb (63.12 keV) is overlapped by a ^{177}Lu gamma-line only to a small extent. U(n, f) means that an analyzed radionuclide (^{40}La and others) is produced by the fission of the uranium containing in the sample. ^{133}Xe is a uranium fission product too, but it was accounted as a spectral interference. Other interferences in the similar aluminum-siliceous matrixes are insignificant and hence were ignored.

Table 1 – Main nuclear parameters and interferences of the radionuclides used to calculate lanthanides by INAA internal standard method

Radionuclide	Half-life, days	Energy, keV	Quantum yield, %	Interferences	Energy, keV	Quantum yield, %
^{140}La	1.7	328.76	20.3	U(n,f)	-	-
^{141}Ce	32.5	145.44	48.3	U(n,f)	-	-
^{147}Nd	11.0	91.11	28.1	U(n,f)	-	-
^{153}Sm	1.9	69.67	4.73	^{187}W	69.31	3.17
^{152}Eu	4943	121.78	28.7	-	-	-
^{161}Tb (^{161}Gd)	6.9	25.65	23.2	^{122}Sb	25.27	0.95
^{160}Tb	72.3	298.58	26.1	^{233}Pa	298.81	0.088
^{166}Ho	1.1	80.57	6.71	^{133}Xe	81.00	36.9
^{170}Tm	128.6	84.25	2.48	^{182}Ta	84.68	2.65
^{169}Yb	32.0	63.12	43.6	^{177}Lu	63.24	0.599
^{177}Lu	6.6	208.37	10.4	^{176}Yb→^{177}Lu	208.37	10.4
^{233}Pa (^{233}Th)	27.0	311.90	38.5	-	-	-

Contribution coefficients F_{Ui} of uranium fission products to analyze La, Ce, and Nd contents were evaluated empirically with the help of a CRM of uranium ion solution (by Perkin Elmer). F_{Ui} values were assessed as the ratios of the count rates of the corresponding radionuclide analytical gamma-lines to the count rate of ^{239}Np (106.12 keV) under the same counting conditions.

REE ore samples were scanned at first with the help of XRF. Then the selected samples with the enhanced thorium content were analyzed by IGS. About 100 g (±0.1 g) of each assay measured by an analytical balance was placed in a cylindrical polyethylene beaker. To provide gamma-spectrometric counting a HPGe coaxial detector GX5019 (relative efficiency is 50% and an energy resolution is 1.86 keV at the 1332 keV peak of ^{60}Co) was used connected to an Canberra multi-channel analyzer. The spectrometer was calibrated for detection efficiency using a volumetric gamma-ray source – thorium ore CRM IAEA-RgTh-1 and the homemade software. Counting time of the investigated assays amounted to 3–4 h.

Thorium content was determined by the equilibrium activity of its daughter radionuclide ^{212}Pb using the 238.6 keV gamma-line, quantum yield is 43.6%, on the assumption of undisturbed secular equilibrium with the other members (^{228}Ra and ^{228}Th) of the decay chain. If the rocks were not being subjected to geochemical leaching, equilibrium in the thorium nuclear series usually maintains [29]. Moreover, due to the short half-time

of ^{220}Rn (56 s) – a predecessor of ^{212}Pb – it's no need to seal the assays.

Results and discussion

Lanthanide contents C_a (%) of the analyzed samples were calculated according to the equation of simple comparator method of standardization in INAA [30] (lower case indices *a* and *c* mean an analyzed element and the comparator, respectively):

$$C_a = C_c \frac{k_{0,c} N_{p,a} \varepsilon(E_c)(f + Q_0^c)(SD)_c}{k_{0,a} N_{p,c} \varepsilon(E_a)(f + Q_0^a)(SD)_a} K_{a,c}, \quad (1)$$

where C_c is the element comparator content of the sample (%), k_0 is k_0-factor relatively to the 411.8 keV gamma-line of radionuclide ^{198}Au for the gamma-lines of the comparator and an analyzed element [31], N_p is the net peak area of the analytical gamma-line of the corresponding radionuclide (cps), Q_0 is the resonance integral I_0 (cm^2) to the thermal neutron cross-section σ_0 (cm^2) ratio, f is the thermal to epithermal neutron flux ratio, $S = 1 - \exp(-\lambda t_{irr})$ is saturation factor depending on the irradiation time t_{irr} and decay constant λ, $D = \exp(-\lambda t_d)$ is decay factor depending on the decay time t_d after the end of irradiation. Since there is no a k_0-factor for radionuclide ^{161}Tb in the data base [31], a *k*-factor was used instead composed of the nuclear constant product:

$$k = \sigma_0 \theta P_\gamma M^{-1}, \quad (2)$$

where θ is isotopic abundance (%), P_γ is the yield of the measured gamma-line (%), M is the atomic mass (Da). Here σ_0, θ, and M relate to the activated short-lived radionuclide ^{160}Gd, and P_γ – to the gamma-line of the daughter long-lived ^{161}Tb (25.7 keV).

When INAA of rock samples for the long-lived radionuclides is carried out correction for the measuring time is always <1% and can be neglected. Neutron self-shielding of the thermal and resonance neutron flux by a 100 mg rock sample was assessed following C.Chilian, et al. [32] using a spreadsheet kindly presented by the authors. The correction factor does not exceed 1% up-to the twenty-fold excess of Gd, Sm, and Eu contents over their Clarke values. Gamma-ray self-absorption by the rock samples was evaluated using a model sample corresponding to the crust averages of the main rock-forming elements in the approximation of a thin irradiating layer [33]. Gadolinium content being analyzed by ^{161}Tb (E = 25.7 keV, Table 1) photoelectric absorption and scattering [34] of the analytical gamma-line in a typical plane sample (1 mm of the thickness) comes up to approximately 9%. However self-absorption by the sample of the next low-energy gamma-line – ^{169}Yb (E = 63.1 keV) is lower 1%, i.e. it can be neglected.

The empirical correction factor $K_{a,c}$ is applied to compensate for an analytical bias caused by the errors of detector calibration for detection efficiency, absence of Q_0 correction for the deviation of thermal neutron flux from 1/E law, and by other reasons. In particular, using the same counting geometries, there is no need to correct J for true coincidences. $K_{a,c}$ values were assessed by the repeated irradiation and counting of the CRMs certified for REE and thorium contents.

The model resonance to thermal neutron flux ratio 1/f was evaluated using the "bare bi-isotopic method" [35] with the help of a monitor of the neutron flux spectral composition – a ZrO_2 sample [13]:

$$\frac{1}{f} = \frac{\sigma_{0,2} - B\sigma_{0,1}}{BI_{0,1} - I_{0,2}}, \qquad B = \frac{N_{p,2} \varepsilon(E_1) \theta_1 P_{\gamma,1} (SD)_1}{N_{p,1} \varepsilon(E_2) \theta_2 P_{\gamma,2} (SD)_2}, \quad (3)$$

where lower indices 1 and 2 correspond to two Zr isotopes ($Q_{0,1} << Q_{0,2}$). During the investigation 1/f values in the irradiation position varied within the small range 0.029–0.034.

To assess accuracy of lanthanide determination by comparator INAA the following four rock CRMs certified for REE content were selected thorium content of which was sufficient to apply IGS: SG-4 (Russian Federation), GBW-07110 (China), DC-73301 (China), and OREAS 100a (Australia). REE mass fractions of these CRMs ranged from approximately Clarke ones (DC-73301) to several Clarke values (OREAS 100a) (Tables 2–5). The CRM samples were prepared, irradiated and analyzed as described above. To avoid overirradiation the assay mass of OREAS 100a was diminished to 50 mg. A single measurement of each CRM was carried out.

Uranium content of DC-73301 reaches 18.8 μg/g and comes up to 135 μg/g in OREAS 100a. GBW-07110 is characterized by a negligible

contribution of uranium fission products to the count rate of La analytical gamma-line and a minimum contribution to Ce and Nd gamma-lines, no more than 1–1.5%. In case of OREAS 100a analysis the corresponding correction reached 10% for Ce, 16% for Nd and 1% for La.

As for the other spectral interferences presented in Table 1, W contribution to Sm analytical gamma-line count rate ranged within 1.5–2.5%, Ta to Tm – from 29% (SG-4) to 68% (DC-73301), and Lu to Yb – within 2.5–6%. ^{133}Xe contribution to the area of unresolved double peak ^{166}Ho + ^{133}Xe came up to 24–25% for GBW-07110 and SG-4, and 48% for DC-73301 after 7 days of the decay time. The corresponding contribution reached 59.5% in case of OREAS 100a counting 6 days after irradiation. Due to Sb low content, 2.5 μg/g of OREAS 100a and no more than 1.3 μg/g of the other CRMs, contribution of Sn$K\alpha_1$ X-ray line resulting from ^{122}Sb decay (Table 1) to ^{161}Tb gamma-line was neglected.

Expanded uncertainty of the INAA results was estimated as follows (P = 0.95):

$$U(C_a) \approx \approx 2C_a\sqrt{\frac{u(J_a)^2}{J_a^{\,2}}+\frac{u(J_c)^2}{J_c^{\,2}}+\frac{u(C_c)^2}{C_c^{\,2}}+\delta_a^{\,2}}, \quad (4)$$

where $u(J_a)$, $u(J_c)$, and $u(C_c)$ are standard uncertainties of the corresponding values as in Eq. 1, δ_a is the standard deviation of element analysis (methodical uncertainty) by comparator INAA (all the ratios and δ_a are in %). δ_a values were assessed earlier with the help of the CRMs and ranged from 2.6% (Eu determination) to 5.0% (determination of Ho and Tm). Relative standard uncertainty of the ^{233}Pa analytical gamma-line count rate amounted to <2%.

To assess relative standard uncertainty (%) of thorium content determination by IGS the next expression was used (P = 0.68):

$$\frac{u(C_c)}{C_c} \approx \approx \sqrt{\frac{u(J_a)^2}{J_a^{\,2}}+\frac{u(J_r)^2}{J_r^{\,2}}+\frac{u(C_r)^2}{C_r^{\,2}}+\delta_m^{\,2}}, \quad (5)$$

where $u(J_a)$ and $u(J_r)$ are standard (statistical) uncertainties of the ^{212}Pb analytical gamma-line count rates of the investigated sample and CRM IAEA-RgTh-1 (P = 0.68), $u(C_r)$ is standard uncertainty of the thorium certified content C_r of IAEA-RgTh-1(1%, P = 0.68), δ_m is relative methodical uncertainty resulting from measuring of the cylindrical assay height (≈1%). Relative standard uncertainty of ^{212}Pb analytical gamma-line count rate never exceeded 2.5%. So, relative standard uncertainty of thorium comparator determination was no more than 4% (P = 0.68).

The results of four CRM analyses for lanthanide contents by comparator INAA including thorium content by IGS are presented in Tables 2–5.

Table 2 – REE contents of SG-4 (subalkaline granite) by comparator INAA, μg/g (P = 0.95)

Element	Certified value	Measured value	E_n-number
La	91 ± 7	86.0 ± 8.2	-0.47
Ce	177 ± 27	191 ± 17	0.44
Nd	84 ± 14	84.6 ± 8.5	0.04
Sm	19 ± 3	17.3 ± 1.7	-0.49
Eu	0.64 ± 0.06	0.64 ± 0.05	0.01
Gd	15 ± 2	15.1 ± 1.7	0.04
Tb	2.5 ± 0.3	2.59 ± 0.26	0.23
Ho	2.6 ± 0.5	2.48 ± 0.35	-0.20
Tm	1.1 ± 0.2	1.18 ± 0.15	0.32
Yb	7.4 ± 1.4	7.95 ± 0.82	0.34
Lu	1.3 ± 0.3	1.31 ± 0.13	0.03
Th	20 ± 3	20.1 ± 1.4	0.04

Table 4 – REE contents of DC-73301 (rock) by comparator INAA, μg/g (P = 0.95)

Element	Certified value	Measured value	E_n-number
La	54 ± 4	53.7 ± 4.8	-0.05
Ce	108 ± 7	106 ± 10	-0.17
Nd	47 ± 4	44.0 ± 4.4	-0.50
Sm	9.7 ± 0.8	9.57 ± 0.91	-0.11
Eu	0.85 ± 0.07	0.83 ± 0.07	-0.19
Gd	9.3 ± 0.7	9.1 ± 1.2	-0.18
Tb	1.65 ± 0.09	1.67 ± 0.17	0.10
Ho	2.05 ± 0.17	2.08 ± 0.29	0.09
Tm	1.06 ± 0.09	0.99 ± 0.12	-0.49
Yb	7.4 ± 0.5	7.32 ± 0.75	-0.09
Lu	1.15 ± 0.09	1.11 ± 0.12	-0.27
Th	54 ± 3	53.9 ± 3.5	-0.02

Table 3 – REE contents of GBW-07110 (trachyte andesite) by comparator INAA, μg/g (P = 0.95)

Element	Certified Value	Measured value	E_n-number
La	62.5 ± 2.5	61.9 ± 5.8	-0.09
Ce	117 ± 7	121 ± 11	0.31
Nd	47.2 ± 2.5	49.0 ± 4.9	0.33
Sm	8.63 ± 0.23	8.60 ± 0.86	-0.03
Eu	1.96 ± 0.07	2.03 ± 0.16	0.40
Gd	6.54 ± 0.40	6.37 ± 0.92	-0.17
Tb	0.99 ± 0.07	0.99 ± 0.11	0.04
Ho	1.1 ± 0.1	1.12 ± 0.19	0.10
Tm	0.50 ± 0.04	0.463 ± 0.073	-0.44
Yb	3.15 ± 0.10	3.12 ± 0.32	-0.09
Lu	0.49 ± 0.04	0.511 ± 0.052	0.32
Th	16.7 ± 0.6	16.2 ± 1.1	-0.41

The measured thorium internal standard contents are well comparable with the certified ones within ≤3% of discrepancy. All the lanthanides analyzed mass fractions differ from their certified contents by no more than 10%. Expanded uncertainty of lanthanides analysis in all the four CRMs $U(C_a)$ by comparator INAA doesn't exceed the allowable standard deviation of the results of their determination directed by the III category of precision (of analysis) according to OST 41-08-221-04 [36].

E_n-number of lanthanides determination was additionally evaluated as a criterion recommended by IUPAC to verify the laboratory performance [37]:

$$E_n = \frac{C_a - C_r}{\sqrt{U(C_a)^2 + U(C_r)^2}}, \qquad (6)$$

where $U(C_r)$ is expanded uncertainty of the analyzed element certified value C_r (P = 0.95). E_n-number values within $-1<E_n<1$ interval are considered admissible if the relative deviation $C_a - C_r$ doesn't exceed a predetermined quantity. In the present investigation maximum deviation ±10% was accepted.

Table 5 – REE contents of OREAS 100a (uranium-bearing rock) by comparator INAA, μg/g (P = 0.95)

Element	Certified Value	Measured value	E_n-number
La	260 ± 8	269 ± 25	0.34
Ce	463 ± 20	477 ± 43	0.30
Nd	152 ± 8	156 ± 15	0.24
Sm	23.6 ± 0.4	24.2 ± 2.4	0.25
Eu	3.71 ± 0.23	3.89 ± 0.31	0.47
Gd	23.6 ± 1.4	23.5 ± 2.9	-0.03
Tb	3.80 ± 0.23	3.82 ± 0.38	0.05
Ho	4.81 ± 0.14	4.99 ± 0.66	0.27
Tm	2.31 ± 0.12	2.22 ± 0.27	-0.30
Yb	14.9 ± 0.4	14.9 ± 1.5	0.00
Lu	2.26 ± 0.11	2.37 ± 0.26	0.39
Th	51.6 ± 2.7	52.4 ± 3.3	0.19

Since E_n-number absolute values appeared less than unity (Tables 2–5) and the relative bias – less than 10%, the results of lanthanide analysis can be considered acceptable by E_n-number criterion too.

So the opportunity to use comparator INAA by long-lived radionuclides with a planar type HP Ge detector and thorium as the internal standard to analyze the rock CRMs for lanthanide contents was demonstrated. Then to verify this approach it was tried for real geological objects.

One of them is the rare earth deposit Shock-Karagai in North Kazakhstan, a part of the big complex rare metal and rare earth province Syrymbet. Industrially significant agglomerations of REEs in the deposit are associated with the weathering crusts and Cenozoic loose sediments. Placers are enriched with the light lanthanides and accompanied by thorium increased contents 0.008–0.02% [38].

The results of eleven lanthanides determinations in twenty REE ore samples by comparator INAA (P = 0.95) are presented in Table 6. Preliminary elemental analysis of the core material was carried out by XRF. All the samples are characterized by relatively low iron mass fractions 0.5–3.3%, insufficient to measure ^{59}Fe count rate by a planar detector in the "far" geometry with the necessary statistical uncertainty. Thorium content of the samples is high enough and therefore was determined by IGS.

The ratio of sum contents of the cerium and yttrium groups (Table 6) confirms the conclusion that the light lanthanides are characteristic of the Shock-Karagai weathering crust [38] unlike that of some other Kazakhstan's REE deposits. Several samples such as 2001/5, 7005/14, 7008/12 and TT-2 are distinguished by the enhanced relative sum mass fraction of the heavy REEs.

It may be noted that a high enough value of the thermal neutron cross-section and monoisotopic composition makes possible to use thorium as an internal standard in comparator INAA beginning from its Clarke contents. This opportunity is restricted only by the sensitivity of thorium determination by an independent method. Neutron activation analysis of the REE ores characterized by thorium enhanced mass fractions for lanthanide contents causes no difficulties and may be regarded as a major application of the planar type detectors in comparator INAA.

Typical gamma-ray spectra of an REE ore sample (№ 7004/2) are presented in Fig. 1 in a log-linear scale after 7 days (a) and 3 weeks (b) of decay. The first spectrum was counted for 35 min and the second one – for about 50 min. Fig. 1(b) displays a low-energy part of the spectrum with the analytical lines of ^{169}Yb and ^{170}Tm. GLP36360 doesn't discriminate between ^{170}Tm and ^{182}Ta gamma-peak energies (84.3 and 84.7 keV) but it resolves the sum peak up to the background, unlike coaxial detectors. Gamma-lines of ^{160}Tb (298.6 keV) and ^{233}Pa (300.1 keV) partly resolved by the planar detector are usually reliably divided by the software even when thorium content of the samples exceeds 100 μg/g. Despite the much lower count rate of 298.6 keV gamma-line comparing with 86.8 keV one of ^{160}Tb, the latter was not chosen as the analytical line because of the frequently fallible results caused by ^{233}Pa spectral interference (86.6 keV). ^{152}Eu and ^{141}Ce gamma-lines are not shown in Fig. 1(b) since there is no problem with corresponding element determination.

Table 6 – Lanthanides and thorium contents of the Shock-Karagai REE ore samples by comparator INAA, μg/g ($P = 0.95$)

Sample	Th	La	Ce	Nd	Sm	Eu	Gd	Tb	Ho	Tm	Yb	Lu
463	41.3 ± 2.1	103 ± 10	209 ± 21	98.7 ± 9.9	21.2 ± 2.1	1.31 ± 0.13	17.5 ± 1.4	3.06 ± 0.31	3.91 ± 0.45	1.53 ± 0.18	10.6 ± 1.1	1.60 ± 0.16
2001/5	41.8 ± 2.1	88.5 ± 8.9	146 ± 15	60.6 ± 6.6	12.2 ± 1.2	0.56 ± 0.06	12.4 ± 1.2	2.75 ± 0.28	3.38 ± 0.39	1.69 ± 0.19	12.3 ± 1.2	1.92 ± 0.19
7002/7	102.5 ± 5.1	171 ± 17	321 ± 32	109 ± 11	19.1 ± 1.9	0.86 ± 0.09	14.9 ± 1.5	2.53 ± 0.25	2.59 ± 0.32	0.93 ± 0.12	7.03 ± 0.70	1.04 ± 0.11
7002/8	123.9 ± 6.2	274 ± 27	494 ± 50	176 ± 18	32.2 ± 3.2	1.38 ± 0.14	26.9 ± 2.7	4.58 ± 0.46	4.68 ± 0.55	1.48 ± 0.18	9.64 ± 0.95	1.38 ± 0.14
7002/9	107.1 ± 5.4	225 ± 23	403 ± 40	144 ± 15	26.1 ± 2.6	1.17 ± 0.12	23.8 ± 2.4	3.96 ± 0.40	3.73 ± 0.44	1.38 ± 0.16	8.71 ± 0.87	1.24 ± 0.13
7002/12	45.2 ± 2.4	76.5 ± 6.9	113 ± 10	58.3 ± 5.8	11.8 ± 1.2	0.55 ± 0.05	11.4 ± 1.3	2.28 ± 0.23	3.21 ± 0.40	1.56 ± 0.20	10.8 ± 1.1	1.69 ± 0.17
7004/2	70.5 ± 3.5	113 ± 11	314 ± 32	86.3 ± 8.6	15.8 ± 1.6	2.06 ± 0.21	13.6 ± 1.4	2.22 ± 0.22	2.48 ± 0.29	0.81 ± 0.11	6.86 ± 0.69	1.09 ± 0.11
7004/5	82.7 ± 4.1	96.1 ± 9.6	198 ± 20	58.2 ± 5.8	11.8 ± 1.2	0.55 ± 0.06	11.4 ± 1.1	2.09 ± 0.21	2.52 ± 0.29	0.69 ± 0.10	5.63 ± 0.56	0.83 ± 0.08
7004/10	65.4 ± 3.3	915 ± 92	601 ± 60	473 ± 47	88.5 ± 8.9	3.86 ± 0.39	83.6 ± 8.4	13.8 ± 1.4	12.2 ± 1.4	3.64 ± 0.41	20.4 ± 2.1	2.84 ± 0.29
7005/6	103.1 ± 5.2	68.8 ± 6.9	236 ± 24	47.5 ± 4.8	8.60 ± 0.86	0.45 ± 0.05	8.23 ± 0.98	1.51 ± 0.15	1.85 ± 0.23	0.69 ± 0.12	6.78 ± 0.68	1.07 ± 0.11
7005/9	89.8 ± 4.5	178 ± 18	304 ± 31	126 ± 13	23.6 ± 2.4	1.20 ± 0.12	20.2 ± 2.0	3.86 ± 0.39	4.56 ± 0.52	1.94 ± 0.23	12.9 ± 1.3	1.95 ± 0.20
7005/14	63.9 ± 3.2	399 ± 40	251 ± 25	237 ± 24	45.7 ± 4.6	2.68 ± 0.27	43.2 ± 4.3	8.77 ± 0.88	12.1 ± 1.4	5.45 ± 0.60	33.8 ± 3.4	5.15 ± 0.52
7006/4	80.0 ± 4.0	674 ± 67	1080 ± 110	349 ± 35	58.5 ± 5.9	2.90 ± 0.29	46.0 ± 4.6	6.81 ± 0.68	6.14 ± 0.75	1.72 ± 0.22	10.0 ± 1.0	1.43 ± 0.15
7006/6	63.0 ± 3.2	263 ± 26	468 ± 47	158 ± 16	27.7 ± 2.8	1.23 ± 0.14	24.7 ± 2.5	4.21 ± 0.42	4.84 ± 0.57	1.67 ± 0.20	10.4 ± 1.1	1.59 ± 0.16
7006/7A	54.3 ± 2.9	169 ± 17	277 ± 28	95.7 ± 9.6	16.4 ± 1.6	0.93 ± 0.09	14.6 ± 1.5	2.69 ± 0.27	3.08 ± 0.37	1.14 ± 0.14	7.50 ± 0.75	1.14 ± 0.11
7006/8A	65.0 ± 3.3	227 ± 23	361 ± 36	130 ± 13	23.4 ± 2.4	1.14 ± 0.12	22.8 ± 2.3	3.72 ± 0.37	4.02 ± 0.47	1.49 ± 0.18	8.95 ± 0.90	1.36 ± 0.14
7007/10	64.0 ± 3.2	173 ± 17	357 ± 36	113 ± 11	20.5 ± 2.1	1.19 ± 0.13	17.2 ± 1.6	2.87 ± 0.29	2.93 ± 0.35	1.13 ± 0.16	8.18 ± 0.82	1.26 ± 0.13
7007/11	71.9 ± 3.6	778 ± 78	608 ± 61	532 ± 53	98.6 ± 9.9	6.03 ± 0.60	73.4 ± 7.5	12.4 ± 1.3	13.1 ± 1.5	4.73 ± 0.54	29.2 ± 2.9	4.24 ± 0.43
7008/12	79.8 ± 4.0	101 ± 10	116 ± 12	72.2 ± 7.2	14.4 ± 1.5	1.00 ± 0.010	13.7 ± 1.4	3.57 ± 0.36	5.88 ± 0.65	3.21 ± 0.38	24.4 ± 2.5	3.90 ± 0.39
TT-2	59.1 ± 3.0	130 ± 13	222 ± 22	70.6 ± 7.1	15.9 ± 1.6	0.34 ± 0.04	14.2 ± 1.4	3.27 ± 0.33	5.02 ± 0.55	2.37 ± 0.26	17.2 ± 1.7	2.72 ± 0.27

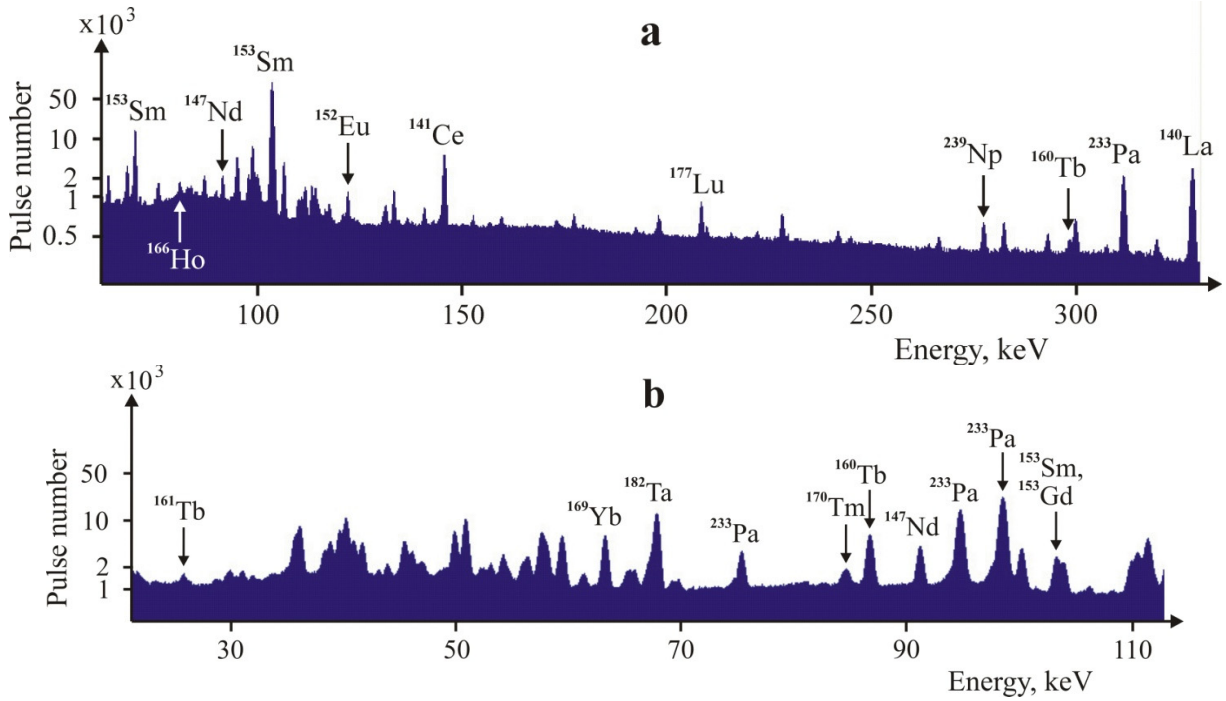

Figure 1 – Parts of the gamma-ray spectra of REE ore sample № 7004/2 counted by GLP36360 after 7 days (a) and 3 weeks (b) of decay (in a log-linear scale)

Another example of the approach verification relates to a nontraditional REE source such as rare metal deposits. As throughout the world, rare earth elements in Kazakhstan are often found in close association with zirconium, niobium, tantalum, and thorium [39]. In the absence of the samples collected from the corresponding fields, several different types of rare metal CRMs with sufficiently high thorium contents were selected for investigation. They are: GSO-2273 (a zirconium ore), NFS-15 (a tantalum-niobium-zirconium ore), both by Russian Federation, GSO-1711 (a tungsten ore, Kazakhstan), and IAEA-RgTh-1. All these CRMs were not certified for lanthanide mass fractions. Thorium content of GSO-2273 and GSO-1711 was determined by IGS and certified in the other samples. Based on preliminary analysis, to conduct INAA IAEA-RgTh-1 assay was significantly diminished to 20 mg, and the other CRM assays – to 40–50 mg.

The results of REE determination in the four rare metal ore samples by comparator INAA (P = 0.95) are presented in Table 7. Certified contents of the elements or their oxides accounting for the ore types are tabulated too. The table is supplemented with the certified or measured mass fractions of uranium since it often accompanies rare metal ores in higher contents.

In case of zirconium ore analysis, contribution of the uranium fission products to the count rate of La analytical gamma-line were negligible and reached approximately 6% and 11% to Ce and Nd ones. Sm gamma-line count rate was corrected for ≈8%. Due to a rather high tantalum content, correction to Tm gamma-line intensity amounted to 82%. ^{161}Tb count rate was increased by 8% comparing with INAA of a typical (model) rock according to the estimated self-absorption of the 25.7 keV gamma-line by zirconium.

The tungsten ore sample was analyzed in the standard manner with the exception that Sm content was found by the 103.2 keV gamma-line because of the extremely high correction of the 69.7 keV line count rate. Uranium contribution as a spectral interference to 103.2 keV gamma-line amounted to 10%.

The sample of complex tantalum-niobium-zirconium ore presented a rather difficult challenge resulted from the high contents of three interfering elements – uranium, thorium and tantalum. The former one caused substantial corrections to the intensities of La, Ce, and Nd analytical gamma-lines amounted to approximately 10%, 39% and 62%, correspondingly. Thorium contribution to Tb gamma-line count rate reached 15%. Very high correction in the case of Tm analysis (≈97%) made the result a rather approximate one.

Table 7 – Lanthanides, thorium and some basic element contents of the rare metal ore samples by comparator INAA, μg/g (P = 0.95)

Element	Zirconium ore	Tungsten ore	Tantalum-niobium-zirconium ore	Thorium ore
La	56.1 ± 5.8	16.3 ± 1.6	19.9 ± 2.0	1530 ± 140
Ce	119 ± 11	51.2 ± 5.1	63.3 ± 6.3	3640 ± 330
Nd	48.4 ± 5.1	25.6 ± 2.6	24.4 ± 3.2	1740 ± 160
Sm	8.33 ± 0.89	9.16 ± 0.85	10.6 ± 1.0	280 ± 27
Eu	1.04 ± 0.10	0.122 ± 0.011	0.119 ± 0.013	69.1 ± 5.8
Gd	7.7 ± 1.6	8.5 ± 1.0	9.2 ± 1.8	154 ± 17
Tb	1.77 ± 0.18	2.01 ± 0.20	3.97 ± 0.40	15.5 ± 1.5
Ho	3.77 ± 0.53	3.03 ± 0.32	7.6 ± 1.0	5.2 ± 1.5
Tm	1.52 ± 0.24	1.86 ± 0.23	1.0 ± 0.3	< 0.2
Yb	33.9 ± 3.4	15.8 ± 1.6	53.5 ± 5.3	2.58 ± 0.29
Lu	5.03 ± 0.48	2.76 ± 0.26	8.61 ± 0.87	0.32 ± 0.04
Zr, %	3.87 ± 0.09 [a]	-	0.35 ± 0.02 [a]	-
Nb_2O_5, %	-	-	0.199 ± 0.009 [a]	-
Ta_2O_5, %	0.0039 ± 0.0004	0.0020 ± 0.0002	0.019 ± 0.002 [a]	-
W	17.7 ± 1.8	286 ± 16 [a]	-	-
U	21.3 ± 1.9	10.0 ± 1.0	134 ± 7 [a]	6.3 ± 0.4 [a]
Th	34.6 ± 1.4	38.9 ± 1.8	740 ± 38 [a]	800 ± 16 [a]

[a] Certified value

All the three samples are characterized by the Clarke, or sub-Clarke contents of the light lanthanides and by the several times increased contents of the heavy ones, from Ho to Lu, comparing with their Clarkes. This allows considering the corresponding ore types as a valuable source of heavy lanthanide by-product production.

The thorium ore sample differs from the three above in high industrial contents of the light REEs, while the heavier ones correspond to their crust averages.

In several cases the planar detector enabled to determine the elements inaccessible to coaxial ones due to the very high thorium content. The first of them is Gd since the 103.2 keV analytical gamma-line of ^{153}Gd can't be reliably separated from the far more intensive 103.9 keV line of ^{233}Pa. The other examples include Eu and Nd determination in the sample of tantalum-niobium-zirconium ore, Yb and Lu in the thorium ore sample. These failures of the coaxial detectors result from the very poor peak-to-background ratios of the corresponding radionuclides due to their low count rates and a high Compton continuum of the spectra.

Conclusion

A variant of comparator INAA using a planar type HPGe detector and thorium as the internal standard was shown as a reliable method for eleven lanthanides analyses by the long-lived radionuclides in the REE ore samples characterized by the enhanced thorium contents and low contents of iron insufficient to use it as the internal comparator. Thorium mass fraction of the samples was conveniently found by the method of IGS insuring in this case better precision than usually used XRF. A planar type detector makes possible to determine gadolinium by the generally interference-free analytical gamma-line of ^{161}Tb (25.7 keV) thus reducing the whole time of the analyses by one-two

weeks and making free coaxial detectors for other applications.

By the example of INAA of several rock CRMs and the ore samples from the Shock-Karagai REE deposit the possibility of routine analysis of the similar objects by the III category of precision according to OST 41-08-221-04 was demonstrated.

The proposed variant of comparator INAA also suggests an advantage in the analysis of REE and thorium-containing rare metal ores comparing with the traditional application of the coaxial detectors.

Acknowledgments

The work was supported by a grant from Ministry of Education and Sciences of the Republic of Kazakhstan (BR05236400).

References

1 Hoffman E.L. (1992) Instrumental neutron activation in geoanalysis. *J Geochem Explor*, vol. 44(1-3), pp. 297-319. https://doi.org/10.1016/0375-6742(92)90053-B.

2 Bulska E., Ruszczyńska A. (2017) Analytical techniques for trace element determination. *Phys Sci Rev*, vol. 2(5). https://www.degruyter.com/view/journals/psr/2/5/article-20178002.xml (10.11.2020). https://doi.org/10.1515/psr-2017-8002.

3 Baccolo G., Clemenza M., Delmonte B., et al. (2015) Assessing the geochemical fingerprint of the 2010 Eyjafjallajokull tephra through instrumental neutron activation analysis: A trace element approach. *J Radioanal Nucl Chem*, vol. 306(2), pp. 429-435. https://doi.org/10.1007/s10967-015-4092-7.

4 Alnour I.A., Wagiran H., Ibrahim N., et al. (2015) Rare earth elements determination and distribution patterns in granite rock samples by using INAA absolute method. *J Radioanal Nucl Chem*, vol. 303(3), pp. 1999-2009. https://doi.org/10.1007/s10967-014-3756-z.

5 El-Taher A., Abdelhalim M.A.K. (2014) Elemental analysis of limestone by instrumental neutron activation analysis. *J Radioanal Nucl Chem*, vol. 299(5), pp. 1949-1953. https://doi.org/10.1007/s10967-014-2925-4.

6 Mizera J., Řanda Z., Košťák M. (2010) Neutron activation analysis in geochemical characterization of Jurassic–Cretaceous sedimentary rocks from the Nordvik Peninsula. *J Radioanal Nucl Chem*, vol. 284(1), pp. 211-219. https://doi.org/10.1007/s10967-010-0472-1.

7 Avino P., Manigrasso M., Capannesi G., et al. (2015) Classification of an area as metallogenic province: environmental importance and problems. *J Radioanal Nucl Chem*, vol. 303(3), pp. 1967-1982. https://doi.org/10.1007/s10967-014-3712-y.

8 Balaram V. (2019) Rare earth elements: A review of applications, occurrence, exploration, analysis, recycling, and environmental impact. *Geoscience Frontiers*, vol. 10, pp. 1285-1303. https://doi.org/10.1016/j.gsf.2018.12.005.

9 Akam C., Simandl G.J., Lett R., et al. (2019) Comparison of methods for the geochemical determination of rare earth elements: Rock Canyon Creek REE–F–Ba deposit case study, SE British Columbia, Canada. *GEEA*, vol. 19, pp. 414-430. https://doi.org/10.1144/geochem2018-044.

10 Stosch H.-G. (2016) Neutron activation analysis of the rare earth elements (REE) – with emphasis on geological materials. *Phys Sci Rev*, vol. 1(8). https://www.degruyter.com/view/journals/psr/2016/8/article-201662.xml (10.11.2020). https://doi.org/10.1515/psr-2016-0062.

11 Damascena K., Amaral R., dos Santos Júnior J., et al. (2015) Rare-earth elements in uranium deposits in the municipality of Pedra, Pernambuco, Brazil. *J Radioanal Nucl Chem*, vol. 304(3), pp. 1053-1058. https://doi.org/10.1007/s10967-015-3934-7.

12 Capannesi G., Rosada A., Manigrasso M., et al. (2012) Rare earth elements, thorium and uranium in ores of the North-Latium (Italy). *J Radioanal Nucl Chem*, vol. 291(1), pp. 163-168. https://doi.org/10.1007/s10967-011-1197-5.

13 Silachyov I. (2016) Rare earths analysis of rock samples by instrumental neutron activation analysis, internal standard method. *J Radioanal Nucl Chem*, vol. 310(2), pp. 573-582. https://doi.org/10.1007/s10967-016-4903-5.

14 Krishnan K., Saion E., Mohamed Kamari H., et al. (2014) Rare earth element (REE) in surface mangrove sediment by instrumental neutron activation analysis. *J Radioanal Nucl Chem*, vol. 301(3), pp. 667-676. https://doi.org/10.1007/s10967-014-3221-z.

15 Ravisankar R., Manikandan E., Dheenathayalu M., et al. (2006) Determination and distribution of rare earth elements in beach rock samples using instrumental neutron activation analysis (INAA). *Nucl Instrum Methods Phys Res B*,

vol. 251(2), pp. 496-500. https://doi.org/10.1016/j.nimb.2006.07.021.

16 Chappell B.W., Hergt J.M. (1989) The use of known Fe content as a flux monitor in neutron activation analysis. *Chem Geol*, vol. 78, pp. 151-158. https://doi.org/10.1016/0009-2541(89)90113-7.

17 Potts P.J., Thorpe O.W., Isaacs M.C., et al. (1985) High-precision instrumental neutron-activation analysis of geological samples employing simultaneous counting with both planar and coaxial detectors. *Chem Geol*, vol. 45, pp. 145-155. https://doi.org/10.1016/0009-2541(85)90042-7.

18 Ebihara M. (1987) Determination of ten lanthanides in chondritic meteorites by radiochemical neutron activation analysis using coaxial and planar type Ge detectors. *J Radioanal Nucl Chem*, vol. 111, pp. 385-397. https://doi.org/10.1007/BF02072871.

19 Labrecque J.J., Rosales P.A., Mejias G. (1986) Instrumental neutron activation analysis of river sediments from Rio Tigre (Venezuela) employing a planar germanium detector. *Appl Spectrosc*, vol. 40(8), pp. 1232-1235. https://doi.org/10.1366/0003702864507648.

20 Kaizer J., Kučera J., Kameník J., et al. (2017) Determination of elemental content in the Rumanová, Uhrovec, Vel'ké Borové, Košice and Chelyabinsk chondrites by instrumental neutron activation analysis. *J Radioanal Nucl Chem*, vol. 311(3), pp. 2085-2096. https://doi.org/10.1007/s10967-017-5168-3.

21 Mizera J., Řanda Z. (2010) Instrumental neutron and photon activation analyses of selected geochemical reference materials. *J Radioanal Nucl Chem*, vol. 284(1), pp. 157-163. https://doi.org/10.1007/s10967-010-0447-2.

22 Araújo M.F., Corredeira C., Gouveia A. (2007) Distribution of the rare earth elements in sediments of the Northwestern Iberian Continental Shelf. *J Radioanal Nucl Chem*, vol. 271(2), pp. 255-260. https://doi.org/10.1007/s10967-007-0201-6.

23 De Corte F. (2001) The standardization of standardless NAA. *J Radioanal Nucl Chem*, vol. 248(1), pp. 13-20. https://doi.org/10.1023/A:1010601403010.

24 Lin X., Henkelmann R. (2004) The internal comparator method. *Anal Bioanal Chem*, vol. 379, pp. 210-217. https://doi.org/10.1007/s00216-004-2557-6.

25 Silachyov I.Yu. (2020) Combination of neutron activation analysis with X-ray fluorescence spectrometry for the determination of rare-earth elements in geological samples. *J Analyt Chem*, vol. 75(7), pp. 878-889. https://doi.org/10.1134/S106193482007014X.

26 Tiwari S., Nair A.G.C., Acharya R., et al. (2007) Analysis of uranium bearing samples for rare earth and other elements by k_0-based internal monostandard INAA method. *J Nucl Radioch Sci*, vol. 8(1), pp. 25-30. https://doi.org/10.14494/jnrs2000.8.25.

27 Weng Z., Jowitt S.M., Mudd G.M., et al. (2015) A detailed assessment of global rare earth element resources: opportunities and challenges. *Econ Geol*, vol. 110(8), pp. 1925-1952. https://doi.org/10.2113/econgeo.110.8.1925.

28 Koltochnik S.N., Sairanbayev D.S., Chekushina L.V., et al. (2018) Comparison of neutron spectrum in the WWR-K reactor with LEU fuel against HEU one. *NNC RK Bulletin* [Vestnik NYATS RK], vol. 76(4), pp. 14-17 (in Russian).

29 Potts P.J. (1992) A handbook of silicate rock analysis. Springer Science & Business Media, 622 p. ISBN 978-1-4615-3270-5.

30 Greenberg R.R., Bode P., De Nadai Fernandes E.A. (2011) Neutron activation analysis: A primary method of measurement. *Spectrochim Acta Part B*, vol. 66, pp. 193-241. https://doi:10.1016/j.sab.2010.12.011.

31 k_0-News. Nuclear data sub-committee. http://www.kayzero.com/k0naa/k0naaorg/Nuclear_Data_SC/Nuclear_Data_SC.html (10.11.2020).

32 Chilian C., St-Pierre J., Kennedy G. (2008) Complete thermal and epithermal neutron self-shielding corrections for NAA using a spreadsheet. *J Radioanal Nucl Chem*, vol. 278(3), pp. 745-749. https://doi.org/10.1007/s10967-008-1604-8.

33 Shirai N., Hidaka Y., Yamaguchi A., et al. (2015) Neutron activation analysis of iron meteorites. *J Radioanal Nucl Chem*, vol. 303(2), pp. 1375-1380. https://doi.org/10.1007/s10967-014-3654-4.

34 Hubbell J.H., Seltzer S.M. X-ray mass attenuation coefficients. NIST standard reference database 126. https://www.nist.gov/pml/x-ray-mass-attenuation-coefficients (10.11.2020).

35 Diaz O., Figueiredo A., Nogueira C., et al. (2005) Epithermal neutron flux characterization of the IEA-R1 research reactor, Sao Paulo, Brazil. *J Radioanal Nucl Chem*, vol. 266(1), pp. 153-157. https://doi.org/10.1007/s10967-005-0885-4.

36 OST 41-08-212-04 (2004) Standart otrasli. Upravlenie kachestvom analiticheskih rabot. Normy pogreshnosti pri opredelenii himicheskogo sostava mineralnogo syr'ya i klassifikatsiya metodik laboratornogo analiza po tochnosti rezultatov

(Idustrial standard. Quality management of analytical work. Error guidelines for chemical analysis of mineral resources and precision classification of laboratory analytical techniques). Moscow, VIMS, 23 p. (in Russian).

37 ISO 13528:2015 (2015) Statistical Methods for Use in Proficiency Testing by Interlaboratory Comparisons. Genève, Switzerland, 89 p.

38 Omirserikov M.Sh., Yusupova U.Y., Togizov K.S., et al. (2015) Rare earth elements in the weathering crust of Shock-Karagai deposit (North Kazakhstan). *News of the Academy of Sciences of RK*, *ser*. *geol*., vol. 3, pp. 35-41. (in Russian).

39 Omirserikov M., Stepanenko N., Pankratova N., et al. (2015) Redkometalnye i redkozemelnye mestorozhdenia Kazahstana (Rare metal and rare earth deposits of Kazakhstan). http://metalmininginfo.kz/archives/2256 (25.08.2020). (in Russian).

IRSTI 68.33.29 https://doi.org/10.26577/ijbch.2020.v13.i2.15

R. Jaćimović[1], I.V. Matveyeva[2*], N.A. Nursapina[2], B.A. Shynybek[2], Sh.N. Nazarkulova[2], O.I. Ponomarenko[2]

[1]Jožef Stefan Institute, Ljubljana, Slovenia
[2]Al-Farabi Kazakh National University, Almaty, Kazakhstan
*e-mail: ilona.matveyeva@kaznu.kz

Assessment of minor and trace elements in mineral fertilizers purchased in Almaty city, Kazakhstan, using k_0-INAA

Abstract. The fertilizers are essential in agriculture as they supply macro and micronutrients to growing crops. The appropriate consumption of nutrients, as well as minimized concentrations of pollutants are the basis of good health of human. The control of content of minor and trace elements in fertilizers can lead to improvement of living conditions of local population. The presenting study is aimed on the investigation of concentration of minor and trace elements, purchased in Almaty city, Kazakhstan. The concentrations were found by k_0-INAA method after crushing and homogenization of the samples. Ljubo-zeleno mineral fertilizer contains high concentration of calcium, potassium, sodium, as well as elevated concentrations of strontium and barium. In Fertika main components are calcium and potassium, although strontium and barium are presented in lower concentrations, than in Ljubo-zeleno mineral fertilizer. In Bujskie udobreniya monopotassium phosphate and ammonium nitrate Fasko mineral fertilizers most of analyzed components (except macrocomponents) are contained in concentrations, lower than the limit of detection of the used method.

Key words: mineral fertilizers, minor and trace elements, k_0-INAA.

Introduction

Agriculture plays a great role in modern life, as the exponentially growing population need to increase crop yields to provide food [1]. Deficiencies in essential nutrients or unavailability in soil can result in a lower quantity and quality of produced foods [2-4]. The question of accumulation of different elements by growing crops is complex and very complicated, although the presence of elements in soils is one of the most important factors, influencing on chemical composition of crops. The usage of different types of chemicals for improvement of crops quality also became “normal” for modern society. One type of these chemicals are fertilizers, which serve a source of most important macro and micronutrients for growing plants. Macronutrients include calcium, potassium, magnesium, phosphorus, and sulfur, while selected micronutrients are iron, manganese, sodium, silicon, and zinc, among others [5]. These nutrients are required by plants in various quantities and are essential for crop growth, development, and yield [6-8]. They can enter agroecosystems through both natural (weathering of soil parent material) and anthropogenic processes (use of fertilizers, organic manures, industrial and municipal wastes, metal-based pesticides, irrigation, and atmospheric deposition) [9].

Although fertilizers can consist not only of those elements, which are essential for these crops, but also of other accompanying elements, which in some cases can be dangerous and even poisonous for animals and human. So, for example, in case of phosphate fertilizers used for agricultural purposes, the starting material for their production are phosphate rocks. Phosphate rock is a general term which refers to rock which is most commonly of the apatite group $\{Ca_5(PO_4)_3[F, OH \text{ or } Cl]\}$ [10]. Phosphate rock of sedimentary origin exists in the earth’s crust in the form of calcium phosphates $Ca_3(PO_4)_2$ and the rock contains NORM (naturally occurring radioactive material) [11-12].

Hence, precise control of concentration of elements in fertilizers is one of the factors, which can improve the quality of living conditions of human in general. The presenting study is aimed on determination of minor and trace elements in several mineral

fertilizers, which were purchased in the specialized shops of Almaty city, and hence are used by locals for improvement of quality of crops.

Materials and methods

Description of fertilizers

In the study five different fertilizers were chosen for investigation, among them are "Ljubo-zeleno" (Russian Federation), organic-mineral mixture Fertika (Russian Federation), superphosphate Fasko (Garden Retail Service, Russian Federation), monopotassium phosphate (Bujskie udobreniya, Russian Federation) and ammonium nitrate Fasko (Garden Retail Service, Russian Federation). Most of them are recommended for usage for vegetables, commonly grown in Kazakhstan and used by local population, including private houses and farms.

The content of some components is presented by producer and presented in Table 1.

Table 1 – Content of components, reported by producer

Fertilizer	N, %	P_2O_5, %	K_2O, %
Ljubo-zeleno	10	12	15
Fertika	-	5	8
Superphosphate Fasko	9	30	-
Monopotassium phosphate Bujskie udobreniya	-	50	33
Ammonium nitrate Fasko	33	-	-

All samples of fertilizers were crushed in mortar and homogenized before the analysis.

Description of k_0-INAA

The mass of aliquot taken for k_0-instrumental neutron activation analysis (k_0-INAA) varied from 0.200 g to 0.210 g [13]. The sample was sealed in a pure polyethylene ampoule (SPRONK system, Lexmond, The Netherlands). A sample together with an Al-0.1%Au standard (IRMM-530R produced by Institute for Reference Materials and Measurements (IRMM), Belgium) were stacked together, fixed in the polyethylene vial in sandwich form and irradiated for 18 h in the carousel facility of the TRIGA Mark II reactor of Jožef Stefan Institute (JSI) [14-15] at a thermal neutron flux of 1.1×10^{12} cm^{-2} s^{-1}. Following irradiation the aliquot was measured after 4, 8 and 22 days cooling time on absolutely calibrated high-purity germanium (HPGe) detectors (40% and 45% relative efficiency). For peak area evaluation, the HyperLab 2002 program was used [16]. The values f = 28.43 (thermal to epithermal flux ratio) and α = –0.0042 (epithermal flux deviation from the ideal 1/E distribution) were used to calculate element concentrations. For elemental concentrations and effective solid angle calculations, the software package Kayzero for Windows was applied [17]. The k_0-INAA procedure at the Department of Environmental Sciences of the JSI is accredited according to ISO/IEC 17025 by the Slovenian Accreditation Agency (Accreditation Certificate LP-090). For QA/QC purposes for k_0-INAA the certified reference material BCR-320R channel sediment (produced by IRMM, Belgium) was used.

In order to prove the reliability of the results the calculation of E_n-score via the following equation was used [18]:

$$E_n = \frac{X_{lab} - X_{ref}}{\sqrt{U_{lab}^2 + U_{ref}^2}}, \quad (1)$$

where: X_{lab} and X_{ref} are results of determination of concentration in laboratory and reference values, correspondently; U_{lab} and U_{ref} are uncertainties (k=2) for laboratory and reference values. The results obtained by k_0-INAA with their associated combined standard uncertainties (u_c) are given in Table 2 and compared with certified values. Combined standard uncertainty (u_c) is calculated as follows:

$$u_c = \sqrt{u_{Np,AREA}^2 + u_{c,method}^2} \quad (2)$$

where $u_{Np,AREA}$ is uncertainty for number of counts in net peak area of gamma ray and $u_{c,method}$ is the combined standard uncertainty of the k_0-INAA established as 3.5% with a coverage factor k=1. The overall combined standard uncertainty of 3.5% is obtained by quadratic summation of the individual contributions [k_0 ~ 1%, Q_0 ~ 1%, α ~ 1.5%, f ~ 1%, ε_p ~ 2% and coincidence correction factors (COI) ~ 1.5%] as described elsewhere [19-21].

Table 2 – Results obtained by k_0-INAA for BCR-320R channel sediment on dry mass basis

El.	This work		IRMM		E_n
	Content (mg/kg)	u_c (mg/kg)	Certified value (mg/kg)	U (k=2) (mg/kg)	
Ag	0.517	0.073			
As	23.1	0.8	21.7	2	0.55
Au	0.0076	0.0003			
Ba	263	9			
Br	82.0	2.9			
Ca	36746	1305			
Cd	2.70	0.18	2.64	0.18	0.15
Ce	34.7	1.2			
Co	9.94	0.35	9.7	0.6	0.26
Cr	60.4	2.1	59	4	0.24
Cs	4.32	0.15			
Cu	< 909		46.3	2.9	N/A
Eu	0.695	0.037			
Fe	25746	903	25700	1300	0.02
Ga	8.41	0.75			
Hf	4.77	0.17			
Hg	0.891	0.049	0.85	0.09	0.31
K	12269	452			
La	19.9	0.7			
Mo	1.01	0.09			
Na	9325	329			
Nd	17.6	0.7			
Rb	63.5	2.2			
Sb	1.13	0.04			
Sc	5.39	0.19	5.2	0.4	0.34
Se	0.804	0.092	(0.96)	(0.18)	N/A
Sm	3.07	0.11			
Sr	191	8			
Ta	0.506	0.019			
Tb	0.429	0.015			
Th	5.27	0.19	5.3	0.4	-0.05
U	1.55	0.05	1.56	0.2	-0.04
Yb	1.51	0.05			
Zn	329	12	319	20	0.32
Zr	179	8			

Notes: u_c – combined standard uncertainty; U – expanded uncertainty (k=2); Results in brackets are informative values; N/A – not applicable; < – Limit of detection (LD) of the method used.

The calculated E_n-scores are within the following inequality $|E_n| \leq 1.0$ [18], hence the used method shows good results.

Results and discussion

The measurement of the fertilizers was done in duplicate, the obtained data are presented in Tables 3-7. Averaged value (X_{AVG}) and its associated uncertainty (u_{XAVG}) are calculated as follows:

$$X_{AVG} = \frac{X_1 + X_2}{2} \quad (3)$$

$$u_{X_{AVG}} = \sqrt{\frac{1}{2}\left(X_1^2 + u_{c,1}^2 + X_2^2 + u_{c,2}^2\right) - X_{AVG}^2} \quad (4)$$

where X_1, X_2, $u_{c,1}$, $u_{c,2}$ denote the result and its associated combined standard uncertainty for each replicate, respectively, X_{AVG} is the averaged value of two replicates. For data presented as LD, the averaged value represents the higher value of the replicates if not stated otherwise.

The data of the Table 3 showed that Ljubo-zeleno mineral fertilizer contains high concentration of calcium, potassium, sodium, which were essential components of mineral fertilizers. Although elevated concentrations of strontium and less of barium, which being chemical analogue of calcium, can substitute it in biological systems, causing serious illnesses of animals and human, should be mentioned. Thorium and uranium also were detected in this mineral fertilizer.

Table 3 – The results obtained by k_0-INAA for Ljubo-zeleno are given on air dry mass basis

El.	Replicate 1		Replicate 2		Average			*n*
	Content (mg/kg)	u_c (mg/kg)	Content (mg/kg)	u_c (mg/kg)	Content (mg/kg)	u_c (mg/kg)	u_c (%)	
Ag	< 0.18		< 0.16		< 0.18			2
As	< 1.5		< 1.4		< 1.5			2
Au	< 0.0032		< 0.0024		< 0.0032			2
Ba	123	5	127	5	125	5	4.3	2
Br	43.4	1.5	44.1	1.5	43.7	1.6	3.6	2
Ca	145100	5200	133800	4802	139450	7548	5.4	2
Cd	< 4.8		< 3.8		< 4.8			2
Ce	238	8	244	9	241	9	3.7	2
Co	0.538	0.020	0.539	0.023	0.538	0.021	4.0	2
Cr	3.80	0.33	3.93	0.70	3.86	0.55	14.3	2
Cs	0.195	0.012	0.180	0.008	0.188	0.013	6.7	2
Cu	< 4223		< 4353		< 4353			2
Eu	5.99	0.21	5.90	0.21	5.95	0.22	3.6	2
Fe	1487	53	1462	52	1475	54	3.6	2
Ga	< 7.1		< 6.8		< 7.1			2
Gd	21.2	0.9	21.9	0.9	21.6	0.9	4.3	2
Hf	0.258	0.011	0.277	0.013	0.268	0.016	5.8	2
Hg	< 0.064		< 0.18		< 0.18			2
K	140000	4974	140200	4996	140100	4986	3.6	2
La	135	5	138	5	136	5	3.7	2
Mo	< 3.6		1.87	0.44	1.87	0.44	23.7	1
Na	27740	978	26620	941	27180	1111	4.1	2
Nd	110	4	113	4	111	4	3.9	2
Pr	< 50.7		< 39.9		< 50.7			2
Rb	47.0	1.7	45.8	1.6	46.4	1.8	3.8	2

Continuation of table 3

El.	Replicate 1		Replicate 2		Average			*n*
	Content (mg/kg)	u_c (mg/kg)	Content (mg/kg)	u_c (mg/kg)	Content (mg/kg)	u_c (mg/kg)	u_c (%)	
Sb	0.102	0.006	0.074	0.006	0.088	0.015	17.6	2
Sc	0.165	0.006	0.149	0.005	0.157	0.010	6.1	2
Se	< 0.49		< 0.51		< 0.51			2
Sm	18.0	0.6	18.3	0.6	18.1	0.7	3.6	2
Sn	< 50.7		< 21.6		< 50.7			2
Sr	4726	168	4807	170	4767	174	3.6	2
Ta	0.500	0.018	0.499	0.018	0.499	0.018	3.6	2
Tb	2.14	0.07	2.19	0.08	2.16	0.08	3.7	2
Th	8.36	0.29	8.61	0.30	8.48	0.32	3.8	2
Tm	0.812	0.075	0.773	0.041	0.792	0.063	8.0	2
U	1.86	0.09	1.78	0.08	1.82	0.10	5.4	2
W	< 2.6		< 2.5		< 2.6			2
Yb	2.83	0.10	2.85	0.10	2.84	0.10	3.6	2
Zn	10.6	0.5	11.4	0.5	11.0	0.6	5.7	2
Zr	< 22.6		< 20.5		< 22.6			2

Notes: u_c – combined standard uncertainty; *n* – number of replicates; < – Limit of detection (LD) of the method used.

Table 4 – The results obtained by k_0-INAA for Fertica are given on air dry mass basis

El.	Replicate 1		Replicate 2		Average			*n*
	Content (mg/kg)	u_c (mg/kg)	Content (mg/kg)	u_c (mg/kg)	Content (mg/kg)	u_c (mg/kg)	u_c (%)	
Ag	< 0.14		< 0.14		< 0.14			2
As	0.788	0.039	0.796	0.051	0.792	0.045	5.7	2
Au	< 0.0012		< 0.0011		< 0.0012			2
Ba	43.5	2.5	41.5	2.2	42.5	2.5	6.0	2
Br	131	5	126	4	128	5	4.0	2
Ca	104800	3697	103300	3646	104050	3747	3.6	2
Cd	< 1.0		< 1.2		< 1.2			2
Ce	24.5	0.9	27.4	1.0	25.9	1.7	6.7	2
Co	2.18	0.08	2.25	0.08	2.22	0.08	3.8	2
Cr	11.3	0.4	11.5	0.5	11.4	0.5	4.1	2
Cs	0.328	0.013	0.330	0.012	0.329	0.013	3.8	2
Cu	< 575		< 604		< 604			2
Eu	0.519	0.023	0.477	0.021	0.498	0.031	6.1	2
Fe	3391	119	3495	123	3443	132	3.8	2
Ga	< 1.9		< 2.9		< 2.9			2
Gd	< 1.6		< 1.6		< 1.6			2
Hf	0.354	0.013	0.335	0.013	0.345	0.016	4.7	2
Hg	< 0.060		< 0.125		< 0.125			2

Continuation of table 4

El.	Replicate 1		Replicate 2		Average			*n*
	Content (mg/kg)	u_c (mg/kg)	Content (mg/kg)	u_c (mg/kg)	Content (mg/kg)	u_c (mg/kg)	u_c (%)	
K	64580	2273	64140	2260	64360	2277	3.5	2
La	16.2	0.6	17.8	0.6	17.0	1.0	5.8	2
Mo	0.217	0.097	0.342	0.123	0.279	0.127	45.6	2
Na	1987	70	1995	70	1991	70	3.5	2
Nd	9.93	0.63	11.37	0.67	10.7	1.0	9.1	2
Pr	< 6.0		< 10.2		< 10.2			2
Rb	7.42	0.29	7.62	0.30	7.52	0.31	4.2	2
Sb	0.0867	0.0054	0.0837	0.0041	0.0852	0.0051	5.9	2
Sc	1.15	0.04	1.19	0.04	1.17	0.05	3.9	2
Se	< 0.32		< 0.25		< 0.32			2
Sm	1.55	0.06	1.65	0.06	1.60	0.08	4.8	2
Sn	< 16.0		< 16.6		< 16.6			2
Sr	289	11	303	11	296	13	4.5	2
Ta	0.365	0.013	0.370	0.014	0.367	0.014	3.7	2
Tb	0.231	0.008	0.246	0.009	0.238	0.011	4.8	2
Th	2.35	0.08	2.38	0.08	2.36	0.09	3.6	2
Tm	< 0.13		< 0.13		< 0.13			2
U	0.978	0.036	0.975	0.036	0.977	0.036	3.7	2
W	< 0.32		< 0.54		< 0.54			2
Yb	1.16	0.04	1.17	0.04	1.16	0.04	3.6	2
Zn	12.0	0.5	12.9	0.5	12.4	0.6	5.0	2
Zr	< 15.2		< 15.6		< 15.6			2

Notes: u_c – combined standard uncertainty; *n* – number of replicates; < – Limit of detection (LD) of the method used.

In Fertika (Table 4) main components were calcium and potassium, less – iron and sodium. Strontium and barium were presented in it, but in lower concentrations, than in Ljubo-zeleno mineral fertilizer. The same situation was observed for thorium and uranium.

Table 5 – The results obtained by k_0-INAA for superphosphate Fasko are given on air dry mass basis

El.	Replicate 1		Replicate 2		Average			*n*
	Content (mg/kg)	u_c (mg/kg)	Content (mg/kg)	u_c (mg/kg)	Content (mg/kg)	u_c (mg/kg)	u_c (%)	
Ag	< 0.52		< 0.44		0.52			2
As	2.20	0.32	2.32	0.33	2.26	0.33	14.5	2
Au	< 0.0151		< 0.0195		0.0195			2
Ba	246	17	250	11	248	15	5.9	2
Br	2.81	0.18	3.04	0.25	2.92	0.24	8.3	2
Ca	91750	3803	86250	3673	89000	4641	5.2	2
Cd	< 10.8		< 10.7		10.8			2

Continuation of table 5

El.	Replicate 1		Replicate 2		Average			*n*
	Content (mg/kg)	u_c (mg/kg)	Content (mg/kg)	u_c (mg/kg)	Content (mg/kg)	u_c (mg/kg)	u_c (%)	
Ce	1088	38	1085	38	1087	38	3.5	2
Co	1.49	0.06	1.50	0.06	1.49	0.06	3.7	2
Cr	19.5	0.8	18.5	0.8	19.0	1.0	5.0	2
Cs	0.405	0.020	0.377	0.026	0.391	0.027	6.9	2
Cu	< 6018		< 6466		6466			2
Eu	18.5	0.7	18.6	0.7	18.6	0.7	3.6	2
Fe	3775	134	3756	138	3766	136	3.6	2
Ga	< 18.3		< 19.3		19.3			2
Gd	66.4	2.7	68.3	2.6	67.4	2.8	4.2	2
Hf	0.693	0.031	0.683	0.030	0.688	0.031	4.5	2
Hg	< 0.57		< 0.49		0.57			2
K	2698	329	3672	431	3185	620	19.5	2
La	652	23	650	23	651	23	3.5	2
Mo	3.70	1.36	< 2.1		3.70	1.36	36.8	1
Na	3253	114	3283	116	3268	116	3.5	2
Nd	423	15	424	15	423	15	3.6	2
Pr	117	9	109	9	113	10	8.6	2
Rb	12.6	0.7	11.5	0.6	12.1	0.9	7.1	2
Sb	0.264	0.016	0.249	0.018	0.256	0.019	7.3	2
Sc	0.839	0.030	0.819	0.029	0.829	0.031	3.7	2
Se	< 1.8		< 1.2		1.8			2
Sm	63.1	2.2	63.2	2.2	63.1	2.2	3.5	2
Sn	< 145		< 130		145			2
Sr	6169	220	6137	216	6153	218	3.5	2
Ta	1.27	0.05	1.30	0.05	1.28	0.05	3.9	2
Tb	6.28	0.22	6.23	0.22	6.26	0.22	3.5	2
Th	17.4	0.6	17.4	0.6	17.4	0.6	3.6	2
Tm	5.16	0.31	4.46	0.33	4.81	0.47	9.8	2
U	12.0	0.5	12.1	0.5	12.0	0.5	3.9	2
W	< 3.3		< 3.4		3.4			2
Yb	7.36	0.26	7.29	0.26	7.32	0.26	3.6	2
Zn	33.1	1.6	33.1	1.4	33.1	1.5	4.6	2
Zr	52.8	19.0	< 62.2		52.8	19.0	36.1	1

Notes: u_c – combined standard uncertainty; *n* – number of replicates; < – Limit of detection (LD) of the method used.

In superphosphate Fasko mineral fertilizer (Table 5), calcium, iron, and potassium were the main components. Strontium and barium found in significant concentrations in Fasko mineral fertilizers, as well as uranium and thorium, are present in considerable quantities.

In monopotassium phosphate (Table 6) the dominant component was potassium, which is evident. Most of the rest components were contained in concentrations, lower than the limit of detection of the used method.

Table 6 – The results obtained by k_0-INAA for monopotassium phosphate are given on air dry mass basis

El.	Replicate 1		Replicate 2		Average			*n*
	Content (mg/kg)	u_c (mg/kg)	Content (mg/kg)	u_c (mg/kg)	Content (mg/kg)	u_c (mg/kg)	u_c (%)	
Ag	< 0.20		< 0.18		< 0.20			2
As	< 0.17		< 0.63		< 0.63			2
Au	< 0.0035		< 0.0027		< 0.0035			2
Ba	< 21		< 20		< 21			2
Br	< 0.24		< 0.23		< 0.24			2
Ca	< 894		< 897		< 897			2
Cd	< 4.5		< 3.3		< 4.5			2
Ce	< 1.5		< 1.4		< 1.5			2
Co	< 0.021		< 0.020		< 0.021			2
Cr	< 1.3		< 1.2		< 1.3			2
Cs	< 0.044		< 0.040		< 0.044			2
Cu	< 1049		< 1101		< 1101			2
Eu	< 0.0057		< 0.0030		< 0.0057			2
Fe	< 17		< 11		< 17			2
Ga	< 4.3		< 4.5		< 4.5			2
Gd	< 6.0		< 5.5		< 6.0			2
Hf	< 0.069		< 0.064		< 0.069			2
Hg	< 0.42		< 0.39		< 0.42			2
K	284900	9998	286400	10050	285650	10052	3.5	2
La	< 0.028		< 0.020		< 0.028			2
Mo	< 5.7		< 4.4		< 5.7			2
Na	1751	61	1736	61	1744	62	3.5	2
Nd	< 4.8		< 4.5		< 4.8			2
Pr	< 13.0		< 13.4		< 13.4			2
Rb	33.5	1.2	34.0	1.3	33.8	1.3	3.7	2
Sb	0.314	0.013	0.303	0.014	0.309	0.014	4.7	2
Sc	0.0105	0.0006	0.0104	0.0005	0.0105	0.0006	5.3	2
Se	< 0.99		< 0.91		< 0.99			2
Sm	< 0.081		< 0.057		< 0.081			2
Sn	< 48		< 44		< 48			2
Sr	< 30		< 28		< 30			2
Ta	< 0.016		< 0.014		< 0.016			2
Tb	< 0.018		< 0.016		< 0.018			2
Th	< 0.10		< 0.09		< 0.10			2
Tm	< 0.53		< 0.49		< 0.53			2
U	< 0.54		< 0.40		< 0.54			2
W	< 1.1		< 1.1		< 1.1			2
Yb	< 0.10		< 0.09		< 0.10			2
Zn	1.37	0.15	1.67	0.14	1.52	0.21	13.9	2
Zr	< 21.9		< 20.0		< 21.9			2

Notes: u_c – combined standard uncertainty; *n* – number of replicates; < – Limit of detection (LD) of the method used.

Table 7 – The results obtained by k_0-INAA for ammonium nitrate Fasko are given on air dry mass basis

El.	Replicate 1		Replicate 2		Average			*n*
	Content (mg/kg)	u_c (mg/kg)	Content (mg/kg)	u_c (mg/kg)	Content (mg/kg)	u_c (mg/kg)	u_c (%)	
Ag	< 0.029		< 0.029		< 0.029			2
As	0.0111	0.0016	0.0141	0.0017	0.0126	0.0023	17.9	2
Au	< 0.00004		0.00042	0.00002	0.00042	0.00002	4.8	1
Ba	5.34	0.25	5.16	0.23	5.25	0.26	4.9	2
Br	0.0339	0.0021	0.0237	0.0016	0.0288	0.0055	19.0	2
Ca	< 170		121	20	121	20	16.3	1
Cd	< 0.068		< 0.051		< 0.068			2
Ce	0.0303	0.0051	0.0413	0.0051	0.0358	0.0075	21.0	2
Co	< 0.009		< 0.002		< 0.009			2
Cr	0.523	0.058	0.846	0.058	0.685	0.172	25.1	2
Cs	< 0.004		< 0.003		< 0.004			2
Cu	< 11.7		< 13.6		< 13.6			2
Eu	< 0.001		< 0.001		< 0.001			2
Fe	52.1	2.2	53.2	2.2	52.7	2.3	4.3	2
Ga	< 0.071		< 0.077		< 0.077			2
Gd	< 0.095		< 0.057		< 0.095			2
Hf	< 0.005		0.00678	0.00068	0.00678	0.00068	10.1	1
Hg	< 0.017		< 0.017		< 0.017			2
K	< 7.4		7.85	1.60	7.85	1.60	20.4	1
La	0.0138	0.0009	0.0214	0.0012	0.0176	0.0039	22.4	2
Mo	< 0.027		< 0.015		< 0.027			2
Na	14.7	0.5	15.8	0.6	15.2	0.8	5.1	2
Nd	< 0.053		< 0.051		< 0.053			2
Pr	< 0.27		< 0.28		< 0.28			2
Rb	< 0.17		< 0.16		< 0.17			2
Sb	0.00770	0.00040	0.00743	0.00036	0.00757	0.00040	5.3	2
Sc	0.00268	0.00015	0.00299	0.00013	0.00283	0.00021	7.4	2
Se	< 0.031		< 0.014		< 0.031			2
Sm	0.00354	0.00015	0.00455	0.00019	0.00404	0.00053	13.1	2
Sn	5.05	0.46	7.09	0.46	6.07	1.12	18.4	2
Sr	30.8	1.3	31.1	1.2	30.9	1.3	4.1	2
Ta	< 0.0028		< 0.0028		< 0.0028			2
Tb	< 0.0012		< 0.0009		< 0.0012			2
Th	< 0.0021		0.00420	0.00057	0.00420	0.00057	13.5	1
Tm	< 0.0078		< 0.0079		< 0.0079			2
U	0.00637	0.00045	0.00512	0.00037	0.00574	0.00075	13.1	2
W	< 0.013		< 0.016		< 0.016			2
Yb	0.00369	0.00046	0.00338	0.00035	0.00353	0.00044	12.4	2
Zn	0.245	0.062	0.200	0.040	0.223	0.057	25.6	2
Zr	< 3.6		< 1.6		< 3.6			2

Notes: u_c – combined standard uncertainty; *n* – number of replicates; < – Limit of detection (LD) of the method used.

In ammonium nitrate Fasko mineral fertilizer (Table 7), most of the analyzed elements were presented in very low concentrations.

Conclusion

The current investigation provided the data on minor and trace elements, presented in five fertilizers, purchased in specialized shops of Almaty city, Kazakhstan. Among them are "Ljubo-zeleno" (Russian Federation), organic-mineral mixture Fertika (Russian Federation), superphosphate Fasko (Garden Retail Service, Russian Federation), monopotassium phosphate (Bujskie udobreniya, Russian Federation) and ammonium nitrate Fasko (Garden Retail Service, Russian Federation). The fertilizers under investigation are recommended for growing of vegetables, commonly used by local population for everyday consumption.

The analysis was done by k_0-instrumental neutron activation analysis. The quality control of the method was done, based on measurements of certified reference material BCR-320R channel sediment. The obtained values of E_n-scores varied within the interval from -0.05 to 0.55, so the method validified the accuracy.

According to the obtained results, Ljubo-zeleno mineral fertilizer contains high concentration of calcium, potassium, sodium, as well as elevated concentrations of strontium and barium, which being chemical analogue of calcium, can substitute it in biological systems, causing serious illnesses of animals and human. In Fertika main components are calcium and potassium, although strontium and barium are presented in lower concentrations, than in Ljubo-zeleno mineral fertilizer.

In monopotassium phosphate and ammonium nitrate Fasko mineral fertilizer most of analyzed components (except macrocomponents) are contained in concentrations, lower than the limit of detection of the used method, hence can be recommended to utilization by local population.

Based on data presented in this work obtained by k_0-INAA and data presented by the producer, we can confirm that content of K in K_2O is in good agreement with stated the producer declaration in Table 1 for Ljubo-zeleno, Fertika and monopotassium phosphate Bujskie udobreniya (see Tables 3, 4 and 6, respectively).

It is necessary to note, that for more precise conclusion, detailed investigations of the bioavailability of minor and trace elements of the investigated fertilizers should be done in future.

Acknowledgments

The work was supported by a project of Ministry of Education and science of the Republic of Kazakhstan "Influence of application of mineral fertilizers on accumulation ability of radionuclides and heavy metals in root vegetables" (#0120PK00099).

References

1 Almeida H.J., Carmona V.M.V., Inocencio, M.F., Neto A.E.F., Mauad M. (2020) Zinc application improves the yield and nutritional quality of three green bean genotypes grown in a Red Latosol. Sci. Hortic. Amsterdam, vol. 274, pp. 2-10. https://doi.org/10.1016/j.scienta.2020.109636

2 Fischer S., Hilger T., Piepho H.P., Jordan I., Karungi J., Towett E., Shepherd K., Cadisch G. (2020) Soil and farm management effects on yield and nutrient concentrations of food crops in East Africa. Sci. Total Environ., vol. 716, pp. 2-13. https://doi.org/10.1016/j.scitotenv.2020.137078

3 Fischer S., Hilger T., Piepho H., Jordan I., Cadisch G. (2019) Do we need more drought for better nutrition? The effect of precipitation on nutrient concentration in east African food crops. Sci. Total Environ., vol. 658, pp. 405–415. https://doi.org/S0048969718350265.;

4 Joy E.J.M., Broadley M.R., Young S.D., Black C.R., Chilimba A.D.C., Ander E.L., Barlow T.S., Watts M.J. (2015) Soil type influences crop mineral composition in Malawi. Sci. Total Environ., vol. 505, pp. 587–595. https://doi.org/10.1016/j.scitotenv.2014.10.038

5 Pisani O., Liebert D., Bosch D.D., Coffn A.W., Endale D.M., Potter T.L. and Strickland T.C. (2020) Element losses from felds in conventional and conservation tillage in the Atlantic Coastal Plain, Georgia, United States. J. Soil Water Conserv., vol. 75, no. 3, pp. 376-386. doi:10.2489/jswc.75.3.376

6 Nagajyoti P.C., Lee K.D. and Sreekanth T.V.M. (2010) Heavy metals, occurrence and toxicity for plants: A review. Environ. Chem. Lett., vol. 8, pp. 199-216. DOI: 10.1007/s10311-010-0297-8

7 Rashid A., Ryan J. (2004) Micronutrient constraints to crop production in soils with Mediterranean-type characteristics: A review. J. Plant Nutr., vol. 27, pp.959-975. DOI: 10.1081/PLN-120037530

8 Reeves R.D., Baker A.J.M. (2000) Metal-accumulating plants. In Phytoremediation of Toxic Metals: Using Plants to Clean Up the Environment, ed. I. Raskin and B.D. Ensley, 193-229. New York: Wiley, 304 p. ISBN: 978-0-471-19254-1

9 He Z.L., Zhang M.K., Calvert D.V., Stoffella P.J., Yang X.E., Yu S. (2004) Transport of heavy metals in surface runoff from vegetable and citrus fields. Soil Sci. Soc. Am. J., vol. 68, pp. 1662-1669. https://doi.org/10.2136/sssaj2004.1662

10 Mar S.S., Okazaki M. (2012) Investigation of Cd contents in several phosphate rocks used for the production of fertilizer. Microchem. J., vol. 104, pp. 17–21. DOI: 10.1016/j.microc.2012.03.020

11 Abbady A.G.E., Uosif M.A.M., Ei-Taher A. (2005) Natural radioactivity and dose assessment for phosphate rocks from Wadi EI-Mashash and EI-Mahamid Mines, Egypt. J. Environ. Radioact., vol. 84, pp. 65–78. DOI: 10.1016/j.jenvrad.2005.04.003

12 Chauhan, P., Chauhan R.P., Gupta M. (2013) Estimation of naturally occurring radionuclides in fertilizers using gamma spectrometry and elemental analysis by XRF and XRD techniques. Microchemi. J., vol. 106, pp. 73–78. DOI: 10.1016/j.microc.2012.05.007

13 Matveyeva I., Jaćimović R., Planinšek P., Stegnar P., Smodiš B., Burkitbayev M. (2014) Assessment of the main natural radionuclides, minor and trace elements in soils and sediments of the Shu valley (near the border of Kazakhstan and Kyrgyzstan). J. Radioanal. Nucl. Chem., vol. 299, pp. 1399–1409. DOI 10.1007/s10967-013-2902-3

14 Snoj L, Žerovnik G, Trkov A (2012) Computational analysis of irradiation facilities at the JSI TRIGA reactor. Appl Radiat Isot, vol. 70, pp. 483–488. DOI: 10.1016/j.apradiso.2011.11.042

15 Radulović V., Jaćimović R., Pungerčič A., Vavtar I., Snol L., Trkov A. (2020) Characterization of the neutron spectra in three irradiation channels of the JSI TRIGA reactor using the GRUPINT spectrum adjustment code. Nuclear Data Sheets, vol. 167, pp. 61–75. https://doi.org/10.1016/j.nds.2020.07.003

16 HyperLab 2002 System (2002) Installation and quick start guide. HyperLabs Software, Budapest.

17 Kayzero for Windows (KayWin®), User's Manual for reactor neutron activation analysis (NAA) using the k0 standardization method, Version 2, November 2005.

18 ISO 13528 (2015) Statistical methods for use in proficiency testing by interlaboratory comparisons, Second edition 2015-08-01, ISO, Genève, Switzerland.

19 De Corte F. (1987) The k0-standardization method: a move to the optimization of neutron activation analysis. Habil. Thesis, Ghent University, Belgium.

20 Jaćimović R., De Corte F., Kennedy G., Vermaercke P., Revay Z. (2014) The 2012 recommended k0 database, J. Radioanal. Nucl. Chem., vol. 300, pp. 589–592. https://doi.org/10.1007/s10967-014-3085-2

21 Bučar T., Smodiš B. (2008) Computer-assisted uncertainty assessment of k0-NAA measurement results, Nucl. Instr. and Meth., A, vol. 595, pp. 647–652. https://doi.org/10.1016/j.nima.2008.07.146

IRSTI 544.42 https://doi.org/10.26577/ijbch.2020.v13.i2.16

R.K. Nadirov[1,2*], M.D. Turan[3], G.A. Karamyrzayev[1]

[1] Al-Farabi Kazakh national university, Almaty, Kazakhstan
[2]Institute of Combustion Problems, Almaty, Kazakhstan
[3]Firat University, Elazig, Turkey
*e-mail: nadirov.rashid@gmail.com

Copper smelter slag leaching with hydrochloric acid in isopropyl alcohol: kinetic study

Abstract. The solvometallurgical approach was applied for the first time for processing copper smelter slag. A comparative analysis of the processes of slag leaching with hydrochloric acid dissolved in water, as well as in isopropanol is presented. The use of isopropanol as a solvent leads to an increase in the extraction of copper in comparison with an aqueous solution (84 and 66%, respectively, at 348 K). The rate constants of leaching processes in an alcohol environment are an order of magnitude higher than those in aqueous solutions at 298, 328 and 348 K. The calculated activation energy values were 28.1±0.8 and 15.7±0.5 kJ/mol for aqueous and alcohol environments, respectively. Diffusion and chemical reactions are the limiting stages of the leaching in aqueous solution while the only diffusion limits the leaching rate in alcohol environment, according to the shrinking core model. The much higher leaching ability of the isopropanol solution is explained by the lower energy of acid solvation in alcohol in comparison with the energy of hydration in an aqueous solution.
Key words: copper smelter slag, copper dissolution, leaching, solvometallurgy.

Introduction

Pyrometallurgical copper production is accompanied by the formation of smelter slag, with about three tons of slag being formed for each ton of copper produced. The copper content in the slag is on average about 1%, depending on the smelting mode used [1]. Being under the open air and exposed to temperature changes and atmospheric precipitation, the slag components partially dissolve and pass into the soil and water. Thus, copper smelter slag should be considered in two aspects: as a raw material for copper production and as a potential source of environmental pollution [2, 3]. Slag is currently processed in three ways: (i) flotation (mainly); (ii) pyrometallurgy; (iii) hydrometallurgy. All these routes have significant disadvantages: flotation loses up to 50% of copper; pyrometallurgy is energy-intensive and an expensive way of processing raw materials with low content of valuable metals. Hydrometallurgical processing of slag seems to be attractive [4-6]. However, the action of the acid on the silicon-containing components of the slag dissolves silicon in the form of silicic acid [7-10]. The dissolved silicon undergoes polymerization to form a gel. This gel makes it practically impossible to separate the pulp into solid and liquid phases [11-12]. Dissolved silicon is a problem not only in acid leaching but also in alkaline processing.

For the formation of silicic acid, water is required; thus, the use of non-aqueous solvents for leaching will avoid the problems associated with the formation of siliceous gels.

Solvometallurgy is a promising approach to the processing of metallurgical raw materials containing a significant amount of silicon. The difference between this approach and the hydrometallurgical one lies in the use of non-aqueous solutions for leaching raw materials [13-16]. Despite the well-known examples of use, solvometallurgy is today considered a new branch of extractive metallurgy [17].

We assumed the possibility of using solvometallurgy for processing copper smelter slag. Isopropyl alcohol was used as a non-aqueous solvent. Aliphatic alcohols are known as ionizing solvents capable of dissolving ionic and covalent compounds; in this case, the molecules and ions of the solute in the solution are strongly solvated [18]. Hydrochloric acid was used as a leaching agent, which is an effective reagent for leaching copper minerals [19, 20]. To the best of our knowledge, the solvometallurgical approach has not previously been used to process copper smelter slag.

Materials and methods

Copper smelter slag samples. Copper smelter slag was sampled at the slag dump of the «Kazakhmys Smelting» copper smelter (Balkhash, Central Kazakhstan), by hand. XRD analysis demonstrated that the major minerals were fayalite (Fe_2SiO_4) and quartz (SiO_2); copper presented mostly as chalcopyrite ($CuFeS_2$) and chalcocite (Cu_2S). The chemical composition of the slag sample determined by ICP-AES (Perkin Elmer, Optima 8000) was, wt %: Fe 35.17, Si 15.28, Zn 2.73, Al 1.12, Cu 1.09, S 0.85. After milling, slag was sieved; samples with particle size 90% ≥ 200 mesh were used for leaching experiments.

Reagents. Isopropyl alcohol (≥98%) and hydrochloric acid (37%) were purchased from Sigma-Aldrich and used without further purification.

Leaching. The leaching tests were performed in a thermostated 1-L flask. The slag sample (15 g) was placed in the flask filled with aqueous or alcohol solution of hydrochloric acid with pre-determined concentration. A magnetic stirrer was used to stir the pulp. After pre-determined leaching time, quantitative analysis of copper ions in the leachate was performed by using ICP-AES (Perkin Elmer, Optima 8000). All experiments were repeated 3 times; the averaged results were used further.

Results and discussion

Dissolution of copper-bearing minerals present in the slag sample. In the presence of hydrochloric acid, the following basic reactions are possible with the participation of copper-containing minerals:

$$CuFeS_2 + 4HCl = CuCl_2 + FeCl_2 + 2H_2S \quad (1)$$

$$CuFeS_2 + 3CuCl_2 = 4CuCl + FeCl_2 + 2S \quad (2)$$

$$Cu_2S + 2HCl = 2CuCl + H_2S \quad (3)$$

Leaching of chalcopyrite with hydrochloric acid leads to the formation of copper (II) chloride, which, in turn, is also a leaching agent.

In general, the above reactions are rather slow because chalcocite and (especially) chalcopyrite are refractory minerals. Besides, the vitreous matrix of the slag prevents the leaching agent from accessing the copper minerals. Acceptable leaching rates and recovery rates are achieved only when the slurry is heated.

Slag leaching in the aqueous and isopropanol solutions. To reveal the role of isopropyl alcohol in the process of copper leaching from slag, comparative experiments were carried out in aqueous and alcoholic media. The concentrations of hydrochloric acid in both media were kept the same for correct comparison.

Figure 1 demonstrates the dependences of the degree of copper extraction into an aqueous solution on the hydrochloric acid concentration and the leaching duration. Solution temperature was maintained at 298 K, the liquid-to-solid ratio was 20: 1, and the stirring rate was kept at 600 rpm.

Increasing both the leach time and the acid concentration increased the copper recovery to a certain limit. After 240 minutes of leaching and using 1M HCl, copper recovery reached 42%; further, the increase in acid concentration and leaching duration did not increase copper recovery.

It should be noted that as a result of leaching, a hard-to-filter slurry was formed; the separation of the solids from the liquid was a difficult task.

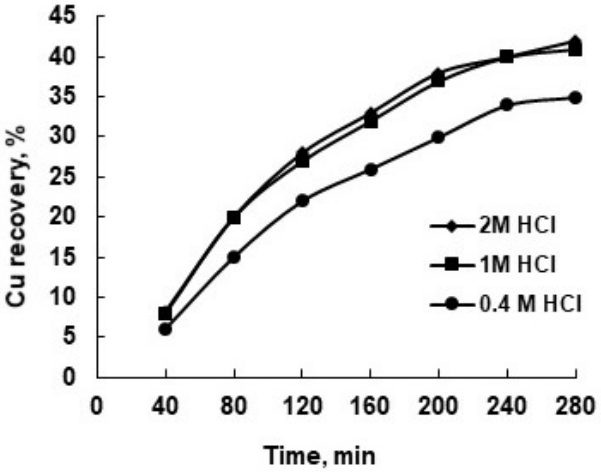

Figure 1 – Effect of hydrochloric acid concentration and leaching duration on copper recovery (%) into an aqueous solution (298 K, liquid-to-solid ratio = 20:1, 600 rpm)

A similar series of experiments were also performed for an alcoholic solution of hydrochloric acid. The results are presented in Figure 2.

It can be noted that the nature of the curves in Figure 2 is similar to that for Figure 1. An increase in the leaching duration, as well as an increase in the acid concentration from 0.4 M to 1.0 M, led to an increase in the copper extraction into solution. Meanwhile, the maximum achievable copper recovery is higher than in aqueous solution (46% vs 42%); besides, the maximum copper recovery in an alcoholic solution was achieved in less time than in an aqueous one (200 min vs 240

min). Thus, it can be assumed that the isopropanol medium favours the leaching of copper from the slag from both thermodynamic (increased recovery) and kinetic (decrease in leaching duration) points of view.

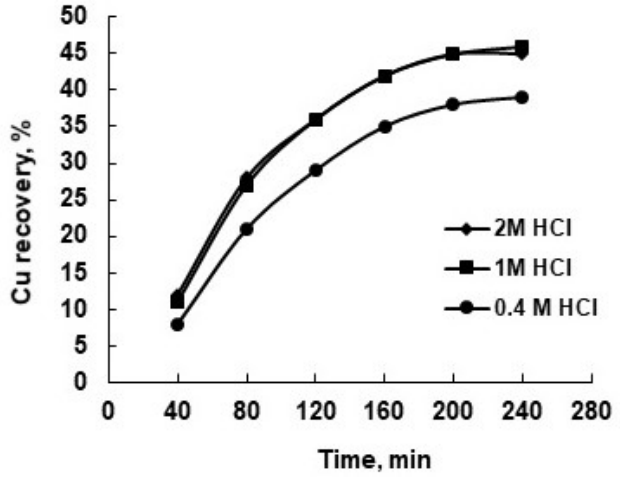

Figure 2 – Effect of hydrochloric acid concentration and leaching duration on copper recovery (%) into alcohol solution (298 K, liquid-to-solid ratio = 20:1, 600 rpm)

In contrast to the aqueous solution, the alcoholic solution after leaching was filtered quite easily. Visually, no siliceous gel was observed, as in the case of an aqueous environment.

In the next series of experiments, the temperature was varied; acid concentration was maintained at 1M (since further increase in acid concentration did not increase copper recovery, see Figs. 1 and 2), the liquid-to-solid ratio was 20: 1, and the stirring rate was kept at 600 rpm.

Figures 3 and 4 demonstrate the dependences of the degree of copper recovery into aqueous and alcoholic solutions, respectively.

It can be seen that with increasing temperature, the degree of copper extraction into solution also increases, in both media. Upon reaching 200 min (in an aqueous medium) and 160 min (in an alcoholic medium), the curves reached a plateau. The maximum extraction of copper in solution was 66% (aqueous solution) and 84% (an alcohol solution).

To determine the limiting stage of leaching in both studied media, as well as the kinetic parameters, the shrinking core model [21] was applied. According to this model, slag particles were considered as ideal spheres, the radius of which decreased over time. Depending on which stage of leaching is the limiting one, one of the following straight-line relationships can be observed:

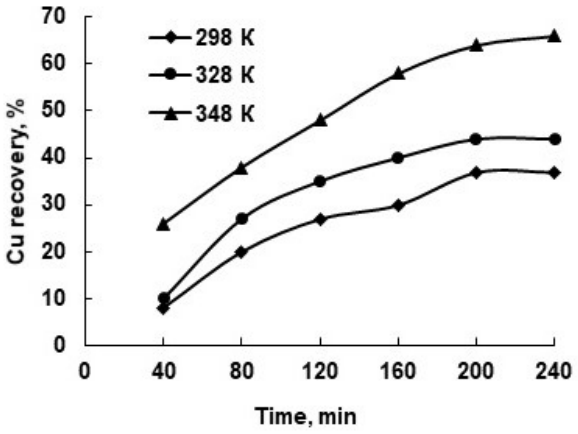

Figure 3 – Effect of leaching duration and temperature on copper recovery (%) into an aqueous solution (1 M HCl, liquid-to-solid ratio = 20:1, 600 rpm)

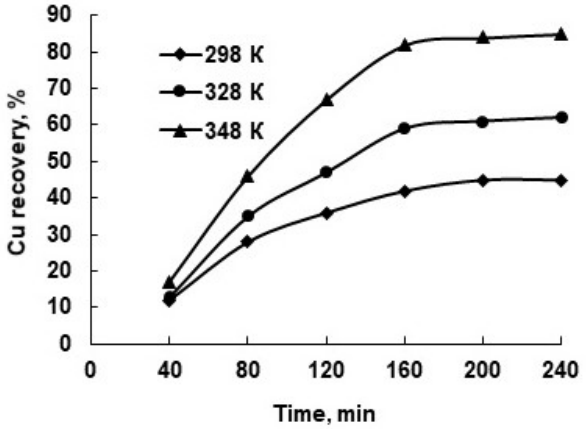

Figure 4 – Effect of leaching duration and temperature on copper recovery (%) into alcohol solution (1 M HCl, liquid-to-solid ratio = 20:1, 600 rpm)

$$1 - (1\text{-}X)^{2/3} = k\tau \quad (4)$$

$$1 - (1\text{-}X)^{1/3} = k\tau \quad (5)$$

$$1 - 2(1\text{-}X)^{1/3} + (1\text{-}X)^{2/3} = k\tau \quad (6)$$

where X is the fraction of the recovered component at the leaching time τ, and k is the apparent rate constant.

Eqs. 4, 5 and 6 correspond to diffusion, kinetic and mixed control leaching processes, respectively. By substituting the values of the degree of copper extraction (X) into the above equations, it was determined which equation led to the straight-line dependence.

Calculations demonstrated that for an aqueous solution, a linear dependence was observed corresponding to the equation (6), see Fig.5.

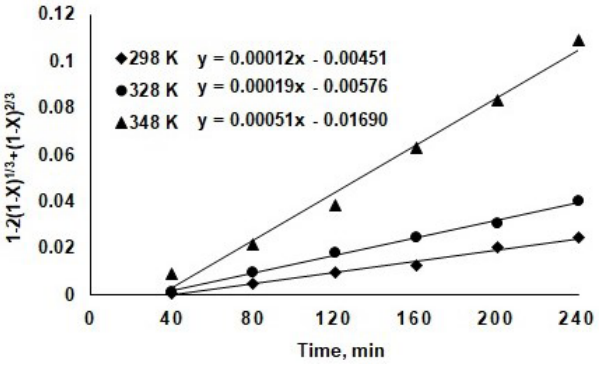

Figure 5 – Plot of $1-2(1-X)^{1/3}+(1-X)^{2/3} = k\tau$ vs time for leaching in aqueous solution(1 M HCl, liquid-to-solid ratio = 20:1, 600 rpm)

This fact indicates a mixed, diffusion-kinetic control of the process of dissolution of copper in an aqueous solution of hydrochloric acid. The apparent rate constants for these reactions have been found as 0.00012, 0.00019, and 0.00051 min^{-1} for 298, 328 and 348 K, respectively.

For the alcoholic solution, a different rectilinear relationship was observed (Fig. 6), that can be described by Eq.(4).

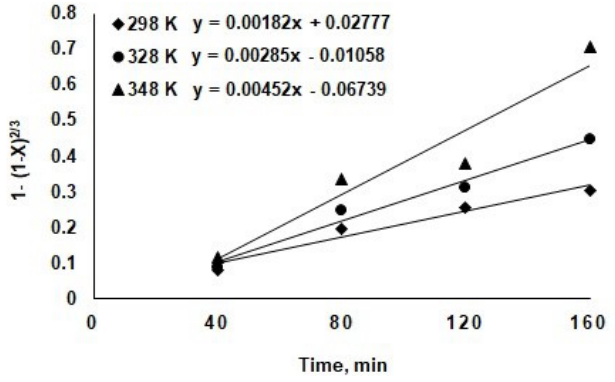

Figure 6 – Plot of $1-2(1-X)^{1/3}+(1-X)^{2/3} = k\tau$ vs time for leaching in alcohol solution (1 M HCl, liquid-to-solid ratio = 20:1, 600 rpm)

This fact testifies in favour of diffusion control of the copper dissolution process in isopropanol solution of hydrochloric acid. The apparent rate constants for these reactions have been found as 0.00182, 0.00285, and 0.00452 min^{-1} for 298, 328 and 348 K, respectively.

It can be seen that the apparent rate constants in the case of an alcohol solution are an order of magnitude higher than those for an aqueous solution.

By using the Arrhenius plot (Fig.7), the activation energies have been calculated for copper leaching processes in both aqueous and alcohol environments.

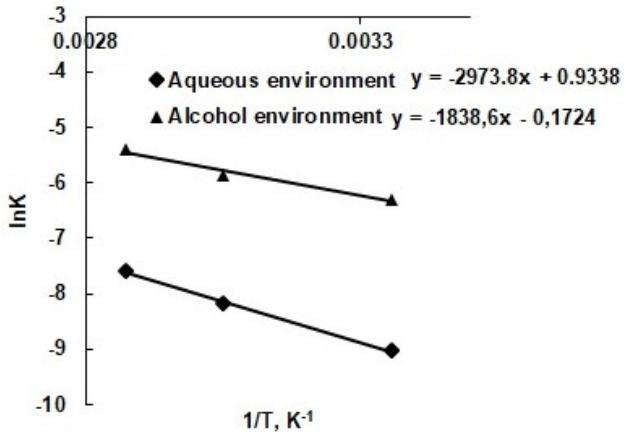

Figure 7 – Arrhenius plot for copper dissolution from slag in aqueous and alcohol environments (1 M HCl, liquid-to-solid ratio = 20:1, 600 rpm)

The activation energy values were 28.1±0.8 and 15.7±0.5 kJ/mol for aqueous and alcohol solutions, respectively. The activation energies values confirmed the initial assumptions about mixed control for a process in an aqueous environment and diffusion control for a process in an alcohol environment.

We assume that the higher capacity of hydrochloric acid in a non-aqueous (alcoholic) solution is due to the lower energy of acid solvation compared to its energy of hydration in an aqueous solution.

Thus, the use of isopropanol hydrochloric acid solution has the following advantages in comparison with an aqueous solution: (i) higher extraction of copper into solution, (ii) higher copper leaching rate, (iii) much easier filterability of the pulp.

The above advantages determine the promising use of the solvometallurgical approach for leaching the copper smelter slag.

Conclusion

The traditional ways of processing copper smelter slag are characterized by various disadvantages, such as significant losses of copper with tailings (flota-

tion enrichment), energy intensity (pyrometallurgy), as well as the formation of hard-to-filter pulp due to acid dissolution of silicon (hydrometallurgy). In this work, a solvometallurgical approach to the processing of copper slag has been applied for the first time.

It was found that the use of isopropanol as a solvent for hydrochloric acid leads to an increase in the extraction of copper in comparison with an aqueous solution (84 and 66%, respectively, at 348 K).

The kinetic characteristics of slag leaching in aqueous and isopropanol hydrochloric acid solutions have been compared. The rate constants of leaching processes in an alcohol environment are an order of magnitude higher than those for an aqueous one at the three operating temperatures (298, 328 and 348 K). The calculated activation energy values were 28.1±0.8 and 15.7±0.5 kJ/mol for aqueous and alcohol solutions, respectively. It has been demonstrated that during leaching in an aqueous solution, diffusion process and chemical reactions are the limiting stages, while when using an isopropanol environment, the leaching process is controlled only by the diffusion stage.

The much higher ability of the isopropanol solution to leach copper from the slag is explained by the lower energy of acid solvation in alcohol in comparison with the energy of hydration in an aqueous solution.

In contrast to leaching with an aqueous solution, the use of an alcohol environment results in the formation of an easily filterable slurry.

The results obtained demonstrate the promise of applying the solvometallurgical approach to the processing of copper smelter slag.

Acknowledgements

This research was funded by the Science Committee of the Ministry of Education and Science of the Republic of Kazakhstan (Grant No. AP08856414).

References

1 Wang J. P., Erdenebold U. (2020). A study on reduction of copper smelting slag by carbon for recycling into metal values and cement raw material. Sustainability-Basel, vol. 12, no. 4, p. 1421. https://doi.org/10.3390/su12041421.

2 Gorai B., Jana R. K. (2003). Characteristics and utilisation of copper slag—a review. Resour Conserv Recy., vol. 39, no. 4, pp. 299-313. https://doi.org/10.1016/S0921-3449(02)00171-4.

3 Sarfo P., Das A., Wyss G., Young C. (2017). Recovery of metal values from copper slag and reuse of residual secondary slag. Waste Manage, vol. 70, pp. 272-281. https://doi.org/10.1016/j.wasman.2017.09.024.

4 Nadirov R. K. (2019). Recovery of valuable metals from copper smelter slag by sulfation roasting. T Indian I Metals, vol. 72, no. 3, pp. 603-607. https://doi.org/10.1007/s12666-018-1507-5.

5 Khalid M. K., Hamuyuni J., Agarwal V., Pihlasalo J., Haapalainen M., Lundström M. (2019). Sulfuric acid leaching for capturing value from copper rich converter slag. J Clean Prod., vol. 215, pp. 1005-1013. https://doi.org/10.1016/j.jclepro.2019.01.083.

6 Banza A. N., Gock E., Kongolo K. (2002). Base metals recovery from copper smelter slag by oxidising leaching and solvent extraction. Hydrometallurgy, vol. 67, no. 1-3, pp. 63-69. https://doi.org/10.1016/S0304-386X(02)00138-X.

7 Turan M. D., Sari Z. A., Miller J. D. (2017). Leaching of blended copper slag in microwave oven. T Nonfer Metal Soc., vol. 27, no. 6, pp. 1404-1410. https://doi.org/10.1016/S1003-6326%2817%2960161-4.

8 Piatak N. M., Parsons M. B., Seal II R. R. (2015). Characteristics and environmental aspects of slag: A review. Appl Geochem., vol. 57, pp. 236-266.

9 Potysz A., van Hullebusch E. D., Kierczak J., Grybos M., Lens P. N., Guibaud G. (2015). Copper metallurgical slags–current knowledge and fate: a review. Crit Rev Env Sci Tec., vol. 45, no. 22, pp. 2424-2488. https://doi.org/10.1080/10643389.2015.1046769.

10 Shi G., Liao Y., Su B., Zhang Y., Wang W., Xi J. (2020). Kinetics of copper extraction from copper smelting slag by pressure oxidative leaching with sulfuric acid. Sep Purif Technol., vol. 241, p. 116699. https://doi.org/10.1016/j.seppur.2020.116699.

11 Cao L., Liao Y. L., Shi G. C., Zhang Y., Guo M. Y. (2019). Leaching behavior of zinc and copper from zinc refinery residue and filtration performance of pulp under the hydrothermal process. Int J Min Met Mater., vol. 26, no. 1, pp. 21-32. https://doi.org/10.1007/s12613-019-1706-z

12 Gyurov S., Marinkov N., Kostova Y., Rabadjieva D., Kovacheva D., Tzvetkova, C., Penkov I. (2017). Technological scheme for copper slag processing. Int J Miner Process., vol. 158, pp. 1-7. http://dx.doi.org/10.1016/j.minpro.2016.11.008.

13 Kopkova E. K., Shchelokova E. A., Gromov P. B. (2015). Processing of titanomagnetite concentrate with a hydrochloric extract of n-octanol. Hydrometallurgy, vol. 156, pp. 21-27. https://doi.org/10.1016/j.hydromet.2015.05.007.

14 Li X., Monnens W., Li Z., Fransaer J., Binnemans K. (2020). Solvometallurgical process

for extraction of copper from chalcopyrite and other sulfidic ore minerals. Green Chem., vol. 22, no. 2, pp. 417-426. https://doi.org/10.1039/C9GC02983D.

15 Whitehead J. A., Lawrance G. A., McCluskey A. (2004). 'Green'leaching: recyclable and selective leaching of gold-bearing ore in an ionic liquid. Green Chem., vol. 6, no. 7, pp. 313-315. https://doi.org/10.1039/B406148A.

16 Önal M. A. R., Riaño S., Binnemans K. (2020). Alkali baking and solvometallurgical leaching of NdFeB magnets. Hydrometallurgy, vol. 191, p. 105213. https://doi.org/10.1016/j.hydromet.2019.105213.

17 Binnemans K., Jones P. T. (2017). Solvometallurgy: an emerging branch of extractive metallurgy. J Sustain Met., vol. 3, no. 3, pp. 570-600. https://doi.org/10.1007/s40831-017-0128-2.

18 Nagrimanov R. N., Samatov A. A., Solomonov B. N. (2019). Additive scheme of solvation enthalpy for linear, cyclic and branched-chain aliphatic compounds at 298.15 K. J Mol Liq., vol. 292, p. 111365. https://doi.org/10.1016/j.molliq.2019.111365.

19 Cai Y., Chen X., Ding J., Zhou, D. (2012). Leaching mechanism for chalcopyrite in hydrochloric acid. Hydrometallurgy, vol. 113, pp. 109-118. https://doi.org/10.1016/j.hydromet.2011.12.002.

20 Petrović S. J., Bogdanović G. D., Antonijević M. M. (2018). Leaching of chalcopyrite with hydrogen peroxide in hydrochloric acid solution. T Nonfer Metal Soc., vol. 28, no. 7, pp. 1444-1455. https://doi.org/10.1016/S1003-6326(18)64788-0.

21 Gbor P. K., Jia C. Q. (2004). Critical evaluation of coupling particle size distribution with the shrinking core model. Chem Eng Sci., vol. 59, no. 10, pp. 1979-1987. https://doi.org/10.1016/j.ces.2004.01.047.

Contents

T.T. Nurkenov, A.K. Tsoy, G.E. Zhusupova, F.S. Olzhayev, M.Zh. Shertay, T.M. Shalakhmetova, J.C.-M. Lee, Sh.N. Askarova
Therapeutic effectiveness of *Limonium gmelinii* extract in experimentally – induced ischemic brain damage *in vivo* 4

G. Sypabekkyzy, M. Sedlářová, Y.V. Rakhimova, B.D. Yermekova, L.A. Kyzmetova, A.M. Assylbek
Diversity of rust fungi on woody and shrubby vegetation of the Zailiysky Alatau.....14

Hatice Aysun Mercimek Takcı, Pemra Bakirhan, Kıvılcım Caktu Guler
Urease purification from indigenous soil bacteria and accumulation of $CaCO_3$ crystals 24

A.M. Belkozhayev, R.Ye. Niyazova, C.M. Wilson
The features of novel miRNAs interaction with mRNA candidate genes having trinucleotide repeats in coding sequences and untranslated regions 30

Ayse Gul Sarıkaya, Seydi Ahmet Kavaklı
Some morphological and phenological characteristics and volatile components of *Campanula rapunculus* L. var. *rapunculus* 38

L.Zh. Gumarova, D. Hillman, A.T. Mansharipova, G. Sadyrbayeva, M. Tauassarova
Geomagnetic, cardiovascular and geo-cardiovascular congruences of cycles: putative co-periodisms.....46

O.K. Khamdiyeva, Z.B. Tileulesa, G.S. Baratzhanova, S.S. Murzataeva, E.M. Khussainova, S. Abdikerim, A. Childebayeva, L.D. Djansugurova
Next Generation Sequencing in diagnosis of mitochondrial epilepsy.....53

Z. Zakaria, L. Bekbayeva, A.V. Goncharova, E.-S. Negim
Effects of blended polyvinyl alcohol/urea on the growth, yield and chemical content of tomato (*Lycopersicon esculentum* L. Mill) 59

T.N. Kobylina, N.M. Mukhitdinov, K.T. Abidkulova, N.V. Kurbatova, N.O. Kudrina, M.B. Alimkulova, Jurate Zaltauskaite
Anatomic-morphological and phytochemical study of a rare species – *Rheum wittrockii* Lundstr. 69

O.A. Iksan, I.A. Kisselev, A.A Garshin, L.A. Skvortsova, Zh.A. Zhaniyazov, M.A. Alpysbes, Charleston W.K. Chiang, L.Z. Musralina, G.S. Zhunussova, E.M. Khussainova
Analysis of the Kazakh tribe Baiuly based on the distribution of the Y-chromosome haplogroups 80

M. Irfan, J. Bakhtawar, S. Sadia, H.A. Shakir, M. Khan, S. Ali
Utilization of fruit wastes for enzyme production in submerged fermentation 88

E.S. Jafarov, M.Z. Velijanova
Study of the adaptive reaction to salt stress of *Cicer arietinum* L., grown from seeds exposed to presowing γ – irradiation 96

A.K. Martusevich, O.B. Zhdanova
Dynamics of some physical and chemical properties of biological fluids in surgical treatment of alveolar hydatid disease of liver.....110

I.Yu. Silachyov
Neutron activation analysis of rare earth raw material using a planar detector and thorium as an internal standard 117

R. Jaćimović, I.V. Matveyeva, N.A. Nursapina, B.A. Shynybek, Sh.N. Nazarkulova, O.I. Ponomarenko
Assessment of minor and trace elements in mineral fertilizers purchased in Almaty city, Kazakhstan, using k0-INAA 130

R.K. Nadirov, M.D. Turan, G.A. Karamyrzayev
Copper smelter slag leaching with hydrochloric acid in isopropyl alcohol: kinetic study 141